

UNCLASSIFIED

AD 402 623

*Reproduced
by the*

DEFENSE DOCUMENTATION CENTER

FOR

SCIENTIFIC AND TECHNICAL INFORMATION

CAMERON STATION, ALEXANDRIA, VIRGINIA



UNCLASSIFIED

NOTICE: When government or other drawings, specifications or other data are used for any purpose other than in connection with a definitely related government procurement operation, the U. S. Government thereby incurs no responsibility, nor any obligation whatsoever; and the fact that the Government may have formulated, furnished, or in any way supplied the said drawings, specifications, or other data is not to be regarded by implication or otherwise as in any manner licensing the holder or any other person or corporation, or conveying any rights or permission to manufacture, use or sell any patented invention that may in any way be related thereto.

402623

PROPERTIES OF STRIP
TRANSMISSION LINE

by

A. D. Stiles

Department of Defense

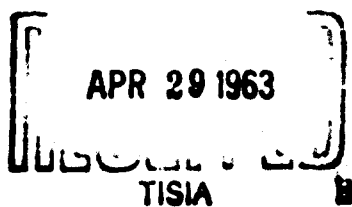


TABLE OF CONTENTS

Chapter	Page
I Introduction	1
II Determination of stripline Characteristic Impedance	
A. History	7
B. Recommended Approach	11
C. Derivation of Characteristic Impedance in the Low Range	11
D. Determination of Characteristic Impedance in the High Range	17
E. Comparison with an Exact Case	20
F. Graphical Presentation of Z_0	21
G. Conclusions	21
II. Characteristic Impedance Measurement	
1. Theory	25
2. Hardware	26
3. Measurement Technique	27
4. Source of Error	28
Bibliography	32

TABLE OF CONTENTS

Appendix I Size and Cost Calculations for a 1000 Logical Element Computer

A.	Waveguide Construction	
1.	Size	A1
2.	Cost	A2
B.	Stripline Constriction	
1.	Size	A2
2.	Cost	A4

Appendix II A Discussion of the TEM Mode

A.	Maxwells First Law	A5
B.	Maxwells Second Law	A9
C.	Maxwells Third Law	A13
D.	Maxwells Fourth Law	A17
E.	The Wave Equations Governing Electric and Magnetic Phenomena in Charge Free Dielectric	A17

Appendix III Elements of Complex Variable Theory and a Discussion of the Schwarz-Christoffel Transformation

A.	Elements of Complex Variable Theory	
1.	The Cauchy Riemann Equations . . .	A24
2.	Conformal Mapping	A28
B.	The Schwarz-Christoffel Transformation .	A30
C.	The Inverse Function	A38
D.	Successive Transformation	A45

Appendix IV Determination of the Capacitance of
Stripline

- A. Capacitance of Stripline per unit length neglecting Fringing A⁴⁷
- B. Capacitance of Stripline including fringing capacitance A⁴⁹
- C. Development of an expression for fringing capacitance C_f' A⁵⁰

Appendix V Polygonal Cross Section A⁵⁷

Appendix VA Reduction of

$$2\sqrt{2} \int_0^{\frac{\pi}{2}} \sqrt{\cos 2\psi + \sin 2\beta} d\psi \text{ to complete}$$

elliptic integrals A⁵¹

LIST OF FIGURES

Figure	Page
1-1 Microstrip Cross Section	3
1-2 stripline Cross Section	4
2-1 Treatment of the low Z_0 Range	12
2-2 Cross Section of "Stripline" used for Capacitance Calculations	15
2-3 Treatment of the high Z_0 range	18
2-4 Center Conductors of Small Cross Section Yielding Equivalent Characteristic Impedance	19
2-5 Equivalence between a Rectangular and Circular Cross Section	22
2-6 Comparison of the Two Approximate Formulas with the Exact Formula for $t = 0$	23
2-7 Graph of Z_0 versus w/b for various values of t/b	24
2-8 Test Set Up for Measurement of stripline Capacity	29
2-9 Theoretical vs. Measured Values of Characteristic Impedance	31

LIST OF FIGURES

Figure	Page	
A1-1	A 3 kmc Magic Tee	A1
A1-2	Configuration of a Hybrid Ring	A2
A2-1	Element of volume in the electromagnetic field. Cartesian Coordinates	A5
A2-2	Derivation of Divergence	A14
A3-1	Illustration of Z and W Planes	A25
A3-2	Conformal Mapping in the Complex Domain . .	A28
A3-3	Representation of $(z-z_v)$ in polar form in the study of dw/dz	A32
A3-4	The path along which dw/dz is studied in the Schwartz-Christoffel Transformation . .	A34
A3-5	The map in the W-plane of the real axis in the Z-plane shown in Fig A3-4	A36
A3-6	Relation of interior to exterior angles . .	A37
A4-1	Cross Section of stripline	A47
A4-2	Upper Half of Fig A4-1	A48
A4-3	Schwarz-Christoffel - Mapping of stripline: Z plane representation	A51
A4-4	Schwarz-Christoffel	A52
A4-5	Transformation from the Z_1 to the W plane .	A59

Figure		Page
A4-6	Cross Section of Stripline as given by Cohn	A64
A4-7	Exact Fringing Capacitance for a Semi- Infinite Plate Centered between Parallel Ground Planes	A66
A5-1	Mapping of the Region outside a Rectangle on the Outside of a Circle	A71
A5-2	The Equivalent Radius a_{eq} of a Rectangle as a Function of the Ratio of Thickness t to width s	A77

CHAPTER I

INTRODUCTION

As man endeavors to delve further and further into the realm of the unknown, his problems become more and more complex. The invention of the electronic computer has greatly aided this quest for knowledge in that it enables problems that would have taken a lifetime using antiquated methods to be solved in a short length of time. Computing speed has gradually been increased in order to handle extremely complex problems in a reasonable length of time.

Of course there are many problems whose answers would be useless if not obtainable in a specified length of time. This type of problem dictates the realization of even faster computing speeds than are now available. Here lies the problem. Existing lumped constant systems are limited in their upper operating frequencies by the stray capacitance and inductance associated with them.

The logical question asked at this point then: "Why not use standard microwave techniques to build a computer?". The question is easily answered by two considerations: Size and cost. A simple example will serve to show how bulky even the simplest waveguide computer would be. Suppose a computer having a carrier

frequency of 3 kmc is made of 1000 logical elements, the logical elements being Magic T's. A rough calculation shows that the logical elements and their associated interconnections exclusive of power supplies, signal generators etc. would require a room of 1000 cubic feet (see Appendix 1). Considering the logical element to be made up of one Magic Tee and a small amount of flexible waveguide or coaxial cable as required by the logical configuration, the cost of 1,000 elements would be roughly \$160,000 plus the cost of connecting sections. These simple examples serve to show the inadvisability of attempting to build a computer out of waveguide.

Once a computer built of waveguide components has been ruled out, the reader will undoubtedly ask, "Why not build it out of some configuration of coaxial and multiple wire transmission line?".

In the first place, the author has never heard of logical elements made of coaxial or wire transmission lines. However, even assuming that such logical elements could be made, the bulk of the resulting computer would be prohibitive. Admittedly its cost would be considerably less than that of a microwave computer.

How then are we to build a computer operating at microwave frequencies? The answer lies in a new type of transmission line called strip transmission line. Two basic types of strip

transmission line exist; the so called "Microstrip", which consists of a strip conductor over a single ground plane, and the type consisting of a strip placed symmetrically between two ground planes. This latter type is variously termed as "Stripline", "Tri-Plate", balanced strip line, shielded strip line, etc. In this paper it will be referred to as "Stripline".

While both "Microstrip" and "Stripline" possess merit, the latter type is in more popular demand due to its lower loss and smaller stray coupling as compared to "Microstrip". These considerations indicate a greater versatility of application for "Stripline" and lead to the conclusion that for our purposes only "Stripline" need be considered. All analysis therefore, will be done in terms of the "Stripline" configuration. "Microstrip" will not be considered further. Figures 1-1 and 1-2 show the physical configurations of "Microstrip" and "Stripline" respectively.

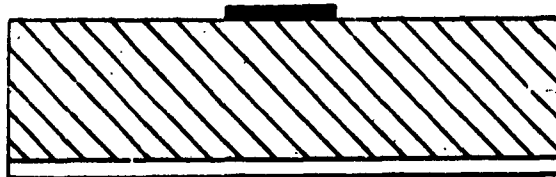


Fig 1-1 "Microstrip Cross Section"

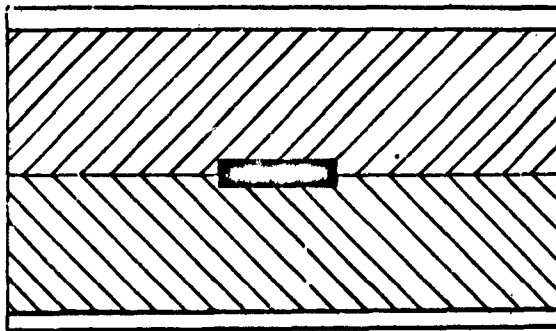


Fig 1-2 "Stripline Cross Section"

The explanation for the continuing interest in "Stripline" lies in its advantages over coaxial and waveguide construction, notably savings in production cost, in weight and volume and in time and expense in the development of new circuits.

However certain disadvantages exist also. The principal of these are: (1) an apparent unsuitability for long runs of line; (2) a higher attenuation, lower resonant Q and lower power capacity than waveguide (although the parameters are at least comparable to those of coaxial line); (3) a dependence upon dielectric materials for dimensional stability and strength and (4) a partial loss of constructional advantages in the case of circuits that cannot be reduced to planar form.

For many circuit applications these disadvantages are unimportant and are far outweighed by the advantages. Also each disadvantage can be minimized through careful design procedure.

The manufacture of "Stripline" is well suited to printed circuit techniques such as photo-etching of copper foil laminated on a dielectric surface. As such it bears all of the advantages of printed circuits, i.e. ease of reproducability, low cost and small size.

A comparison of a 1000 logical element computer made of waveguide and of "Stripline" is in order. The cost of our 1000 element "Stripline" computer would be in the neighborhood of \$4,700 plus connecting sections as opposed to \$160,000 plus connecting sections for waveguide (see Appendix 1). If the 1,000 logical elements in the waveguide example were made of "Stripline" the resulting volume would be only 1.95 cu. ft. as compared to 1,000 cu. ft. for waveguide.

Logical elements are realized by printing hybrid rings and using them to perform the logical functions. To realize a given logical configuration then, say an adder, we would (1) draw the circuits; (2) make a drawing and photograph it to get a negative; (3) reduce the negative to the required size; (4) print two double clad boards on one side and (5) attach connectors and bolt the boards together with their printed sides facing each other.

The previous paragraphs have shown that "Stripline" could indeed be used to construct a practical computer operating at microwave frequencies. The following chapters of this report will therefore concern themselves with the

basic characteristics of "Stripline" such as characteristic impedance, attenuation, transient response, etc. in order that we may exploit "Stripline" to build an operating device. A second report will be written describing the logical design of a toy computer.

CHAPTER II

DETERMINATION OF STRIPLINE CHARACTERISTIC IMPEDANCE

A. History.

Close examination of the literature discloses that several articles concerning strip transmission lines have been written. In the opinion of the author the article done by Oliner² is by far the best. As a result the past history of Characteristic Impedance analysis as done in this paper is essentially that of Oliner.

Most of the people engaged in theoretical work on symmetric strip lines have in one way or another been concerned with the determination of suitable expressions for its Characteristic Impedance. While it is almost impossible to include the contributions of everyone involved, the discussion below is felt to be fairly inclusive and typical of the different methods of approach that have been used. The earlier efforts on this topic dealt with expressions for zero-thickness center strips while the later investigations were concerned with strips of finite thickness.

Since the dominant mode in symmetrical strip line is a TEM mode, the field distribution in the transverse plane is a static one, and the Characteristic Impedance follows directly from the knowledge of the static capacity of the line. This point was recognized by all investigators.

For zero-thickness center strips, pioneer work was conducted by Barrett³ for the low impedance range, which corresponds to lines for which the strip width is greater than one-half the ground plane spacing. He considered the line cross-section to be made up of a parallel-plate region in the center and fringing capacities at the sides, and on this basis derived a simple and useful expression. At the time he was unaware of a rigorous solution for zero-thickness strips by Oberhettinger and Magnus,⁴ which is based on a conformal mapping and is valid for any ratio of strip width to ground plane spacing. Hayt⁵ has more recently considered the effect of finite width ground planes. He obtained a rigorous solution via conformal mapping procedures for ground planes of finite width in which the center strip and the ground planes are all of zero-thickness, and he concluded that for the line dimensions employed in practice the assumption of infinite width ground planes introduces negligible error.

A variety of approximate expressions has been obtained for lines with center strips of finite thickness. The first of these expressions, historically, was deduced by Begovich,⁶

who followed the lead of Barrett³ but employed the fringing capacity appropriate to a strip of finite thickness. While such a procedure would yield an expression suitable for the low impedance range, his result is of questionable value because the fringing capacity employed was given in a very slowly convergent form. The next contribution along these lines was due to Cohn⁷ and Oliner,^{8,9} working independently but arriving at identical results. These results apply separately to the low impedance and the high impedance ranges, and very satisfactorily overlap in the intermediate region (strip width to ground plane spacing ratio approximately equal to 0.35). The expression for the low impedance range is that of Begovich,⁶ except for the use of a fringing capacity which is exact and explicit. The expression for the high impedance range was based upon a far field equivalence between a rectangular and circular cylinder. These points are elaborated upon somewhat below.

Approximate expressions for lines of finite thickness center strips were also derived by Pease,¹⁰ following a suggestion of Wheeler. Their results yield rigorous upper and lower bounds for Characteristic Impedance, and an approximate expression which lies between these bounds. The results are best applicable to the low impedance range.

Pease and Mingins¹¹ have also derived a "universal" expression which is a composite of simpler ones applicable only to

special ranges of line dimensions. Their composite expression yields the Characteristic Impedance to a high degree of accuracy, and is valid for a center conductor of arbitrary, but rectangular, aspect ratio. Skiles and Higgins¹² have also developed an approximate procedure for the case of arbitrary but rectangular aspect ratio; their method is capable of arbitrarily high accuracy if the procedure is carried out far enough.

Several rigorous solutions have also been derived for lines with center conductors of finite thickness. An expression due to Greenhill¹³ has long been in the literature, but it is in implicit form and is not amenable to calculation. Begovich¹⁴ has derived a rigorous result which is expressible as the sum of a parallel plate term, a fringing capacity term, and correction terms. He proceeded by breaking up the cross-section into elementary regions, solving Laplace's equation in each region separately, and then matching the solutions across the respective boundaries. The infinite set of equations obtained thereby was then solved and the solution cast into the above-mentioned form. A rigorous solution, obtained via conformal mapping procedures, has also been derived by Snow.¹⁵ Although his result is in implicit form, numerical results may readily be obtained from it. His result has not been published, however, but remains in his unpublished notes. A recent solution, due to Bates,¹⁶

has also been derived by conformal mapping methods. It is also in implicit form, and readily yields numerical results.

B. Recommended Approach.

In the opinion of the writer, the solutions of Cohn serve as the most practical expressions available for the Characteristic Impedance of lines with center conductors of finite thickness, since the expressions are simple in form and are rather accurate (about 2% at worst). In addition, Cohn's published curves⁷ are in very useful form. In order that the reader may understand Cohn's derivation, it is included in this paper. Cohn's derivation is divided into two parts, namely (1) the low impedance range and (2) the high impedance range. Each case will be discussed in general terms in the text in order to satisfy the casual reader. If rigor is desired, the complete mathematical analysis will be found in the Appendices. An Appendix containing an abbreviated discussion of Theory of A Complex Variable is included for the reader who may need a short review of complex variable theory before attempting to understand the Characteristic Impedance derivation.

C. Derivation of Characteristic Impedance in the Low Range.

The treatment of the low impedance range parallels that of Barrett³ and Begovich⁶, and proceeds as shown in Fig 2-1. The actual line cross-section of Fig 2-1a is regarded as composed of a central parallel plate region with fringing capacity at

the sides. A knowledge of this fringing capacity permits the construction of the equivalent structure of Fig 2-1b, which is a parallel plate line of width D. The expression for D in terms of the parameters of the line of Fig 2-1a is given in Appendix IV.

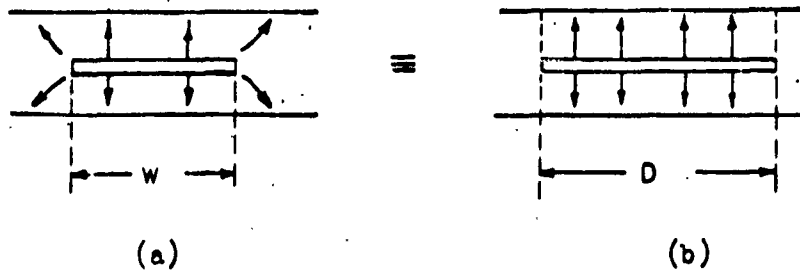


Fig 2-1 Treatment of the low Z_0 Range

The general development procedure has been described in the above paragraph. Let us now consider it in some detail.

Stripline, like coaxial and transmission line operates in the TEM mode. This mode is characterized by the property that the electromagnetic waves contain neither electric nor magnetic fields in the direction of propagation. Since electric and magnetic field lines both lie entirely in the transverse plane, these may be called transverse electromagnetic waves (abbreviated TEM).

The above explanation of the TEM mode of propagation will probably satisfy the casual reader but if more rigor

is desired Appendix II may be consulted. This Appendix contains a mathematical derivation of the TEM mode beginning with such basic relations as the circuital law of magnetism and Faraday's law and concludes with Laplace's equation. Since Laplace's equation has a static solution, we may conclude that the TEM mode is exactly a static distribution and analyze it as such. The equations for Characteristic Impedance, velocity of propagation etc. are therefore the same as these for any standard transmission line. The well known expression for Characteristic Impedance in Transmission line theory is:

$$Z_0 = \sqrt{L/C} \quad (2-1)$$

Where:

L equals inductance/unit length

and

C equals capacitance per unit length

The velocity of propagation of the principal mode is given by

$$v = \frac{1}{\sqrt{LC}} \quad (2-2)$$

Solving (2-1) and (2-2) simultaneously

$$Z_0 = \frac{1}{vC} \quad (2-3)$$

but $v = \frac{c\sqrt{\mu\epsilon_0}}{\sqrt{\mu\epsilon}} = \frac{c}{\sqrt{\epsilon_r}}$ (2-4)

where: μ = magnetic permeability (Equals 1 for air and most dielectrics).

ϵ = permittivity of the medium.

v = velocity in the medium with properties μ and ϵ

and

c = the velocity of light

$$= 3 \times 10^8 \text{ meters/sec}$$

therefore:

$$Z_0 = \frac{\sqrt{\epsilon_r}}{3 \times 10^8} \quad (2-5)$$

To find Z_0 we must now develop an expression for C .

Knowing this quantity we can also find attenuation and power handling capabilities as will be seen later.

In the finding of the correct value of capacitance to use in formula (2-5), it will be necessary to perform a Schwarz-Christoffel mapping in the complex plane. Such a mapping requires a knowledge of Theory of a Complex Variable for an understanding of the procedure. A short review of complex variable theory and the theory of the Schwartz-Christoffel transformation is included as Appendix III. Such a review should be sufficient for the reader already somewhat familiar with this theory. The reader who is not familiar with complex variables is referred to the many excellent texts on the subject, of which Churchill,¹⁷ Ahlfors,¹⁸ or Guillemin,¹⁹ are best in the author's opinion.

Consider the cross-section of Stripline as shown in Fig 2-2 .

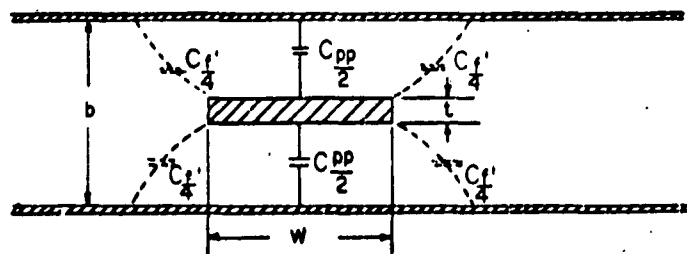


Fig 2-2 Cross Section of "Stripline" used for Capacitance Calculations

As can be seen by inspection, the capacity of the Stripline configuration is essentially that of two parallel plate capacitors connected in parallel plus a correction for fringing capacitance C_f' . The parallel plate capacitance for Stripline is derived in Appendix IV. The result may be used to compute Characteristic Impedance up to 25 ohms and is:

$$C_{pp} = 4 \times 10^{14} \left(\frac{8.842 \epsilon_r w}{b-t} \right) \quad (2-6)$$

where

w = Center conductor strip width-cm

b = Ground plane spacing - cm

t = Plate Thickness - cm

ϵ_r = Dielectric Constant

C_{pp} = Parallel Plate Capacitance - f/cm

Above 25 ohms we must add a term for fringing capacitance to C_{pp} . The total capacitance per unit length of line is then:

$$C_{tp} = C_{pp} + C_f' \quad (2-7)$$

where

$$C_f' = f(w, \frac{t}{b}) \quad (\text{Fringing field capacitance in f/cm})$$

C_{tp} = Total capacitance per unit length of line

Equation (2-6) then becomes:

$$C_{tp} = 4 \times 10^{-14} \left(\frac{8.842 \epsilon_r w}{b-t} + C_f' \right) \quad (2-8)$$

Inserting the results of equation (2-8) into equation (2-3) there is obtained:

$$Z_0 = \frac{94.15}{\sqrt{\epsilon_r} \left(\frac{w/b}{1-t/b} + 0.0885 \epsilon_r \right)} \quad (2-9)$$

Equation (2-9) is precisely Cohn's result and is in a convenient working form.

Before equation (2-9) is of any use to us, we must find an expression for the fringing capacitance C_f' . This required expression is obtained through the use of a Schwarz-Christoffel mapping in the complex plane. The essential procedure is described in the introduction to this section i.e. finding an equivalent stripline structure which takes into account fringing capacitance and can therefore be treated as an ideal parallel plate capacitor. The author has performed this mapping to check the results given in the literature.

The results check those given by Cohn and can be conveniently expressed in working form as:

$$C_f' = \frac{0.0885 \epsilon_r}{\pi} \left(\left(\frac{2}{1-t/b} \right) \ln \left(\frac{1}{1-t/b} + 1 \right) - \left(\frac{1}{1-t/b} - 1 \right) \ln \left(\frac{1}{(1-t/b)^2} - 1 \right) \right) \text{ mmf/cm} \quad (2-10)$$

D. Determination of Characteristic Impedance in the High Range.

In the high impedance range, the strip width is small compared to the ground plane spacing, as shown in Fig 2-3a, and the approximation employed assumes that the ground planes are far away from the center strip. As a result, one can employ a far field equivalence between the actual rectangular center conductor and a circular or a zero-thickness strip center conductor, as indicated in Fig 2-3b. The insertion of this equivalence into the known expressions for the Characteristic Impedance of a round conductor between ground planes, or a stripline with a zero-thickness center conductor, yields expressions simple in form for the high impedance range. While only the equivalence to a round conductor is employed in Cohn's curves,⁷ the equivalence to a zero-thickness strip⁸ yields a result of high accuracy for very thin center strips. It has also been recognized by Pease²² that the Characteristic Impedance in the high range of the line possessing a rectangular center conductor lies between that

of the lines with a flat center strip placed horizontally and that with a similar strip placed vertically. The situation is illustrated by Fig 2-3c. Since the Characteristic Impedances Z'_0 and Z''_0 of Fig 2-3c are known, this recognition makes available upper and lower bounds on the result of interest.

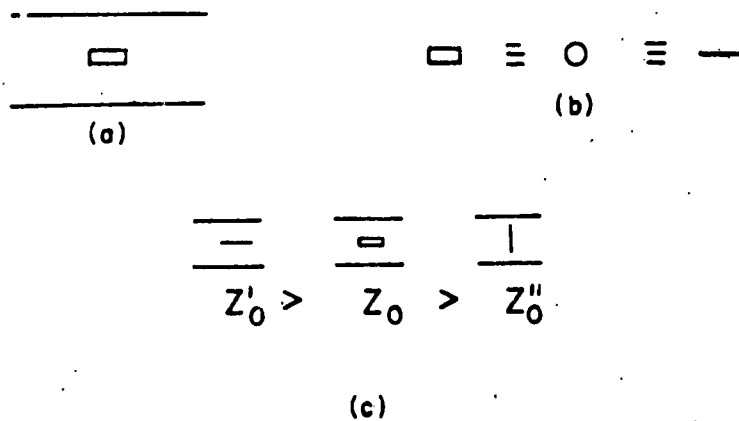


Fig 2-3 Treatment of the high Z_0 range

Examination of the literature shows Cohn's results to be the most widely accepted. As a result, the derivation given here will be essentially that of Cohn.

The Characteristic Impedance of a transmission line consisting of a circular conductor of diameter d_0 centered between two parallel ground planes is well known. It was derived by Frankel²³ in 1943 and as it has stood the test of time, its derivation will not be included here; only the result will be stated. It is:

$$Z_0 = \frac{60}{\sqrt{\epsilon_r}} \ln \frac{4b}{\pi d_0} \text{ ohms} \quad (2-11)$$

where the parameters are as shown in Fig 2-4a. Fig 2-4b is the familiar cross section of "Stripline" which is repeated here for convenience. As shown in Fig 2-3 and discussed in the beginning of this section, if "d_o" is



Fig 2-4 Center Conductors of Small Cross Section Yielding Equivalent Characteristic Impedance

small compared to "b", we can find an equivalence between round and rectangular cross sections via the Schwarz-Christoffel Transformation and then use equation (2-11). This mapping between rectangular and circular cross section has been performed by Flammer²⁴ and is included as Appendix V. The results are given in graphical form and are shown as Fig 2-5. When Fig 2-5 is used in conjunction with equation

(2-11), the accuracy increases as $d_o \rightarrow 0$. However comparison with a more precise analysis by Wholey and Eldred²⁵ shows equation (2-11) to be accurate to within one per cent for d_o as large as $b/2$.

E. Comparison with an Exact Case.

The accuracy of equation (2-9) and (2-11) may be tested by comparing them to an exact solution given by Oberhettinger and Magnus⁴ which is valid for $t = 0$. Their result is

$$z_o = \frac{30 \pi K(k)}{K(k')} \quad (2-12)$$

where $K(k)$ and $K(k')$ are complete elliptic integrals of the first kind and where

$$k = \operatorname{sech} \frac{\pi w}{2b}$$

$$k' = \tanh \frac{\pi w}{2b}$$

Fig 2-6 shows a comparison of equations (2-9), (2-11) and (2-12). The maximum error occurs at $w/b = 0.35$ where (2-9) and (2-11) intersect and is only 1.2 per cent. At $w/b = 0.2$ and 0.5, the error is reduced to 0.4 per cent while for lesser and greater w/b , the error rapidly approaches zero.

Similar plots of (2-9) and (2-11) have been made for strips having t/b up to 0.25, and in all cases, the curves tend to merge together at least as well as in Fig 2-6.

As one would expect from a consideration of fringing-field interaction, the intersection of the curves remains very near the same value of $w/(b-t) = 0.35$. A study of flux plots for $t = 0$ and $t > 0$ leads one to believe that the error at the intersection point will be no greater in the latter case than in the former, and very likely will be smaller. Hence the proper use of (2-9) and (2-11) in their assigned parameter ranges is believed to result in an error of no more than 1.2 per cent near $w/(b-t) = 0.35$, and considerably less at other values of $w/(b-t)$.

F. Graphical Presentation of Z_0 .

In Fig 2-7, a family of Z_0 curves are plotted versus w/b with t/b as parameter. The curve for $t/b = 0$ is exact, the points having been computed from (2-12). The other curves are computed from (2-9) and (2-11). Equation (2-9) was used for $w/(b-t) > 0.35$ and (2-11) for $w/(b-t) < 0.35$. It is seen that the effect of thickness on the characteristic impedance is substantial, even for thicknesses only a few per cent of the plate spacing.

G. Conclusions.

Two simple formulas and auxiliary curves are presented for the characteristic impedance of the shielded stripline. By means of these formulas, accuracy sufficient for any engineering purpose is obtainable for all strip widths and for thicknesses up to at least a quarter of the plate spacing. Fig 2-7 displays the characteristic impedance in a form that should be particularly useful to the design engineer.

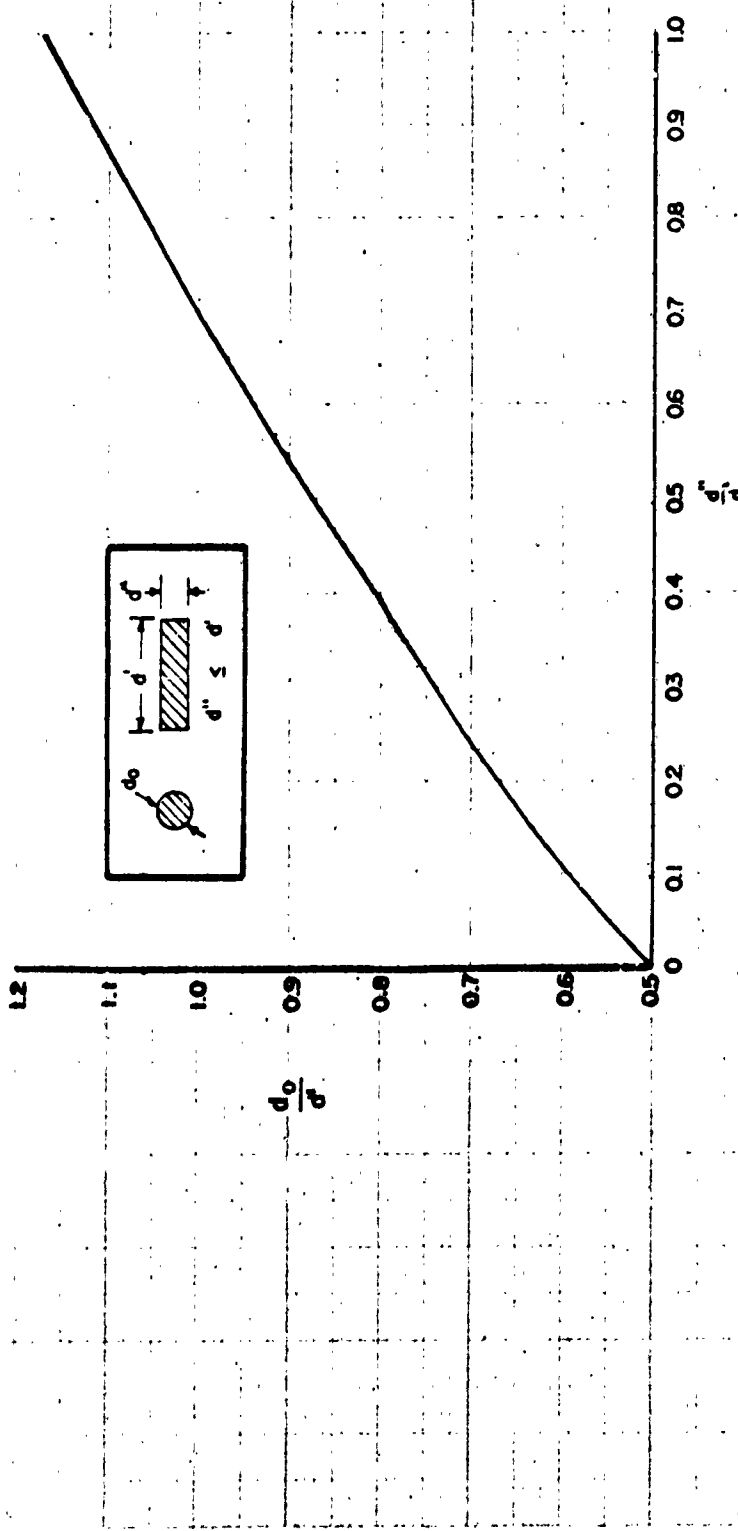


Fig. 2-5 EQUIVALENCE BETWEEN A RECTANGULAR AND CIRCULAR CROSS SECTION

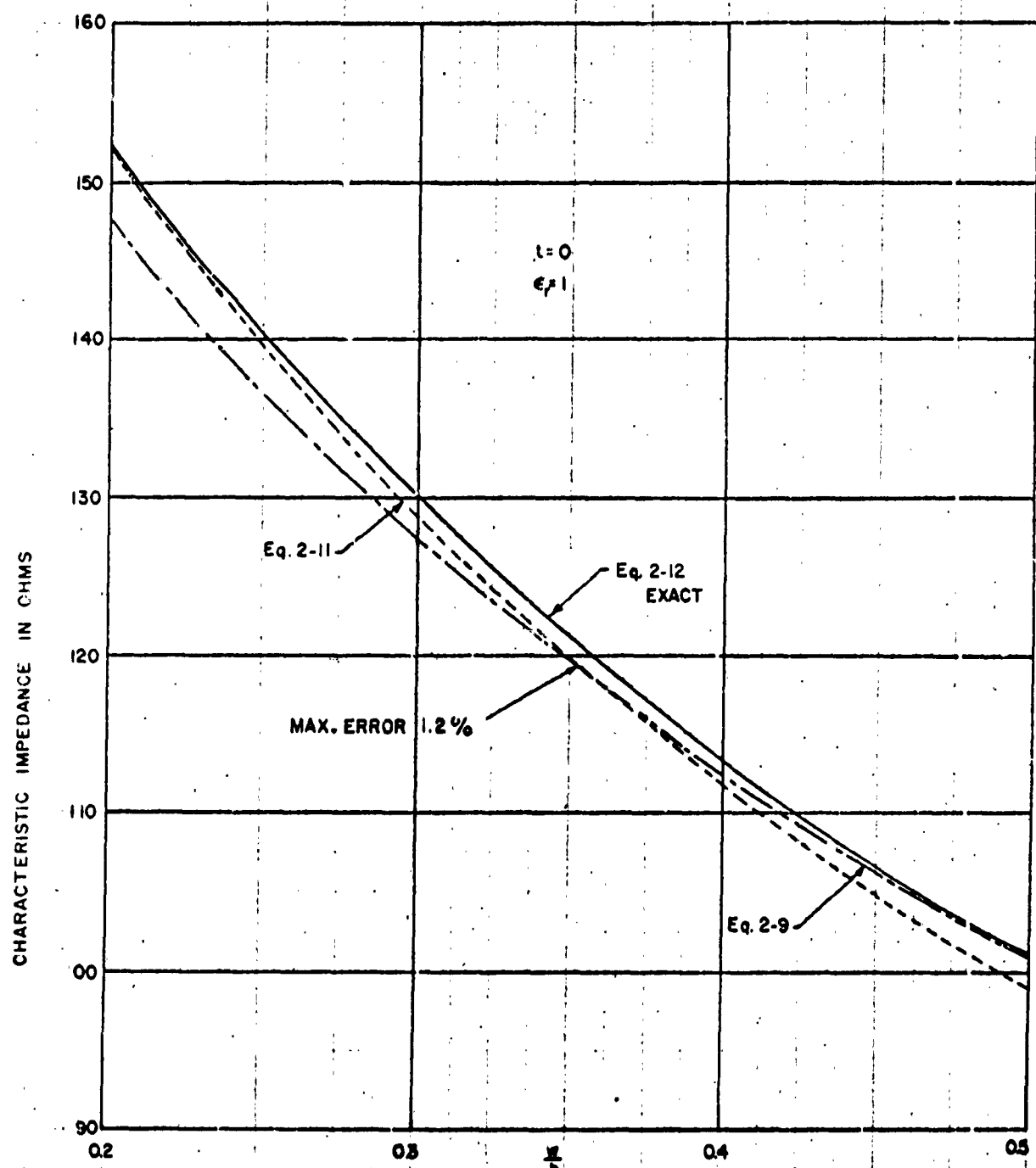


Fig. 2-6 COMPARISON OF THE TWO APPROXIMATE FORMULAS WITH THE EXACT FORMULA FOR $L=0$.

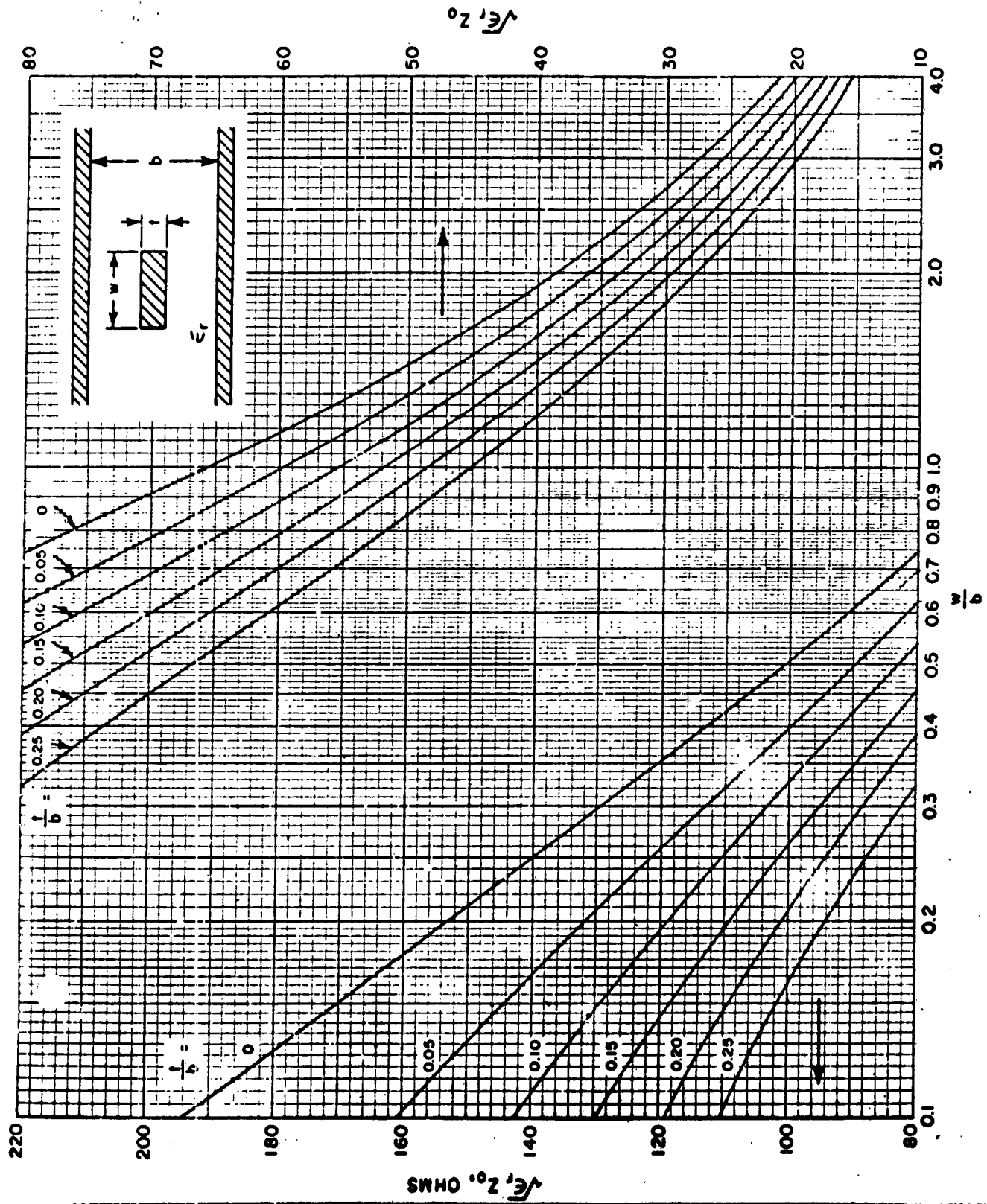


FIG 2-7 Graph of Z_0 versus V_E/Z_0 for various values of w/b .

H. Characteristic Impedance Measurement.

1. Theory.

Much time has been spent in the theoretical development of expressions for the Characteristic Impedance of Stripline. This investigation resulted in two equations. The first applies when the condition $\frac{w}{b-t} > 0.35$ is met and is

$$Z_0 = \frac{94.15}{\sqrt{\epsilon_r} \left(\frac{w/b}{1-t/b} + \frac{cr'}{0.0885 \epsilon_r} \right)} \text{ ohms} \quad (2-9)$$

The second equation applies when $\frac{w}{b-t} < 0.35$ and was given as

$$Z_0 = \frac{60}{\sqrt{\epsilon_r}} \ln \frac{4b}{\pi d_0} \text{ ohms} \quad (2-11)$$

Let us examine equations (2-9) and (2-11) to see how Characteristic Impedance may be measured in order to determine the validity of the theoretical development. We see that if samples of Stripline were built using two double clad boards, the thickness of the center strip (t) and the distance between ground planes (b) would be fixed, as would the dielectric constant and the fringing capacitances (assuming the ground plane is at least eight times wider than the center strip). The only variable is then the strip width (w).

2. Hardware.

In line with this reasoning, a number of Stripline samples were built having various strip widths. The boards were double clad with two ounce copper having an average thickness of 2.7 mils. Since two of these boards are placed back-to-back, the thickness of the center strip was 5.4 mils. The dielectric material goes under the trade name of "Dilectro" or "GB 112 T" and was made by Continental Diamond Fiber Co. It has a dielectric constant of 2.73 and has an average thickness of 57 mils. Consideration of the cross section of Stripline then shows that the distance between ground planes is 119 mils. The strip width (w) was determined by using the average of five readings made through the use of a measuring device accurate to 0.1 mil. The C_f' term is a function only of t and b and can be determined from the results of Appendix IV (i.e. Fig A4-7). Thus all the parameters in equation (2-9) are known. In equation (2-11), the quantity d_o must be determined. Knowing w and t and using Fig 2-5, d_o is easily found. The resulting Characteristic Impedances for the various strip widths as calculated from equation (2-9) and (2-11) are shown in the second column of Table 2-1 and as the broken line on Fig 2-9.

3. Measurement Technique.

We now know what that Characteristic Impedance of the stripline samples should be. The question now is, "How do we measure it?" Consider equation (2-5) which was

$$Z_0 = \frac{\sqrt{\epsilon_r}}{3 \times 10^8 C} \quad (2-5)$$

Equation (2-5) has two unknowns, $\sqrt{\epsilon_r}$ and the capacitance C. The dielectric constant is given in most handbooks and for GB 11. T is 2.73. Since the initial uses of stripline will be at 3 Mc, it would be desirable to make Characteristic Impedance measurements at that frequency. However, to the authors' knowledge, the best RF bridges have a cut off frequency of 100 mc. It was therefore desirable to make the measurements at a relatively low frequency and extrapolate the answer to 3 kmc. Discussions between the author and the Bureau of Standards indicated that the dielectric constant is unchanged at frequencies below 20 kmc and perhaps 30 kmc.* Two bridges were obtained; a Model B 801 Wayne Kerr V.H.F. Admittance Bridge usable in the frequency range 1 to 100 megacycles and a Model B 601 R. F. Impedance Bridge usable in the frequency range 15 kilocycles to 5 megacycles. The Model B 801 Bridge had an accuracy of ± 2 per cent $\pm 0.5 \mu\mu f$ while the Model B 601 has an accuracy of ± 1 per cent.

* There seems to be some disagreement on this point (see Wild et al "Handbook of Triplate Microwave Components", Sanders Associates Inc., 1956, page 134).

Measurements were made on various components in the overlapping frequency range. Agreement was found to be good. Further experiment with the Model B 801 showed it to be inaccurate at frequencies above 50 megacycles. Since the Model B 801 has a finer vernier scale, it was decided to use it at a frequency of 5 megacycles and check the results with the Model E 601.

4. Source of Error.

Several difficulties were encountered. For the lengths of stripline used, narrow strip widths resulted in low values of capacitances as can be seen by reference to column five of Table 2-1. Since the accuracy of the Model B 801 is \pm 2 percent \pm 0.5 $\mu\mu f$ and the null was not determinable to more than \pm 1 $\mu\mu f$, it can be seen that the reading could be 1.5 $\mu\mu f$ off quite easily. For large values of capacitance (wide strips), this error is small, but it becomes significant for narrow strip width and is believed to account for at least a part of the deviation between theoretical and measured values of Characteristic Impedance. Other sources of error arise from the fact that averages were used for t, b, w and the dielectric constant ϵ_r .

5. Step-by-Step Measurement Procedure.

This test set up is shown in Fig 2-8.

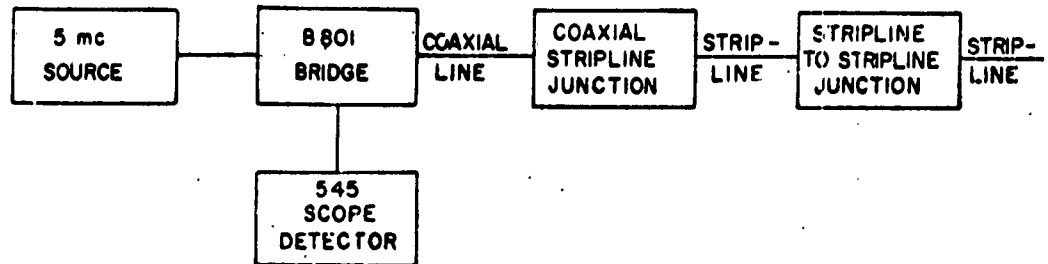


Fig 2-8 Test Set Up for Measurement of Stripline Capacity

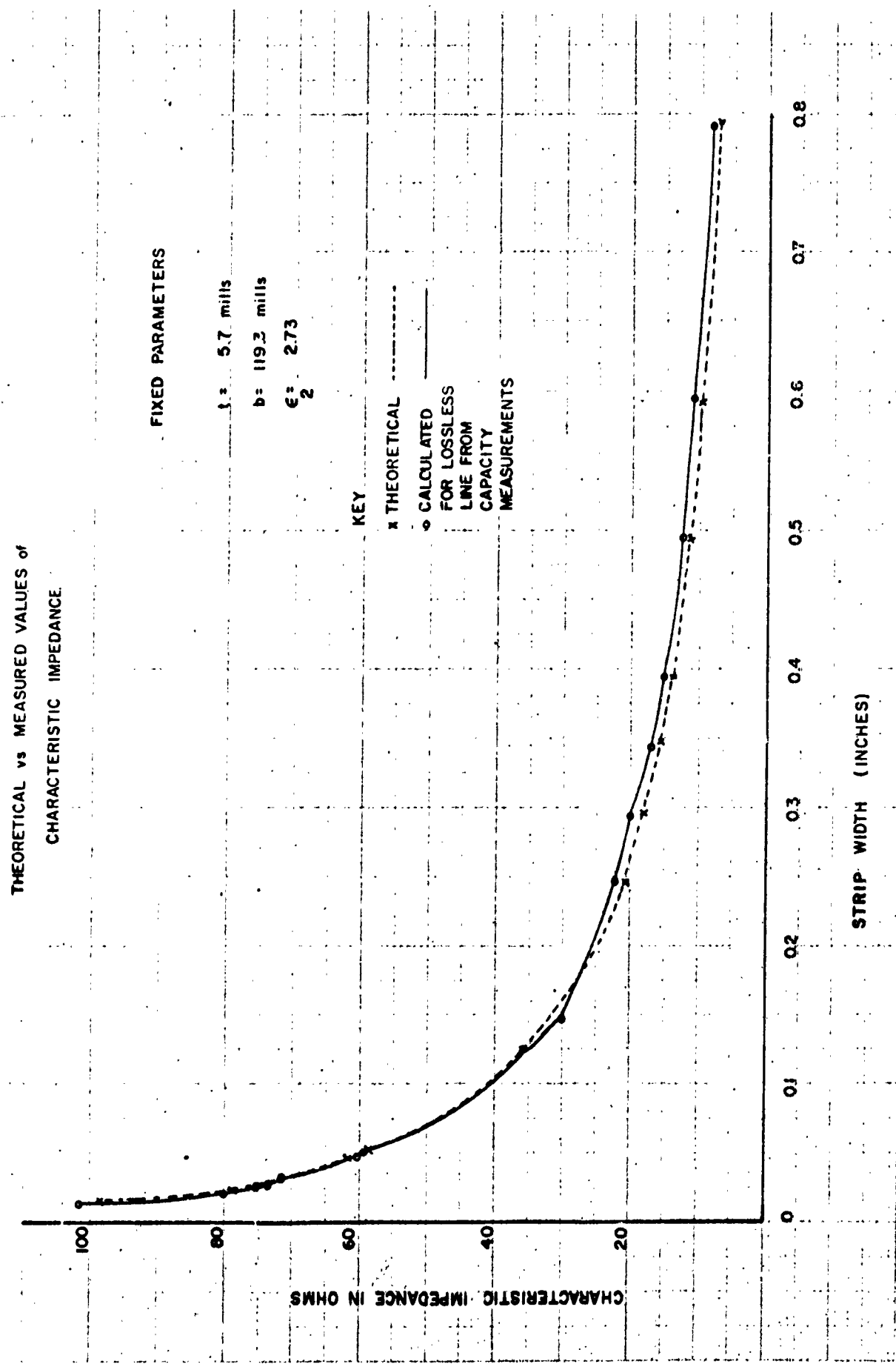
The oscillator and oscilloscope were allowed to warm up. The bridge was then balanced with no load attached. The short piece of coaxial cable and the coaxial cable to Stripline junction having a short section of Stripline attached were then attached to the bridge and a measurement made. Finally the length of Stripline to be measured was attached and a measurement made. The difference between the two measurements was the capacity of the section of Stripline. Knowing the length of the measured section, the per unit capacitance was obtained. The Characteristic Impedance was then calculated through the use of equation (2-5). The results are expressed in tabular form as Table 2-1 and in graphical form as Fig 2-9.

TABLE 2-1

MEASUREMENT OF STRIPLINE CHARACTERISTIC IMPEDANCE

STRIP WIDTH (INCHES)	CALCULATED CHARACTERISTIC IMPEDANCE (OHMS)	CALCULATED CAPACITANCE per UNIT LENGTH $\mu\text{uf}/\text{cm}$	MEASURED CAPACITANCE per UNIT LENGTH $\mu\text{uf}/\text{cm}$	MEASURED CHARACTERISTIC IMPEDANCE (ohms)
0.0121	98.5	0.553	0.558	101.5
0.0228	79.4	0.693	0.698	79.8
0.0279	74.5	0.734	0.744	75.0
0.0293	73.5	0.749	0.743	74.4
0.0365	71.0	0.776	0.772	71.0
0.0456	62.1	0.885	0.900	61.0
0.0471	61.2	0.902	0.878	62.7
0.0516	58.6	0.938	0.932	60.0
0.1204	36.2	1.50	1.51	36.2
0.1441	30.0	1.71	1.78	30.9
0.1462	31.7	1.74	1.88	29.2
0.2453	20.9	2.64	2.47	22.4
0.2947	18.4	2.94	2.74	20.1
0.3468	16.0	3.41	3.25	17.0
0.3974	14.5	3.76	3.69	14.9
0.4955	11.7	4.71	4.54	12.1
0.5976	9.9	5.54	5.39	10.2
0.7954	7.6	6.34	6.76	8.1

Fig.2-9
THEORETICAL vs MEASURED VALUES of
CHARACTERISTIC IMPEDANCE



BIBLIOGRAPHY

1. W. E. Fromm, "Characteristics and some Applications of Stripline Components", IRE Transactions, MTT 3, No. 2, March 1955, pp 13-20.
2. A. A. Oliner, "Theoretical Developments in Symmetrical Strip Transmission Lines", Proceedings of the Symposium on Modern Advances in Microwave Techniques, pp 380-383, Ann Arbor Michigan, Edwards Brothers Inc., 1955.
3. R. L. Barrett and M. H. Barnes, "Etched Sheets Serve as Microwave Components", Electronics, Vol 25, pp 114-118, June 1952.
4. F. Oberhettinger and W. Magnus, "Anwendung der Elliptische Funktionen in Physik und Technik", J. Springer, Berlin, Germany, pp 63-65, 1949.
5. W. H. Hayt, Jr., "A Study of Radiation and Mutual Impedance Problems in Strip Transmission Lines", Ph.D. Thesis, University of Illinois, Part V, 1954.
6. N. A. Begovich and A. R. Margolin, "Theoretical and Experimental Study of a Strip Transmission Line", Hughes Aircraft Company Report TM No. 234, May 1950.
7. S. B. Cohn, "Characteristic Impedance of the Shielded-Strip Transmission Line", Trans. I.R.E., Vol MTP-2, pp. 52-57, July 1954.
8. A. A. Oliner, "The Effect of Thickness on the Characteristic Impedance of Strip Transmission Lines", memorandum to L. C. Van Atta, Hughes Aircraft Company, July 31, 1953.
9. A. A. Oliner, "private communication to W. E. Fromm", Airborne Instruments Laboratory, Feb 17, 1954.
10. R. L. Pease, "Characteristic Impedance of Strip Transmission Lines with Rectangular Inner Conductors in the Low Impedance Region", Interim Report No. 2 on Contract No. AF 19(604)-575 Tufts College, Jan 12, 1954.
11. R. L. Pease and C. R. Mingins, "A Universal Approximate Formula for Characteristic Impedance of Strip Transmission Lines with Rectangular Inner Conductors", Symposium on Microwave Strip Circuits.

12. J. J. Skiles and R. J. Higgins, "Determination of the Characteristic Impedance of UHF Coaxial Rectangular Transmission Lines, National Electronics Conference, Chicago, Illinois, Oct 4, 1954.
13. Sir G. Greenhill, "Report on the Theory of a Stream Line Past a Plane Barrier and of the Discontinuity Arising at the Edge with an Application of the Theory to an Aeroplane," Advisory Committee for Aeronautics, Reports and Memoranda, No. 19, pp 86-92, 1910.
14. N. A. Begovich, "Characteristic Impedance of Strip Transmission Lines," Symposium on Microwave Strip Circuits.
15. C. Snow, unpublished notes.
16. R. H. T. Bates, "The Characteristic Impedance of the Shielded Slab Line, paper submitted to the I.R.E.
17. R. V. Churchill, "Introduction to Complex Variables and Applications," 1948, New York, McGraw Hill Book Co.
18. L. V. Ahlfors, "Complex Analysis," 1953, New York, McGraw Hill Book Co., Inc.
19. E. A. Guillemin, "The Mathematics of Circuit Analysis," Chapter VI, 1949, New York, John Wiley and Sons, Inc.
20. Ware and Reed, "Communications Circuits," pp 370-374, 1955, New York, John Wiley and Sons, Inc.
21. H. H. Skilling, "Fundamentals of Electric Waves," pp 38-40, 1948, New York, John Wiley and Sons, Inc.
22. R. L. Pease, "Characteristic Impedance of Strip Transmission Lines with Rectangular Inner conductors in the High Impedance Region," Interim Report No. 5 on Contract No. AF 19(604)-575, Tufts College, May 10, 1954.
23. S. Frankel, "Characteristic Functions of Transmission Lines," Communications, pp 32-35, March 1943.
24. C. Flammer, "Equivalent Radii of Thin Cylindrical Antennas with Arbitrary Cross Sections," Stanford Research Institute of Technology Report, March 1950.
25. W. B. Wholey and W. M. Eldred, "A New Type of Slotted Line Section," Proc. I.R.E., Vol 38, pp 244-248, March 1950.

26. Dwight, "Tables of Integrals and other Mathematical Data", McMillan Co., New York.

APPENDIX I

SIZE AND COST CALCULATIONS FOR A 1000 LOGICAL ELEMENT COMPUTER

A. Waveguide Construction.

1. Size

Logical operations in waveguide may be performed through the use of a Magic Tee. The dimensions of a commercially available 3 kmc Magic Tee are shown in Fig Al-1.

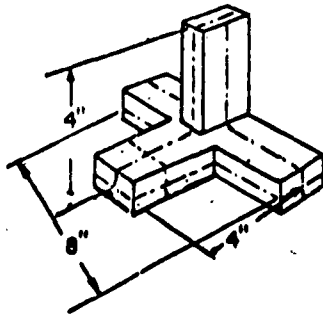


Fig Al-1 A 3 kmc Magic Tee

To allow for terminations and space occupied by interconnecting cables, assume each Magic Tee occupies 1 cu. ft. One Thousand Magic Tee's would therefore occupy 1000 cu. ft.

APPENDIX I

SIZE AND COST CALCULATIONS FOR A 1000 LOGICAL ELEMENT COMPUTER

A. Waveguide Construction.

1. Size

Logical operations in waveguide may be performed through the use of a Magic Tee. The dimensions of a commercially available 3 kmc Magic Tee are shown in Fig Al-1.

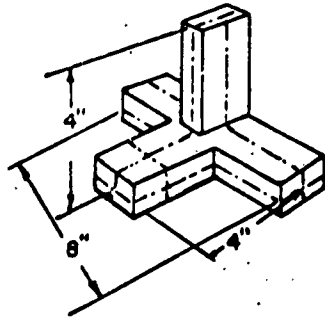


Fig Al-1 A 3 kmc Magic Tee

To allow for terminations and space occupied by interconnecting cables, assume each Magic Tee occupies 1 cu. ft. One Thousand Magic Tee's would therefore occupy 1000 cu. ft.

2. Cost

The catalog retail price of a 3 kmc Magic Tee is \$160. The cost of 1000 Magic Tee's would therefore be \$160,000.

B. Stripline Construction.

1. Size

Logical operations in Stripline may be performed through the use of Hybrid Rings. The theory of the Hybrid Ring dictates that its minimum circumference be $1.5 \lambda_g$ where λ_g is the wavelength in Stripline. The configuration of a Hybrid Ring is shown as Fig Al-2.

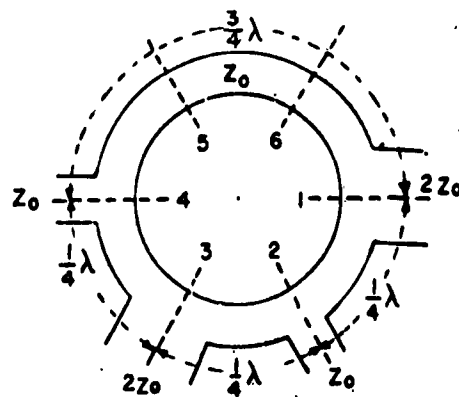


Fig Al-2 Configuration of a Hybrid Ring

The free space wavelength at 3 kmc may be found from the relation

$$\lambda = \frac{3 \times 10^8}{3 \times 10^9} = 10 \text{ cm} \quad (\text{Al-1})$$

Stripline wavelength is related to free space wavelength by:

$$\lambda_t = \frac{\lambda}{\sqrt{\epsilon_r}} \quad (\text{Al-2})$$

where ϵ_r is the relative permittivity of the dielectric.

Present day Stripline has a Glass Teflon dielectric whose relative permittivity is 2.82. The wavelength in Stripline is then:

$$\lambda_t = \frac{\lambda}{\sqrt{\epsilon_r}} = \frac{10 \text{ cm}}{\sqrt{2.82}} = 5.95 \text{ cm}$$

The circumference of the Hybrid Ring is then:

$$C = 1.5 \lambda = 1.5 \times 5.95 = 8.93 \text{ cm} \quad (\text{Al-3})$$

This circumference corresponds to a diameter of

$$D = \frac{C}{\pi} = \frac{8.93 \text{ cm}}{\pi} \approx 2.84 \text{ cm} = 1.12 \text{ in} \quad (\text{Al-4})$$

This stray coupling between rings must be considered next. It has been noted in literature that "separation by approximately the ground plane spacing is sufficient to achieve negligible coupling between adjacent lines."¹ Application of this statement to a ground plane spacing of 1/8 inch leads to the conclusion that the adjacent Hybrid Ring should be at least 1/4 inch apart. For our approximation let each Hybrid Ring be centered on a square of Stripline 1 1/2 inches in a side. Now suppose the 1000 logical element computer is

constructed of 100 sheets of Stripline with 10 Hybrid Rings per sheet. Each sheet will be 15 inches on a side and 1/8 inch thick. A stack of 100 sheets would therefore occupy about 2 cu. ft.

2. Cost.

The cost of producing a 1000 logical element Stripline computer can be broken down as follows:

200 Double Clad Teflon Fiberglass boards	\$4,000.00
Developer, Sensitizer, and Laquer	\$ 100.00
Labor, Art Work and negative	\$ 500.00
Drilling and shearing	<u>\$1,000.00</u>
	\$4,700.00

It must be remembered that Stripline consists of two Double Clad boards sandwiched together. Therefore 200 double clad boards are required for 100 Stripline components.

APPENDIX II

A DISCUSSION OF THE TEM MODE

A. Maxwell's First Law.²⁰

The first set of equations is based on the circuital law of magnetism which in equation form and in rationalized units is:

$$\oint \mathbf{H} \cdot d\mathbf{l} = I \quad (\text{A2-1})$$

where \mathbf{H} is the magnetic field intensity in amperes per meter and l is the displacement or distance along the closed path which encircles the current. In this derivation, the current I is expressed in amperes and is equal to the sum of conduction and displacement currents, and the displacement l is expressed in meters. (It is understood that in general \mathbf{H} is a function of both time and space).

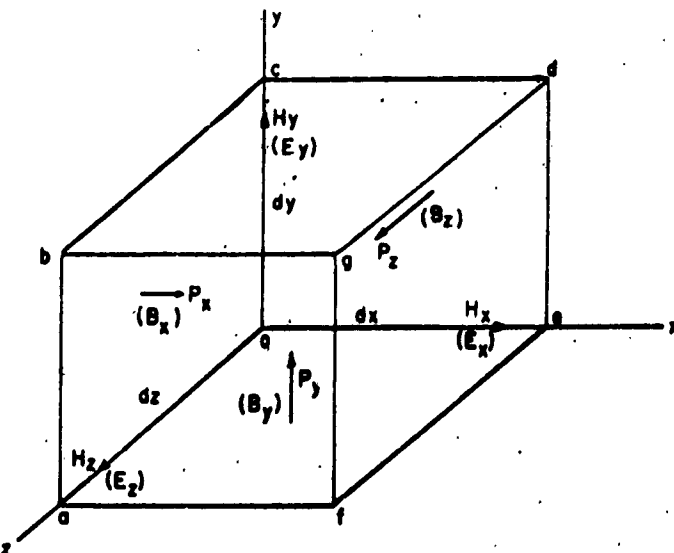


Fig A2-1 Element of volume in the electromagnetic field.
Cartesian Coordinates.

If all space is assumed to be filled with electric currents and the associated magnetic fields, it is a relatively simple matter to establish the relationships between the space variations in H and the current densities which exist at any point in space. This set of relationships is sometimes referred to as Maxwell's first law.

Let Fig A2-1 represent an elemental section of space filled with electric and magnetic fields, and with the associated currents. Also ρ_x , ρ_y and ρ_z represent the current densities in the x , y and z directions respectively. The magnetic-field intensities along the x , y and z axis respectively will be represented by H_x , H_y and H_z . The general principle involved in the establishment of the first equation to be considered can be seen by treating only one surface of the element of volume. Assume that the area ocba is selected. Through this area the total current is

$$I_x = \rho_x dy dz = \rho_x dA \quad (A2-2)$$

Around the boundary of this surface there exist magnetic intensity or H vectors, two of which are indicated in Fig A2-1, namely H_y along the dy path and H_z along the dz path.

The magnetic potential drops around the ocba loop taken individually are:

$$dU_1(\text{along } oc) = H_y dy$$

$$dU_2(\text{along cb}) = H_z dz + \frac{\partial(H_z dz)}{\partial y} dy = H_z dz + \frac{\partial H_z}{\partial y} dy dz$$

$$dU_3(\text{along ba}) = - \left[H_y dy + \frac{\partial(H_y dy)}{\partial z} dz \right] = - H_y dy - \frac{\partial H_y}{\partial z} dy dz$$

$$dU_4(\text{along ao}) = - H_z dz$$

In arriving at these expressions it is of course recognized that dz is not a function of y and neither is dy a function of z . The four magnetic potential drops are to be taken in the ocba_{ao} direction around the loop since $+ I_x$ establishes H vectors in this direction around the loop in accordance with the right-hand rule.

From the circuital law of magnetism (equation A2-1), it is plain that

$$\begin{aligned} \oint H \cdot dl &= dU_1 + dU_2 + dU_3 + dU_4 \\ &= \left(\frac{\partial H_z}{\partial y} - \frac{\partial H_y}{\partial z} \right) dy dz = \rho_x dy dz \end{aligned} \quad (\text{A2-3})$$

$$\text{or } \frac{\partial H_z}{\partial y} - \frac{\partial H_y}{\partial z} = \rho_x \quad (\text{A2-4})$$

In this equation ρ_x the current density existing over the $dy dz$ face and directed along the x axis is made up of

two parts. One is the conduction current density gE_x , where g is the specific conductance per unit volume and E_x is the x component of the electric-field intensity in volts per meter. The other is the displacement current density,

$\frac{\partial D_x}{\partial t}$, where D_x is the electric flux density. Since $D = \epsilon E$, where ϵ is the permittivity of the medium, the total current density may be written,

$$\rho_x = gE_x + \epsilon \frac{\partial E_x}{\partial t}$$

Equation (A2-4) now becomes

$$\frac{\partial H_z}{\partial y} - \frac{\partial H_y}{\partial z} = gE_x + \epsilon \frac{\partial E_x}{\partial t} \quad (A2-5)$$

In an exactly similar manner two other equations, for the remaining two coordinate directions, may be derived. They are

$$\frac{\partial H_x}{\partial z} - \frac{\partial H_z}{\partial x} = gE_y + \epsilon \frac{\partial E_y}{\partial t} \quad (A2-6)$$

$$\text{and } \frac{\partial H_y}{\partial x} - \frac{\partial H_x}{\partial y} = gE_z + \epsilon \frac{\partial E_z}{\partial t} \quad (A2-7)$$

These three equations together make up the expression of one of Maxwell's laws. They express three of the necessary relations which must always exist between H and E in the electromagnetic field.

B. Maxwell's Second Law.

Equations (A2-5), (A2-6) and (A2-7) are based on the circuital law of magnetism. Another set of three equations based on Faraday's law will now be derived. Again Fig A2-1 will be used with the ρ 's replaced by flux densities B and with the H 's giving place to corresponding electric intensities (E 's) expressed in volts per meter.

Consider the area ocba and assume that the flux density B_x is decreasing so that its derivative with respect to time is negative. Also assume for the moment that the boundaries of the area are fine wires, with practically infinite resistance if we wish, in which emf's are induced by the time rate of change of B_x . The decrease of flux through the area will induce a voltage e in the wire boundary which will be in the sense ocba. The magnitude of this voltage is given by Faraday's law to be

$$e = \oint E \cdot dl = - \frac{d\phi_x}{dt} = - \frac{\partial B_x}{\partial t} dydz \quad (A2-8)$$

where E is the electric intensity vector

l is the displacement directed along the periphery of loop oabco

ϕ_x is the magnetic flux crossing the $dydz$ surface

B_x is the flux density at the $dydz$ surface

The minus sign accounts for the fact that the voltage induced in the ocba loop is measured by the time rate of decrease of magnetic flux through the loop.

The electric potential differences around the closed path ocba (taken in the right-hand screw direction around $+B_x$) are individually

$$dv_1(\text{along } oc) = E_y dy$$

$$dv_2(\text{along cb}) = E_z dz + \frac{\partial(E_z dz)}{\partial y} dy = E_z dz + \frac{\partial E_z}{\partial y} dy dz$$

$$dv_3(\text{along ba}) = - \left[E_y dy + \frac{\partial(E_y dy)}{\partial z} dz \right] = - E_y dy - \frac{\partial E_y}{\partial z} dy dz$$

$$dv_4(\text{along ao}) = - E_z dz$$

From equation (A2-8) it is seen that

$$e = dv_1 + dv_2 + dv_3 + dv_4 = \left(\frac{\partial E_z}{\partial y} - \frac{\partial E_y}{\partial z} \right) dy dz = - \frac{\partial B_x}{\partial t} dy dz \quad (\text{A2-9})$$

Recognizing that $B_x = \mu H_x$

$$\frac{\partial E_z}{\partial y} - \frac{\partial E_y}{\partial z} = -\mu \frac{\partial H_x}{\partial t} \quad (\text{A2-10})$$

If the same procedure is applied to faces $dxdz$ and to $dxdy$ respectively, we find that:

$$\frac{\partial \overline{E}_x}{\partial z} - \frac{\partial \overline{E}_z}{\partial x} = -\mu \frac{\partial \overline{H}_y}{\partial t} \quad (A2-11)$$

and

$$\frac{\partial \overline{E}_y}{\partial x} - \frac{\partial \overline{E}_x}{\partial y} = -\mu \frac{\partial \overline{H}_z}{\partial t} \quad (A2-12)$$

Equations (A2-5) through (A2-7) and (A2-10) through (A2-12) are generalized solutions to Maxwell's first two laws in Cartesian coordinates. We are interested primarily in the steady state sinusoidal solution. Since the \overline{H} 's and \overline{E} 's of the above equations are functions of time and space, we may therefore make the substitutions:

$$\overline{E}_x = \overline{E}_x' e^{(j\omega t - \gamma z)} \quad (A2-13)$$

$$\overline{E}_y = \overline{E}_y' e^{(j\omega t - \gamma z)} \quad (A2-14)$$

$$\overline{E}_z = \overline{E}_z' e^{(j\omega t - \gamma z)} \quad (A2-15)$$

and

$$\overline{H}_x = \overline{H}_x' e^{(j\omega t - \gamma z)} \quad (A2-16)$$

$$\overline{H}_y = \overline{H}_y' e^{(j\omega t - \gamma z)} \quad (A2-17)$$

$$\overline{H}_z = \overline{H}_z' e^{(j\omega t - \gamma z)} \quad (A2-18)$$

where the \overline{H}' 's and \overline{E}' 's are functions of space only, γ is the propagation constant and z is the assumed direction of propagation.

If equations (A2-13) - (A2-18) are substituted in equations (A2-5) thru (A2-7) and (A2-10) thru (A2-12), the following relations are obtained (assuming $g = 0$):

$$\frac{\partial \bar{E}_z}{\partial y} - \gamma \bar{E}_y = -j \omega \mu \bar{H}_x \quad (A2-19)$$

$$-\gamma \bar{E}_x - \frac{\partial \bar{E}_z}{\partial x} = -j \omega \mu \bar{H}_y \quad (A2-20)$$

$$\frac{\partial \bar{E}_y}{\partial x} - \frac{\partial \bar{E}_x}{\partial y} = -j \omega \mu \bar{H}_z \quad (A2-21)$$

$$\frac{\partial \bar{H}_z}{\partial y} + \gamma \bar{H}_y = j \omega \epsilon \bar{E}_x \quad (A2-22)$$

$$-\gamma \bar{H}_x - \frac{\partial \bar{H}_z}{\partial x} = j \omega \epsilon \bar{E}_y \quad (A2-23)$$

$$\frac{\partial \bar{H}_y}{\partial x} - \frac{\partial \bar{H}_x}{\partial y} = j \omega \epsilon \bar{E}_z \quad (A2-24)$$

Equations (A2-19) - (A2-24) may be solved simultaneously for the \bar{E} 's and \bar{H} 's. The results are:

$$\bar{H}_x = \frac{1}{r^2 + k_1^2} \left(j\omega \epsilon \frac{\partial \bar{E}_z}{\partial y} - r \frac{\partial \bar{H}_z}{\partial x} \right) \quad (A2-25)$$

$$\bar{H}_y = \frac{-1}{r^2 + k_1^2} \left(j\omega \epsilon \frac{\partial \bar{E}_z}{\partial x} + r \frac{\partial \bar{H}_z}{\partial y} \right) \quad (A2-26)$$

$$\bar{E}_x = \frac{-1}{r^2 + k_1^2} \left(r \frac{\partial \bar{E}_z}{\partial x} + j\omega \mu_x \frac{\partial \bar{H}_z}{\partial y} \right) \quad (A2-27)$$

$$\bar{E}_y = \frac{1}{r^2 + k_1^2} \left(-r \frac{\partial \bar{E}_z}{\partial y} + j\omega \mu_x \frac{\partial \bar{H}_z}{\partial z} \right) \quad (A2-28)$$

where $k_1 = \omega^2 \mu \epsilon$

C. Maxwell's Third Law.²¹

Consider a small rectangular prism with its edges parallel to three coordinate axis X, Y and Z, as in Fig A2-2. The limiting case is to be considered, in which the prism is so small that its edges are dx , dy and dz in length. Fig A2-2 shows a side view of this prism, with the plane of the figure parallel to the X-Y plane. We are looking upon a side with area $dx dy$. Each end has area $dy dz$, and the top and bottom $dx dz$.

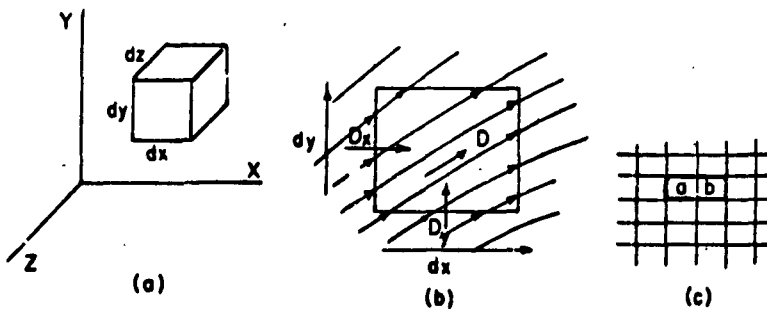


Fig A2-2 Derivation of Divergence

This small prismatic volume is located in a vector field which, for convenience, we will call D . Flux lines of this field pass through the prism, entering through one surface and leaving through another. We wish to find how many lines, if any, originate within the volume.

Referring to Fig A2-2, the number of flux lines entering the left-hand side of the prism is equal to the area of the left-hand surface times the normal component of field strength, which is $D_x dy dz$. The number leaving the right-hand surface is different if D_x changes in the distance dx . If D_x is changing at the rate $\frac{\partial D_x}{\partial x}$ as one passes from left to right, the amount of change in the distance dx is $\frac{\partial D_x}{\partial x} dx$. Hence the number of flux lines leaving the right-hand surface is $(D_x + \frac{\partial D_x}{\partial x} dx) dy dz$. Subtracting, the number of lines that leave the right-hand side in excess of the number that enter the left-hand side is $\frac{\partial D_x}{\partial x} dx dy dz$.

Similarly, the number of lines leaving the top of the prism in excess of those entering the bottom is $\frac{\partial D_y}{\partial y} dy dx dz$; and the number leaving the front surface is greater than the number entering the back by $\frac{\partial D_z}{\partial z} dz dx dy$.

Combining these quantities, the total number of flux lines leaving the volume that do not enter it is

$$\left(\frac{\partial D_x}{\partial x} + \frac{\partial D_y}{\partial y} + \frac{\partial D_z}{\partial z} \right) dx dy dz \quad (A2-29)$$

But divergence is defined as the number of flux lines originating per unit volume; so, if the volume of the prism is dv ,

$$\nabla \cdot D = \left(\frac{\partial D_x}{\partial x} + \frac{\partial D_y}{\partial y} + \frac{\partial D_z}{\partial z} \right) \frac{dx dy dz}{dv} \quad (A2-30)$$

Since the volume of the prism dv is equal to $dx dy dz$, it follows that

$$\nabla \cdot D = \frac{\partial D_x}{\partial x} + \frac{\partial D_y}{\partial y} + \frac{\partial D_z}{\partial z} \quad (A2-31)$$

Now consider that space is divided into an unlimited number of small cells of volume dv , as in Fig A2-2. The number of flux lines leaving one such cell, marked "a" in the figure, is greater than the number entering that cell by $\nabla \cdot D dv$. The number originating within the adjoining cell "b" is likewise the divergence at that location times the

volume of that cell. The number of lines emanating from the two cells together, considered as a unit, is the sum of the two products of divergence and volume. Adding more cells to the group thus begun, the number of lines of flux issuing from any volume is greater than the number entering that volume by the summation (or integral) of all the individual products of divergence and volume. Hence,

$$\text{Excess outward flux} = \int_V \nabla \cdot D \, dv = Q \quad (\text{A2-32})$$

The flux of the vector field D passing through an area a is defined as

$$\int D \cdot da \quad (\text{A2-33})$$

and from this it follows that the net flux passing outward through any closed surface (the excess of the outward flux over the inward flux) is found by integrating over the whole closed surface:

$$\int D \cdot da \quad (\text{A2-34})$$

Now equation (A2-34) and equation (A2-32) are different expressions for the same quantity of flux and hence may be equated, giving

$$\oint \mathbf{D} \cdot d\mathbf{a} = \int \nabla \cdot \mathbf{D} dv = Q \quad (\text{A2-35})$$

In any region in which there is no electric charge, so

$$Q = 0, \int (\nabla \cdot \mathbf{D}) dv = 0, \text{ and hence } \nabla \cdot \mathbf{D} = 0 \quad (\text{A2-36})$$

D. Maxwell's Fourth Law.

A basic experiment in the theory of magnetic fields leads to the equation

$$\oint \mathbf{B} \cdot d\mathbf{a} = 0 \quad (\text{A2-37})$$

Applying Gauss' theorem to this experimental result, it appears that the magnetic field has no divergence under any circumstances. i.e.

$$\nabla \cdot \mathbf{B} = 0 \quad (\text{A2-38})$$

The discussion of Maxwell's first and second laws is essentially that of Ware and Reed,²⁰ while the discussion of the third and fourth laws follow Skilling²¹ closely.

E. The Wave Equations Governing Electric and Magnetic Phenomena in Charge-Free Dielectric.

We now wish to operate on Maxwell's equations to obtain the wave equations. Consider a dielectric containing no charges

and with zero conductivity, so that there are no conduction currents in the dielectric. Since these are the conditions implied in the previous development of Maxwell's laws, the final equations can just be reproduced for convenience.

They are:

$$\nabla \times H = \epsilon \frac{\partial E}{\partial t} \quad (\text{A2-5) thru (A2-7)}$$

$$\nabla \times E = -\mu \frac{\partial H}{\partial t} \quad (\text{A2-10) thru (A2-12})$$

$$\nabla \cdot D = 0 \quad (\text{A2-36})$$

$$\nabla \cdot B = 0 \quad (\text{A2-38})$$

It will be observed that the first two equations have been written in their vector form rather than in the expanded Cartesian coordinate form used previously. This was done simply for convenience in developing the wave equations. The reader unfamiliar with vector operations will find an adequate discussion in Skilling.²¹

In order to realize the wave equations, let us first take the curl of (A2-10) thru (A2-12)

$$\nabla \times \nabla \times \mathbf{E} = -\mu \nabla \times \frac{\partial \mathbf{H}}{\partial t} \quad (\text{A2-39})$$

Now there is an identity in vector analysis which states:

$$\nabla \times \nabla \times \mathbf{A} = -\nabla^2 \mathbf{A} + \nabla (\nabla \cdot \mathbf{A}) \quad (\text{A2-40})$$

Substituting (A2-40) into (A2-39)

$$\nabla (\nabla \cdot \mathbf{E}) - \nabla^2 \mathbf{E} = -\mu \nabla \times \frac{\partial \mathbf{H}}{\partial t} \quad (\text{A2-41})$$

But by equation (A2-36)

$$\nabla \cdot \mathbf{D} = \nabla \cdot \epsilon \mathbf{E} = 0 \quad (\text{A2-36})$$

Inserting (A2-36) into (A2-41), there is obtained

$$\nabla^2 \mathbf{E} = \mu \nabla \times \frac{\partial \mathbf{H}}{\partial t} \quad (\text{A2-42})$$

A little reflection reveals that \mathbf{E} and \mathbf{H} are continuous functions of time and space and that their partial derivatives may be taken in any order. Utilizing this result, equation (A2-42) can be put in the form

$$\nabla^2 \mathbf{E} = \mu \frac{\partial}{\partial t} (\nabla \times \mathbf{H}) \quad (\text{A2-43})$$

But equation (A2-5) thru (A2-7) states

$$\nabla \times H = \epsilon \frac{\partial E}{\partial t} \quad (A2-5) \text{ thru } (A2-7)$$

Inserting this result in (A2-44), we get

$$\nabla^2 E = \frac{\mu_0}{\epsilon} \left(\epsilon \frac{\partial^2 E}{\partial t^2} \right) \quad (A2-44)$$

or

$$\nabla^2 E = \mu \epsilon \frac{\partial^2 E}{\partial t^2} \quad (A2-45)$$

This is the general form of the wave equation. A wave equation in terms of H can also be obtained simply by starting with equations (A2-5) thru (A2-7) and proceeding in precisely the same manner as in the electric field case.

The result is:

$$\nabla^2 H = \mu \epsilon \frac{\partial^2 H}{\partial t^2} \quad (A2-46)$$

Again we assumed a sinusoidal steady state solution, so that the E 's and H 's of equations (A2-45) and (A2-46) are those of equations (A2-13) thru (A2-18). Therefore for sinusoidal variations equation (A2-45) may be written as:

$$\nabla^2 E = -\omega^2 \mu \epsilon E \quad (A2-47)$$

and (A2-46) as:

$$\nabla^2 H = -\omega^2 \mu \epsilon H \quad (A2-48)$$

where E and H are functions of time and space.

Now as was used in equations (A2-25) thru (A2-28)

let $k_1 = \omega^2 \mu \epsilon$. Making this substitution, equation (A2-47) becomes:

$$\nabla^2 E = -k_1^2 E \quad (A2-49)$$

and relation (A2-48) becomes:

$$\nabla^2 H = -k_1^2 H \quad (A2-50)$$

Now let us look at the expanded form of equations (A2-49)

$$\frac{\partial^2 E_x}{\partial x^2} + \frac{\partial^2 E_x}{\partial y^2} + \frac{\partial^2 E_x}{\partial z^2} = -k_1^2 E_x \quad (A2-51)$$

$$\frac{\partial^2 E_y}{\partial x^2} + \frac{\partial^2 E_y}{\partial y^2} + \frac{\partial^2 E_y}{\partial z^2} = -k_1^2 E_y$$

$$\frac{\partial^2 E_z}{\partial x^2} + \frac{\partial^2 E_z}{\partial y^2} + \frac{\partial^2 E_z}{\partial z^2} = -k_1^2 E_z$$

Equation (A2-50) is similar in form. It should be obvious by inspection that (A2-49) can be split into two parts as follows:

$$\nabla^2 E = \nabla_{xy}^2 E + \frac{\partial^2 E}{\partial z^2} = -k_1^2 E \quad (A2-52)$$

Assuming our sinusoidal variation $E e^{(j\omega t - \gamma z)}$:

$$\frac{\partial^2 E}{\partial z^2} = \gamma^2 E \quad (A2-53)$$

Substituting (A2-53) into (A2-52), we obtain

$$\nabla_{xy}^2 E = -(\gamma^2 + k_1^2) E \quad (A2-54)$$

Equation (A2-50) is operated in a similar manner to obtain

$$\nabla_{xy}^2 H = -(\gamma^2 + k_1^2) H \quad (A2-55)$$

The mode of propagation under discussion is the TEM mode. This mode is characterized by the property that the E and H fields in the direction of propagation is zero i.e. if Z is the direction of propagation, E_z and H_z are zero.

The general relations between wave components as expressed by equations (A2-25) thru (A2-28) show that with E_z and H_z zero, then all other components must of necessity also be zero, unless $\gamma^2 + k_1^2$ is at the same time equal to zero. Thus, a transverse electromagnetic wave must satisfy the condition

$$\gamma^2 + k_1^2 = 0 \quad (A2-56)$$

or

$$\gamma = \pm jk_1 = \pm \sqrt{j\omega \mu \epsilon}$$

If equation (A2-56) is inserted in equations (A2-54) and (A2-55), then is obtained

$$\nabla_{xy}^2 E = 0 \quad (A2-57)$$

and

$$\nabla_{xy}^2 H = 0 \quad (A2-58)$$

But relations (A2-57) and (A2-58) are Laplace's equations for E and H in the transverse plane. Since E_z and H_z are zero, the field is transverse. The solutions for Laplace's equation are electric and magnetic fields under static conditions. Therefore we may conclude that the TEM mode is exactly a static distribution and analyze it as such. The equations for Z_0 , velocity in the medium, etc. are the same as those for any standard transmission line.

APPENDIX III

ELEMENTS OF COMPLEX VARIABLE THEORY AND A DISCUSSION OF THE SCHWARZ-CHRISTOFFEL TRANSFORMATION

A. Elements of Complex Variable Theory.

1. The Cauchy-Riemann equations.

We are aware that a complex plane exists that has a real and complex axis. We call this complex plane the Z plane. Any point in this plane may be identified by the coordinates:

$$z = x + jy \quad (A3-1)$$

We may further define the W plane,

$$w = f(z) = u + jv \quad (A3-2)$$

where: u is the real part of $f(z)$
and v is the imaginary part.

Fig A3-1 A and B illustrate the Z and W planes.

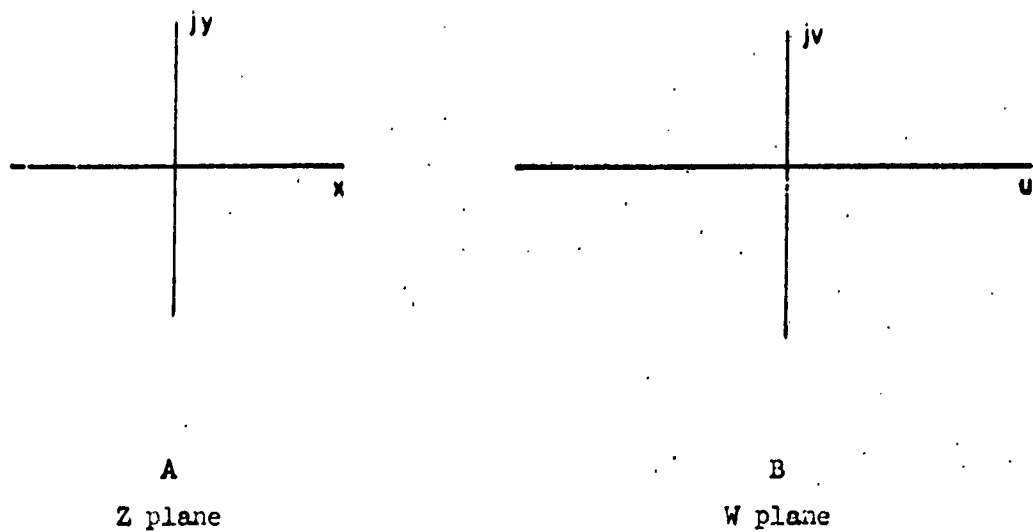


Fig A3-1 Illustration of Z and W Planes

To determine what conditions $f(z)$ must satisfy to fulfill the above relations, let us examine the derivative:

$$\frac{dw}{dz} = \lim_{\Delta z \rightarrow 0} \frac{\Delta w}{\Delta z} \quad (A3-3)$$

In order for the limit (A3-3) to be valid, Δz must be able to approach zero from any direction. Let us write

$$\frac{dv}{dz} = \frac{du}{dx} + j\frac{dv}{dy} \quad (A3-4)$$

Remembering that

$u = \text{Real part of } f(z)$

we may write:

$$du = \frac{\partial u}{\partial x} dx + \frac{\partial u}{\partial y} dy \quad (A3-5)$$

Also $v =$ Imaginary part of $f(z)$, so

$$dv = \frac{\partial v}{\partial x} dx + \frac{\partial v}{\partial y} dy \quad (A3-6)$$

Substituting (A3-5) and (A3-6) into (A3-4), there is obtained:

$$\frac{dw}{dz} = \frac{\left(\frac{\partial u}{\partial x} + j \frac{\partial v}{\partial x} \right) + \left(\frac{\partial u}{\partial y} + j \frac{\partial v}{\partial y} \right) \frac{dy}{dx}}{1 + j \frac{dy}{dx}} \quad (A3-7)$$

Inspection of (A3-7) shows that the direction of dz is determined by dy/dx . If (A3-7) is to be independent of direction, certain conditions must be satisfied. Dividing numerator and denominator of (A3-7) by

$$\frac{\left(\frac{\partial u}{\partial x} + j \frac{\partial v}{\partial x} \right)}{\left(\frac{\partial u}{\partial y} + j \frac{\partial v}{\partial y} \right)} + \frac{\frac{dy}{dx}}{\left(\frac{\partial u}{\partial y} + j \frac{\partial v}{\partial x} \right)} \quad (A3-8)$$

Now let:

$$\frac{\left(\frac{\partial u}{\partial x} + j \frac{\partial v}{\partial x} \right)}{\left(\frac{\partial u}{\partial y} + j \frac{\partial v}{\partial y} \right)} = \frac{1}{j} \quad (A3-9)$$

Substituting (A3-9) into (A3-8):

$$\frac{dw}{dz} = j \frac{\left(\frac{1}{j} + \frac{dy}{dx} \right)}{1 + j \frac{dy}{dx}} = 1 \quad (\text{A3-10})$$

Equation (A3-10) is obviously independent of direction and therefore meets our criterion. The restriction on u and v may be gotten from the equation (A3-9) which may be written as:

$$\frac{\partial u}{\partial y} + j \frac{\partial v}{\partial y} = - \frac{\partial v}{\partial x} + j \frac{\partial u}{\partial x} \quad (\text{A3-11})$$

Now in order for (A3-11) to be true the Real parts must be equal and the Imaginary parts must be equal; i.e.,

$$\frac{\partial u}{\partial x} = \frac{\partial v}{\partial y} \quad (\text{A3-12})$$

and

$$\frac{\partial u}{\partial y} = - \frac{\partial v}{\partial x} \quad (\text{A3-13})$$

Equations (A3-12) and (A3-13) are known as the Cauchy-Riemann equations. Only those functions $w = u + j v$ which satisfy these equations can be called functions of a complex variable. Such functions are analytic functions i.e. they have a derivative everywhere within a arbitrarily small region in the vicinity of some point.

2. Conformal Mapping.

Conformal mapping applies only to analytic functions.

Since we now have a mathematical relationship between the Z and W planes, it is possible to map the points of z on the Z plane and the corresponding (or image) points on the $W = F(Z)$ plane.

If to each point there corresponds only one point w, the function $W = F(Z)$ is said to be single valued.

Now let us see what is meant by the word "conformal".

In Fig A3-2(a) let the element of distance pp' in the Z plane represent dz . Then there will be an image distance dw represented by qq' in the W plane. Now dw may be written as:

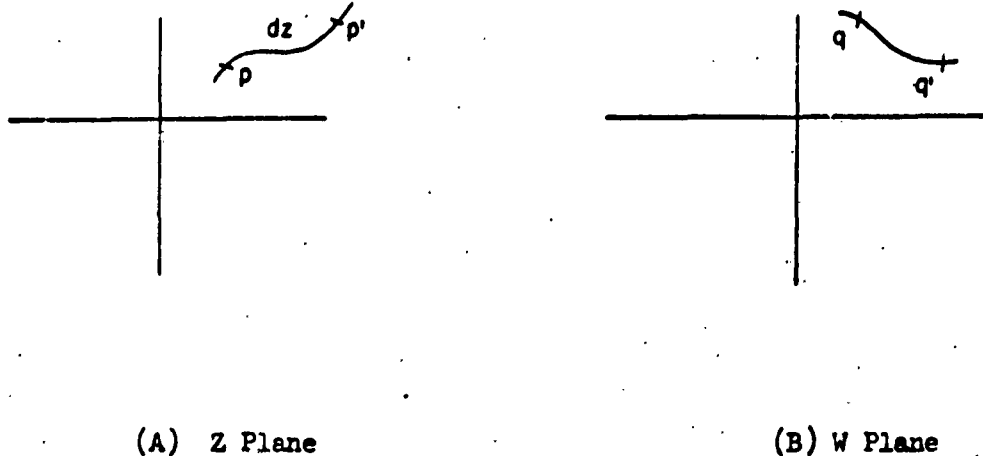


Fig A3-2 Conformal Mapping in the Complex Domain

$$dw = \left(\frac{dw}{dz}\right) dz \quad (A3-14)$$

Now $\frac{dw}{dz}$ is complex and may be written as:

$$\frac{dw}{dz} = a e^{j\phi} \quad (A3-15)$$

where

$$\left| \frac{dw}{dz} \right| = a$$

and

$$\phi = \text{argument} \left(\frac{dw}{dz} \right)$$

Substituting (A3-15) into (A3-14), there is obtained:

$$dw = (a e^{j\phi}) dz \quad (A3-16)$$

We therefore find that an element dw can be obtained from the corresponding element dz by multiplying its length by "a" and rotating it through an angle ϕ . It therefore follows that any element of area in the Z plane is represented in the W plane by an element of area that has the same form as the original element but whose linear dimensions are "a" times as great and whose orientation is obtained by turning the original element through an angle ϕ . Because angles are preserved (lines at right angles to each other in the Z plane remain at right angles in the W plane), the transformation is called "conformal".

B. The Schwarz-Christoffel Transformation.

An extremely useful mapping function, of considerable generality in its ability to meet various geometrical configurations, is given by the so-called Schwarz-Christoffel formula, which reads

$$w(z) = M \int_{z_0}^z (\delta - z_1)^{-\mu_1} (\delta - z_2)^{-\mu_2} \cdots (\delta - z_n)^{-\mu_n} d\delta + N \quad (A3-17)$$

Here δ is a running variable in the Z-plane, z_1, z_2, \dots, z_n are n finite points on the real axis, numbered in such an order that

$$z_1 < z_2 < \cdots < z_n \quad (A3-18)$$

and the quantities $\mu_1, \mu_2, \dots, \mu_n$ appearing in the exponents are any set of positive or negative real numbers.

The constants M and N may have complex values, with the possibility that N be zero, but M must, of course, have a non-zero value. The lower limit z_0 of the integral is an arbitrary point in the upper half plane. It may be chosen equal to zero, or equal to one of the points z_1, \dots, z_n . The independent variable for the mapping function $w(z)$ is the upper limit of the integral. For this reason the derivative of the function is given by

* This development follows that of Guillemin as given in "Mathematics of Circuit Analysis" ¹⁹, pp 380-384.

$$\frac{dw}{dz} = M (z-z_1)^{-\mu_1} (z-z_2)^{-\mu_2} \cdots (z-z_n)^{-\mu_n} \quad (A3-19)$$

as may be seen from the fact that if one has

$$w(z) = \int_{z_0}^z f(\delta) d\delta \quad (A3-20)$$

the usual definition for the derivative

$$\frac{dw}{dz} = \lim_{\Delta z \rightarrow 0} \left[\frac{w(z + \Delta z) - w(z)}{\Delta z} \right] \quad (A3-21)$$

yields

$$w(z + \Delta z) - w(z) = \int_z^{z + \Delta z} f(\delta) d\delta \quad (A3-22)$$

Since Δz is a small displacement (becoming zero in the limit), one may say that for the integration in equation (A3-22) the function $f(\delta)$ is essentially constant and equal to the value $f(z)$. It is assumed, of course, that the function $f(\delta)$ is continuous in the vicinity of the point $\delta=z$, which is a recognized condition for the existence of the derivative in the first place. With $f(\delta)$ equal to the constant value $f(z)$, it may be placed in front of the integral sign, and (A3-22) yields

$$w(z + \Delta z) - w(z) \approx f(z) \int_z^{z + \Delta z} d\delta = f(z) \Delta z \quad (A3-23)$$

the approximation becoming exact in the limit $\Delta z \rightarrow 0$.

Completing the limit, one finds, therefore, that

$$\frac{dw}{dz} = f(z) \quad (A3-24)$$

The essential character of the function $w(z)$ may now be recognized from a study of the behavior of the derivative (A3-19) in the vicinity of the point $z = z_v$. The first step in this direction is to represent the factor $(z - z_v)$ in the polar form as illustrated in Fig A3-3. This representation reads

$$(z - z_v) = |z - z_v| e^{j(\phi_v + 2\pi k)} \quad (A3-25)$$

in which k is an integer.

Then

$$(z - z_v)^{-\mu_v} = |z - z_v|^{-\mu_v} e^{-j(\mu_v \phi_v + 2\pi k \mu_v)} \quad (A3-26)$$

Since the quantity μ_v is not necessarily an integer, the right-hand side of equation (A3-26) may have many different values for different integer values of k .

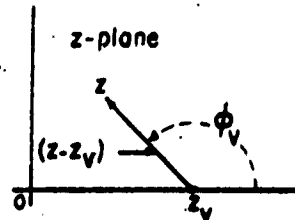


Fig A3-3 Representation of $(z - z_v)$ in polar form in the study of dw/dz .

In order to remove this multivaluedness of the factor $(z - z_v)^{-\mu_v}$, it is specified at the outset that k shall assume only the value zero. This specification is equivalent to stating that the function dw/dz is to be studied on only one of the many leaves of its Riemann surface, namely, on that one which corresponds to $k = 0$ in (A3-26). A typical factor in (A3-19) then becomes

$$(z - z_v)^{-\mu_v} = |z - z_v|^{-\mu_v} e^{-j \mu_v \phi_v} \quad (\text{A3-27})$$

and if the point z is allowed to lie only in the upper half plane or on the real axis of the Z -plane, it is clear from Fig A3-3 that

$$0 \leq \phi_v \leq \pi \quad (\text{A3-28})$$

When the polar forms

$$M = |M| e^{j\alpha} \quad (\text{A3-29})$$

and

$$\frac{dw}{dz} = \left| \frac{dw}{dz} \right| e^{j\theta} = \left[|M| |z - z_1|^{-\mu_1} |z - z_2|^{-\mu_2} \cdots |z - z_n|^{-\mu_n} \right] e^{j[\alpha - \mu_1 \phi_1 - \mu_2 \phi_2 - \cdots - \mu_n \phi_n]} \quad (\text{A3-30})$$

are introduced, it follows that

$$\theta = \alpha - \mu_1 \phi_1 - \mu_2 \phi_2 - \cdots - \mu_n \phi_n \quad (\text{A3-31})$$

It is now assumed that the variable z in the function (A3-19) is restricted to real values only; that is, the variable point z is thought of as moving along the real axis from $-\infty$ to ∞ , the only deviation from this behavior occurring wherever the variable point z encounters one of the critical points z_v .

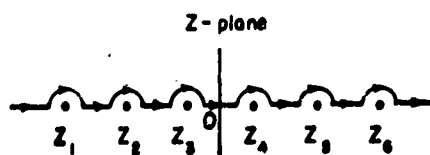


Fig A3-4 The path along which dw/dz is studied in the Schwartz-Christoffel transformation

There it makes a slight detour around the critical point instead of passing directly through it. These detours may be visualized as having the form of vanishingly small semicircular arcs lying in the upper half plane, as shown in Fig A3-4. As the point z traverses a small semicircular arc in the vicinity of the point z_v , the angle Φ_v changes from the value π to zero, whereas the angles of the remaining factors do not change at all because of the assumed vanishingly small radius of the semicircular detour. Hence for the range

$$z_{v-1} < z < z_v + 1 \quad (A3-32)$$

one has

$$\phi_1 = \phi_2 = \dots = \phi_{v-1} = 0 \quad \pi \geq \theta \geq 0 \quad (A3-33)$$

$$\phi_{v+1} = \phi_{v+2} = \dots = \phi_n = \pi$$

and* according to (A3-31)

$$\alpha - (\mu_v + \mu_{v+1} + \dots + \mu_n) \pi \leq \theta \leq \alpha - (\mu_{v+1} + \mu_{v+2} + \dots + \mu_n) \pi \quad (A3-34)$$

Throughout the range (A3-32), the angle θ is, therefore, increased by the amount

$$\Delta \theta = \mu_v \pi \quad (A3-35)$$

the important feature being that this increment occurs only as the point z traverses the small semicircular arc. In other words, as the point z moves along the real axis, the angle θ remains constant as z proceeds from one of the critical points to the next, receiving a sudden increment $\Delta \theta = \mu_v \pi$ only as z passes directly over the critical point z_v .

According to the discussion of conformal mapping, it is recognized that the map of the function $w(z)$ in the W -plane, corresponding to the real axis in the Z -plane, consists of a succession of straight-line segments between the points w_1, w_2, \dots corresponding respectively to z_1, z_2, \dots , the angular

* If μ_v is negative, the inequalities are reversed.

directions of two consecutive segments confluent in the point w_v differing by $\mu_v\pi$. That is, the map in the W-plane of the function (A3-17), corresponding to the real axis in the Z-plane, traversed from $-\infty$ to ∞ , has the general character shown in Fig A3-5. This result follows from the fact that the angle of dw/dz equals the difference between the angles of the increments dw and dz , and since the angle of the latter remains zero as the point z moves along the real axis, the angle of dw/dz must equal that of dw .

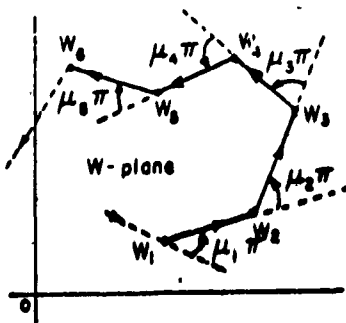


Fig A3-5 The map in the W-plane of the real axis in the Z-plane shown in Fig A3-4

This angle, however, is shown to remain constant except when z passes over one of the critical quantities z_v . At the corresponding points w_v then, the direction of the increment dw suddenly changes by the amount $\mu_v\pi$.

The plot in the W-plane corresponding to the real axis in the Z-plane is thus seen to be a polygon with the points w_1, \dots, w_n as its vertexes. If

$$\mu_1 + \mu_2 + \dots + \mu_n = 2 \quad (\text{A3-36})$$

the sum of the increments $\Delta\theta$ at the n vertexes w_1, \dots, w_n equals 2π . We may relate the exterior angles to the interior angles by the relation

$$\alpha_v - \pi\mu_v = \pi \quad (\text{A3-37})$$

or

$$\frac{\alpha_v}{\pi} - 1 = \mu_v \quad (\text{A3-38})$$

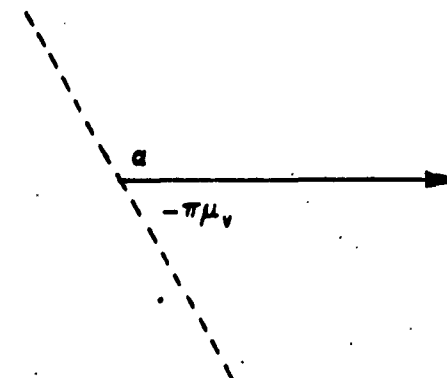


Fig A3-6 Relation of interior to exterior angles

Substituting this result into equation (A3-19), there is obtained:

$$\frac{dw}{dz} = M (z-z_1)^{\frac{\alpha_1}{\pi}-1} (z-z_2)^{\frac{\alpha_2}{\pi}-1} (z-z_3)^{\frac{\alpha_3}{\pi}-1} \dots (z-z_n)^{\frac{\alpha_n}{\pi}-1} \quad (\text{A3-39})$$

C. The Inverse Function.

Suppose we are interested in going from the W to the Z plane via the Schwarz-Christoffel Transformation. We must examine the inverse function dz/dw to do this. It was previously stated that

$$w = f(z) = u(x,y) + jv(x,y) \quad (\text{A3-40})$$

We may invert

$$z = \phi(w) = x(u,v) + jy(u,v) \quad (\text{A3-41})$$

where a 1 to 1 relationship exists between z and w.

Let us consider the following relations:

$$dx = \frac{\partial x}{\partial u} du + \frac{\partial x}{\partial v} dv \quad (\text{A3-42})$$

$$dy = \frac{\partial y}{\partial u} du + \frac{\partial y}{\partial v} dv \quad (\text{A3-43})$$

Equations (A3-42) and A3-43) are the inverse of equations (A3-5) and (A3-6) which are repeated here for convenience.

$$du = \frac{\partial u}{\partial x} dx + \frac{\partial u}{\partial y} dy \quad (A3-5)$$

$$dv = \frac{\partial v}{\partial x} dx + \frac{\partial v}{\partial y} dy \quad (A3-6)$$

We have for the determinant of (A3-5) and (A3-6)

$$D = \frac{\partial u}{\partial x} \frac{\partial v}{\partial y} - \frac{\partial u}{\partial y} \frac{\partial v}{\partial x} \quad (A3-14)$$

But the Cauchy Riemann equations state

$$\frac{\partial u}{\partial x} = \frac{\partial v}{\partial y} \quad (A3-12)$$

and

$$\frac{\partial u}{\partial y} = -\frac{\partial v}{\partial x} \quad (A3-13)$$

Substituting (A3-12) and (A3-13) into (A3-14) we obtain:

$$D = \left(\frac{\partial u}{\partial x} \right)^2 + \left(\frac{\partial u}{\partial y} \right)^2 = \left(\frac{\partial v}{\partial x} \right)^2 + \left(\frac{\partial v}{\partial y} \right)^2 \quad (A3-45)$$

Now it was previously stated that

$$f(z) = u + jv \quad (A3-2)$$

Hence

$$\frac{dw}{dz} = f'(z) = \frac{du + j dv}{dx + j dy} \quad (A3-46)$$

Let us reexamine equation (A3-7). This relation was

$$\frac{dw}{dz} = \frac{(\partial u/\partial x + j\partial v/\partial x) + (\partial u/\partial y + j\partial v/\partial y)}{1 + j\partial y/\partial x} \frac{dy}{dx} \quad (A3-7)$$

We have shown in our earlier discussion that if a function is analytic, the value of the derivative is independent of the angle of the increment $dz = dx + j dy$. If this angle is zero, dy is zero.

Letting dy equal zero in (A3-7)

$$\frac{dw}{dz} = \frac{\partial u}{\partial x} + j \frac{\partial v}{\partial x} \quad (A3-47)$$

Now apply the Cauchy-Riemann conditions.

(Equation (A3-12) and (A3-13) to equation (A3-47)). The result is:

$$\frac{dw}{dz} = \frac{\partial u}{\partial x} + j \frac{\partial v}{\partial x} = \frac{\partial v}{\partial y} + j \frac{\partial v}{\partial x} \quad (A3-48)$$

Recalling equations (A3-45)

$$D = \left(\frac{\partial v}{\partial x} \right)^2 + \left(\frac{\partial v}{\partial y} \right)^2 \quad (A3-45)$$

Comparing equations (A3-45) and (A3-48) and remembering the definition of the absolute value, we see that:

$$D = |f'(z)|^2 = \left| \frac{dw}{dz} \right|^2 \quad (A3-49)$$

We previously made the statement that the following relations were inverse.

$$du = \frac{\partial u}{\partial x} dx + \frac{\partial u}{\partial y} dy \quad (A3-5)$$

$$dv = \frac{\partial v}{\partial x} dx + \frac{\partial v}{\partial y} dy \quad (A3-6)$$

and

$$dx = \frac{\partial x}{\partial u} du + \frac{\partial x}{\partial v} dv \quad (A3-42)$$

$$dy = \frac{\partial y}{\partial u} du + \frac{\partial y}{\partial v} dv$$

If these relations truly are inverse, then their matrixies must be inverse; that is

$$\begin{vmatrix} \frac{\partial x}{\partial u} & \frac{\partial x}{\partial v} \\ \frac{\partial y}{\partial u} & \frac{\partial y}{\partial v} \end{vmatrix} = \begin{vmatrix} \frac{\partial u}{\partial x} & \frac{\partial u}{\partial y} \\ \frac{\partial v}{\partial x} & \frac{\partial v}{\partial y} \end{vmatrix}^{-1} \quad (A3-50)$$

We remember from the determinant theory of inverse matrixies that

$$a_{jk} = \frac{A_{kj}}{D} \quad (A3-51)$$

Where:

a_{jk} is the element belonging to the j th row and k th column

A_{kj} is the minor of the k th row and j th column

and

D is the value of determinant under consideration

In order for (A3-51) to hold, the relations between the matrixies are:

$$\frac{\partial x}{\partial u} = \frac{1}{D} \frac{\partial v}{\partial y} \quad (A3-52)$$

$$\frac{\partial x}{\partial v} = -\frac{1}{D} \frac{\partial u}{\partial y} \quad (A3-53)$$

$$\frac{\partial y}{\partial u} = -\frac{1}{D} \frac{\partial v}{\partial x} \quad (A3-54)$$

$$\frac{\partial y}{\partial v} = \frac{1}{D} \frac{\partial u}{\partial x} \quad (A3-55)$$

Now

$$\frac{dz}{dw} = \frac{dx + j dy}{du + j dv} \quad (A3-56)$$

Inserting dx and dy as given by (A3-42) and (A3-43)

$$\frac{dz}{dw} = \frac{(\partial x/\partial u du + \partial x/\partial v dv) + j (\partial y/\partial u du + \partial y/\partial v dv)}{du + j dv} \quad (A3-57)$$

Divide top and bottom of (A3-57) by du

$$\frac{dz}{dw} = \frac{(\partial x/\partial u + \partial x/\partial v dv/du) + j (\partial y/\partial u + \partial y/\partial v dv/du)}{1 + j dv/du} \quad (A3-58)$$

Rearranging, (A3-58) becomes

$$\frac{dz}{dw} = \frac{(\partial x/\partial u + j \partial y/\partial u) + (\partial x/\partial v + j \partial y/\partial v) \frac{dv}{du}}{1 + j \frac{dv}{du}} \quad (A3-59)$$

Since dz/dw must be independent of the increment of

$$dw = du + j dv,$$

if the angle equals zero (i.e. $j v = 0$).

Then:

$$\frac{dz}{dw} = (\partial x/\partial u + j \partial y/\partial u) \quad (A3-60)$$

But from (A3-52)

$$\frac{\partial x}{\partial u} = \frac{1}{D} \frac{\partial v}{\partial y} \quad (A3-52)$$

and from (A3-54)

$$\frac{\partial y}{\partial u} = -\frac{1}{D} \frac{\partial v}{\partial x} \quad (A3-54)$$

Substituting (A3-52) and (A3-54) into (A3-60) we obtain

$$\frac{dz}{dw} = \frac{\partial v/\partial y - j \partial v/\partial x}{D} \quad (A3-61)$$

Multiply top and bottom of (A3-61) by

$$\left(\frac{\partial v}{\partial y} + j \frac{\partial v}{\partial x} \right)$$

giving

$$\begin{aligned} \frac{dz}{dw} &= \frac{(\partial v/\partial y - j \partial v/\partial x)(\partial v/\partial y + j \partial v/\partial x)}{D \left(\frac{\partial v}{\partial y} + j \frac{\partial v}{\partial x} \right)} \\ &= \frac{(\partial v/\partial y)^2 + (\partial v/\partial x)^2}{D \left(\frac{\partial v}{\partial y} + j \frac{\partial v}{\partial x} \right)} \end{aligned} \quad (A3-62)$$

But equation (A3-45) stated

$$D = \left(\frac{\partial v}{\partial x} \right)^2 + \left(\frac{\partial v}{\partial y} \right)^2 \quad (A3-45)$$

Substituting (A3-45) into (A3-62)

$$\frac{dz}{dw} = \frac{1}{\frac{\partial v}{\partial y} + j \frac{\partial v}{\partial x}} \quad (A3-63)$$

One of the Cauchy conditions states:

$$\frac{\partial v}{\partial y} = \frac{\partial u}{\partial x} \quad (A3-12)$$

Substituting (A3-12) into (A3-63), there is obtained

$$\frac{dz}{dw} = \frac{1}{\frac{\partial u}{\partial x} + j \frac{\partial v}{\partial x}} \quad (A3-64)$$

Equation (A3-47) stated that

$$\frac{dw}{dz} = \frac{\partial u}{\partial x} + j \frac{\partial v}{\partial x} \quad (A3-47)$$

Inserting (A3-47) into (A3-64), the desired result is obtained.

$$\frac{dz}{dw} = \frac{1}{\frac{dw}{dz}} \quad (A3-65)$$

The inverse function therefore has a derivative that is the inverse of the given function. We may therefore map a function from the W to the Z plane, or from the Z to the W plane. The Schwarz-Christoffel transformation from the W to the Z plane has already been written as equation (A3-39). The equation from the Z to the W plane is the inverse and may be written:

$$\frac{dz}{dw} = M (w-u_1)^{\frac{\alpha_1}{\pi}-1} (w-u_2)^{\frac{\alpha_2}{\pi}-1} \dots (w-u_n)^{\frac{\alpha_n}{\pi}-1} \quad (A3-66)$$

where:

M is a complex constant

$u_1 \dots u_n$ are the image points of the corresponding z's in the W plane

$\alpha_1 \dots \alpha_n$ are the interior angles of the polygon.

D. Successive Transformations:

In solving two dimensional potential problems, it is frequently convenient to use successive transformations.

$$\text{Let } W = F_1(z_1) \quad (A3-67)$$

and

$$z_1 = F_2(z) \quad (A3-68)$$

By elimination of z_1 between (A3-67) and (A3-68) we obtain

$$W = F_3(z) \quad (A3-69)$$

The relation (A3-68) expresses a transformation from the Z plane into the Z_1 plane, while (A3-67) expresses a further transformation from the Z_1 plane into the W plane. Therefore the final transformation (A3-69) may be regarded as the result of two successive transformations.

APPENDIX IV

DETERMINATION OF THE CAPACITANCE OF STRIPLINE

A. Capacitance of Stripline per unit length neglecting fringing.

Upon consideration of the cross section of stripline, it can be seen that the capacitance of this configuration is essentially that of two parallel plate condensers connected in parallel, neglecting fringing capacity, C_f' . An expression for C_f' will be developed at a later point in the Appendix.

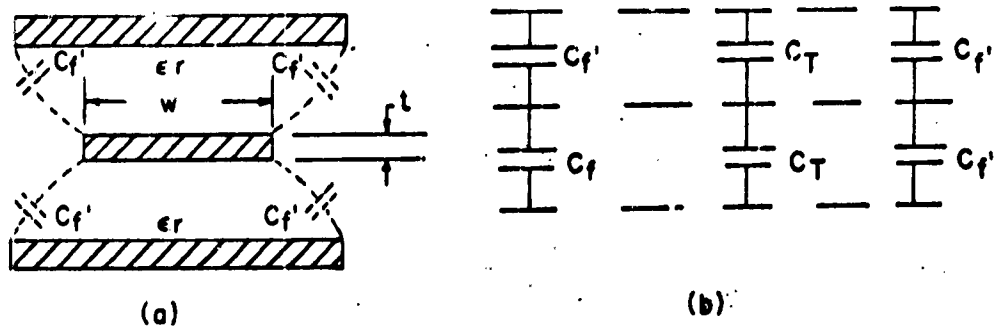


Fig A4-1 Cross Section of Stripline

Fig A4-2 shows the upper half of fig A4-1. From this figure C_T can be determined.

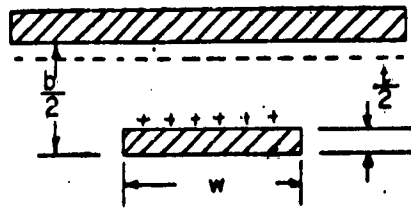


Fig A4-2 Upper Half of Fig A4-1

The electric field between the plates of Fig A2-2
is given by the expression:

$$E = \frac{V}{d} = \frac{V}{\frac{b-t}{2}} \quad (A4-1)$$

where E = electric field between the plates

V = potential difference between the plates

d = distance between plates

b = ground plane spacing - cm

t = plate thickness - cm

The electric flux density is then:

$$\begin{aligned} D &= \epsilon_0 \epsilon_r E \\ &= \epsilon_0 \epsilon_r \frac{V}{\frac{b-t}{2}} \end{aligned} \quad (A4-2)$$

where $D = \text{electric flux density}$
 $\epsilon_0 = \text{permittivity of free space}$
 $\epsilon_r = \text{relative permittivity}$

The electric flux originating at the positive plate
and terminating on the negative plate is:

$$\psi = D A = \frac{\epsilon_0 \epsilon_r V}{\frac{b-t}{2}} (w \times l) = Q \quad (\text{A4-3})$$

where $Q = \text{charge on one plate}$

$A = \text{area of one plate}$

$w = \text{strip width - cm}$

The capacitance of the parallel plate condenser is then:

$$C = \frac{Q}{V} = \frac{2 \epsilon_0 \epsilon_r w}{(b-t)} \quad (\text{A4-4})$$

Now remembering that we have two capacitors in parallel,
we obtain for the stripline capacitance neglecting fringing
effects.

$$C_{pp} = \frac{4 \epsilon_0 \epsilon_r w}{b-t}$$

$$= 4 \times 10^{-14} \frac{(8.842 \epsilon_r w)}{b-t} \quad (\text{A4-5})$$

where C_{pp} is in farad/cm.

B. Capacitance of Stripline including fringing capacitance.

Equation (A4-5) can be used to compute Characteristic
Impedance up to 25 ohms. For Characteristic Impedance calculations

above 25 ohms, a term for fringing capacitance must be added to equation (A4-5). Designating fringing capacitance by C_f' and referring to Fig A4-1, we see that equation (A4-5) becomes:

$$C_{TP} = 4 \times 10^{-14} \frac{(8.842 \epsilon_r w + C_f')}{b-t} \text{ farad/cm.} \quad (A4-6)$$

C. Development of an expression for Fringing Capacitance C_f' .

We now wish to put the Schwarz-Christoffel Transformation to work in order to find an expression for the fringing capacitance C_f' . Equation (A3-66) is repeated here for convenience with w replaced by z_1 .

$$\frac{dz}{dz_1} = M (z_1 - u_1)^{\frac{\alpha_1}{\pi}-1} (z_1 - u_2)^{\frac{\alpha_2}{\pi}-1} \dots (z_1 - u_n)^{\frac{\alpha_n}{\pi}-1} \quad (A3-66)$$

where the notation is the same as that given in Appendix III except for z_1 which represents points in a plane Z_1 intermediate to the A and W planes. In other words we will perform a mapping from the Z to the Z_1 plane and then a second mapping from the Z_1 to the W plane.

Consider Fig A4-3. This figure represents one half of the cross section of stripline. The polygon used to perform the Schwarz-Christoffel Transformation is shown in broken lines. As the points $\pm a_1$ proceed toward infinity, the angles associated with these points approach zero degrees, while the angles associated with the points $\pm b$ approach the value $3\pi/2$.

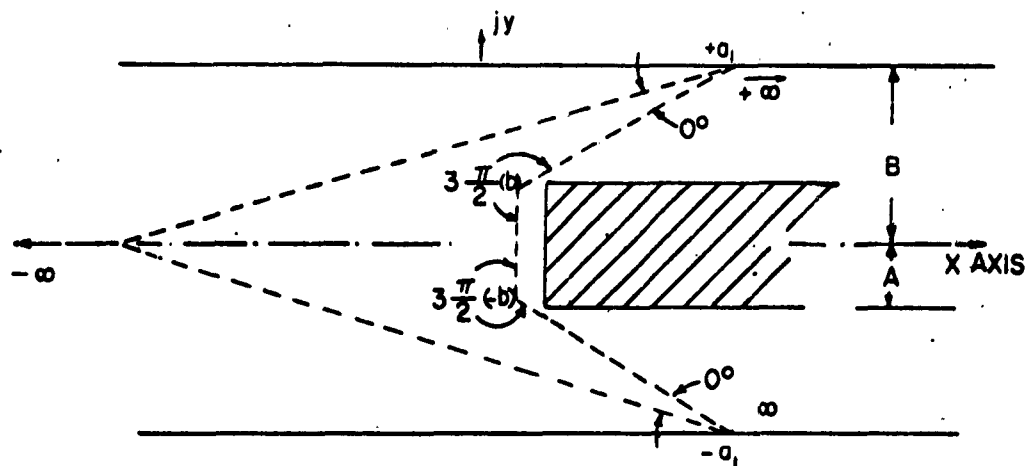


Fig A4-3 Schwarz-Christoffel

Mapping of Stripline: Z plane representation

In the limit, the polygon becomes degenerate and assumes the configuration of the Stripline. It is now necessary to choose the points u_1, \dots, u_n for equation (A3-66). The points u_n are those points in the Z_1 plane corresponding to the points $\pm a_1$ and $\pm b_1$ in the Z plane. We choose the points $z_1 = \pm 1$ to correspond to $z = \pm b_1$ and choose $z_1 = \pm a_1$ to correspond to $z = \pm a_1$. We also choose the image of 0 in the W plane to be infinity in the Z_1 plane. Consideration of Fig A3-4 shows that this drops out the factor $(z - u_n)^{\frac{\alpha}{\pi} - 1}$ connected with the point 0 in equation (A3-66). It is shown in Churchill¹⁷ that only 3 of the u_n are arbitrary. We have picked ± 1 and

infinity as these 3 arbitrary points, leaving $\pm a_1$ to be determined. Inserting these constants into (A3-61), there is obtained:

$$\begin{aligned} \frac{dz}{dz_1} &= M (z_1 - 1)^{\frac{3\pi}{2\pi}-1} (z_1 + 1)^{\frac{3\pi}{2\pi}-1} (z_1 + a_1)^{0-1} (z_1 - a_1)^{0-1} \quad (\text{A4-7}) \\ &= M \frac{(z_1^2 - 1)^{1/2}}{(z_1^2 - a_1^2)} \end{aligned}$$

or in integral form

$$z = M \int \frac{(z_1^2 - 1)^{1/2}}{(z_1^2 - a_1^2)} dz_1 \quad (\text{A4-8})$$

The image of the polygon in the Z_1 plane is shown in Fig A4-4.

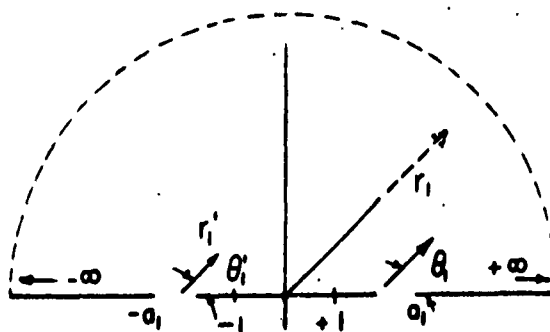


Fig A4-4 Schwarz-Christoffel

Mapping of Stripline: Mapping of Polygon in Z_1 plane

Fig A4-4 is easily understood if the discussion pertinent to Fig A3-4 is remembered. The line segment 0 to $(-a_1)$ in the Z plane corresponds to the segment 0 to $(-a_1)$ in the Z_1 plane; the segment $-a_1$ to $-b_1$ in the Z plane to $-a_1$ to -1 in the Z_1 plane; the segment $-b_1$ to $+b_1$ in the Z plane to -1 to $+1$ in the Z_1 plane; the segment b_1 to a_1 in the Z plane to $+1$ to a_1 in the Z_1 plane and the segment a_1 to 0 in the Z plane to a_1 to 0 in the Z_1 plane. Finally, since the Schwarz-Christoffel transformation maps the polygon onto the upper half of the W plane, the points - infinity and + infinity are joined by a semicircle having an infinite radius.

To evaluate (A4-8), let us first find the values of the constants M and $\pm a_1$. The notation used in this evaluation will be that of Fig A4-4.

To find M, let

$$z_1 = r_1 e^{j\theta_1} \quad (A4-9)$$

Then

$$dz_1 = j r_1 e^{j\theta_1} d\theta_1 = j z_1 d\theta_1 \quad (A4-10)$$

Substituting (A4-10) into (A4-7), we get

$$dz = \frac{j M \sqrt{z_1^2 - 1}}{z_1^2 - a_1^2} (z_1 d\theta) \quad (A4-11)$$

Now let z_1 approach infinity i.e. let r_1 approach infinity.

Assuming z_1 much much greater than 1 and z_1 much much greater than a_1 (A4-11) becomes.

$$dz = j M d\theta \quad (\text{A4-12})$$

Reference to Fig A4-3 and A4-4 show that as z goes from $+jB$ to $-jB$ at the point 0, r_1 rotates through an angle of π radians.
Integrating both sides of (A4-12)

$$\int_{+jB}^{-jB} dz = j M \int_0^\pi d\theta \quad (\text{A4-13})$$

Integrating both sides of (A4-13) and solving for M , we find

$$M = \frac{-2B}{\pi} \quad (\text{A4-14})$$

To determine a_1 , let

$$z_1 = -a_1 + r_1' e^{j\theta_1'} \quad (\text{A4-15})$$

then

$$dz_1 = j r_1' e^{j\theta_1'} d\theta_1' = j z_1' d\theta_1' \quad (\text{A4-16})$$

Substituting (A4-15) and (A4-16) into (A4-7) we obtain:

$$dz = \frac{(-2B)}{\pi} \cdot \frac{(a_1^2 - 2a_1 r_1' e^{j\theta_1'} + r_1'^2 e^{j2\theta_1'} - 1)^{1/2}}{(a_1^2 - 2a_1 r_1' e^{j\theta_1'} + r_1'^2 e^{j2\theta_1'} - 1)^{1/2}} (j r_1' e^{j\theta_1'} d\theta_1') \quad (\text{A4-17})$$

We may simplify the numerator of (A4-17) by observing that as r_1' approaches 0, both $r_1'^2$ and r_1' go to zero very quickly compared to -1. The denominator may be simplified by observing that as r_1' approaches zero, $r_1'^2$ approaches zero much faster than r_1' . Utilizing these observations in (A4-17) and simplifying, we observe that

$$dz = \frac{jB \sqrt{a_1^2 - 1} d\theta}{\pi a_1} \quad (A4-18)$$

From Fig's A4-3 and A4-4, we see that as z goes from $-jB$ to $-jA$ in the Z plane, r_1' rotates from π to 0 in the Z_1 plane. Using these facts we may integrate (A4-18) and solve for a_1 .

The result is:

$$a_1 = \frac{B}{\sqrt{A(2B-A)}} \quad (A4-19)$$

Now that we have determined that constants $\pm a_1$ and M , let us proceed to integrate (A4-8) which is repeated here for convenience.

$$z = \frac{M \int (z_1^2 - 1)^{1/2} dz_1}{(z_1^2 - a_1^2)} \quad (A4-8)$$

To facilitate the integration, let us divide (A4-8) into two parts (after inserting the constant M).

The result is:

$$z = \frac{-2B}{\pi} \int \frac{dz_1}{\sqrt{z_1^2 - 1}} + (a_1^2 - 1) \int \frac{dz_1}{(z_1^2 - a_1^2) \sqrt{z_1^2 - 1}} \quad (A4-20)$$

Consider the first term. We rearrange it to read:

$$\frac{-2B}{\pi} \int \frac{dz_1}{\sqrt{z_1^2 - 1}} = j \frac{2B}{\pi} \int \frac{dz_1}{\sqrt{1 - z_1^2}} \quad (A4-21)$$

Using formula 320.01 of Dwight's Integral Table,²⁶ (A4-21) becomes

$$j \frac{2B}{\pi} \int \frac{dz_1}{\sqrt{1 - z_1^2}} = j \frac{2B}{\pi} \sin^{-1} z_1 \quad (A4-22)$$

The second term of (A4-20) is

$$\frac{-2B (a_1^2 - 1)}{\pi} \int \frac{dz_1}{(z_1^2 - a_1^2) \sqrt{z_1^2 - 1}} \quad (A4-23)$$

We may use formula 367 from Dwight's Integral Tables provided the condition a_1^2 is greater than 1 is met. Therefore, let us examine a practical cross-section of stripline and see whether this condition is met. Utilizing the dimension of one sixteenth inch double clad boards plated with 2 ounce copper, and referring to Fig A4-3, we find A approximately equals 2 mils and B approximately equals 60 mils. Inserting

these results in (A4-19) we find:

$$a_1^2 = 153 \gg 1 \quad (\text{A4-24})$$

The condition a_1^2 greater than 1 is then met and we proceed to use Dwight 387. The result is:

$$\begin{aligned} & \frac{-2B(a_1^2 - 1)}{\pi} \int \frac{dz}{(z_1^2 - a_1^2) \sqrt{z_1^2 - 1}} \\ &= j \frac{2B}{\pi} \frac{(a_1^2 - 1)^{1/2}}{a_1} \tan^{-1} \frac{z_1 \sqrt{a_1^2 - 1}}{a_1 \sqrt{1 - z_1^2}} \end{aligned} \quad (\text{A4-25})$$

The total integration of (A4-8) is therefore:

$$z = \frac{2jB}{\pi} \left[\sin^{-1} z_1 + \frac{(a_1^2 - 1)^{1/2}}{a_1} \tan^{-1} \frac{z_1 \sqrt{a_1^2 - 1}}{a_1 \sqrt{1 - z_1^2}} \right] \quad (\text{A4-26})$$

Several simplifications may be made to equation (A4-26).

By substitution and algebraic manipulation we get the identity:

$$\frac{(a_1^2 - 1)^{1/2}}{a_1} = \frac{B - A}{B} \quad (\text{A4-27})$$

Furthermore a little trigonometric manipulation shows that

$$\tan^{-1} \frac{z_1 \sqrt{a_1^2 - 1}}{a_1 \sqrt{1 - z_1^2}} = \sin^{-1} \frac{z_1 \sqrt{a_1^2 - 1}}{\sqrt{a_1^2 - z_1^2}} \quad (A4-28)$$

Substituting (A4-27) and (A4-28) into (A4-26) there is obtained:

$$z = \frac{2JB}{\pi} \left[\sin^{-1} z_1 + \frac{B-A}{B} \sin^{-1} \frac{z_1 \sqrt{a_1^2 - 1}}{\sqrt{a_1^2 - z_1^2}} \right] \quad (A4-29)$$

We have now transformed the function from the Z or primary plane to the Z_1 or intermediate plane. However, this is not the form we wish for the result. The desired result will be in the form of two parallel planes from which a parallel plate capacity can be found. The required transformation from the Z_1 to the W plane is realized by the relation:

$$z_1 = a_1 \tanh \pi v/2 \quad (A4-30)$$

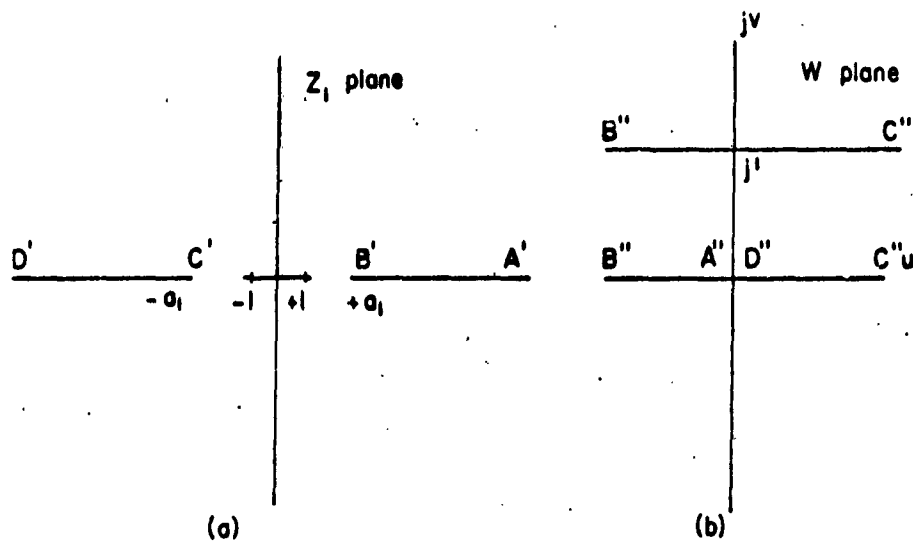


Fig A4-5 Transformation from the Z_1 to the W Plane

The line segment $A'B'$ in the Z_1 plane maps into the segment $A''B''$ in the W plane; the segment $B'C'$ maps into $B''C''$ and $C'D'$ maps into $C''D''$.

We now wish to substitute (A4-30) into (A4-29) and simplify the result: Equation (A4-29) is repeated here for convenience. It is:

$$z = \frac{2JB}{\pi} \left[\sin^{-1} z_1 + \frac{B-A}{B} \sin^{-1} z_1 \frac{\sqrt{a_1^2 - 1}}{\sqrt{a_1^2 - z_1^2}} \right] \quad (\text{A4-29})$$

Consider the 2nd term. Upon substitution of (A4-30) for z_1 and the use of a trigonometric identity we find:

$$\frac{B-A}{B} \sin^{-1} z_1 \cdot \frac{\sqrt{a_1^2 - 1}}{\sqrt{a_1^2 - z_1^2}} = \frac{B-A}{B} \sin^{-1} \sqrt{a_1^2 - 1} \sinh \pi \frac{w}{2} \quad (A4-31)$$

It was previously shown that a_1 is large corresponding to large u in the W plane, (where $w = u + jv$). For large u

$$\sqrt{a_1^2 - 1} \sinh \pi w/2 \rightarrow \frac{\sqrt{a_1^2 - 1} e^{\pi u/2}}{2} \quad (A4-32)$$

as is obvious by expanding $\sinh \pi w/2$ in exponential form and realizing that we are interested in the function on the real axis.

For principal values and remembering that B is much much greater than A , Dwight 507.20 simplifies to:

$$\sin^{-1} x = \pi/2 - j \cosh^{-1} x \quad (A4-33)$$

Substituting (A4-33) and (A4-32) into (A4-29) we find that

$$z = \frac{2jB}{\pi} \left[\pi/2 - j \cosh^{-1} \frac{B}{\sqrt{A(2B-A)}} + \frac{B-A}{B} \right] \quad (A4-34)$$

$$\left(\pi/2 - j \cosh^{-1} \frac{B-A}{\sqrt{A(2B-A)}} e^{\pi u/2} \right]$$

Now we are only interested in the real part of (A4-34). Taking the real part, we get

$$x = \frac{2B}{\pi} \left[\cosh^{-1} \frac{B}{\sqrt{A(2B-A)}} + \frac{B-A}{B} \cosh^{-1} \frac{B-A e^{\pi u/2}}{2\sqrt{A(2B-A)}} \right] \quad (A4-35)$$

Using Dwight 701 and (A4-27), we obtain the relation:

$$\cosh^{-1} a_1 = \tanh^{-1} \frac{B-A}{B} \quad (A4-36)$$

Now remembering the definition of a_1 as given in (A4-19), we may substitute (A4-36) into (A4-35) with the result:

$$x = \frac{2B}{\pi} \left[\tanh^{-1} \frac{B-A}{B} + \frac{B-A}{B} \cosh^{-1} \frac{B-A e^{\pi u/2}}{2\sqrt{A(2B-A)}} \right] \quad (A4-37)$$

Now we wish to solve (A4-37) for u . This can be done by transposing and taking the cosh of both sides. The result is:

$$\frac{(B-A) e^{\pi u/2}}{2\sqrt{A(2B-A)}} = \cosh \left[\frac{\pi x}{2(B-A)} - \frac{B}{B-A} \tanh^{-1} \frac{B-A}{B} \right] \quad (A4-38)$$

Clearing and taking the ln of both sides

$$u = \frac{2}{\pi} \ln \left[\frac{2\sqrt{A(2B-A)}}{B-A} \right] \cosh \left[\frac{\pi x}{2(B-A)} - \frac{B}{B-A} \tanh^{-1} \frac{B-A}{B} \right] \quad (A4-39)$$

Now by definition:

$$\cosh = \frac{e^x + e^{-x}}{2} \quad (A4-40)$$

In actual practice $x \gg B-A$ (i.e. the width of the ground planes is much greater than the distance between ground planes). Therefore the ϵ^{-x} term in (A4-40) is negligible. Making this assumption we may make the following statement:

$$\cosh \left[\frac{\pi x}{2(B-A)} - \frac{B}{B-A} \tanh^{-1} \frac{B-A}{B} \right] \quad (x \gg B-A)$$

$$= \epsilon \left(\frac{\pi x}{2(B-A)} + \frac{B}{B-A} \tanh^{-1} \frac{B-A}{B} \right) \quad (A4-41)$$

Using (A4-41) in (A4-39), we see that

$$u = 2/\pi \ln \left[\sqrt{\frac{A(2B-A)}{B-A}} \epsilon \left(\frac{\pi x}{2(B-A)} + \frac{B}{B-A} \tanh^{-1} \frac{B-A}{B} \right) \right] \quad (A4-42)$$

We may simplify (A4-42) to read

$$u = 2/\pi \ln \sqrt{\frac{A(2B-A)}{B-A}} + \frac{x}{B-A} + \frac{2B}{\pi(B-A)} \tanh^{-1} \frac{B-A}{B} \quad (A4-43)$$

We must now find out what x would be if there were no fringing effect present. If the fringing effect is neglected, the capacitance in the Z and W planes must be the same. We may therefore equate the expression for parallel plate capacitance in the Z and W planes.

$$\frac{\epsilon_0 \epsilon_r A_w}{d_w} = \frac{\epsilon_0 \epsilon_r A_z}{d_z} \quad (A4-44)$$

where the subscripts indicate the plane of applicability.

For unit length (A4-44) simplifies to

$$x = (B-A) u \quad (A4-45)$$

Multiplying sides of (A4-43) by (B-A) we get

$$(B-A) U = 2/\pi (B-A) \ln \frac{\sqrt{A(2B-A)}}{B-A} + x \\ + \frac{2B}{\pi} \tanh^{-1} \frac{B-A}{B} \quad (A4-46)$$

Solving (A4-46) for x we obtain:

$$x = (B-A) U - 2/\pi (B-A) \ln \frac{\sqrt{A(2B-A)}}{B-A} - \frac{2B}{\pi} \tanh^{-1} \frac{B-A}{B} \quad (A4-47)$$

Since in the ideal case of no fringing

$$x = (B-A) U \quad (A4-45)$$

the other terms in (A4-47) must be due to the fringing effect i.e.

$$x + \Delta x = (B-A) U \quad (A4-48)$$

Therefore

$$\Delta x = 2/\pi \left[(B-A) \ln \frac{\sqrt{A(2B-A)}}{B-A} + B \tanh^{-1} \frac{B-A}{B} \right] \quad (A4-49)$$

We may put (A4-49) in a more useful form through the identity

$$\tanh^{-1} x = \ln \left(\frac{1+x}{1-x} \right)^{1/2} \quad (A4-50)$$

Utilizing (A4-50) in (A4-49), we find that

$$\Delta x = 2/\pi \left[B \ln \frac{2B-A}{B-A} - A \frac{\ln \sqrt{A(2B-A)}}{B-A} \right] \quad (A4-51)$$

We may now find an expression for fringing capacity C_f' by inserting (A4-51) into the expression for parallel plate capacitance which is:

$$C = \frac{\epsilon_0 \epsilon_r A}{d} \quad (A4-52)$$

Upon making the substitution of (A4-51) into (A4-52) and remembering that we are considering capacitance per unit length, we get

$$C_f' = \frac{8.842 \times 10^{-2}}{d} \epsilon_r \left[\frac{2}{\pi} B \ln \frac{2B-A}{B-A} - A \frac{\ln \sqrt{A(2B-A)}}{B-A} \right] \frac{\text{mmf}}{\text{cm}} \quad (A4-53)$$

In order to make (A4-53) agree with the notation of the literature, it is necessary to redefine A, B, and d.

Cohn defines his dimensions as shown in Fig A4-6.

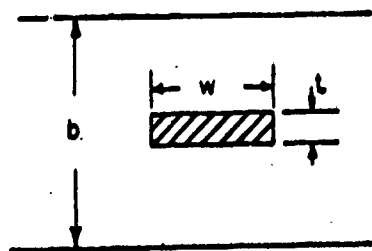


Fig A4-6 Cross Section of Stripline As Given by Cohn

Observation of Fig A4-3 and A4-6 indicates the following equivalence:

$$d = \frac{b-t}{2} \quad (\text{A4-54})$$

$$A = t/2 \quad (\text{A4-55})$$

$$B = b/2 \quad (\text{A4-56})$$

If (A4-54) through (A4-56) are substituted in (A4-5) and a little algebraic manipulation performed, Cohn's result is obtained. It is:

$$cr' = \frac{8.842 \times 10^{-2}}{\pi} \epsilon_r \left[\frac{2}{1-t/b} \ln \left(\frac{1}{1-t/b} + 1 \right) - \left(\frac{1}{1-t/b} - 1 \right) \ln \left(\left(\frac{1}{1-t/b} \right)^2 - 1 \right) \right] \frac{\text{mm}^2}{\text{cm}} \quad (\text{A4-57})$$

Equation (A4-57) has been put in graphical form and is shown as Fig A4-7.

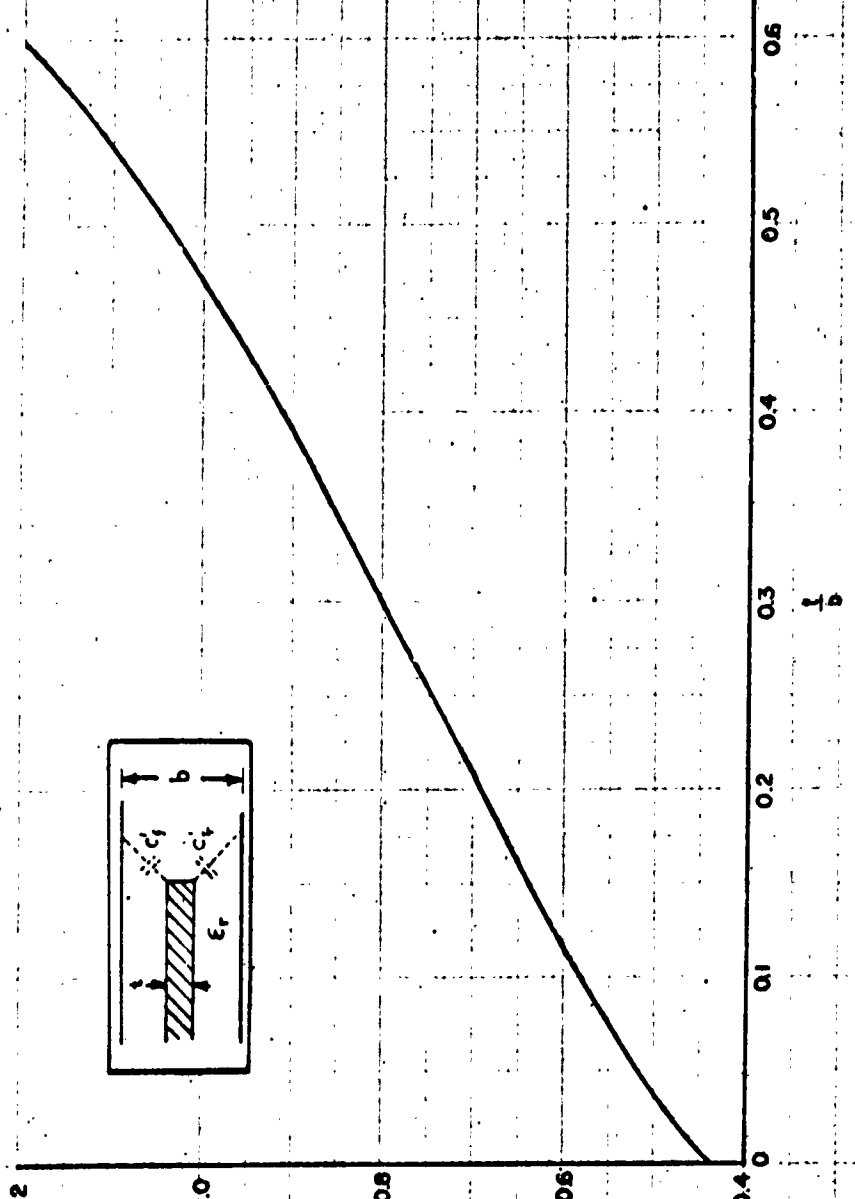


Fig. A4-7. EXACT FRINGING CAPACITANCE FOR A SEMI-INFINITE PLATE CENTERED
BETWEEN PARALLEL GROUND PLANES.

APPENDIX V

POLYGONAL CROSS SECTIONS

Consider cross sections whose peripheral curve is a closed polygon with n sides and external angles, μ_r . To map the outside of the polygon in the z -plane on the outside of the unit circle in the δ -plane, we shall first map the region outside the polygon on the upper half of the t -plane. To do this, an extended version of the Schwarz-Christoffel transformation will be used which is not quite the same as the well-known Schwarz-Christoffel transformation which maps the interior of a closed polygon onto an upper half-plane. The reason for this is that the point in the t -plane which corresponds to the points at infinity in the z -plane must now be considered. It may be shown* that the mapping function for transforming the region outside a closed polygon in the z -plane to the upper half of the t -plane is given by

* O. D. Kellogg, Foundations of Potential Theory,
Julius Springer, Berlin, 1929.

$$z - z_0 = C \int \frac{\prod_{r=1}^n (t - t_{1r})^{\frac{\mu_r}{\pi} - 1}}{(t - \beta)^2 (t - \beta^*)^2} dt \quad (A5-1)$$

where the t_{1r} are the points on the real axis of t corresponding to the vertices of the polygon, C and z_0 are constants, β is the point in the upper half of the t -plane corresponding to $z = \infty$, and the asterisk denotes complex conjugate. Since the sum of the exterior angles of a polygon with n vertices is $(n + 2)\pi$, the necessary condition on the angles is

$$\sum_{r=1}^n \frac{\mu_r}{\pi} - 1 = 2 \quad (A5-2)$$

Now let $\beta = i$, and

$$\delta = \frac{i+t}{i-t}, t = t_1 + it_2 = \frac{i(\delta - 1)}{\delta + 1} \quad (A5-3)$$

so that $t = i$ corresponds to $\delta = \infty$. But $t = \beta = i$ corresponds to $z = \infty$, so that infinitely remote regions in the z -plane and δ -plane correspond. Furthermore,

$$|\delta| = \left| \frac{i+t}{i-t} \right| = \sqrt{\frac{t_1^2 + t_2^2 + 1 + 2t_2}{t_1^2 + t_2^2 + 1 - 2t_2}}$$

so that, for $t_2 = 0$, $|\delta| = 1$. Thus, the t_1 axis is transformed into the unit circle in the δ -plane. Moreover, for $t_2 > 0$, $|\delta| > 1$, that is, the upper half-plane of t goes over into the outside of the unit circle $|\delta| = 1$. Hence, the outside of the polygon in the z -plane is transferred to the outside of the unit circle in the δ -plane, such that infinitely remote points in the two planes correspond.

With the transformation equation (A5-3), the mapping function equation (A5-1) becomes^{*}

$$z - z_0 = a_1 \int_{\delta}^{\infty} \frac{\prod_r^{\mu_r} (\delta - \delta_r)^{\frac{\mu_r}{\pi} - 1}}{\delta^2} d\delta \quad (A5-4)$$

in which the δ_r 's must satisfy the conditions $|\delta_1| = |\delta_2| = \dots = |\delta_n| = 1$ since they lie on the unit circle. Expanding the integrand of equation (A5-4) into inverse powers of δ and using equation (A5-2), we obtain

$$\frac{dz}{d\delta} = a_1 - a_1 \left[\frac{\left(\frac{\mu_1}{\pi} - 1 \right) \delta_1 + \left(\frac{\mu_2}{\pi} - 1 \right) \delta_2 + \dots + \left(\frac{\mu_n}{\pi} - 1 \right) \delta_n}{\delta} - \frac{\dots}{\delta^n} - \dots \right] \quad (A5-5)$$

and, therefore, upon integration, a logarithmic term will arise unless the condition

* For an alternative derivation of this transformation, see P. Frank and R. V. Mises, Differentialgleichungen der Physik, Vol II, p.658-662. Friederich Vieweg and Sohn, Brunswick, Germany, 1935, Mary S. Rosenberg, New York, 1943.

$$\sum_{r=1}^n \delta_r \left(\frac{\mu}{\pi} r - 1 \right) = 0 \quad (A5-6)$$

is satisfied. This condition must be fulfilled in order that the mapping be conformal at ∞ . Integration of equation (A5-5) yields a series development of the form

$$z = a_1 \delta + a_0 + \frac{a_{-1}}{\delta} + \frac{a_{-2}}{\delta^2} + \dots$$

which is valid for large δ . Since the polygon is mapped onto the unit circle, it follows that a_1 is the equivalent radius of the polygon.

We shall restrict ourselves here to the calculation of the equivalent radius of rectangular cross sections. In this case, the angles have a common value $\mu = \frac{3}{2}\pi$, so that $\frac{\mu}{\pi} - 1 = \frac{1}{2}$. The mapping is shown on Fig A5-1. From the condition equation (A5-6), and symmetry considerations, it may be inferred that the points δ_r on the unit circle corresponding to the vertices form an inscribed rectangle. Therefore, we set

$$\delta_1 = e^{i\theta_0}, \delta_2 = e^{i(\pi - \theta_0)}, \delta_3 = e^{i(\pi + \theta_0)}, \delta_4 = e^{-i\theta_0},$$

and obtain

$$\sum_{r=1}^n \delta_r \left(\frac{\mu_r}{\pi} - 1 \right) = 0 \quad (A5-6)$$

is satisfied. This condition must be fulfilled in order that the mapping be conformal at ∞ . Integration of equation (A5-5) yields a series development of the form

$$z = a_1 \delta + a_0 + \frac{a_{-1}}{\delta} + \frac{a_{-2}}{\delta^2} + \dots$$

which is valid for large δ . Since the polygon is mapped onto the unit circle, it follows that a_1 is the equivalent radius of the polygon.

We shall restrict ourselves here to the calculation of the equivalent radius of rectangular cross sections. In this case, the angles have a common value $\mu = \frac{3}{2}\pi$, so that $\frac{\mu}{\pi} - 1 = \frac{1}{2}$. The mapping is shown on Fig A5-1. From the condition equation (A5-6), and symmetry considerations, it may be inferred that the points δ_r on the unit circle corresponding to the vertices form an inscribed rectangle. Therefore, we set

$$\cdot \delta_1 = e^{i\theta_0}, \delta_2 = e^{i(\pi-\theta_0)}, \delta_3 = e^{i(\pi+\theta_0)}, \delta_4 = e^{-i\theta_0},$$

and obtain

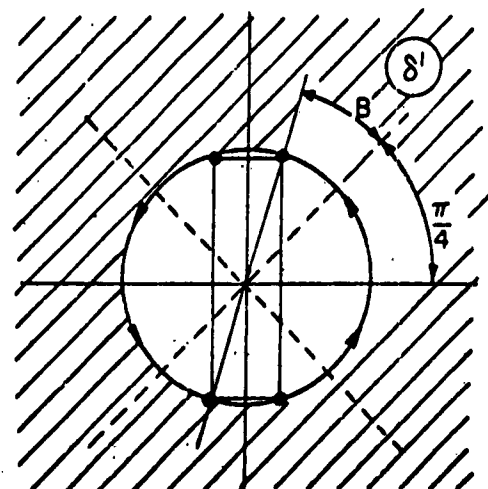
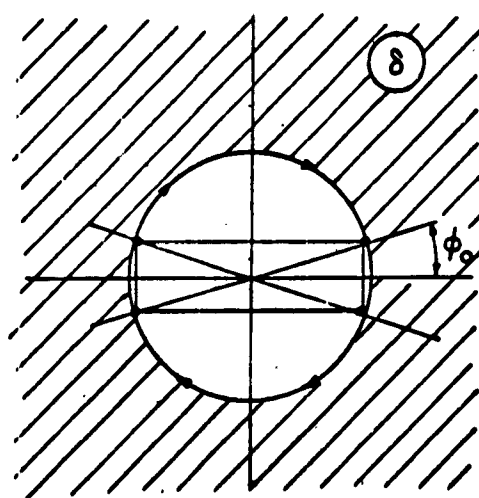
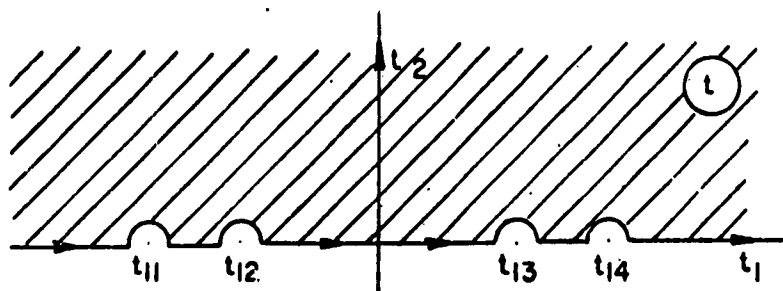
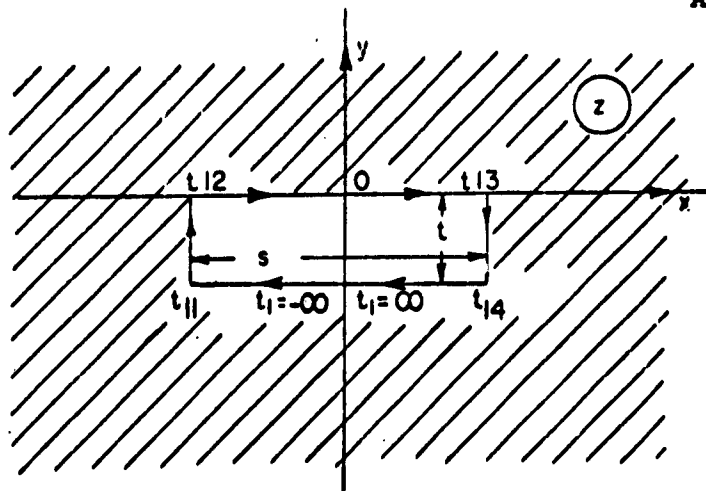


Fig. A5-1 MAPPING OF THE REGION OUTSIDE A RECTANGLE ON THE
OUTSIDE OF A CIRCLE

$$\prod_{r=1}^4 (\delta - \delta_r)^{\frac{1}{2}} = \sqrt{\delta^4 + 1 - 2\delta^2 \cos 2\theta_0}$$

$$z - z_0 = a_1 \int \frac{\sqrt{\delta^2 + \delta^{-2} - \cos 2\theta_0}}{\delta} d\delta$$

Let us integrate along the unit circle; we set $\delta = e^{i\phi}$ and the transformation becomes

$$z - z_0 = ia_1 \int \sqrt{2 \cos 2\phi - 2 \cos 2\theta_0} d\phi$$

Integrating ϕ from $\frac{\pi}{2}$ to 0, we obtain (see Fig A5-1)

$$s - it = i 2a_1 \int_{\pi/2}^0 \sqrt{2 \cos 2\phi - 2 \cos 2\theta_0} d\phi$$

where s is the width of the rectangle, and t the thickness.

With the transformation

$$\psi = -\phi + \frac{\pi}{2}$$

this becomes

$$s - it = 2\sqrt{2} a_1 \int_0^{\pi/2} \sqrt{\cos 2\psi - \cos 2\psi_0} d\psi$$

Making the substitution

$$\psi_0 = \frac{\pi}{4} + \beta$$

we obtain finally

$$s - it = 2\sqrt{2} a_1 \int_0^{\pi/2} \sqrt{\cos 2\psi + \sin 2\beta} d\psi \quad (A5-7)$$

The integral in equation (A5-7) is an elliptic integral and may be expressed in terms of complete elliptic integrals of the first and second kinds. The reduction to complete elliptic integrals is carried out in the appendix. The result is

$$s - it = a_1 \left[\frac{4E(\sqrt{\frac{1+\sin 2\beta}{2}})}{\sqrt{\frac{1+\sin 2\beta}{2}}} - 2(1-\sin 2\beta) K(\sqrt{\frac{1+\sin 2\beta}{2}}) \right] \\ - ia_1 \left[\frac{4E(\sqrt{\frac{1-\sin 2\beta}{2}})}{\sqrt{\frac{1-\sin 2\beta}{2}}} - 2(1+\sin 2\beta) K(\sqrt{\frac{1-\sin 2\beta}{2}}) \right] \quad (A5-8)$$

where

$$K(k) = \int_0^1 \frac{dt}{\sqrt{(1-t^2)(1-k^2t^2)}}$$

$$E(k) = \int_0^1 \frac{1 - k^2 t^2}{\sqrt{(1-t^2)(1-k^2t^2)}} dt$$

with $k \leq 1$, are complete elliptic integrals of the first and second kinds respectively, and are tabulated in the literature.*

From equation (A5-8)

$$s = a_1 \left[4E\left(\sqrt{\frac{1 + \sin 2\beta}{2}}\right) - 2(1 - \sin 2\beta) K\left(\sqrt{\frac{1 + \sin 2\beta}{2}}\right) \right] \quad (\text{A5-9})$$

$$t = a_1 \left[4E\left(\sqrt{\frac{1 - \sin 2\beta}{2}}\right) - 2(1 + \sin 2\beta) K\left(\sqrt{\frac{1 - \sin 2\beta}{2}}\right) \right]$$

and thus,

* E. Jahnke and F. Emde, Tables of Functions, Dover Publications, New York 1945.

$$\frac{t}{s} = \frac{2E(\sqrt{\frac{1 - \sin 2\beta}{2}}) - (1 + \sin 2\beta) K(\sqrt{\frac{1 - \sin 2\beta}{2}})}{2E(\sqrt{\frac{1 + \sin 2\beta}{2}}) - (1 - \sin 2\beta) K(\sqrt{\frac{1 + \sin 2\beta}{2}})} \quad (\text{A5-10})$$

Equation (A5-10) serves to determine β from the ratio of t to s , and equation (A5-9) gives the equivalent radius a_1 in terms of s or t .

Particular cases are:

1. square cross section, $\beta = 0$

$$s = t = a_1 \left[\frac{4E(1/\sqrt{2})}{2K(1/\sqrt{2})} \right]$$

so that

$$a_{eq} = a_1 = 0.59025 s \quad (\text{A5-11})$$

that is

the equivalent radius = 0.59025 side of the square

2. thin strip, $\beta = \frac{\pi}{4}$

$$t = a_1 [2E(0) - 2K(0)] = 0$$

$$s = 4a_1 E(1) = 4a_1$$

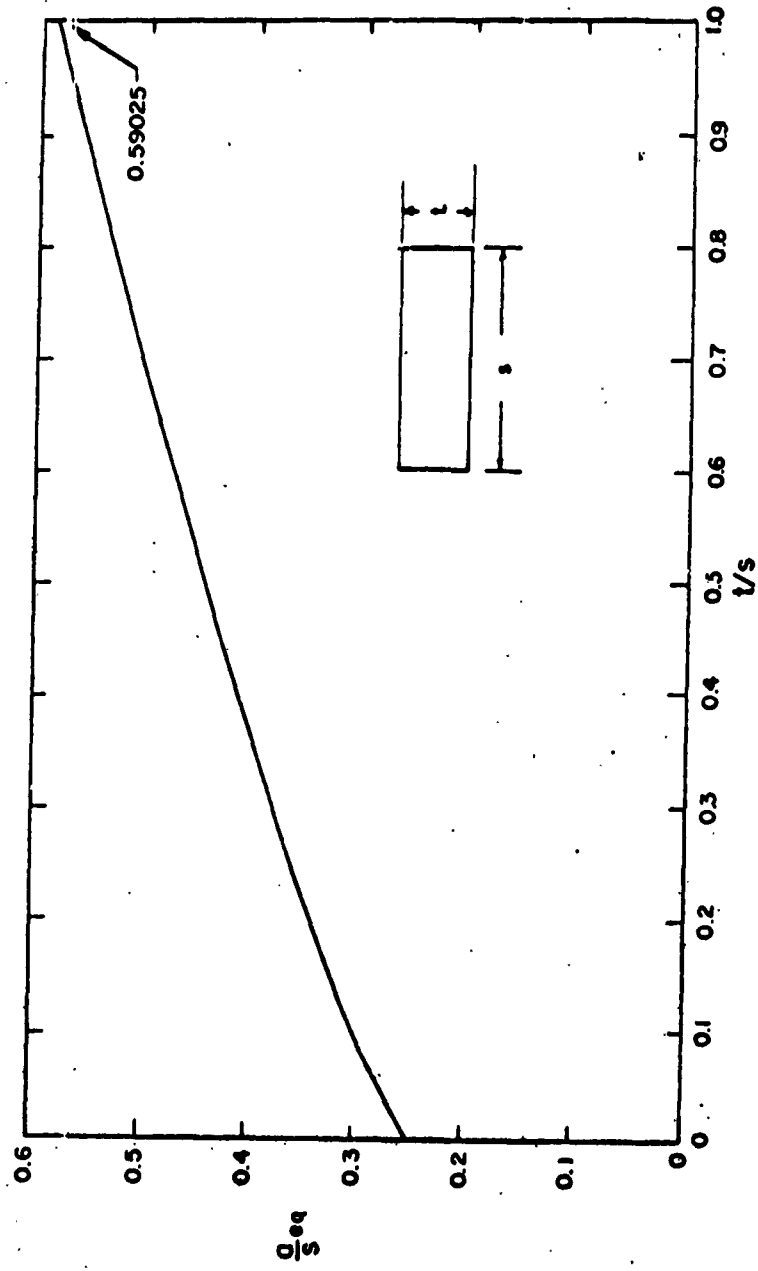
so that

$$a_1 = \frac{1}{4} s$$

that is,

the equivalent radius = 1/4 width of the strip. (A5-12)

The ratio of the equivalent radius to the width of the rectangular cross section is plotted on Fig A5-2 for values of the ratio of thickness to width from 0 to 1.



THE EQUIVALENT RADIUS q_{eq} OF A RECTANGLE AS A FUNCTION OF THE
RATIO OF THICKNESS t TO WIDTH s .

Fig. A5-2

APPENDIX V A

Reduction of $2\sqrt{2} \int_0^{\pi/2} \sqrt{\cos 2\psi + \sin 2\beta} d\psi$ to complete elliptic integrals.

We have

$$\begin{aligned} 2\sqrt{2} \int_0^{\pi/2} \sqrt{\cos 2\psi + \sin 2\beta} d\psi &= 2\sqrt{2} \int_0^{\pi/2} \sqrt{1 + \sin 2\beta - 2 \sin^2 \psi} d\psi \\ &= 2\sqrt{2} \sqrt{1 + \sin 2\beta} \int_0^{\pi/2} \sqrt{1 - \frac{2}{1 + \sin 2\beta} \sin^2 \psi} d\psi \quad (\text{AA-1}) \end{aligned}$$

Let

$$\sin \psi = z \quad d\psi = \frac{dz}{\sqrt{1 - z^2}}$$

then equation (AA-1) becomes

$$2\sqrt{2} \sqrt{1 + \sin 2\beta} \int_0^1 \frac{\sqrt{1 - \frac{2}{1 + \sin 2\beta} z^2}}{\sqrt{1 - z^2}} dz \quad (\text{AA-2})$$

Now set

$$x = \sqrt{\frac{2}{1 + \sin 2\beta}} z$$

then equation (AA-2) becomes

$$2(1 + \sin 2\beta) \int_0^{\sqrt{\frac{2}{1 + \sin 2\beta}}} \frac{\sqrt{1 - x^2}}{\sqrt{1 - \frac{1 + \sin 2\beta}{2} x^2}} dx$$

$$= 2(1 + \sin 2\beta) \int_0^{\sqrt{\frac{2}{1 + \sin 2\beta}}} \frac{(1 - x^2)}{\sqrt{(1 - x^2)(1 - \frac{1 + \sin 2\beta}{2} x^2)}} dx$$

$$= 4(1 + \sin 2\beta) \int_0^{\sqrt{\frac{2}{1 + \sin 2\beta}}} \frac{(1 - \frac{1}{2} x^2) dx}{\sqrt{(1 - x^2)(1 - \frac{1 + \sin 2\beta}{2} x^2)}}$$

$$- 2(1 + \sin 2\beta) \int_0^{\sqrt{\frac{2}{1 + \sin 2\beta}}} \frac{dx}{\sqrt{(1 - x^2)(1 - \frac{1 + \sin 2\beta}{2}x^2)}}$$

$$= 4 \int_0^{\sqrt{\frac{2}{1 + \sin 2\beta}}} \frac{(1 - \frac{1 + \sin 2\beta}{2}x^2) dx}{\sqrt{(1 - x^2)(1 - \frac{1 + \sin 2\beta}{2}x^2)}}$$

$$- 2(1 - \sin 2\beta) \int_0^{\sqrt{\frac{2}{1 + \sin 2\beta}}} \frac{dx}{\sqrt{(1 - x^2)(1 - \frac{1 + \sin 2\beta}{2}x^2)}}$$

$$= 4 \left[E\left(\sqrt{\frac{1 + \sin 2\beta}{2}}\right) + i E_1\left(\sqrt{\frac{1 + \sin 2\beta}{2}}\right) \right]$$

$$- 2(1 - \sin 2\beta) \left[K\left(\sqrt{\frac{1 + \sin 2\beta}{2}}\right) + i K'\left(\sqrt{\frac{1 + \sin 2\beta}{2}}\right) \right] \quad (\text{AA-3})$$

where

$$K(k) = \int_0^1 \frac{dt}{\sqrt{(1-t^2)(1-k^2t^2)}}$$

$$E(k) = \int_0^1 \frac{1-k^2t^2}{\sqrt{(1-t^2)(1-k^2t^2)}} dt$$

with $k \leq 1$, are complete elliptic integrals of the first and second kinds respectively, associated with the modulus k ;

$$K'(k) = K(k') = \int_0^1 \frac{dt}{\sqrt{(1-t^2)(1-k'^2t^2)}} \quad (\text{AA-4})$$

is the complete elliptic integral of the first kind associated with the complementary modulus k' defined by

$$k^2 + k'^2 = 1 \quad (\text{AA-5})$$

and it may be shown that*

$$iK' = \int_1^{1/k} \frac{dt}{\sqrt{(1-t^2)(1-k'^2t^2)}}$$

* Whittaker and Watson, Modern Analysis, Cambridge University Press, 1927.

so that

$$K + iK' = \int_0^{1/k} \frac{dt}{\sqrt{(1-t^2)(1-k^2t^2)}}$$

E_1 is defined by

$$iE_1 = \int_1^{1/k} \frac{1 - k^2 t^2}{\sqrt{(1-t^2)(1-k^2t^2)}} dt$$

and may be reduced to complete elliptic integrals of the first and second kind as follows:

$$iE_1 = \int_1^{1/k} \frac{1 - k^2 x^2}{\sqrt{(1-x^2)(1-k^2x^2)}} dx$$

$$= \int_1^{1/k} \frac{dx}{\sqrt{(1-x^2)(1-k^2x^2)}} - \int_1^{1/k} \frac{k^2 x^2}{\sqrt{(1-x^2)(1-k^2x^2)}} dx$$

The first integral is $iK'(k)$. In the second integral, we let

$$y = \frac{1}{kx} \quad dx = -\frac{1}{ky^2} dy$$

and we obtain

$$\int_1^{1/k} \frac{k^2 x^2}{\sqrt{(1-x^2)(1-k^2 x^2)}} dx = \int_1^{1/k} \frac{y^2}{y^2 \sqrt{(y^2-1)(k^2 y^2-1)}} dy$$

Now we set

$$y^2 = \frac{1}{1 - k'^2 t^2}, \quad \frac{dy}{dt} = \frac{k'^2 t}{(1 - k'^2 t^2)^{3/2}}$$

and we obtain after a few manipulations

$$\int_1^{1/k} \frac{dy}{y^2 \sqrt{(y^2-1)(k^2 y^2-1)}} = i \int_0^1 \frac{\sqrt{1 - k'^2 t^2}}{\sqrt{1 - t^2}} dt$$

$$= iE(k')$$

Hence,

$$iE_1 = iK'(k) - iE(k')$$

or

$$iE_1 = iK(k') - iE(k') \quad (\text{AA-6})$$

Substituting equation (AA-6) in equation (AA-3) and using equations (AA-4) and (AA-5) we get finally

$$2\sqrt{2} \int_0^{\pi/2} \sqrt{\cos 2\psi + \sin 2\beta} d\psi$$

$$= 4E \left(\sqrt{\frac{1 + \sin 2\beta}{2}} \right) - 2(1 + \sin 2\beta) K \left(\sqrt{\frac{1 + \sin 2\beta}{2}} \right)$$

$$- i \left[4E \left(\sqrt{\frac{1 - \sin 2\beta}{2}} \right) - 2(1 + \sin 2\beta) K \left(\sqrt{\frac{1 - \sin 2\beta}{2}} \right) \right]$$

(AA-7)

ABSTRACT

Impedance measurements in Stripline at microwave frequencies require the use of a slotted line. Since no slotted lines in Stripline are commercially available, it is either necessary to build a laboratory model in Stripline or to use a coaxial slotted line and a transition to Stripline. Since commercial coaxial Slotted Lines are readily available and a Stripline laboratory model would be expensive and time consuming to produce, it was decided that the coaxial slotted line with its attendant transition was the best approach. It is in this transition that the problem arises. The junction introduces a discontinuity which must be taken into account. By making the rather good approximation that the junction is lossless, a bilinear transformation may be used to relate the two sides of the junction. A theoretical derivation is made and an example worked to illustrate the practical aspects of the solution. It was found that, while this method cannot be used to find the Characteristic Impedance of Stripline, if the Characteristic Impedance is known, the impedance of any unknown Stripline load can be found.

7

TABLE OF CONTENTS

Chapter		Page
III	Measurement of Unknown stripline Loads Through a Junction	
	A. Impedance	
	1. The Problem	35
	2. Transformation of the Smith Chart Through Lossless Junctions	
	a. The Smith Chart: Derivation of Loci of Constant Normalized Resistance and Reactance	36
	b. Transformation of Circles of Constant V.S.W.R.	40
	c. Transformation of Lines of Constant Phase Angles	45
	d. Transformation of Circles of Constant Resistance and Reactance	47
	B. Determination of Unknown Impedance	
	1. The Problem	51
	2. Determination of the Iconocenter . .	52
	3. An Example Illustrating the Technique	61
	C. Conclusions	68
	Bibliography	70

TABLE OF CCNTENTS

Appendix VI	Relation Between the Iconocenter and the Crossover Point	A78
--------------------	---	------------

(1)

LIST OF FIGURES

Figure	Page
3-1 Definition of Reference Planes 1 and 2	37
3-2 Relation between the representation of a reflection coefficient on the Smith Chart (W) and on the projective chart (\bar{W})	53
3-3 Transformation β and β^{-1} . Construction of \bar{W} from W or of W from \bar{W}	54
3-4 Loci on the projective chart and on the Smith and Carter Charts of constant resistance R , reactance X , impedance magnitude $ Z $ and impedance phase $\hat{\angle} Z$	55
3-5 Definition and evaluation of the Hyperbolic Distance (AB)	56
3-6 Reflectance of four open circuits spaced one eighth wavelength apart on the stripline side of the junction	59
3-7 Reflectances of four open circuits spaced one eighth wavelength apart after being transformed through a lossless junction	60
3-8 Transformation from the Projective to Smith Chart representation	61
3-9 Test Setup for Measurement of an Unknown Load	62
3-10 Determination of the Iconocenter	69

LIST OF FIGURES

Figure		Page
A6.1	Transformation from the Crossover Point to the Iconocenter	A78
A6.2	Relation Between the Iconocenter and the Crossover Point	A79

CHAPTER III

MEASUREMENT OF UNKNOWN STRIPLINE LOADS THROUGH A JUNCTION

A. Impedance.

1. The Problem.

Measurement of Impedance at Microwave frequencies is commonly performed through the use of a slotted line. While there are commercially available coaxial and waveguide slotted lines, none exists for the measurement of Stripline. Several laboratory models have appeared in the literature but the expense of manufacture is not justified in light of an existing method of measurement utilizing a coaxial slotted line.

When a coaxial slotted line is used, the problem becomes one of measuring through a junction. The junction in question of course is the transition between coaxial line and the section of Stripline to be measured. The parameters measured with the slotted line are those on the coaxial side of the junction. However, we are interested not in the coaxial side of the junction, but in the Stripline side of the junction. The question to be answered is then "Knowing the parameters in the coaxial side of the junction, how can we find the same parameters in the Stripline side of the junction?" The answer to this question lies in a conformal transformation between the

two sides of the junction. In the sections to follow, this transformation will be developed and the results used to measure impedance of an unknown load in stripline.

2. Transformation of the Smith Chart Through Lossless Junctions.²⁷

a. The Smith Chart: Derivation of Loci of Constant Normalized Resistance and Reactance.

The Smith Chart is a coordinate system representing reflection coefficient as a complex variable.

For a reflection coefficient of constant amplitude and varying phase, the plot is a circle centered at the origin. The angle subtended by the radius vector to a point on the circle and a reference axis through the origin of the diagram represents the phase angle of the reflection coefficient. One complete rotation about the origin represents a distance of one-half wavelength.

The circle representing unit-amplitude reflection contains the entire diagram. The general equation of circles of constant-amplitude reflection coefficient is written in the notation of complex variables as

$$\bar{\rho\rho} = k^2 \quad (3-1)$$

where:

ρ = Complex reflection coefficient in Plane 1.

$\bar{\rho}$ = Complex conjugate of ρ

k = radius when vector ρ varies in such a manner as to describe a circle (< 1)

A few words are necessary concerning "planes" 1 and 2 which will be referred to in this paper. Since any microwave circuit is one having distributed parameters, it is not possible to pick up two pair of leads and specify them as input and output ports. We therefore establish our input and output ports by means of planes and attempt to find an equivalent circuit for the microwave configuration between these planes. We shall define plane 1 as the reference plane on the stripline side of the junction and plane 2 as the reference plane in the coaxial side of the junction. Figure 3-1 illustrates reference planes 1 and 2.

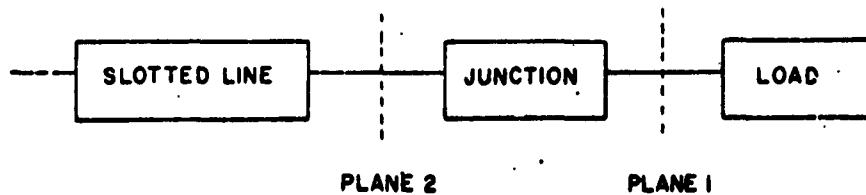


Fig 3-1 Definition of Reference Planes 1 and 2

Voltage Standing Wave Ratio is related to ρ by the expression

$$\text{V.S.W.R.} = \frac{1 + \sqrt{\rho\rho}}{1 - \sqrt{\rho\rho}} \quad (3-2)$$

The radial line representing reflection coefficients of constant phase and varying amplitude may be written in the form

$$\frac{\rho}{\bar{\rho}} = l \quad (l \text{ represents length, not the number one}) \quad (3-3)$$

If ρ is to be written in the form

$$\rho = \sqrt{\rho\rho} e^{j\phi} \quad (3-4)$$

then:

$$l = e^{j2\phi} \quad (3-5)$$

The normalized impedance z at any plane in a transmission line is related to the reflection coefficient at the plane by

$$z = \frac{1 + \rho}{1 - \rho} \quad (3-6)$$

Now z may be written as

$$z = r + jx \quad (3-7)$$

where

z = normalized impedance at any plane

r = normalized resistance at any plane

x = normalized reactance at any plane

If equation (3-6) has its numerator and denominator multiplied by $(1-\bar{\rho})$ and the result split into its real and imaginary

parts, we can identify the real and imaginary parts of equation (3-6) with r and x respectively. The result is:

$$r = \frac{1 - \rho\bar{\rho}}{1 + \rho\bar{\rho} - \rho - \bar{\rho}} \quad (3-8)$$

$$jx = \frac{\rho - \bar{\rho}}{1 + \rho\bar{\rho} - \rho - \bar{\rho}} \quad (3-9)$$

Equation (3-8) may be rearranged to read

$$\rho\bar{\rho} - \frac{r}{1+r} \rho - \frac{r}{1+r} \bar{\rho} - \frac{(1-r)}{(1+r)} = 0 \quad (3-10)$$

The general equation of the circle described by the vector ρ measured from the origin, having radius k with center displaced from the origin by the vector a is

$$(\rho - a)(\bar{\rho} - \bar{a}) = k^2 \quad (3-11)$$

or

$$\rho\bar{\rho} - a\bar{\rho} - \bar{a}\rho + a\bar{a} = k^2$$

If equation (3-10) is compared to equation (3-11) and r is assumed constant, we can see that equation (3-10) represents a circle for which

$$a = \frac{r}{1+r} \quad (3-12)$$

$$k = \frac{1}{1+r} \quad (3-13)$$

In a similar manner equation (3-9) may be rearranged to read

$$\rho \bar{\rho} - (1 - j/x) \rho - (1 + j/x) \bar{\rho} + 1 = 0 \quad (3-14)$$

If x is assumed constant and equation (3-14) is compared to equation (3-11), we see that (3-14) represents a circle for which

$$a = 1 + j/x \quad (3-15)$$

$$k = 1/x \quad (3-16)$$

Equation (3-10) and (3-14) thus represent the familiar circles of constant r and constant x that are found on any Smith Chart.

b. Transformation of Circles of Constant V.S.W.R.

It is well known that the reflection coefficients of any two planes in a transmission line are bilinear functions, related by an equation of the general form

$$\sigma = \frac{ap + b}{cp + 1} \quad \text{or} \quad \rho = \frac{-\sigma + b}{c\sigma - a} \quad (3-17)$$

where

ρ = Complex reflection coefficient in Plane 1.

σ = Complex reflection coefficient in Plane 2.

a,b,c = complex constants

Utilizing equation (3-17), the relation (3-1) may be written:

$$\left(\frac{-\sigma + b}{c\sigma - a} \right) \times \left(\frac{-\bar{\sigma} + \bar{b}}{\bar{c}\bar{\sigma} - \bar{a}} \right) = k^2 \quad (3-18)$$

Rearranging equation (3-18) into the form of equation (3-11), there results

$$\begin{aligned} \sigma\bar{\sigma} - \sigma \left(\frac{\bar{b} - k^2 \bar{a}\bar{c}}{1 - k^2 \bar{c}\bar{c}} \right) - \bar{\sigma} \left(\frac{b - k^2 a\bar{c}}{1 - k^2 c\bar{c}} \right) \\ + \left(\frac{b\bar{b} - k^2 a\bar{a}}{1 - k^2 c\bar{c}} \right) = 0 \end{aligned} \quad (3-19)$$

From the discussion pertinent to equation (3-11), we see that equation (3-19) is a circle displaced from the origin. If A represents the vector by which the center of this circle is displaced from the origin and K represents the radius, then

$$A = \frac{b - k^2 a\bar{c}}{1 - k^2 c\bar{c}} \quad (3-20)$$

and

$$K^2 = A\bar{A} - \left(\frac{b\bar{b} - k^2 a\bar{a}}{1 - k^2 c\bar{c}} \right) \quad (3-21)$$

- The conditions for which equation (3-20) and (3-21) are solved are:
- (1) The transforming section is lossless and is specified in terms of the reflection coefficient at one plane under conditions which give a match at the other.
 - (2) The reference planes are "corresponding planes", i.e. an open circuit at the one gives an open circuit at the other.

According to condition one the transforming section is lossless. This implies that with a purely reactive termination of the line, the modulus of the reflection coefficient is unity at all planes, i.e.

$$k = 1$$

$$K = 1 \quad (3-22)$$

$$A = 0$$

Substituting the values (3-22) into equation (3-20) we find that

$$b = a\bar{c} \quad (3-23)$$

therefore

$$\bar{b} = \bar{a}\bar{c} \quad (3-24)$$

Condition two states that the reference planes are chosen such that an open circuit at one plane gives and open circuit at the other, i.e.

$$\rho = 1$$

when

$$\sigma = 1 \quad (3-25)$$

Using the values (3-25) in equation (3-17) we find that

$$a + b = c + 1 \quad (3-26)$$

So

$$\bar{a} + \bar{b} = \bar{c} + 1$$

(3) The transforming section is specified in terms of the reflection at the one plane under conditions which give a match at the other, i.e. the value of σ corresponding to $\rho = 0$ is known. The substitution of $\rho = 0$ into equation (3-17) gives $\sigma = b$. Thus b and \bar{b} are known constants. The point whose affix is b is called the iconocenter.

Let us now evaluate equation (3-20) in light of the two specified conditions. Substitute (3-23) in equation (3-20) obtaining

$$A = \frac{b(1 - k^2)}{1 - k^2 c\bar{c}} \quad (3-27)$$

Solving equation (3-23) for "a" and substituting the result into equation (3-26), we get

$$b(1 + \frac{c}{c\bar{c}}) = c + 1 \quad (3-28)$$

or

$$c = \frac{1 - b}{\frac{b}{c\bar{c}} - 1}$$

then

$$\bar{c} = \frac{1 - \bar{b}}{\frac{\bar{b}}{c\bar{c}} - 1} \quad (3-29)$$

Multiplying equation (3-28) and (3-29) together and simplifying, there results:

$$(c\bar{c})^2 - (1 + b\bar{b}) c\bar{c} + b\bar{b} = 0$$

which can be factored to yield

$$(c\bar{c} - 1)(c\bar{c} - b\bar{b}) = 0 \quad (3-30)$$

Therefore

$$\bar{cc} = 1 \quad (3-31)$$

or

$$\bar{cc} = \bar{bb} \quad (3-32)$$

If equation (3-31) is substituted into equation (3-27), the result is $A = b$, which is the solution for $\sigma = 0$. The general solution for \bar{cc} is equation (3-32). If equation (3-32) is substituted into equation (3-27), we get the desired result which is

$$A = \frac{b(1 - k^2)}{1 - k^2 \bar{bb}} \quad (3-33)$$

We now wish to evaluate equation (3-21) which is repeated here for convenience. It is

$$k^2 = A\bar{A} - \left(\frac{\bar{bb} - k^2 \bar{aa}}{1 - k^2 \bar{cc}} \right) \quad (3-21)$$

Examination of this equation shows us that \bar{aa} is the only unknown. Remembering that with a purely reactive termination

$$\bar{cc} = \bar{bb} \quad (3-32)$$

$$K = 1 \quad (3-22)$$

$$A = 0$$

$$k = 1$$

we find upon substitution of these values into equation (3-21) that

$$\bar{aa} = 1 \quad (3-34)$$

Since all the parameters of equation (3-21) are now known we may substitute and simply obtaining as a final result

$$K = \frac{k(1 - bb)}{1 - k^2 bb} \quad (3-35)$$

Circles representing constant V.S.W.R. may thus be transferred from the ρ to the σ planes by means of equation (3-33) and (3-35).

c. Transformation of Lines of Constant Phase Angles.

Substitution of equation (3-17) into equation (3-3) gives the equation of the loci in the σ plane of the radial lines in the ρ plane which represent reflection coefficient of constant phase and varying amplitude.

$$\left(\frac{-\sigma + b}{c\sigma - a} \right) \left(\frac{\bar{c}\bar{\sigma} - \bar{a}}{-\bar{\sigma} + \bar{b}} \right) = 1 \quad (3-36)$$

Equation (3-36) may be rearranged into the form of equation (3-11), yielding the form

$$\begin{aligned} \sigma\bar{\sigma} - \left(\frac{la - bc}{lc - c} \right) \bar{\sigma} - \left(\frac{lbc - \bar{a}}{lc - \bar{c}} \right) \sigma \\ + \left(\frac{labc - \bar{a}b}{lc - \bar{c}} \right) = 0 \end{aligned} \quad (3-37)$$

It may be shown that the coefficient for σ and $\bar{\sigma}$ are conjugate terms, so that equation (3-37) represents a circle for which

$$A = \frac{la - b\bar{c}}{lc - \bar{c}} \quad (3-38)$$

and

$$K^2 = A\bar{A} - \left(\frac{lab - \bar{a}\bar{b}}{lc - \bar{c}} \right) \quad (3-39)$$

where K and A are the symbols identified with equation (3-20).

Let us proceed to put equation (3-38) and (3-39) into a more usable form. Equation (3-23) stated:

$$a = b/\bar{c} \quad (3-23)$$

and relation (3-26) was

$$a + b = c + l \quad (3-26)$$

Also equation (3-32) was given as

$$c\bar{c} = b\bar{b} \quad (3-32)$$

If equations (3-23) and (3-32) are substituted into (3-26) and the result solved for \bar{c} , we get

$$\bar{c} = \frac{b(l-b)}{(l-b)} \quad (3-40)$$

Hence

$$c = \frac{\bar{b}(l-b)}{(l-b)} \quad (3-41)$$

We recall that equation (3-38) was

$$A = \frac{la - b\bar{c}}{lc - \bar{c}} \quad (3-38)$$

If equation (3-23), (3-40) and (3-41) are substituted in equation (3-38) for a , \bar{c} and c respectively we get our desired result which is

$$A = \frac{1 - b^2}{1 - b} \frac{-b^2}{1 - b} \frac{(1 - b)^2}{1 - b} \quad (3-42)$$

To put equation (3-39) into the desired form, substitute values of A , a , c , and \bar{c} as given by equations (3-42), (3-23), (3-41), and (3-40) respectively and realize that

$$1\bar{b} = 1 \quad (3-43)$$

The result is then

$$K = \frac{(1 - b\bar{b})}{\sqrt{2 b\bar{b} - b^2 \frac{(1 - b)^2}{1 - b} - b^2 \frac{1}{1 - b} (1 - b)^2}} \quad (3-44)$$

The radial lines representing constant phase angle in the ρ plane may thus be transformed into corresponding circular tracks in the σ plane by means of equations (3-43) and (3-44). Since the radial lines in the ρ plane all pass through the origin, it follows that the family of circles represented by equation (3-37) all pass through the iconocenter, as may be shown by substituting $\sigma = 1$ in equation (3-37).

d. Transformation of Circles of Constant Resistance and Reactance.

The form of equation (3-6) indicates that the normalized impedance and reflection coefficient at any plane

are bilinearly related, and since ρ and σ are bilinear functions, so are z_1 and z_2 (where z_1 and z_2 are the normalized impedance at planes 1. and 2 respectively). We may therefore state

$$z_2 = \frac{\alpha z_1 + \beta}{\gamma z_1 + 1} \quad (3-45)$$

where

α , β , and γ are, in general complex constants.

According to our previously stated conditions (following equation (3-21)), $\rho = 1$ when $\sigma = 1$. Equation (3-6) is repeated for convenience and is

$$z = \frac{1 + \rho}{1 - \rho} \quad (3-6)$$

Thus when $\rho = 1$, $z = \infty$. Since $\sigma = 1$ when $\rho = 1$, it follows that when $z_1 = \infty$, $z_2 = \infty$. This implies that $\gamma = 0$ in equation (3-45). Therefore z_2 is a linear function of z_1 , i.e.

$$z = \alpha z_1 + \beta \quad (3-46)$$

When z_1 is purely imaginary, z_2 is also purely imaginary since we have assumed the junction to be lossless (condition 1). This implies in equation (3-46) that α is real and β is imaginary.

Condition three stated that the junction would be characterized by measuring the reflection coefficient at plane 2 when plane 1 is matched to its Characteristic Impedance. We define.

$$z_{12} = r_{12} + j x_{12} \quad (3-47)$$

(where z_{12} , r_{12} and x_{12} are normalized to plane 2) as the impedance seen from the coaxial side of the junction (plane 2) when the stripline side of the junction (plane 1) is terminated in its Characteristic Impedance ($z_1 = 1$). When z_1 becomes equal to 1, equation (3-46) is

$$z_2 = z_{12} = r_{12} + j x_{12} = \alpha + j\beta \quad (3-48)$$

Therefore

$$\alpha = r_{12}$$

$$\beta = j x_{12}$$

Equation (3-46) may then be written as

$$z_2 = r_{12} z_1 + j x_{12} \quad (3-49)$$

Solving equation (3-49) for z_1 , we may write

$$\frac{z_1}{z_{01}} = \frac{\frac{z_2}{z_{02}} - j \frac{x_{12}}{z_{02}}}{\frac{r_{12}}{z_{02}}} \quad (3-50)$$

where:

z_1 = impedance at plane 1

z_2 = impedance at plane 2

r_{12} = Real part of impedance seen at plane 2 with plane 1 terminated in its Characteristic Impedance ($\rho = 0$)

x_{12} = Imaginary part of impedance seen at plane 2 with plane 1 terminated in to Characteristic Impedance ($\rho = 0$)

z_{01} = Characteristic Impedance - plane 1

z_{02} = Characteristic Impedance - plane 2

Equation (3-50) shows us that if we know r_{12} and x_{12} as well as the impedance of the unknown load as seen on the coaxial side of the junction (plane 2) and the Characteristic Impedance of both sides of the junction, we may find the value of the unknown z_1 . $z_{12} = r_{12} + j x_{12}$ is known as the "iconocenter" and may be found by a graphical procedure to be described.

B. Determination of Unknown Impedance.

1. The Problem.

The original purpose of this paper was to describe a measurement technique for the Characteristic Impedance of Stripline. It was thought that at any given point in the Stripline, the open circuit and short circuit impedance z_{op2} and z_{s2} could be measured on the coaxial side of the junction, transformed to the Stripline side of the junction through the use of equation (3-50) to yield z_{opl} and z_{sl} and the relation

$$z_{01} = \sqrt{z_{opl} z_{sl}} \quad (3-51)$$

used to find the Characteristic Impedance of the Stripline. However the author overlooked one important fact; namely that the answer begs the question. Reference to equation (3-50) shows that we must know Z_{01} in addition to z_2 (z_{s2} or z_{op2} in our case) in order to determine z_1 (z_{opl} or z_{sl}). While this method is useless for determining Characteristic Impedance, it is quite useful in measuring unknown loads in general. It is anticipated that such unknown loads may have to be determined when an investigation is made of various Stripline terminations.

In order to use this method of measurement we must first determine the iconocenter (z_{12}). The following section therefore will concern itself with the graphical determination of z_{12} .

2. Determination of the Iconocenter.

In determining the iconocenter through graphical construction on the Smith Chart, it is necessary to introduce the concept of the projective chart.²⁸

On the Smith Chart, a reflection coefficient or reflectance ρ is represented by a point W just as any complex number is represented on the Argand diagram. The distance OW to the origin is the magnitude r of the reflectance, and all passive loads are represented by points inside the unit circle Γ . If the line $O'V$ cuts Γ at points I and J (Fig 3-2) the ratio

$$\frac{WI}{WJ} = \frac{1+r}{1-r} \quad (3-52)$$

as shown in the pamphlet, is the voltage standing-wave ratio corresponding to the reflectance ρ .

The modification that leads to the projective chart is to represent the reflectance ρ by the point W with the same phase angle as W but at a distance \tilde{r} from the origin given by

$$\tilde{r} = \frac{2r}{1+r^2} \quad (3-53)$$

This makes the ratio WI/WJ equal to the square of the voltage standing-wave ratio.

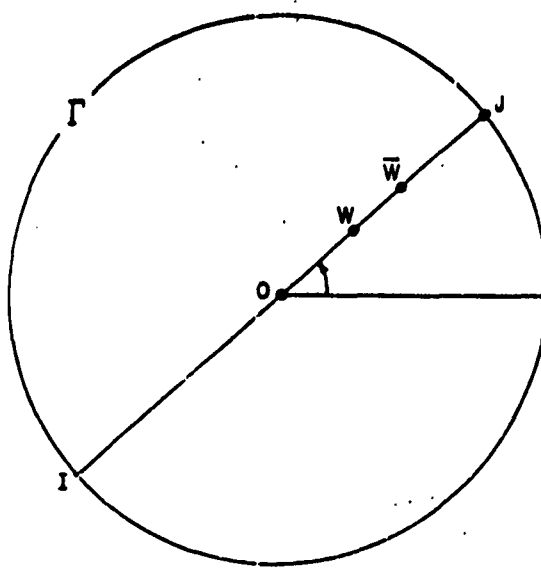


Fig 3-2 Relation between the representation of a reflection coefficient on the Smith Chart (w) and on the projective chart (\bar{w}).

If a radial arm carrying a voltage-standing-wave-ratio graduation in decibels is used with the Smith Chart, the point \bar{w} will be in front of the graduation $2x$ when w is in front of the graduation x . Plotting points on the projective chart or transforming back and forth to the Smith Chart is therefore very simple.

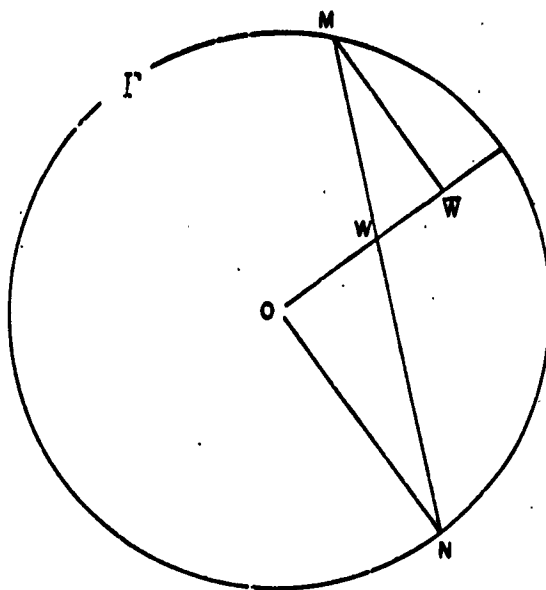


Fig 3-3 Transformation β and β^{-1} . Construction of \bar{W} from W or of W from \bar{W} .

The transformation β from W to \bar{W} can also be obtained²⁹⁻³¹ by projecting W on a sphere with equator from one of its poles and then projecting orthogonally from the sphere on the plane of Γ . Appendix VI shows the derivation of Fig 3-3. This justifies the construction shown in this figure. $\bar{W}M$ and ON are perpendicular to the radius OW and MN goes through W . This can also be used to perform the inverse transformation β^{-1} from \bar{W} to W .

The circles usually drawn on the Smith Chart corresponding to constant resistance or reactance and to constant magnitude or phase of the impedance become on the projective chart straight lines and ellipses as shown in Fig 3-4. These could be drawn in advance and used as on the Smith and Carter charts to plot impedance measurements taken for instance, with a bridge.

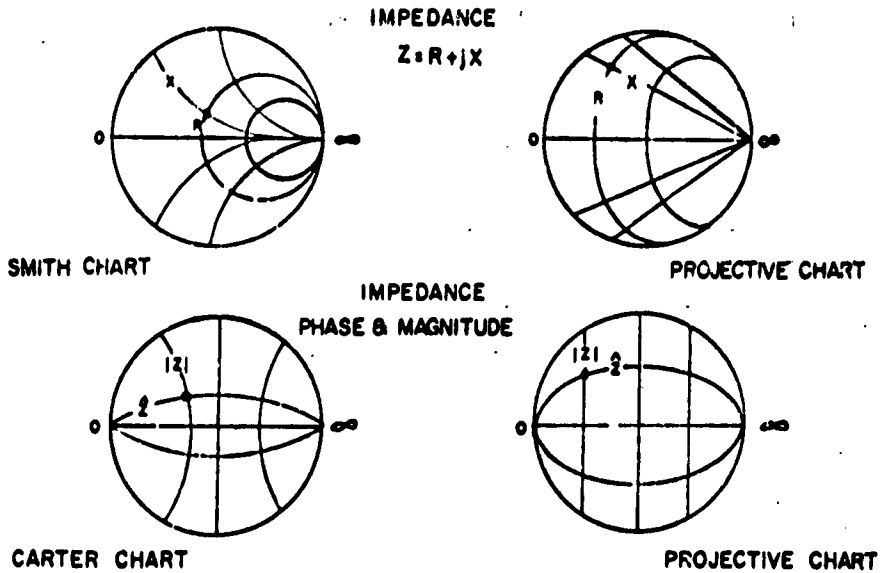


Fig 3-4 Loci on the projective chart and on the Smith and Carter Charts of constant resistance R , reactance X , impedance magnitude $|Z|$ and impedance phase $\angle Z$.

Special notions of distance and angle that have useful interpretations can be introduced on the projective chart.

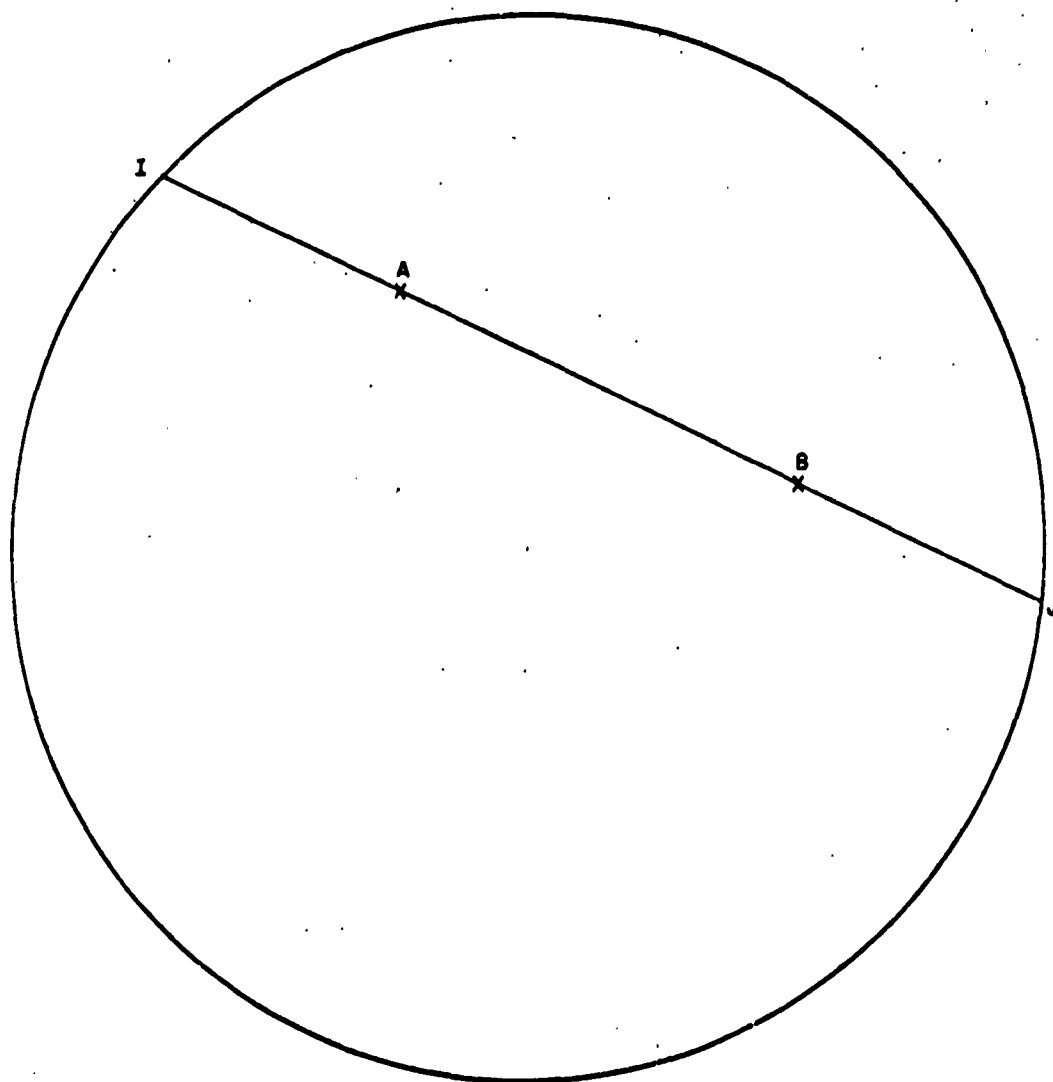


Fig 3-5 Definition and evaluation of the
Hyperbolic Distance (AB)

Given two points, A,B and the intersections I,J of AB with (Fig 3-4), the quantity

$$10 \log_{10} \left(\frac{BI}{BJ} : \frac{AI}{AJ} \right) \quad (A3-54)$$

will be denoted by (AB) and called the hyperbolic distance between A and B. It will usually be expressed in decibels as in (3-54) but can be converted to nepers by substituting $1/2 \ln$, for $10 \log_{10}$.

The quantity (3-54) deserves the name of "distance" because it satisfies the triangular inequality (which shows that straight lines are geodesics for this particular measurement system) and because it is additive; that is, when three points, A,B,C are on a straight line in this order:

$$(AB) + (BC) = (AC) \quad (3-55)$$

The hyperbolic distance between the point \bar{W} and the center of the chart is

$$(\bar{OW}) = 10 \log \frac{1+r}{1-r} = 20 \log \frac{1+r}{1-r} \quad (3-56)$$

and can be interpreted as the voltage standing-wave ratio expressed in decibels.

It has been shown in the discussion concerning equation (3-17) that a lossless transformer may be represented by the relation

$$\rho = \frac{-\sigma + b}{c\sigma - a} \quad (3-17)$$

We further saw from Section B that circles in the ρ plane go over to the σ plane as circles under the transformation (3-17). Equation (3-17) is also a conformal transformation (angles are preserved). It follows that hyperbolic distances are also preserved in the following sense. If A, B are transformed into A', B' while Γ becomes Γ' , the distance (AB) defined above is equal to the distance $(A'B')$ measured as if Γ' were the unit circle:

$$(AB)_{\Gamma} = (A'B')_{\Gamma'}, \quad (3-57)$$

the subscript indicating with respect to what circle the distance is measured.

The special transformation (3-17) that preserves the unit circle (lossless transformations of reflectance for instance) are represented on the projective chart by projective transformations. They transform straight lines into straight lines and as a consequence also leave the hyperbolic distances and elliptic angles invariant.

Let us now put the fact that straight lines go to straight lines (in the projective chart) under the transformation (3-17) to work for us. The iconocenter is defined as the impedance seen on the coaxial side of the junction

(plane 2) when the stripline side of the junction is terminated in its characteristic impedance. If the Smith Chart representation is used, the impedance seen at reference plane 1 (stripline side of the junction) will be Z_{01} , since the stripline is terminated in its characteristic impedance. On a normalized basis, Z_{01} corresponds to the center of the Smith Chart ($\rho = 0$). If A, B, C and D are four equivalent points on the $\rho = 1$ circle (corresponding to four open circuit measurements one eighth electrical wavelength apart), the diameter AC and BD will pass through the center of the circle ($\rho = 0$) as shown in Fig 3-6.

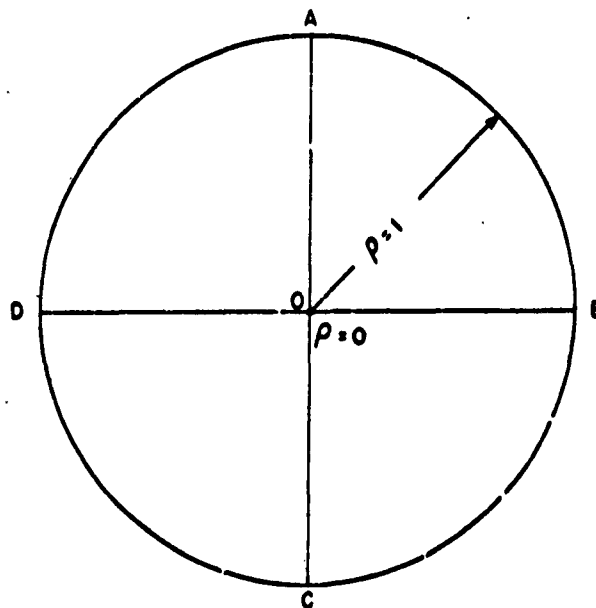


Fig 3-6 Reflectance of four open circuits spaced one eighth wavelength apart on the stripline side of the junction.

If A,B,C and D are transformed through the junction and measured on the coaxial side of the lossless junction, we have the points A',B',C',D'. If the projective representation is used, the straight lines AC and BD go over the straight lines A'C' and B'C' as shown in Fig 3-7. Since the junction is lossless, the unit circle is preserved and the points A', B', C', and D' lie on it.

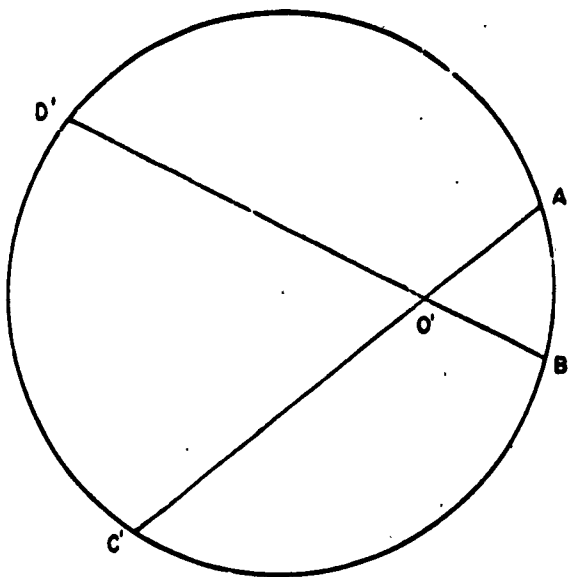


Fig 3-7 Reflectances of four open circuits spaced one eighth wavelength apart after being transformed through a lossless junction.

Point O' in Fig 3-7 is therefore the point corresponding to the point O in Fig 3-6. However Fig 3-7 is the projective representation of Fig 3-6 and not the Smith Chart representation. We therefore perform the construction

shown in Fig 3-3 where $\bar{W} = 0'$ and is known as the "crossover" point. The result is shown as Fig 3-8. The point W is the iconocenter i.e. the impedance in plane 2 corresponding to a matched load in plane 1.

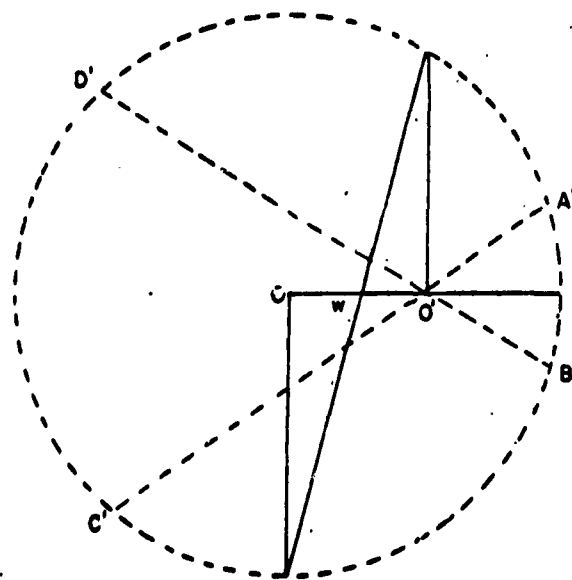


Fig 3-8 Transformation from the Projective to Smith Chart representation.

3. An Example Illustrating the Technique.

In order to clarify the actual measurement procedure, let us work an example. The test setup is shown in Fig 3-9. The first step is to establish a reference plane according to condition 2 assumed in the solution of the preceding equations. It was decided that the reference plane

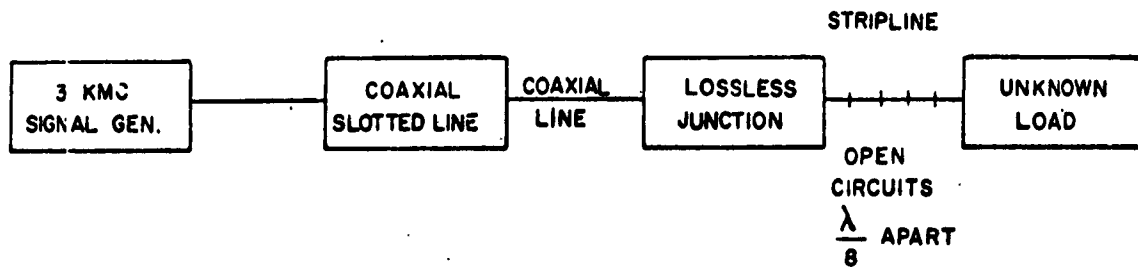


Fig 3-9 Test Setup for Measurement of an Unknown Load

on the Stripline side of the junction would be established directly to the right of the junction. Accordingly the junction was attached to the coaxial cable on the right of the dotted line and the position of the first voltage maximum was recorded. A section of Stripline with known Characteristic Impedance of arbitrary length and open circuited on the load end was then attached to the junction. The VSWR and position of the first maximum were noted. It was next desired to remove one-eighth electrical wavelength from the Stripline. The wavelength in Stripline is related to the wavelength in free space by

$$\lambda_s = \sqrt{\frac{\lambda_f}{\epsilon_r}} \quad (3-58)$$

where

- λ_s = Stripline wavelength
- λ_f = Free Space wavelength
- ϵ_r = Dielectric constant of Stripline

The free space wavelength at 3 kmc is 10 centimeters. Teflon-Fiberglass (GB-112T) was the dielectric used. This material has a dielectric constant of 2.6. We therefore find from equation (3-58) that $\lambda_s/8 = 0.305$ inch. This length was then removed from the load end of the Stripline and another measurement of VSWR and the position of the first voltage maximum made. By repeating the procedure of removing $\lambda_s/8$ three times and measuring the VSWR and the position of the first voltage maximum, the four points A', B', C' and D' are obtained (one point was obtained from the measurement made before any Stripline was removed). The results are shown in Table 3-1.

From Table 3-1, it is first necessary to determine the wavelength in the slotted line. This is done by subtracting minima from their corresponding maxima and averaging the results of all readings. Knowing that the difference between any maximum and minimum is one fourth wavelength, we can find the wavelength in the coaxial line. The position of each maximum is then subtracted from the reference position.

TABLE 3-1

Measurements Relevant to the Determination of an
Unknown Load as Measured Through a Junction

Reference Position on Slotted Line - 378.9		
Maximum	VSWR	Minimum
350.6	39.2	325.9
Remove 0.305 inch of Stripline		
387.2	60	363.8
Remove 0.305 inch of Stripline		
378.5	61	353.9
Remove 0.305 inch of Stripline		
366.8	47	344.3

This difference is then expressed as a percentage of the slotted line wavelength. If the position of a voltage maximum is numerically greater than that of the position of the reference, the maximum has shifted toward the load; if it is less the maximum has shifted toward the generator. The results are shown as Table 3-2.

It has been assumed that the junction is lossless. This means that the VSWR on the coaxial side of the junction can be shown to be infinite or that $\sigma = 1$ since

$$\sigma = \frac{\text{VSWR}-1}{\text{VSWR}+1} \quad (3-59)$$

Table 3-1 shows that the measured standing wave ratios were not infinite. Table 3-3 shows how good an approximation we have to the ideal case ($\sigma = 1$).

Reference to the reflection coefficient scale of Fig 3-10 shows that the approximation is not bad. We will make the assumption that $\sigma = 1$ for all measurements to avoid the more difficult problem of having to consider a lossy junction.

The points of Table 3-2 are plotted on Fig 3-10 using $R = \infty$ as the reference point. We use this reference because our measurement reference was an open circuit corresponding to a voltage maximum. Since a voltage minimum occurs at a current minimum, a resistive maximum is obtained. As discussed previously

TABLE 3-2

Location of Points A',B',C',D'
with Respect to the Reference Plane

	Shift		Direction
1.	0.286	λ	toward generator
2.	0.084	λ	toward load
3.	0.00405	λ	toward generator
4.	0.1224	λ	toward generator

TABLE 3-3

Comparison of Measured VSWR with the ideal value

VSWR	σ
39.2	0.948
60	0.97
61	0.97
47	0.96

the points A' and C' are joined with a straight line across B' and D'. This intersection yields the point O'. The construction of Fig 3-3 is then used to obtain the point W, which is the iconocenter. From Fig 3-10 we see that

$$W = z_{12} = 1.4 + j 0.2 \quad (3-60)$$

Let us now attach the unknown load to the stripline and measure the VSWR and position of the voltage maximum. The VSWR is observed to be 10 while the position of the first voltage maximum is at 370.0 centimeters. From equation (3-59), $\sigma = 0.82$ while the voltage maximum has shifted 0.09 wavelengths or 64.8 degrees toward the generator. A shift toward the generator is negative according to standard transmission line theory. Hence normalized, to z_{02}

$$\begin{aligned} z_2 &= 0.82 \angle -64.8 \\ &= 0.348 - j 0.74 \end{aligned} \quad (3-61)$$

Equation (3-48) is now used to transform z_2 back through the junction. It is

$$\frac{z_1}{z_{01}} = \frac{\frac{z_2 - x_{12}}{z_{02}} - j \frac{x_{12}}{z_{02}}}{\frac{r_{12}}{z_{02}}} \quad (3-50)$$

It is known that the Characteristic Impedance of the stripline is 50 ohms while that of the coaxial cable is 51 ohms. r_{12} and x_{12} are the real and imaginary parts of the iconocenter and are given by equation (3-60). Inserting those values in equation (3-50) we get

$$\frac{z_1}{50} = \frac{\frac{0.348 - j 0.74}{51} - j \frac{0.2}{51}}{\frac{1.4}{51}}$$

$$= 12.7 - j 34.2$$

It will of course be noted that it is not necessary to know z_{02} since it drops out of the equation. It was put in merely to show that z_{12} and z_2 are both normalized to z_{02} .

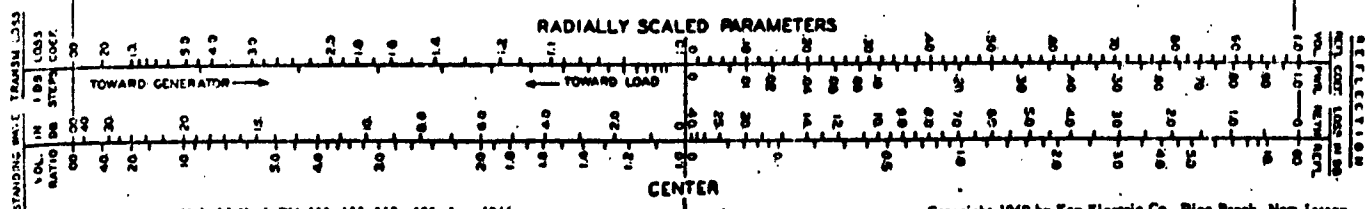
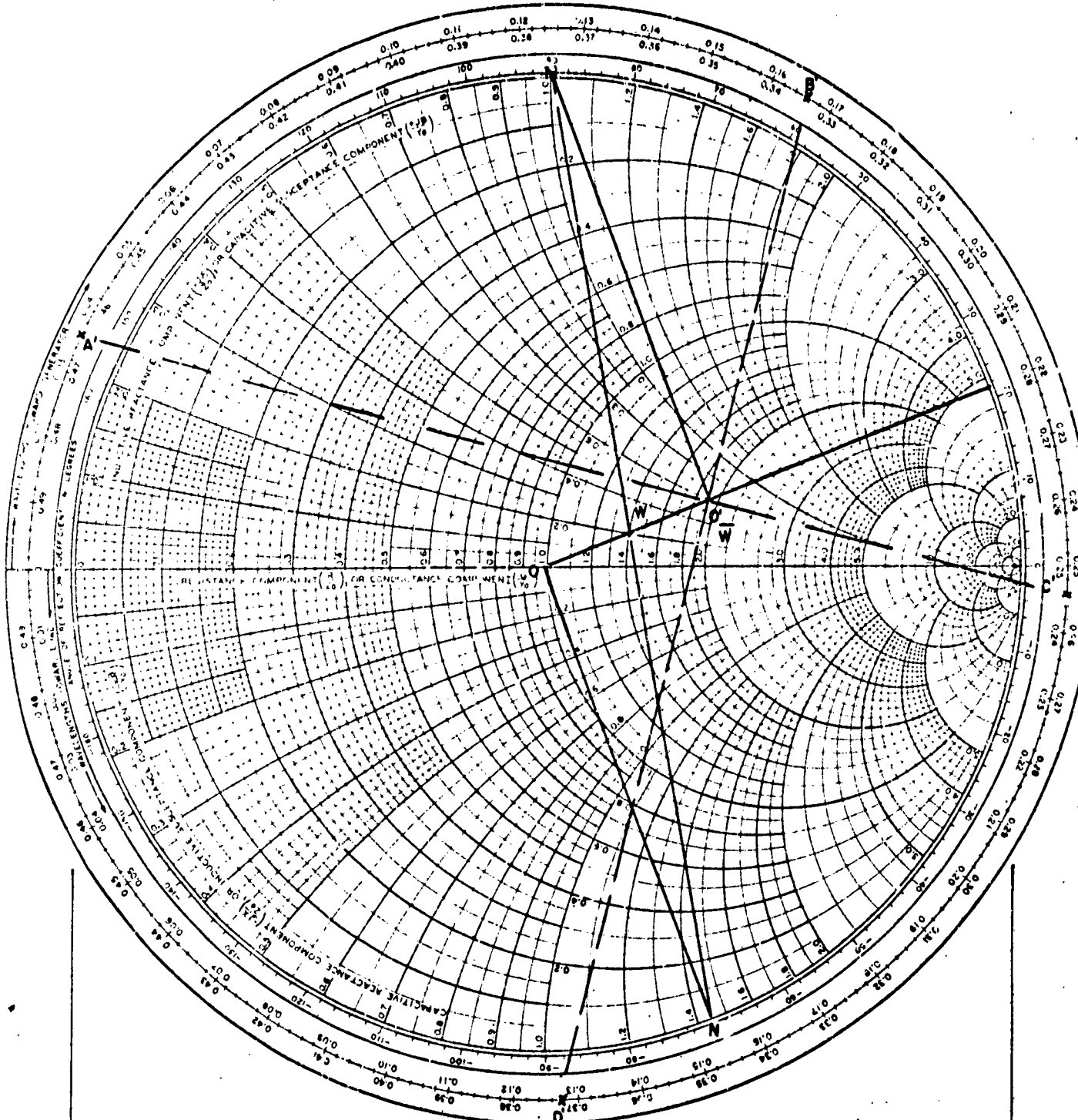
C. Conclusions:

It has been shown that it is possible to measure an arbitrary unknown impedance through a lossless junction thereby allowing the use of an existing coaxial slotted line to determine the value of Stripline Loads. We can not however determine the Characteristic Impedance of the Stripline by this method since our result will be a single equation in two unknowns.

NAME	TITLE Fig. 3-10 DETERMINATION OF THE ICONOCENTER	DWG. NO.
SMITH CHART FORM 756-N	GENERAL RADIO COMPANY, WEST CONCORD, MASSACHUSETTS	DATE

IMPEDANCE OR ADMITTANCE COORDINATES

69



BIBLIOGRAPHY

27. H. V. Shurmer, "Transformation of the Smith Chart Through Lossless Junctions", B.I.E.E., Vol 105, Part C, March 1958, pages 177-182.
28. G. A. Deschamps, "A Hyperbolic Protractor for Microwave Impedance Measurements and Other Purposes", Federal Telecommunication Laboratories, Nutley, N.J., 1953.
29. G. A. Deschamps, "Geometrical Representation of the Polarization of a Plane Electromagnetic Wave", Proceedings of the IRE, Vol 39, pages 540-544, May 1951.
30. G. A. Deschamps, "Application of Non-Euclidean Geometry to the Analysis of Waveguide Junctions", presented at the Joint Spring Meeting of the American Section of the International Scientific Radio Union and the Institute of Radio Engineers, Washington, District of Columbia; April 23, 1952, published in part as, "Determination of the Reflection Coefficients and Insertion Loss of a Waveguide Junction", in Journal of Applied Physics, Vol 24, pages 1046-1050, August 1953.
31. G. A. Deschamps, "Geometric Viewpoints in the Representation of Waveguides and Waveguide Junctions", Proceedings of the Symposium on Modern Network Synthesis, pages 277-295, September 30, 1952. Presented at the Symposium sponsored by the Polytechnic Institute of Brooklyn and the Office of Naval Research in New York, New York on April 18, 1952.

APPENDIX VI

Relation Between the Iconocenter and the Crossover Point

The existence of the crossover point and its relation to the iconocenter may be proved by considering the sphere S having Γ' as its equator (Fig A6-1). By stereographic projection from the pole L , any circle γ' passing through O' and orthogonal to Γ' is transformed into circle γ on S , also orthogonal to Γ' and passing through the stereographic projection K of O' . By projection on the plane of the equator, this circle becomes a straight line, which goes through the projection \bar{O} of K . The construction of Fig A6-2 is a reproduction of $LCO'K\bar{O}$ on the plane of Γ' obtained for instance by rotation through 90 degrees about CO' .

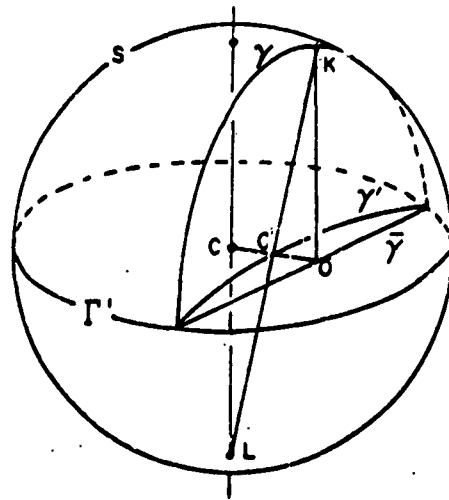


Fig A6-1 Transformation from the Crossover Point to the Iconocenter.

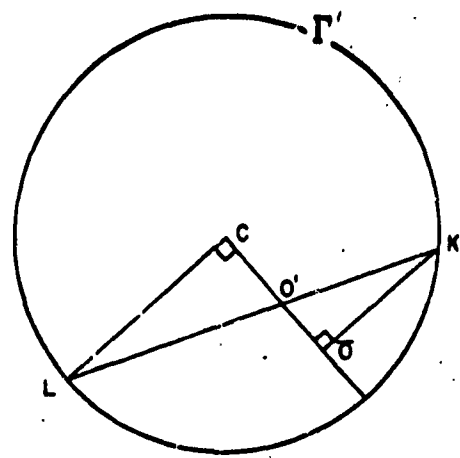


Fig A6-2 Relation Between the Iconocenter and the Crossover Point.

ABSTRACT

The history of work done on Stripline attenuation is discussed. Cohn's³⁷ analysis is accepted as the most desirable for engineering use since his results are expressed in a convenient graphical form. Following Cohn, the attenuation is expressed as the sum of dielectric attenuation and conductor attenuation. Working expressions are developed for dielectric and conductor attenuation, the "incremental inductance" rule of Wheeler³⁸ being used to determine conductor attenuation. The results are shown in easy-to-use graphical form. Finally experimental verification of Stripline attenuation is shown using a Stripline Spiral. Good correlation is obtained between measured and theoretical values of attenuation up to 3.5 Kmc. It is believed that the discrepancy above 3.5 Kmc is due to an increase in loss tangent and a decrease in dielectric constant above this frequency.

TABLE OF CONTENTS

Chapter	Page
IV Determination of Stripline Attenuation	
A. History of Problem	
1. Current Distribution on the Conductors	71
2. Attenuation Constant	74
B. Recommended Approach	76
C. Derivation of a Expression for Stripline Attenuation	77
1. Dielectric Attenuation	77
2. Conductor Attenuation	80
a. Wide Strip case	97
b. Narrow Strip case	101
3. Attenuation Graphs	106
4. Measurement of Attenuation	108
Bibliography	117

LIST OF FIGURES

Figure	Page
4-1 Rigorous Conformal Mapping of Stripline Geometry	72
4-2 Field or Current Distributions Across Outer Conductor Surface	74
4-3 Current Flow in a Plane Conductor	83
4-4 Cross Section of Stripline	95
4-5 Partial Derivative Summation for Use in Equation 4-88	104
4-6 Comparison of the Wide- and Narrow-Strip Attenuation Formulas in their Transition Region	107
4-7 Theoretical Attenuation of Copper Shielded Stripline in a Dielectric Medium ϵ_r	109
4-8 Attenuation Measurements, Method and Equipment	111
4-9a Attenuation Measurements for Lines A and B	113
4-9b Attenuation Measurements for Line C . .	114

CHAPTER IV

DETERMINATION OF STRIPLINE ATTENUATION

A. History of the Problem.³²

1. Current Distribution on the Conductors.

Before Stripline attenuation can be intelligently discussed a few words must be said concerning the distribution of current in Stripline.

Many of the people who have worked on the Characteristic Impedance of this line have, in conjunction with that work, carried out a conformal mapping of the stripline geometry into some simpler geometry. One by-product of such calculations is the current distribution of the inner and outer conductors. The rigorous conformal mapping carried out by Oliner,² and illustrated in Fig 4-1, is therefore meant to be typical of the work of a number of people.

The mapping outlined in Fig 4-1 proceeds by first mapping the upper half region (b) of the Stripline shown in (a) onto the upper half plane (c), by means of a tanh function. The rectangle (d) is then also mapped onto the upper half plane (c), employing a sn function, and the mappings are compared in order to determine the overall mapping from (b) to (d). By taking appropriate derivatives, one finds the following functional

dependence for the current distribution on the ground planes in terms of the notation of Fig 4-1 (b):

$$I(x, b/2) = \frac{1}{\sqrt{1 + k'^2 \sinh^2(\pi x/b)}} \quad (4-1)$$

where

$$k = \tanh(\pi w/2 b), \quad k'^2 = 1 - k^2. \quad (4-2)$$

The current on the center strip conductor is similarly shown to be

$$I(x, 0) \approx \frac{-1}{\sqrt{1 - (k'^2/k^2) \sinh^2(\pi x/b)}} \quad (4-3)$$

where k and k' are given by Fig 4-2.

It is seen from (4-1) that the current on the outer conductors is a maximum at the midplane of the cross-section, and decreased monotonically away from this point on either side. From (4-3), on the other hand, one notes that the current on the inner strip conductor is a minimum at the

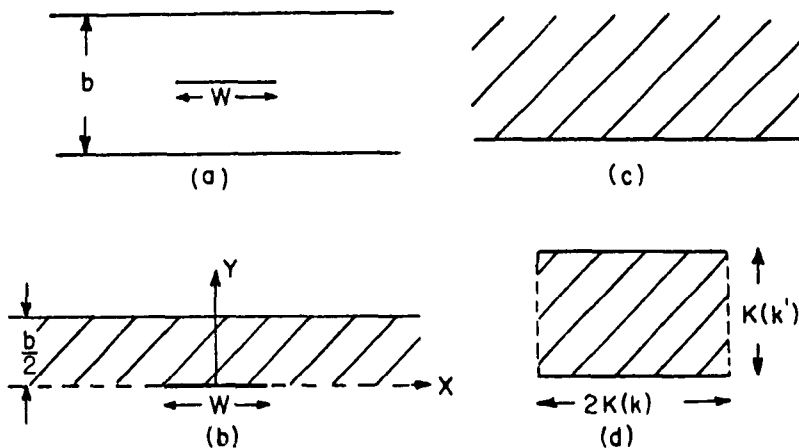


Fig 4-1 - Rigorous Conformal Mapping of Stripline Geometry

midplane and becomes divergent at the strip edges (as one would expect). The actual variations given by (4-1) and (4-3) have a relatively simple form.

Experimental confirmation of the validity of relation (1) in a practical situation is afforded by Fig 4-2 which presents a comparison of the theoretical values predicted by (4-1) with experimental data taken at the Hughes Aircraft Company.³⁴ As seen, the theoretical values agree quite well with the measurements. Fig 4-2 also serves to illustrate the rapid decay encountered as one moves transversely away from the center strip; at a distance away from the strip equal to the strip width the square of the field intensity is 27 db down from its maximum value.

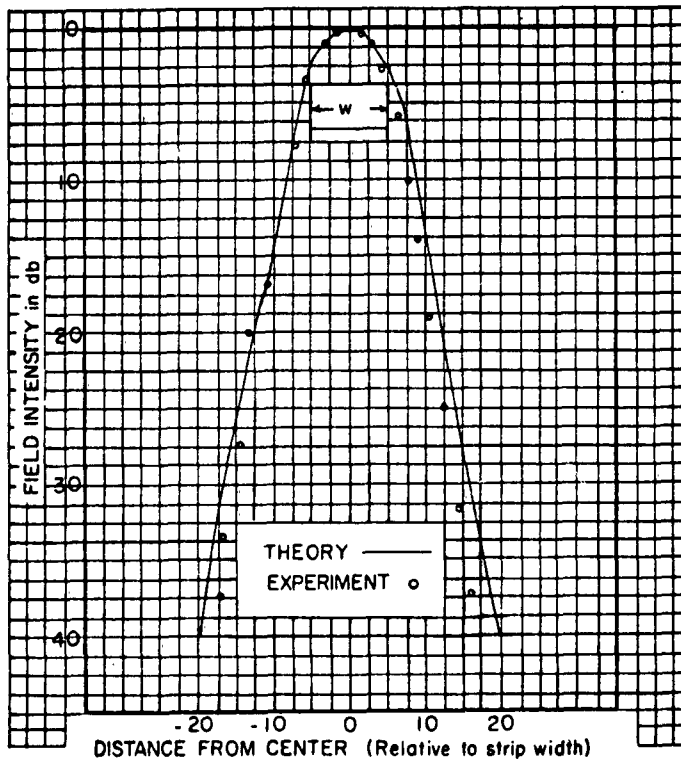


Fig 4-2 - Field or Current Distributions Across
Outer Conductor Surface

2. Attenuation Constant.

The evaluation of the attenuation constant is generally a rather prosaic task, once the appropriate current distributions are known. If one employs the current distribution (4-1), and performs the necessary integrations, one finds for the attenuation constant due to the loss in the outer conductors only,³⁵

$$\alpha_{\text{outer plates}} = \frac{\pi^2 \delta}{4 k b \lambda} \frac{1}{K(k) K(k')} \ln \frac{1+k}{1-k} \quad (4-4)$$

(where k and k' are defined in 4-2, $K(k)$ is the complete elliptic integral of the first kind of modulus k , λ is the wavelength of the line, b is the ground plane spacing, and δ is the conductor

skin depth. When similar integrations are performed for the inner conductor, using current distribution (4-3), a divergent result is obtained for the attenuation constant due to loss in the inner conductor alone. This divergence is due to the divergence in the current distribution at the sides of the inner strip conductor for an inner conductor of finite thickness (rectangular shape) the current distribution at the edges possesses a divergence of lower order and thus permits a finite result for the attenuation constant.

In the course of his work on Characteristic Impedance,¹⁰ Pease had determined the current distributions on the inner and outer conductors in the low impedance range when the inner conductor is of finite thickness. Employing these current distributions in the computation of attenuation constant, Pease³⁶ obtained explicit expressions valid for both inner and outer conductors. While the results are approximate, they are estimated to be accurate to within 1% for $Z_0 < 75$ ohms. The contributions due to the inner and outer conductors are given separately; the result for the outer conductors alone is numerically in very close agreement with (4-4) when the inner conductor thickness is small. While these attenuation constant results are in explicit form, they require the insertion of a quantity related to the Characteristic Impedance which must be determined via a transcendental relation. The form is definitely computable

but more involved than that of (4-4). It is suggested, therefore, if accurate results are desired for lines in the low impedance range with small thickness inner conductors, to employ the formulation of Pease for the inner conductor contributions and expression (4-4) for the contributions of the outer conductors.

More recently, Cohn³⁷ has evaluated expressions for the attenuation constant which are valid over the whole range of Characteristic Impedances, but which are not as accurate as (4-4) or those of Pease. Cohn's approximate results are based on a general formula for the computation of attenuation constants published by Wheeler.³⁸ The procedure involves the evaluation of the derivatives of the Characteristic Impedance with respect to each of the line dimensions; in order to obtain results in reasonably simple form Cohn employed simple, approximate formulas for the Characteristic Impedance. He obtains separate results for the high and low impedance ranges, and the contributions from the inner and outer conductors are not separately determined. Although the results from the high and low impedance ranges differ by 8% in the overlap region, they are recommended which approximate answers are sufficient.

B. Recommended Approach.

Cohn's results seem to be most widely accepted in the literature and are expressed in graphical form for convenience.



The following dissertation will therefore follow Cohn although it will be considerably more complete than that given by Cohn.

C. Derivation of an expression for Stripline Attenuation.

In general, two types of losses occur in a transmission line. These are dissipation in the conductors and dissipation in the dielectric medium filling the line. In the usual case these losses are small enough to permit the total attenuation to be expressed as the sum of each type of attenuation computed individually.

That is:

$$\alpha = \alpha_c + \alpha_d \quad (4-5)$$

where

α = total attenuation per unit length

α_c = conductor attenuation per unit length

α_d = dielectric attenuation per unit length

1. Dielectric Attenuation.

Let us first consider the dielectric attenuation, α_d . It was shown in Appendix II that

$$\gamma = jk_1 = \pm j \omega \sqrt{\mu \epsilon} \quad (A2-56)$$

Furthermore if equations (A2-22) through (A2-24) of Appendix II are written in vector notation (assuming conductivity $\neq 0$), there results

$$\gamma = j \omega \sqrt{\mu \epsilon \left(1 + \frac{\sigma}{j \omega \epsilon} \right)} \quad (4-8)$$

Now

$$\gamma = \alpha + j \beta \quad (4-9)$$

In equation (4-9) α is the attenuation constant and β is the phase constant. We wish to find the attenuation constant α . To do so, we must divide equation (4-8) into its Real and Imaginary parts. We therefore proceed as follows.

$$\begin{aligned} \gamma^2 &= (\alpha + j \beta)^2 \\ &= j^2 \omega^2 \left[\mu \epsilon \left(1 + \frac{\sigma}{j \omega \epsilon} \right) \right] \end{aligned} \quad (4-10)$$

Expanding equation (4-10) and separating Real and Imaginary Parts, we find the Real part to be

$$\alpha^2 - \beta^2 = -\omega^2 \mu \epsilon \quad (4-11)$$

In order to solve equation (4-11) for α , another equation is needed. Equation (4-8) may be rearranged to read

$$\gamma = \sqrt{-\omega^2 \mu \epsilon + j \omega \sigma \mu} \quad (4-12)$$

Now

$$\begin{aligned} |\gamma|^2 &= \gamma \bar{\gamma} = \alpha^2 + \beta^2 \\ &= (\omega^4 \mu^2 \epsilon^2 + \omega^2 \sigma^2 \mu^2)^{1/2} \end{aligned} \quad (4-13)$$

Solving equations (4-12) and (4-13) simultaneously for α there results

$$\alpha = \omega \sqrt{\mu \epsilon \left(1 + \frac{\sigma^2}{\epsilon \omega^2} \right)^{1/2} - 1} \quad (4-14)$$

The quantity $\sigma/\omega\epsilon$ in equation (4-14) is defined as the loss tangent ($\tan \delta$).

For the dielectric materials of interest $\sigma/\omega\epsilon \ll 1$.

Expanding the term

$$\left[1 + \left(\frac{\sigma}{\omega\epsilon} \right)^2 \right]^{1/2}$$

in equation (4-14) in a binominal series, we get

$$\left[1 + \left(\frac{\sigma}{\omega\epsilon} \right)^2 \right]^{1/2} = 1 + 1/2 \left(\frac{\sigma}{\omega\epsilon} \right)^2 - 1/8 \left(\frac{\sigma}{\omega\epsilon} \right)^4 \dots \quad (4-15)$$

Since $\tan \delta \ll 1$, we may neglect all terms after the second term in equation (4-15). Substituting equation (4-15) into equation (4-14), we obtain the result

$$\alpha = \omega \sqrt{\frac{\mu \epsilon \tan^2 \delta}{4}} \quad \text{nepers/unit length} \quad (4-16)$$

Equation (4-16) may be simplified by realizing that

$$\omega = 2 \pi f = \frac{2 \pi c}{\lambda_0} = \frac{2 \pi}{\lambda_0 \sqrt{\mu_0 \epsilon_0}} \quad (4-17)$$

where:

c = velocity light

λ_0 = free space wavelength

μ_0 = free space permeability

ϵ_0 = free space permittivity

Equation (4-17) can be used to simplify (4-16) to read

$$\alpha = \frac{\pi \sqrt{\epsilon_r}}{\lambda_0} \tan \delta \quad \text{nepers/unit length} \quad (4-18)$$

A convenient working form of equation (4-16) is

$$\alpha = \frac{27.3 \sqrt{\epsilon_r} \tan \delta}{\lambda_0} \quad \text{db/unit length} \quad (4-19)$$

where:

λ_0 = free space wavelength

ϵ_r = relative dielectric constant

$\tan \delta$ = loss tangent of the dielectric

2. Conductor Attenuation.

We begin our investigation of conductor losses by rewriting equation (4-6) which was

$$\nabla \times H = (\sigma + j \omega \epsilon) E \quad (4-6)$$

Equation (4-6) may be further simplified, since the displacement current will never be appreciable in any reasonably good conductor, even at the highest radio frequencies. The terms to be compared in equation (4-6) are σ and $\omega\epsilon$. The precise values of ϵ for conductors are not known, yet most indications show that range of dielectric constants is much the same for conductors as for dielectrics. For platinum, a relatively poor conductor, the term $\omega\epsilon$ becomes equal to σ at about 1.5×10^{15} cps, if the dielectric constant is taken as ten times that of free space. This frequency is in the range of ultraviolet light. Consequently, for all but the poorest conductors (such as earth) the displacement current term is completely negligible compared to the conduction current at any frequency. Assuming $\sigma > > \omega\epsilon$, equation (4-6) simplifies to:

$$\nabla \times H = \sigma E \quad (4-20)$$

Taken the curl of both sides of (4-20)

$$\nabla \times \nabla \times H = \nabla \times \sigma E \quad (4-21)$$

But, there is a vector identity which states

$$\nabla \times \nabla \times H = \nabla (\nabla \cdot H) - \nabla^2 H \quad (4-22)$$

Utilizing equation (4-22) equation (4-21) becomes:

$$(\nabla \cdot H) - \nabla^2 H = \sigma \nabla \times E \quad (4-23)$$

Now Maxwell's 2nd and 3rd Laws were derived in Appendix II
and were in vector form

$$\nabla \times E = - \frac{\partial B}{\partial t} \quad (A2-10 \text{ thru } A2-12)$$

and

$$\nabla \cdot B = \nabla \cdot \mu H = 0 \quad (A2-38)$$

Using these two laws in equation (4-23), there results

$$\nabla^2 H = \sigma \mu \frac{\partial H}{\partial t} \quad (4-24)$$

This equation for the variation of H in a conductor
is in the form of a standard differential equation similar to
Laplace's equation, in the wave equation. The equation is
often called the skin effect or distribution equation and may
also be derived in terms of E, yielding

$$\nabla^2 E = \sigma \mu \frac{\partial E}{\partial t} \quad (4-25)$$

Since $i = \sigma E$, equation (4-25) may also be written in terms
of current density (i).

$$\nabla^2 i = \sigma \mu \frac{\partial i}{\partial t} \quad (4-26)$$

If sinusoidal distribution is assumed, equations (4-24) thru (4-26) become

$$\nabla^2 H = j \omega \sigma \mu H \quad (4-27)$$

$$\nabla^2 E = j \omega \sigma \mu E \quad (4-28)$$

$$\nabla^2 i = j \omega \sigma \mu i \quad (4-29)$$

These equations give the relation between space and time derivatives of magnetic field, electric field, or current density at any point in a conductor.

Let us now consider the case of a plane conductor with current flow in the z direction, x normal to the surface and no variations in the y and z directions. Fig 4-3 illustrates this concept. If equation (4-29) is expanded in Cartesian coordinates, there results:

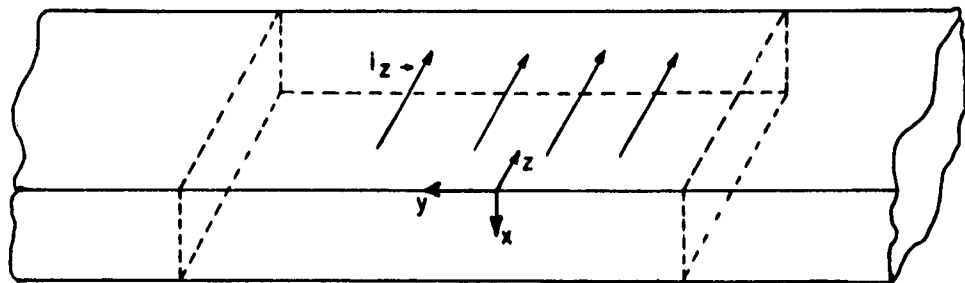


Fig 4-3 - Current Flow in a Plane Conductor

$$\left(\frac{\partial^2}{\partial x^2} + \frac{\partial^2}{\partial y^2} + \frac{\partial^2}{\partial z^2} \right) i = j \omega \sigma \mu i \quad (4-30)$$

However, we have stated that there are no variations in the y or z directions thus simplifying equation (4-30) to

$$\frac{\partial^2}{\partial x^2} i_z = j \omega \mu \sigma i_z$$

$$= \tau i_z \quad (4-31)$$

where

$$\tau^2 = j \omega \mu \sigma$$

or

$$\tau = (1 + j) \sqrt{\pi f \mu \sigma}$$

The solution to equation (4-31) is of the form

$$i_z = C_1 e^{-\tau x} + C_2 e^{+\tau x} \quad (4-32)$$

Current density would increase to the impossible value of infinity at $x = \infty$ unless C_2 is zero. C_1 may be written as the current density at the surface if we let $i_z = i_0$ when $x = 0$. Then

$$i_z = i_0 e^{-\tau x} \quad (4-33)$$

Define

$$\delta = \frac{1}{\sqrt{\pi f \mu \sigma}} \quad (4-34)$$

Then utilizing equation (4-34) in the definition of τ , there results

$$\tau = \frac{1 + j}{\delta}$$

Using equation (4-35), equation (4-33) may be rewritten as:

$$\begin{aligned} i_z &= i_0 e^{-(1+j)x/\delta} \\ &= i_0 e^{-x/\delta} e^{-j x/\delta} \end{aligned} \quad (4-36)$$

From the form of equation (4-36) it is apparent that magnitude of current decreases exponentially with penetration into the conductor, and δ has significance as the depth at which current density to $1/e$ (about 36.9 per cent) of its value at the surface. The phase of current also changes with increasing depth into the conductor according to the factor $e^{-j x/\delta}$.

To find the total current (I) flowing in the plane conductor, we must integrate the current density over a width w and to an infinite depth.

$$I = w \int_0^\infty i_z dx \quad (4-37)$$

Using equation (4-36) for i_z , we get



$$I = i_0 w \int_0^{\infty} e^{-(1+j) x/\delta} dx$$

$$= \frac{i_0 w d}{1+j} \quad (4-38)$$

The voltage E on the surface along the length of this conductor is obtained from the current density (i_0) and the volume resistivity (ρ).

$$E = i_0 z \rho \quad (4-39)$$

The "internal impedance" or "surface impedance" is computed from the ratio of the voltage E given by equation (4-39) and the current I as given by equation (4-38)

$$Z = \frac{E}{I} = (1+j) \frac{z_0}{w\delta} \quad (4-40)$$

Recalling that

$$\delta = \frac{1}{\sqrt{\pi f \mu \sigma}} \quad (4-34)$$

equation (4-40) becomes:

$$Z = (1+j) z_0 / w \sqrt{\pi f \mu \rho} \quad (4-41)$$

Dividing Z into its Real and Imaginary Parts results in

$$R = X = z/w \sqrt{\pi f \mu \rho} \quad (4-45)$$

Let us now define the resistance of a surface of unit length and width and of depth δ by

$$R_s = \rho/\delta \quad (4-46)$$

Equation (4-46) may be simplified by using the definition of δ as given in equation (4-34). The resultant expression is:

$$R_s = \sqrt{\rho \pi \mu f} \quad (4-47)$$

Comparing equations (4-45) and (4-47), we see that

$$R = z/w R_s \quad (4-48)$$

The internal inductance can be calculated from equations (4-45) and (4-34). After rearrangement of terms, there results

$$L = X/w = z/w (\mu \delta/2) \quad (4-49)$$

This is the inductance of a layer of conductive material having a thickness of $\delta/2$, one half of the depth of penetration. This merely means that the mean depth of the current is one half the thickness of the conducting layer.

Some inductance formulas carry the assumption that the current travels in a thin sheet on the surface of the conductor, as if the resistivity were zero. Such assumptions are usual for transmission lines, wave guides, cavity resonators, and piston attenuations. Such formulas can be corrected for the depth of penetration by assuming that the current sheet is at depth $\delta/2$ from the surface. This is the same as assuming that the surface of the conductor recedes by the amount

$$\frac{\delta}{2} \cdot \frac{\mu}{\mu_0} \quad (4-50)$$

The second factor has an effect only if the conductive material has a permeability μ differing from that of space μ_0 . The same correction is applicable to shielding partitions, regarding their effect on the inductance of near-by circuits.

There is sometimes a question which surface of a conductor will carry the current. The rule is, that the current follows the path of least impedance. Since the impedance is mainly inductive reactance, in the common cases, the current tends to follow the path of least inductance. In a ring, for example,

the current density is greater on the inner surface. In a coaxial line, the current flows one way on the outer surface of the inner conductor and returns on the inner surface of the outer conductor.

In determining whether the thickness is much greater than the depth of penetration, the effective thickness corresponds to the depth of a hypothetical line. In a symmetrical conductor with penetration from both sides, as in a strip or a wire, the effective thickness is the depth to the center of the conductor. In a shielding partition with penetration into the surface on one side and with open space on the other side, the effective thickness is the actual thickness. If the effective thickness exceeds twice the depth of a penetration, the accuracy of the above impedance formulas is sufficient for most purposes, within two per cent of a plane surface.

The "incremental-inductance rule" is a formula which gives the effective resistance caused by the skin effect, but is based entirely on inductance computations. Its great value lies in its general validity for all metal objects in which the current and magnetic intensity are governed by the skin effect. In other words, the thickness and the radius of curvature of exposed metal surfaces must be much greater than the depth of penetration, say at least twice as great. It is equally applicable to current conductors, shields, and iron cores.



This rule is generalization of (4-48) which states that the surface resistance R is equal to the internal reactance X as governed by the skin effect. The internal reactance is the reactance of the internal inductance L in (4-49). This inductance is the increment of the total inductance which is caused by the penetration of magnetic flux under the conductive surface. This change of inductance is the same as would be caused by the surface receding to the depth given in (4-50). Starting with a knowledge of this depth, the reverse process of computation gives the increment of inductance caused by the penetration, and from that the effective resistance as governed by the skin effect.

The incremental-inductance rule is stated, that the effective resistance in a circuit is equal to the change of reactance caused by the penetration of magnetic flux into metal objects. It is valid for all exposed metal surfaces which have thickness and radius of curvature much greater than the depth of penetration, say at least twice as great.

The application of the incremental-inductance rule involves the following steps:

- (a) Select the circuit in which the effective resistance is to be evaluated, and identify the exposed metal surfaces in which the skin effect is prevalent.

- (b) Compute the rate of change of inductance of this circuit with recession of each of the metal surfaces, $\frac{\partial L_o}{\partial x}$, assuming zero depth of penetration.*
- (c) Note that the increment of inductance caused by penetration into each surface is

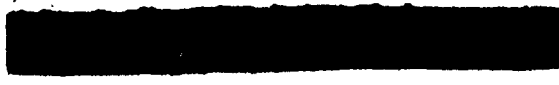
$$L = \frac{\mu}{\mu_0} \cdot \frac{\delta}{2} \cdot \frac{L_o}{\partial x} \quad (4-51)$$

- (d) Compute the effective resistance contributed by each surface.

$$R = \omega L = \frac{1}{\mu_0} \cdot \frac{\partial L_o}{\partial x} \quad R_s \text{ ohms} \quad (4-52)$$

For a surface carrying the current of the circuit, this is identical with (4-48). For the effect of near-by metal objects, such as shields, this formula is easily applied in many practical cases. It is most useful in cases of non-uniform current distribution, which otherwise would require integrations.

* A second-order approximation is secured if $\frac{\partial L_o}{\partial x}$ is computed assuming that the surface is below the actual surface by the amount given in (4-50).



We must now develop an expression for conductor attenuation in terms of R and the Characteristic Impedance Z_0 . In the initial discussion of the theory of stripline, we saw that since a TEM mode is generated, the expressions for transmission lines hold. One of the most basic parameters is the propagation constant.

$$\gamma = \sqrt{zy} = \sqrt{(R + j\omega L)(G + j\omega C)} \quad (4-53)$$

In the construction of well designed transmission lines, it is found that $R \ll \omega L$ and $G \ll \omega C$. Using these approximations, we can therefore write our propagation constant as a Taylor's Series and consider only the first several terms.

$$\sqrt{z} = (j\omega L + R)^{1/2} = \sqrt{j\omega L} \left(1 + \frac{R}{j^2 \omega L} \dots \right) \quad (4-54)$$

and

$$\begin{aligned} \sqrt{y} &= (j\omega C + G)^{1/2} = j\omega \sqrt{LC} \left[1 + \frac{RG}{4\omega^2 LC} \right. \\ &\quad \left. - j \left(\frac{G}{2\omega C} - \frac{R}{2\omega L} \right) \right] \end{aligned}$$

Then

$$j = \sqrt{zy} = R/2 \sqrt{C/L} + G/2 \sqrt{L/C} + j\omega \sqrt{LC} \left[1 - \frac{RG}{4\omega^2 LC} \right] \quad (4-55)$$

Since

$$\gamma = \alpha_c + j\beta \quad (4-56)$$

the attenuation constant α_c may be found by taking the Real part of equation (4-55) resulting in

$$\alpha_c = R/2 \sqrt{C/L} + G/2 \sqrt{L/C} \text{ neper/m} \quad (4-57)$$

From transmission line theory, we know that

$$Z_0 = \sqrt{L/C} \quad (4-58)$$

Substituting equation (4-58) into equation (4-57) we get

$$\alpha_c = \frac{R}{2 Z_0} + \frac{G Z_0}{2} \text{ nepers/m} \quad (4-59)$$

Let us examine equation (4-59) more closely. G is the shunt conductance between conductors. With the common dielectrics in use, it is small enough to be neglected. Using this approximation, equation (4-59) becomes:

$$\alpha_c \approx \frac{R}{2 Z_0} \text{ nepers/m} \quad (4-60)$$

Equation (4-60) is not in a convenient working form and must therefore be modified further. In Chapter II of this report were given the relations

$$Z_0 = \sqrt{L/C} \quad (2-1)$$

and

$$Z_0 = \frac{1}{\sqrt{C}} \quad (2-3)$$

Equating equations (2-1) and (2-3) and solving for L, we get

$$L = \frac{Z_0}{v} \quad (4-61)$$

An expression for velocity of propagation (v) as compared to the velocity of light (c) was also given in Chapter II.

It was

$$v = \frac{c}{\sqrt{\epsilon_r}} \quad (2-4)$$

The substitution of equation (2-4) into equation (2-61)

leads to

$$L = \frac{Z_0 \sqrt{\epsilon_r}}{c} \quad (4-62)$$

If equation (4-62) is used in equation (4-52), there results

$$R_s = \frac{R_s}{\mu_0} - \frac{\partial}{\partial x} \left(\frac{Z_0 \sqrt{\epsilon_r}}{c} \right) \quad (4-63)$$

$$= \frac{R_s}{\mu_0 c} \sqrt{\epsilon_r} - \frac{\partial Z_0}{\partial x}$$

But

$$\mu_0 c = 4 \pi \times 10^{-7} \times 3 \times 10^8 = 376.7$$

so that

$$R = \frac{R_s \sqrt{\epsilon_r}}{376.7} \quad \frac{\partial Z_0}{\partial x} \quad (4-64)$$

If equation (4-64) is now used in equation (4-60) we get a more desirable form for the attenuation constant.

$$\alpha_c = \frac{R_s \sqrt{\epsilon_r}}{753.2 Z_0} \quad \frac{\partial Z_0}{\partial n} \quad \text{nepers/cm} \quad (4-65)$$

where x has been changed to n to conform to Cohn's notation of distance perpendicular to the conductor surface.

We must now evaluate the term $\frac{\partial Z_0}{\partial n}$ in equation (4-65).

Consider the cross section of Stripline as shown in Fig 4-4.

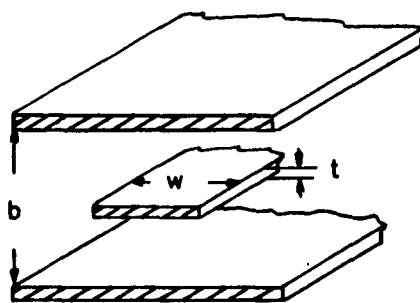


Fig 4-4 - Cross Section of Stripline

δn is perpendicular to the current carrying conductors.

We must therefore consider the inner surfaces of the two ground planes and the four surfaces of the center strip. A change δn inwardly normal to the ground planes requires a change $\delta b = 2 \delta n$ in ground plane spacing. Similarly, in the strip, the necessary changes in dimensions are $w = -2 \delta n$ and $t = -2 \delta n$. The total change (total differential) for a uniform change in δn is therefore:

$$\frac{\partial Z_o}{\partial n} = \frac{\frac{\partial Z_o}{\partial b} \delta b + \frac{\partial Z_o}{\partial w} \delta w + \frac{\partial Z_o}{\partial t} \delta t}{\delta n} \quad (4-66)$$

Substituting the values for δb , δw and δt as given above in equation (4-66), there results

$$\frac{\partial Z_o}{\partial n} = \frac{2 \partial Z_o}{\partial b} - \frac{2 \partial Z_o}{\partial w} - \frac{2 \partial Z_o}{\partial t} \quad (4-67)$$

When equation (4-67) is incorporated into equation (4-65), the desired expression for the attenuation constant α_c results and is

$$\alpha_c = \frac{R_s \sqrt{\epsilon_r}}{376.6 Z_o} \left(\frac{\partial Z_o}{\partial b} - \frac{\partial Z_o}{\partial w} - \frac{\partial Z_o}{\partial t} \right) \text{nepers/m} \quad (4-68)$$

a. Wide Strip case.

Equation (4-68) will first be evaluated for the wide strip case ($w/b - t > 0.35$) using equation (2-9) which is

$$Z_o = \frac{94.15}{\sqrt{\epsilon_r} \left(\frac{w/b}{1-t/b} + \frac{c_f'}{0.0885 \epsilon_r} \right)} \text{ ohms} \quad (2-9)$$

If the partial derivatives of equation (4-68) are evaluated using equation (2-9), the following results are obtained:

$$\frac{\partial Z_o}{\partial b} = \frac{\sqrt{\epsilon_r} Z_o^2}{94.15 b} \left(\frac{w/b}{1-t/b} + \frac{w/b \cdot t/b}{(1-t/b)^2} - \frac{b}{0.0885 \epsilon_r} \frac{\partial c_f'}{\partial b} \right) \quad (4-69)$$

$$\frac{\partial Z_o}{\partial w} = \frac{-\sqrt{\epsilon_r} Z_o^2}{94.15 b} \left(\frac{1}{1-t/b} + \frac{b}{0.0885 \epsilon_r} \frac{\partial c_f'}{\partial w} \right) \quad (4-70)$$

$$\frac{\partial Z_o}{\partial t} = \frac{-\sqrt{\epsilon_r} Z_o^2}{94.15 b} \left(\frac{w/b}{(1-t/b)^2} - \frac{b}{0.0885 \epsilon_r} \frac{\partial c_f'}{\partial t} \right) \quad (4-71)$$

If equations (4-69) through (4-71) are substituted into equation (4-68), there results

$$\alpha_c = \frac{\frac{4}{3} R_s \epsilon_r Z_0}{(376.6)^2 b} \left[\frac{1}{1 - t/b} + \frac{2 w/b}{(1 - t/b)^2} \right. \\ \left. \frac{+b}{0.0885 \epsilon_r} \left(- \frac{\partial c_f'}{\partial b} + \frac{\partial c_f'}{\partial w} + \frac{\partial c_f'}{\partial t} \right) \right] \text{nepers/m}$$
(4-72)

The partial derivatives of c_f' may be evaluated through the use of equation (2-10) which was

$$c_f' = \frac{0.0885 \epsilon_r}{\pi} \left[\frac{2}{1-t/b} \ln \left(\frac{1}{1-t/b} + 1 \right) \right. \\ \left. - \left(\frac{1}{1-t/b} - 1 \right) \ln \left(\frac{1}{(1-t/b)^2} - 1 \right) \right] \text{mmf/cm}$$
(2-10)

Make the substitution

$$x = \frac{1}{1 - t/b}$$
(4-73)

in equation (2-10). The result is

$$c_f' = \frac{0.0885 \epsilon_r}{\pi} \left[2x \ln(x+1) - (x-1) \ln(x^2-1) \right]$$
(2-74)

Taking the partial derivative of equation (4-74) with respect to x , we find that

$$\frac{\partial c_f'}{\partial x} = \frac{0.0885 \epsilon_r}{\pi} \ln \left(\frac{x+1}{x-1} \right)$$
(4-75)

Now

$$\frac{\partial x}{\partial w} = \frac{\partial}{\partial w} \left(\frac{1}{1 - t/b} \right) = 0 \quad (4-76)$$

since x is not a function of w .

Also

$$\frac{\partial x}{\partial b} = \frac{t/b}{b (1 - t/b)^2} \quad (4-77)$$

and

$$\frac{\partial x}{\partial t} = \frac{1}{b (1 - t/b)^2} \quad (4-78)$$

Therefore

$$\begin{aligned} \frac{\partial c_f'}{\partial b} &= \frac{\partial c_f'}{\partial x} \cdot \frac{x}{b} = \\ \frac{0.0885 \epsilon_r}{\pi} &\left(\ln \frac{x+1}{x-1} \right) \cdot \frac{-t/b}{b (1 - t/b)^2} \end{aligned} \quad (4-79)$$

$$\begin{aligned} \frac{\partial c_f'}{\partial w} &= \frac{\partial c_f'}{\partial x} \cdot \frac{\partial x}{\partial w} \\ &= \frac{0.0885 \epsilon_r}{\pi} \left(\ln \frac{x+1}{x-1} \right) \cdot 0 = 0 \end{aligned} \quad (4-80)$$

and

$$\frac{\partial C_f'}{\partial t} = \frac{\partial C_f'}{\partial x} \cdot \frac{\partial x}{\partial t}$$

$$= \frac{0.0885 \epsilon_r}{\pi} \left(\ln \frac{x+1}{x-1} \right) \cdot \frac{1}{b (1-t/b)^2} \quad (4-81)$$

If equations (4-79) through (4-81) are substituted into equation (4-72), we see that

$$\alpha_c = \frac{4 R_s \sqrt{\epsilon_r} Z_0 \sqrt{\epsilon_r}}{(376.6)^2 b} \left[\frac{1}{1-t/b} + \frac{2 w/b}{(1-t/b)^2} \right. \\ \left. + \frac{1}{\pi} \frac{(1+t/b)}{(1-t/b)^2} \ln \left(\frac{\frac{1}{1-t/b} + 1}{\frac{1}{1-t/b} - 1} \right) \right] \text{nepers/unit length} \quad (4-82)$$

For copper $R_s = 8.25 \times 10^{-3} \sqrt{f_{kmc}}$ ohms/square

We also wish our result in decibels per unit length rather than in nepers per unit length. Remembering that one neper equals 8.686 decibels and using R_s for copper in equation (4-82) we obtain the final result, which is

$$\alpha_c = \frac{2.02 \times 10^{-5} \sqrt{f_{kmc}} \sqrt{\epsilon_r} Z_0 \sqrt{\epsilon_r}}{b} x$$

$$\left[\frac{1}{1 - t/b} + \frac{2w}{(1 - t/b)^2} + \frac{1}{\pi} \left(\frac{(1 + t/b)}{(1 - t/b)^2} \right) \ln \left(\frac{\frac{1}{1 - t/b} + 1}{\frac{1}{1 - t/b} - 1} \right) \right]$$

Equation (4-83) is valid in the same range as $w/b - t \geq 0.35$.

The term $(\sqrt{\epsilon_r} Z_0)$ is determined as a function of the cross sectional dimensions. The term α_c is expressed in db/unit length where the unit length is that used to measure b . For example if b is in inches, α_c is db/inch. If the conducting surface is other than copper, the result should be scaled by the ratio of the surface resistivity of this metal to that of copper.

b. Narrow Strip case.

Let us now evaluate equation (4-68) for narrow Strip widths. It was shown in Chapter II that for $w/b - t \leq 0.35$ the Characteristic Impedance could be expressed by equation (2-11) which is

$$Z_0 = \frac{60}{\sqrt{\epsilon_r}} \ln \frac{4b}{d_o} \text{ ohms} \quad (2-11)$$

To evaluate equation (4-68) which is

$$\alpha_c = \frac{R_s \sqrt{\epsilon_r}}{376.6 Z_o} \left(\frac{\partial Z_o}{\partial b} - \frac{\partial Z_o}{\partial w} - \frac{\partial Z_o}{\partial t} \right) \text{nepers/m} \quad (4-68)$$

$\frac{\partial Z_o}{\partial b}$, $\frac{\partial Z_o}{\partial w}$ and $\frac{\partial Z_o}{\partial t}$ must be evaluated.

Utilizing equation (2-11), we see that

$$\frac{\partial Z_o}{\partial b} = \frac{60}{\sqrt{\epsilon_r} b} \quad (4-84)$$

$$\frac{\partial Z_o}{\partial w} = \frac{\partial Z_o}{\partial d_o} \cdot \frac{\partial d_o}{\partial w} = - \frac{60}{\sqrt{\epsilon_r} d_o} \cdot \frac{\partial d_o}{\partial w} \quad (4-85)$$

and

$$\frac{\partial Z_o}{\partial t} = \frac{\partial Z_o}{\partial d_o} \frac{\partial d_o}{\partial t} = - \frac{60}{\sqrt{\epsilon_r} d_o} \frac{\partial d_o}{\partial t} \quad (4-86)$$

Incorporating equation (4-84) thru equation (4-86) into equation (4-68), there results

$$\alpha_c = \frac{R_s}{2\pi Z_o b} \left[1 + \frac{b}{d_o} \left(\frac{\partial d_o}{\partial w} + \frac{\partial d_o}{\partial t} \right) \right] \text{nepers/unit length} \quad (4-87)$$

Making the substitutions $R_s = 8.25 \times 10^{-3} \sqrt{f_{kmc}}$ and one neper = 8.686 db, equation (4-88) results and is

$$\alpha_c = \frac{0.018402 \sqrt{\epsilon_r f_{kmc}}}{(\sqrt{\epsilon_r Z_0}) b} \left[1 + \frac{b}{d_o} \left(\frac{\partial d_o}{\partial w} + \frac{\partial d_o}{\partial t} \right) \right] \text{db/unit length}$$
(4-88)

Equation (4-88) is valid for $\frac{w}{b-t} \leq 0.35$ and $t/b \leq 0.25$.

Although the equation relating d_o , w and t is known, it is an implicit function of the variables and too complex to permit derivation of exact formulas for the partial derivatives. However, a set of five place values of do/d' , versus d''/d' were available,^{*} and permitted a precise numerical evaluation of these derivatives. A plot of $(\partial do/\partial w + \partial do/\partial t)$ as a function of the strip cross section ratio if given in Fig 4-5. Values from this curve may be used in equation (4-88) to obtain the attenuation per unit length of narrow strip lines.

For d''/d' small, where "d''" is the smaller and "d'" the larger of the two dimensions "w" and "t", an approximate formula for d_o exists.³⁹

^{*} These were computed in 1950 by C. Flammer of Stanford Research Institute.

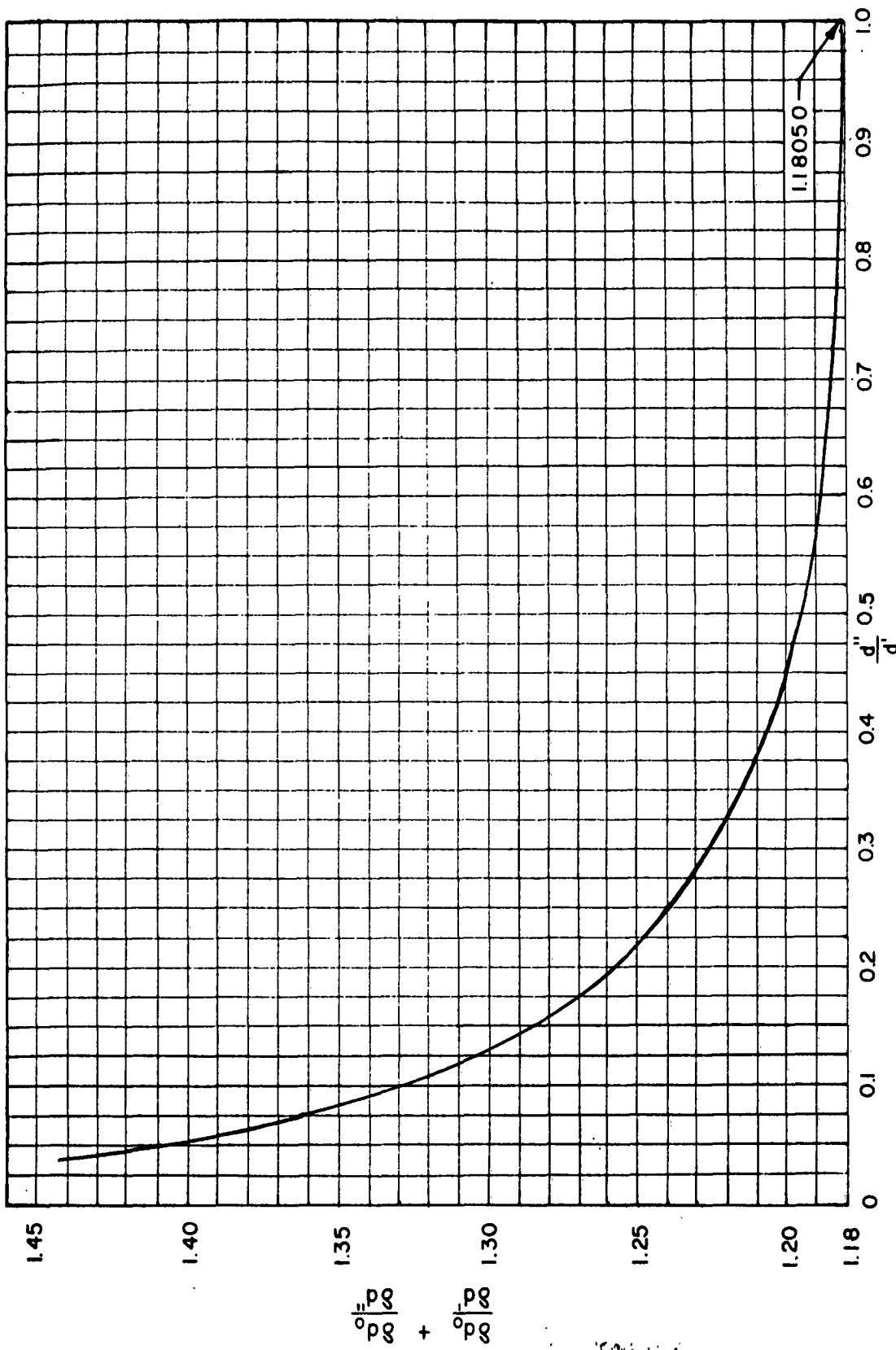
10^4 

Fig. 4-5 PARTIAL DERIVATIVE SUMMATION FOR USE IN EQUATION 4-88

$$\frac{d_o}{d'} = 1/2 \left[1 + \frac{d''}{\pi d'} \left(1 + \ln \frac{4\pi d'}{d''} \right) \right] \quad (4-89)$$

Equation (4-89) is accurate for $d''/d' \leq 0.06$. It was found by Cohn³⁷ that an improvement occurs in equation (4-89) if it is modified to read

$$\begin{aligned} \frac{d_o}{d'} &= 1/2 \left[1 + \frac{d''}{\pi d'} \left(1 + \ln \frac{4\pi d'}{d''} \right) \right. \\ &\quad \left. + 0.510 \left(\frac{d''}{d'} \right)^2 \right] \end{aligned} \quad (4-90)$$

With this modification, equation (4-90) is extremely accurate for d''/d' up to at least 0.11.

Differentiation of equation (4-90) yields

$$\begin{aligned} \frac{\partial d_o}{\partial w} + \frac{\partial d_o}{\partial t} &= \frac{\partial d_o}{\partial d'} + \frac{\partial d_o}{\partial d''} = 1/2 + 0.669 \frac{d''}{d'} \\ &- 0.255 \left(\frac{d''}{d'} \right)^2 + 1/2 \pi \ln 4 \pi \frac{d'}{d''} \end{aligned} \quad (4-91)$$

Inserting the results of equation (4-91) into equation (4-88) gives the final result which is:

$$\alpha_c = \frac{0.011402 \sqrt{\epsilon_r} f_{kmc}}{(\sqrt{\epsilon_r} - z_o) b} \left[1 + \frac{b}{d_o} \left(\frac{1}{2} + 0.669 \frac{d''}{d'} \right. \right. \\ \left. \left. - 0.255 \left(\frac{d''}{d'} \right)^2 + \frac{1}{2} \pi \ln 4 \pi d'/d'' \right) \right] \quad (4-92)$$

Equation (4-92) is applicable for $w/b - t \leq 0.35$, $t/b \leq 0.25$ and either $t/b \leq 0.11$ or $w/t \leq 0.11$.

3. Attenuation Graphs.

It is of considerable interest to compare the formulas for the wide and narrow strip cases in the vicinity of the transition point $w/(b-t) = 0.35$. Fig 4-6 shows curves computed from equations (4-83) and (4-92) for the typical case of $t/b = 0.01$. It is seen that the curves show an approximate agreement near $w/(b-t) = 0.35$, but differ by about eight per cent. This discrepancy is reasonable since the two attenuation formulas utilize the derivatives of two approximate Characteristic Impedance formulas, and, although the latter agree very closely, their errors will necessarily show up most strongly in their derivatives. A reasonable transition between the two attenuation curves is shown in Fig 4-6. It is reasonable to believe that the resulting composite curve is within a few per cent of the true one.

The above process has been carried out for t/b ratios from 0.001 to 0.1. Equations (4-83) and (4-88) and (4-92) were used in their respective ranges of validity. In

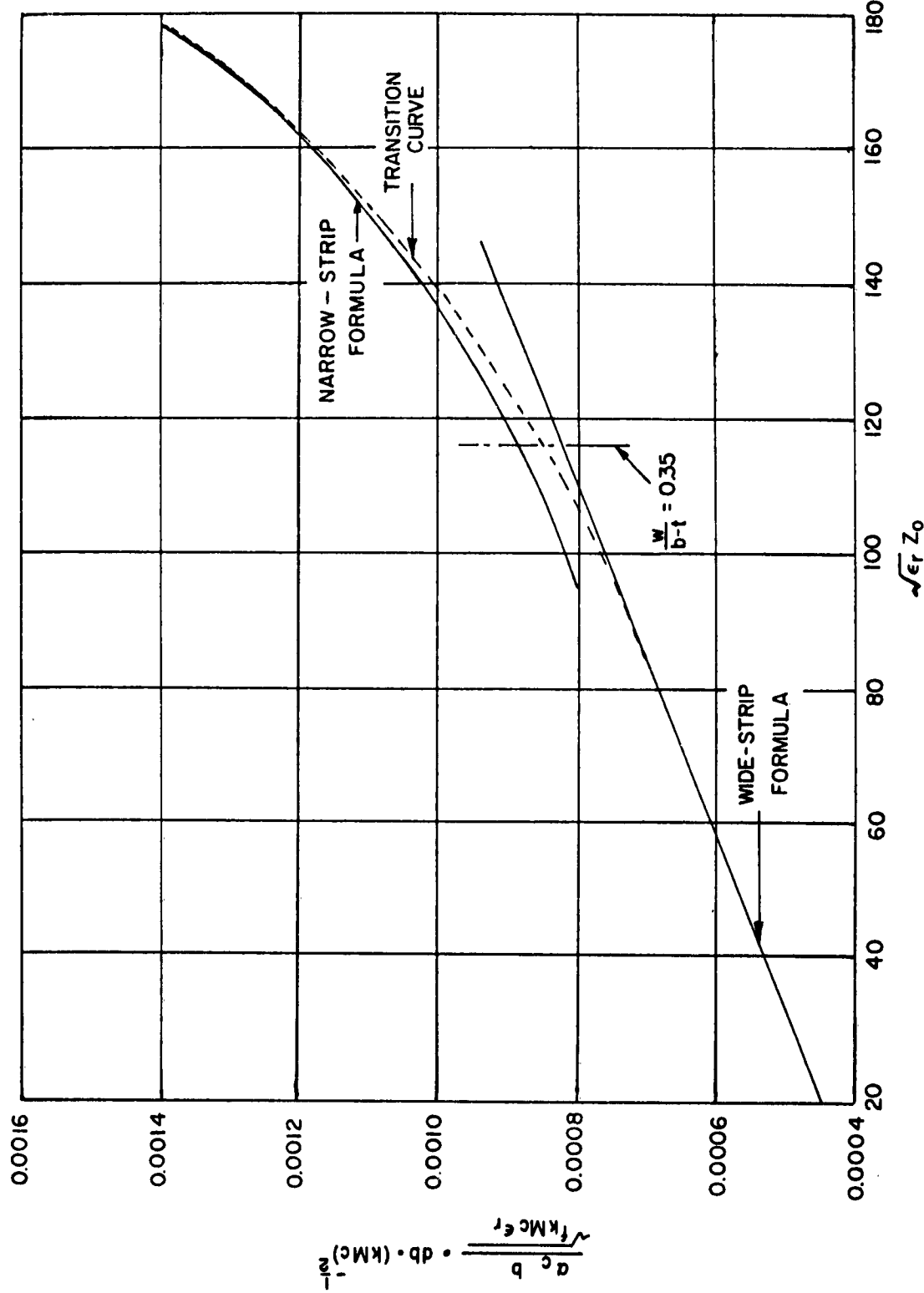


Fig. 4-6 COMPARISON OF THE WIDE- and NARROW-STRIP ATTENUATION FORMULAS IN THEIR TRANSITION REGION.

all cases the curves for narrow and wide strips agree at $w/(b-t) = 0.35$ within 10%. The family of composite curves is given in Fig 4-7, as a function of Z_0 and various values of t/b . It is seen that minimum attenuation is approached at Z_0 , which corresponds to the case of an infinite parallel-plane transmission line of spacing $(b-t)/2$. If field fringing did not occur, with consequent non-uniformity of current distribution, the attenuation would be independent of strip width and Characteristic Impedance. The effect of this current non-uniformity is therefore quite large in the useful range of Characteristic Impedance.

Fig 4-7 applies to copper conductors. For other conductors the attenuation should be scaled proportional to R_s . The ordinate parameter is $\alpha_c b / \sqrt{f_{kmc} \epsilon_r}$ in db(kmc) $^{-1/2}$. Note that this gives α_c directly in db per inch at a frequency of 1 kmc, when $\epsilon_r = 1$ and $b = 1$ in. The total attenuation when a dielectric material fills the line is given by

$$\alpha = \alpha_c + \frac{27.3 \sqrt{\epsilon_r} \tan \delta}{\lambda_0} \text{ db/unit length} \quad (4-93)$$

4. Measurement of Attenuation.

In order to check the correlation between theoretical and measured values of attenuation several stripline spirals were built and evaluated. A spiral was used since it was felt that this was the only practical way to get a representative length of Stripline in a reasonable amount of space. All spirals had a Characteristic Impedance of 50 ohms. Lines A and B were built and tested by Wigington,⁴⁰ while line C was constructed and evaluated by the author.

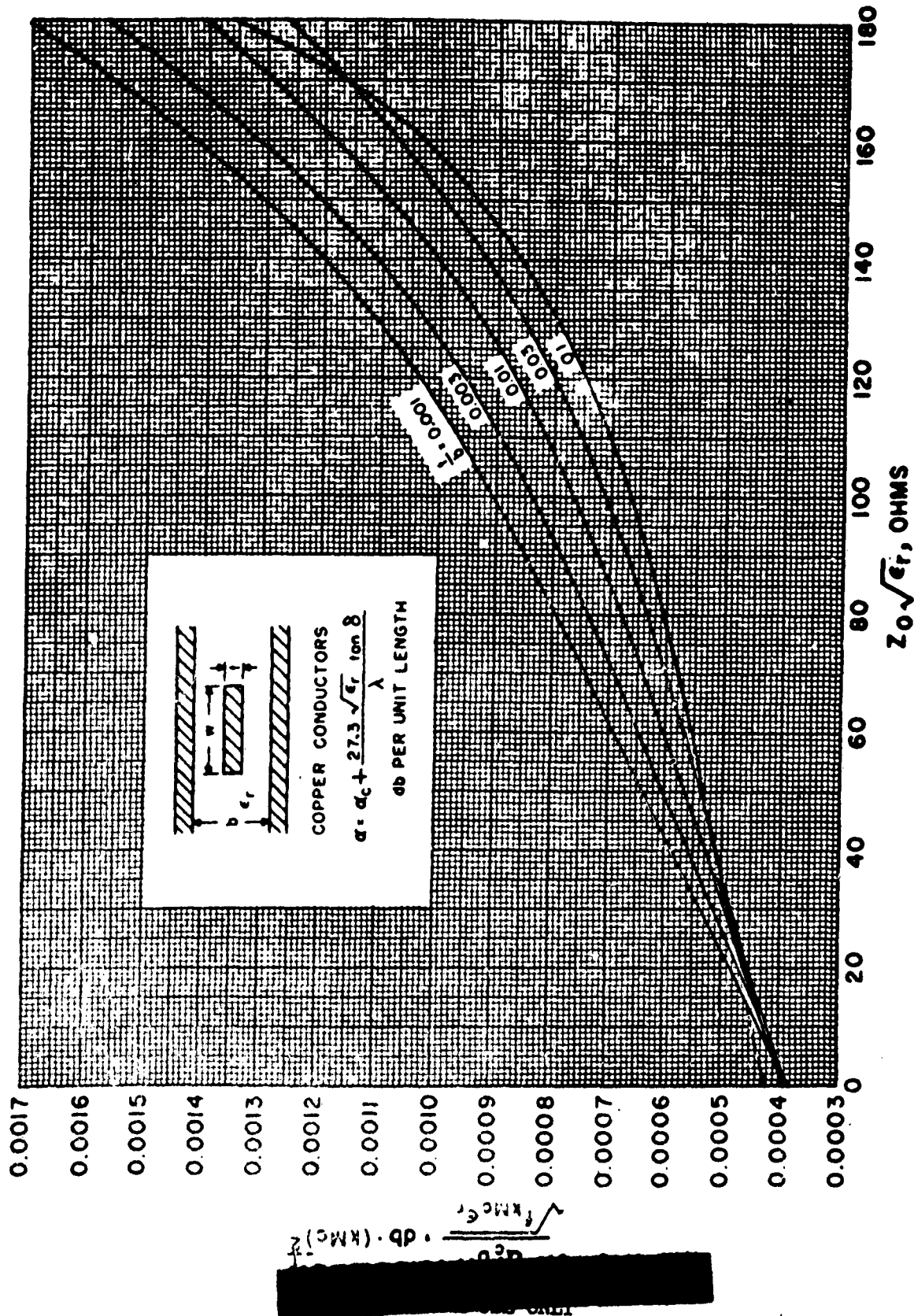
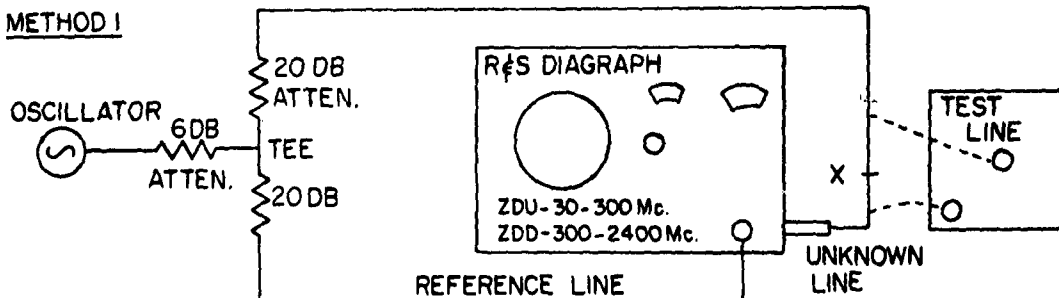


Fig. 4-7 - Theoretical attenuation of copper shielded strip line in a dielectric medium ϵ_r .

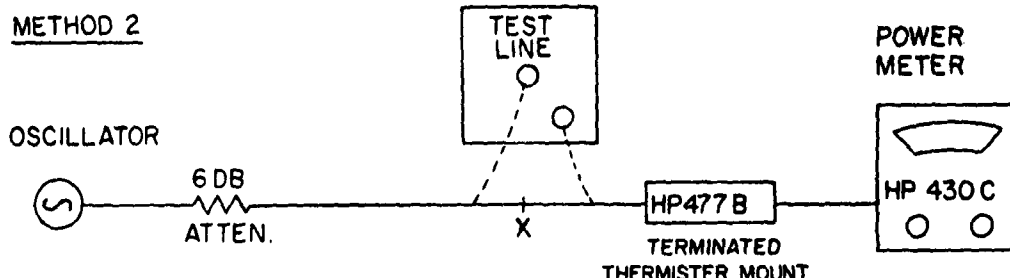
The method of measurement is shown in Fig 4-8. From frequencies of 30 to 2400 megacycles simultaneous measurements were made using both a Rhodes and Schwarz Diagraph and a Hewlett Packard power meter with its accompanying thermistor mount. Good correlation was found between the values of attenuation determined from the Diagraph and from the power meter. The power meter reading was used since it could be more accurately read.

The Diagraph is essentially an automatic Smith Chart which will read attenuation and phase shift directly through the use of a moving spot of light. The power meter was balanced with the Stripline Spiral out of the circuit. The line was then broken and the Spiral inserted. The attenuation due to the Spiral is then read directly from the meter.

Above 2400 megacycles only the power meter was used. When total Spiral attenuation exceeded 10 decibels, the power meter could not be used directly and a slight modification was necessary. Individual General Radio pads were measured at a given frequency. Enough of these pads were inserted in the line so that the difference between the total value of the pads and the expected attenuation of the Stripline was less than 10 decibels. The power meter was then balanced with the pads in the line. Finally, the pads were removed and the Spiral inserted. The total attenuation was then the sum of the pad attenuation and the reading on the power meter.

METHOD 1

1. SET POWER LEVEL AND DIAGRAPH TO READ 0 DB.
2. BREAK UNKNOWN LINE AT X AND INSERT TEST LINE.
3. READ ATTENUATION DIRECTLY FROM DIAGRAPH.

METHOD 2

1. ESTABLISH REFERENCE POWER.
2. BREAK LINE AT X AND INSERT TEST LINE.
3. READ ATTENUATED POWER.
4. CALCULATE ATTENUATION.

COAXIAL COMPONENTS

GR 50 Ohm CABLE, ADAPTERS, TEES, ATTENUATORS, ELLS.

OSCILLATORS

RFS SMLM OSC., 30-300 Mc.
 GR 1021 SIG. GEN., PLUG-IN P2,250-920 Mc.
 P 4,900-2000 Mc.
 GR 1218-A UNIT OSC., 900-2000 Mc.
 HP MOD. 616A SIG. GEN., 1800-4000 Mc.
 HP MOD. 685A 5200-8300 Mc.

RFS = RHODE AND SCHWARTZ

GR = GENERAL RADIO CO.

HP = HEWLETT-PACKARD CO.

Fig. 4-8. ATTENUATION MEASUREMENTS, METHOD AND EQUIPMENT

It should be noted that no measurements were made on Spirals A and B above 4000 megacycles. Above this frequency values were calculated from equation (5-25). This equation appears in the chapter on stripline Transient Behavior.

In the measurement of Spiral C, it was observed that the attenuation began to rise sharply above 3500 megacycles. No information was available as to the increase of loss tangent and the decrease of dielectric constant with frequency was available locally. Correspondence with the manufacturer (Minnesota Manufacturing and Mining Company) provided only one additional value of loss tangent and dielectric constant. Since theoretical attenuation depends on these two constants directly, its accuracy is only as good as that of these parameters. Wigington's¹⁴⁰ results are shown as Fig 4-9a and the author's as Fig 4-9b. Table 4-1 is also included to show the information of Fig 4-9b in numerical form. Finally a picture of stripline Spirals A and C is shown. Spiral A is opened up to show its interior, while Spiral C is in its assembled form.

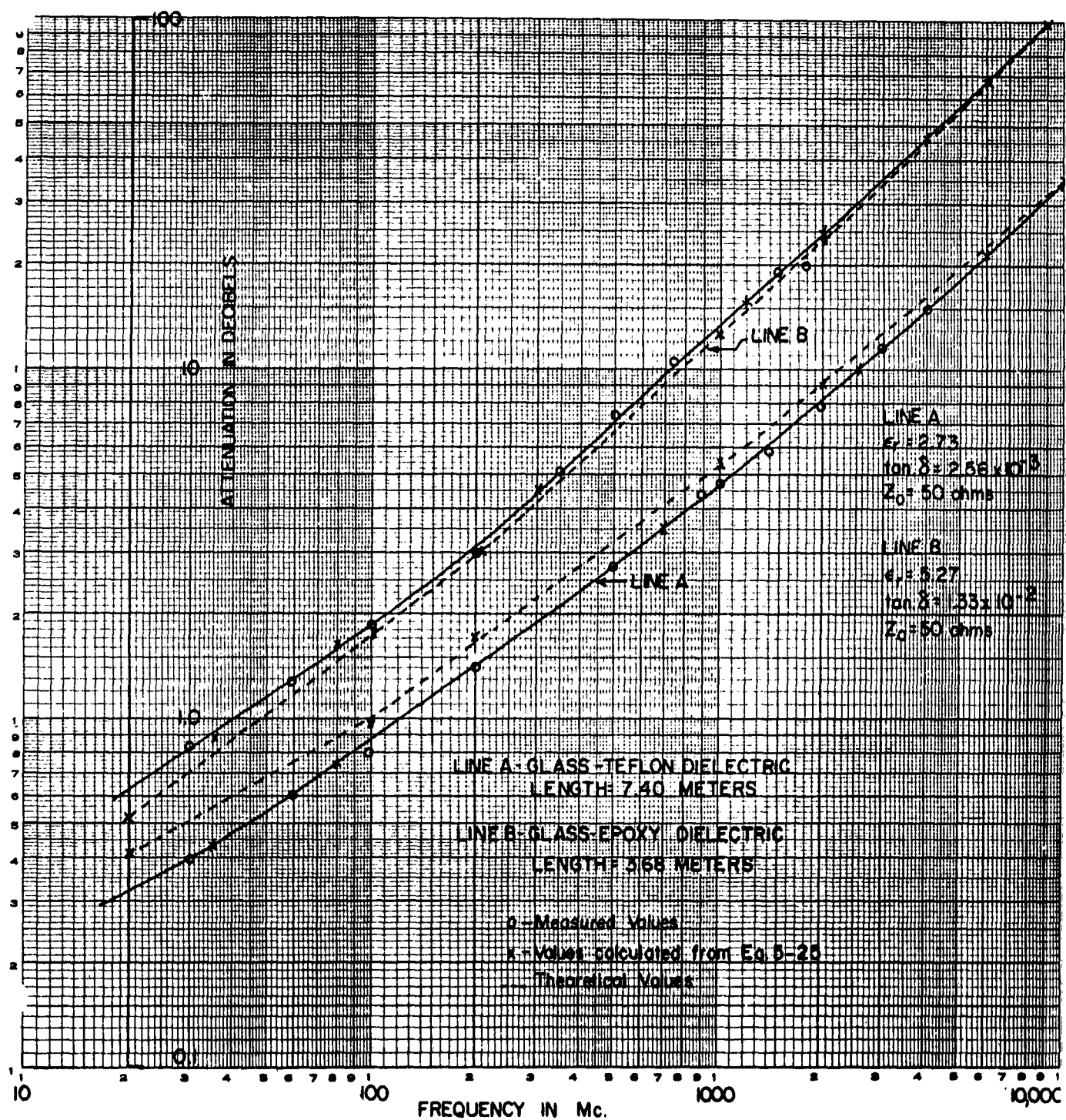


Fig. 4-9a. ATTENUATION MEASUREMENTS FOR LINES A and B

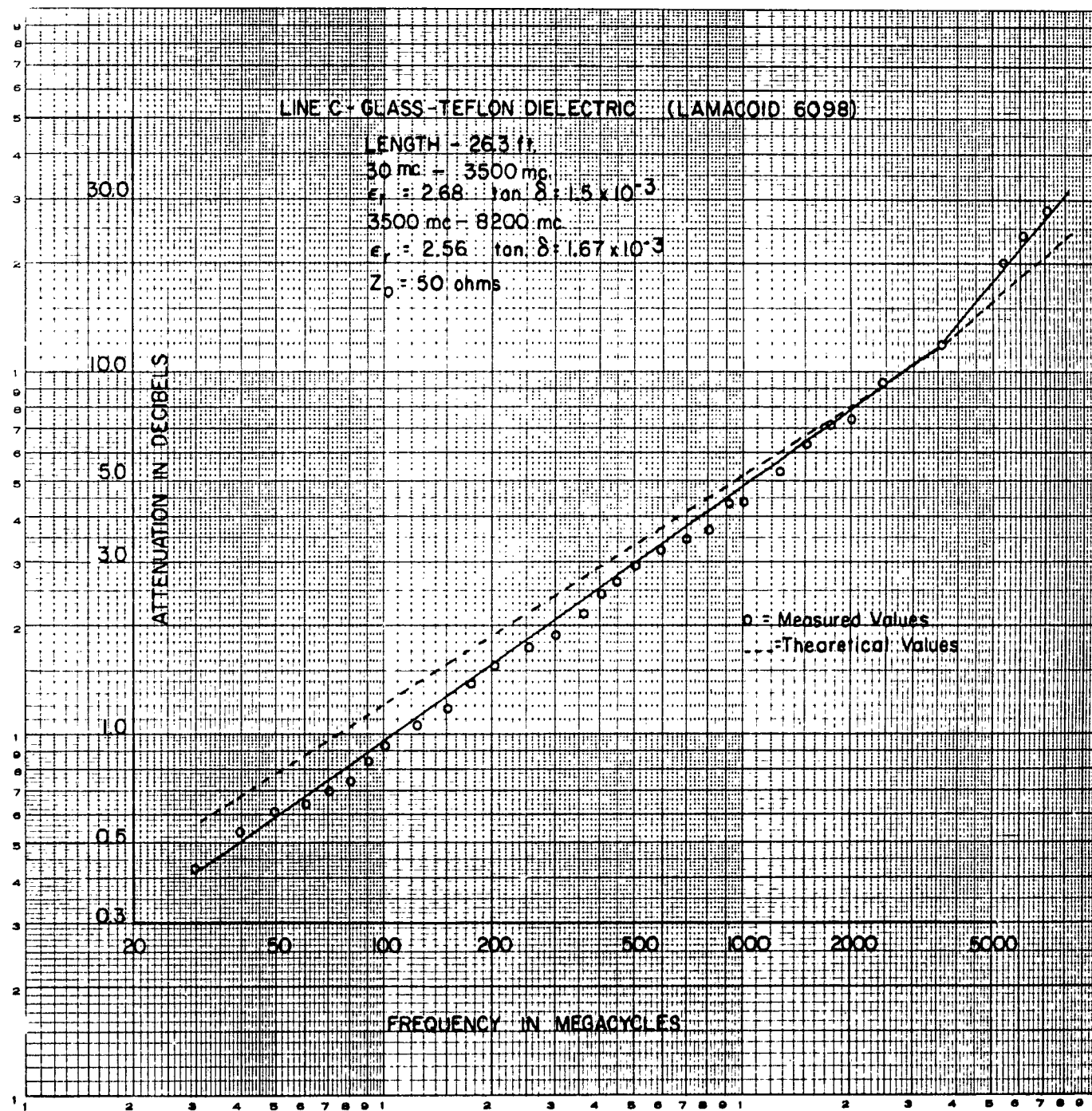


Fig. 4-9b. ATTENUATION MEASUREMENTS FOR LINE C

TABLE 4-1
Theoretical vs. Measured Attenuation of Spiral C.

Frequency (mc)	Calculated Attenuation (db)	Measured Attenuation (db)
30	0.5674	0.41
40	0.6522	0.52
50	0.7400	0.60
60	0.8244	0.63
70	0.8943	0.68
80	0.9622	0.72
90	1.033	0.82
100	1.098	0.9
125	1.251	1.04
150	1.395	1.15
175	1.518	1.36
200	1.657	1.50
250	1.899	1.70
300	2.126	1.82
350	2.244	2.10
400	2.452	2.40
450	2.722	2.60
500	2.947	2.90
600	3.321	3.20
700	3.680	3.41
800	4.026	3.63
900	4.262	4.2
1000	4.689	4.3
1250	5.389	5.2
1500	6.313	6.2
1750	7.064	7.0
2000	7.674	7.2
2400	8.780	9.0
3500	11.667	11.60
5200	15.890	19.90
6000	17.810	23.50
7000	20.240	27.70
8000	22.470	28.80
8200	22.960	28.90



BIBLIOGRAPHY

32. A. A. Oliner, "Theoretical Developments in Symmetrical Strip Transmission Line", Proceedings of the Symposium on Modern Advances in Microwave Techniques, Edwards Brothers Inc., Ann Arbor, Michigan, 1955.
33. A. A. Oliner, "The Radiation Conductance of a Series Slot in Strip Transmission Line", forthcoming Hughes Aircraft Company report.
34. E. Strumwasser, R. J. Stegen, J. A. Short and J. R. Miller, "Slot Study in Rectangular TEM Transmission Line", Hughes Aircraft Company Report TM No. 265, Jan. 1952.
35. A. A. Oliner, "private communication to C. R. Mingins", Tufts College, Feb. 2, 1954.
36. R. L. Pease, "Conductor Heating Losses in Strip Transmission Lines with Rectangular Inner Conductors in the Low Impedance Region", Interim Report No. 3 on Contract No. AF 19(604)-575, Tufts College, March 10, 1954.
37. S. B. Cohn, "Problems in Strip Transmission Lines", Symposium on Microwave Strip Circuits, pp 119-126.
38. H. A. Wheeler, "Formulas for the Skin Effect", Proc. I.R.E., Vol. 30, pp 412-424, Eq. (18), Sept. 1942.
39. N. Marcuvitz, "Waveguide Handbook", McGraw Hill, pp 263-265, 1951.

ABSTRACT

A transfer function for Stripline is found using standard transmission line formulation. This transfer function is broken into two parts, dielectric response and skin effect response. A set of curves is given for dielectric response. Skin effect response is found from the curves in an article by Wigington and Nahman⁴⁶ which is included as an Appendix. Finally, a practical example is worked demonstrating the use of the analysis. Comparison of the results of this example with those determined experimentally shows good correlation.

TABLE OF CONTENTS

Chapter	Page
V. A Transient Analysis of stripline	
A. Introduction	118
B. Theoretical Model	118
C. Stripline Transfer Functions	129
D. Skin Effect Transient	135
E. Transient Due to Dielectric Loss	137
F. Experimental Verification	148
1. Measurement Procedure	148
2. Transient Response Example	149
a. Dielectric Response	153
a1. First Ramp	153
a2. Second Ramp	154
a3. Third Ramp	156
a4. Fourth Ramp	157
a5. Total Dielectric Response . .	159
b. Skin Effect Response	160
b1. First Ramp	160
b2. Second Ramp	163
b3. Third Ramp	165
b4. Fourth Ramp	166
b5. Total Skin Effect Response .	167
G. Summary	174
Bibliography	175

TABLE OF CONTENTS

Appendix VII	Transient Analysis of Coaxial Cables Considering Skin Effect	A80
Appendix VIII	Use of an X-Y Recorder with a Sampling Oscilloscope	A81
Appendix IX	Properties of Materials, Measurement Results, Calculation of Line Parameters. .	A82

LIST OF FIGURES

Figure	Page
5-1 Dielectric Term Impulse Response	139
5-2 Dielectric Term Step Response	143
5-3 Normalized Ramp Responses for Dielectric . .	147
5-4 stripline Input Pulse Approximation	150
5-5 Total Dielectric Response of a stripline Spiral	161
5-6 Theoretical Transient Response for a stripline Spiral	170
5-7 Approximation of Test Pulse Used for stripline Spirals A and B	172
5-8 Calculated Response of stripline Spirals A and B	173

CHAPTER V

A TRANSIENT ANALYSIS OF STRIPLINE

A. Introduction.

Since the use of Stripline to perform logical operations in a computer is a basic aim of this investigation, it will be necessary to consider its transient properties. Any digital logic operation depending on signal amplitude will necessarily involve square pulses to represent the "1" and "0" states. The maximum possible rate of performing logical operations will then be limited in part by the maximum achievable rise time of Stripline. The means of predicting this maximum rise time as well as the variables determining it will be found from a transient analysis. This analysis will follow an analysis done by Wigington.⁴⁰ Wigington's paper is the only transient analysis that has been done to the author's knowledge.

B. Theoretical Model.

To begin the transient analysis of Stripline it is necessary to find its voltage transfer function. It was shown earlier in this report that Stripline operates in the TEM mode. Since this is the case, the formulas for general transmission lines hold. The steady state solution for a voltage wave on a general transmission line is

$$v = A e^{-\gamma l} + B e^{+\gamma l} \quad (5-1)$$

where

$$\gamma = \alpha + j\beta = \sqrt{(R + j\omega L)(G + j\omega C)}$$

l = distance from the sending end of the transmission line

R, L, G, C = resistance, inductance, conductance and capacitance per unit length of line

A and B = Complex constants

The function of interest is that of a voltage transfer in a matched line. The first term of equation (5-1) represents the incident wave while the second term represents the reflected wave. Since a matched line has no reflected wave, the second term of equation (5-1) will be absent. Equation (5-1) then becomes:

$$v = v(0) e^{-\gamma l} \quad (5-2)$$

where

$v(0)$ is the sending end voltage

From equation (5-2) the voltage transfer function becomes:

$$\begin{aligned} F(\omega) &= \frac{v(l)}{v(0)} = e^{-\gamma l} = e^{-\alpha l} e^{-j\beta l} \\ &= e^{-\alpha l} (\cos \beta l - j \sin \beta l) \end{aligned} \quad (5-3)$$

In equation (5-1) the propagation constant γ was defined as

$$\gamma = \left[(R + j\omega L)(G + j\omega C) \right]^{1/2} \quad (5-4)$$

Let us now examine the parameters R, L, G and C for the case of stripline. In Chapter IV of this report, it was shown that

$$Z_{\infty} = \sqrt{\frac{\pi f \mu}{\sigma}} (1 + j) \quad (4-41)$$

where

Z_{∞} = Impedance of a round wire for very high frequencies

f = frequency of interest

μ = permeability of the medium

σ = conductivity of the medium

r_o = radius of wire

It is shown in Ramo and Whinnery⁴¹ that equation (4-41) is valid for $r_o/\delta > 5.5$ if a 10% error can be tolerated (where δ is the depth of current penetration into the conductor).

In stripline $r_o \rightarrow \infty$ since the conductors are actually plane rather than circular. Also for copper at 3 K mc, $\delta = 1.22 \times 10^{-6}$ meters. The assumption that $r_o/\delta > 5.5$ is therefore quite valid.

Equation (4-41) may be rearranged to read

$$Z_{\infty} = \sqrt{\frac{\omega \mu}{8 \pi^2 r_o^2 \sigma}} (1 + j) \quad (5-5)$$

Let us define

$$K_1^2 = \frac{\mu^2}{(4\pi^2 r_o^2 \sigma)^2} \quad (5-6)$$

Inserting equation (5-6) into (5-5) there results

$$Z_\infty = \frac{K_1 \sqrt{\omega}}{\sqrt{2}} (1 + j) \quad (5-7)$$

In the discussion following equation (4-14) it was shown that

$$\tan \delta = \frac{\sigma}{\epsilon \omega} \quad (5-8)$$

where

$\tan \delta$ = loss tangent

σ = conductivity

ϵ = permittivity of the medium

ω = angular frequency in radians

The equation for a parallel plate capacitor is

$$C = \frac{\epsilon A}{d} \quad (5-9)$$

where:

ϵ = permittivity of the medium

A = Area of one plate

d = distance between plates

Equation (5-8) may be rearranged to read

$$\tan \delta = \frac{\frac{\sigma A}{d}}{\omega \left(\frac{\epsilon A}{d} \right)} \quad (5-10)$$

Utilizing equation (5-9) and the basic definition of conductance, there results

$$\tan \delta = \frac{G}{\omega C} \quad (5-11)$$

Now let us examine equation (5-4) which was

$$r = \left[(R + j \omega L) (G + j \omega C) \right]^{1/2} \quad (5-4)$$

Consider the term $(R + j \omega L)$. It must be remembered that there are two types of inductance to be considered, that due to skin effect and that calculated assuming no current penetration into the conductor (L_∞). The resistor term R is essentially due to skin effect. The term $(R + j \omega L)$ may therefore be expressed with the help of equation (5-7) as

$$(R + j \omega L) = (Z_\infty + j \omega L_\infty)$$

$$= \left(\frac{K_1 \sqrt{\omega}}{\sqrt{2}} + j \frac{K_2 \sqrt{\omega}}{\sqrt{2}} + j \omega L_\infty \right) \quad (5-12)$$

Now equation (5-11) is

$$\tan \delta = \frac{G}{\omega C} \quad (5-11)$$

Define

$$C \tan \delta = K_2 \quad (5-13)$$

Then equation (5-12) becomes

$$G = K_2 \omega \quad (5-14)$$

Through the use of equations (5-12) and (5-14), equation (5-14) becomes

$$r = \left[\left(\frac{K_1 \sqrt{\omega}}{\sqrt{2}} + j \frac{K_1 \sqrt{\omega}}{\sqrt{2}} + j \omega L_{\infty} \right) (K_2 \omega + j \omega C) \right]^{1/2} \quad (5-15)$$

Equation (5-15) can be rearranged to read

$$r = j \omega \sqrt{L_{\infty} C} \left[1 + \frac{\frac{K_1 \sqrt{\omega}}{\sqrt{2}} (1+j)}{j \omega L_{\infty}} \right]^{1/2} \left[1 + \frac{K_2}{jC} \right]^{1/2} \quad (5-16)$$

Equation (5-16) is rather unwieldy and may be simplified by expanding each one of its bracketed terms in a binomial series. The general binomial series expansions is

$$(1+x)^n = 1 + nx + \frac{n(n-1)x^2}{2!} \dots x^2 < 1 \quad (5-17)$$

We must first examine the bracketed terms of (5-16) to see if the condition ($x^2 < 1$) is met. The "x" term in the first bracketed term is

$$\frac{\frac{K_1\sqrt{\omega}}{\sqrt{2}}(1+j)}{j\omega L\infty} = \frac{K_1}{\sqrt{\omega}L\infty} \quad (5-18)$$

Evaluation of (5-18) depends on evaluation of K_1 . K_1 in turn depends on the assumption that

$$\frac{K_1}{\sqrt{\omega}L\infty} << 1$$

This assumption will therefore be made and its validity checked after K_1 has been evaluated. In the second term of equation (5-16), the validity of

$$\left| \frac{K_2}{jC} \right| << 1 \quad (5-19)$$

must be checked. Now

$$\left| \frac{K_2}{jC} \right| = \frac{K_2}{C} \quad (5-20)$$

But from equation (5-13)

$$\tan \delta = \frac{K_2}{C} \quad (5-21)$$

At 3 kmc $\tan \delta < 0.01$ for GB 112 T Dielectric. The assumption of (5-19) is therefore justified.

Using the first two terms of the binomial expansion in each term of equation (5-16), there is obtained

$$\begin{aligned} r &\approx j \omega \sqrt{L \infty C} \left[1 - \frac{j K_1 (1+j)}{2 \sqrt{2} \sqrt{\omega} L \infty} \right] \left[1 - j \frac{K_2}{2C} \right] \\ &= j \omega \sqrt{L \infty C} \left[1 - j \frac{K_1 (1+j)}{2 \sqrt{2} \sqrt{\omega} L \infty} - j \frac{K_2}{2C} - \left(\frac{K_1 (1+j)}{2 \sqrt{2} \sqrt{\omega} L \infty} \right) \left(\frac{K_2}{2C} \right) \right] \quad (5-22) \end{aligned}$$

Now it was shown that $\left(\frac{K_2}{2C} \right) \ll 1$ and it will be subsequently shown that

$$\frac{K_1 (1+j)}{2 \sqrt{2} \sqrt{\omega} L \infty} \ll 1.$$

It is therefore valid to drop the last term of equation (5-22). Under this assumption equation (5-22) becomes

$$\gamma \approx j \omega \sqrt{L \infty C} \left[1 - \frac{j K_1 (1 + j)}{2 \sqrt{2} \sqrt{\omega} L \infty} - j \frac{K_2}{2C} \right]. \quad (5-23)$$

or

$$\gamma \approx j \omega T + \frac{K_1}{2 R_o} \frac{(1 + j) \sqrt{\omega}}{\sqrt{2}} + \frac{K_2 R_o \omega}{2} \quad (5-24)$$

where

$$T = \sqrt{L C}$$

and

$$R_o = \sqrt{\frac{L \infty}{C}}$$

The first term is a simple delay and is not of interest in this analysis. We may therefore conclude from equation (5-24) that

$$\alpha = \frac{K_1 \sqrt{\omega}}{2 \sqrt{2} R_o} + \frac{K_2 R_o}{2} \omega \quad (5-25)$$

and

$$\beta = \frac{K_1 \sqrt{\omega}}{2 \sqrt{2} R_o} \quad (5-26)$$

The development has now proceeded far enough to evaluate the constant K_1 . The work of Chapter IV resulted in Fig 4-7 which expresses stripline attenuation as a function of its parameters. The ordinate of Fig 4-7 is

$$y = \frac{\alpha_c^{\text{db}} b (K_{mc})^{-1/2}}{\sqrt{f_{Kmc} \epsilon_r}} \quad (5-27)$$

The attenuation constant α in equation (5-27) is in decibels, whereas the attenuation constant of equation (5-25) is in nepers. Using the conversion factor from decibels to nepers, we see that

$$y' = \frac{\alpha_c^{\text{nep}} b}{\sqrt{f \epsilon_r}} \quad \text{nepers (cycle)}^{-1/2}$$

$$= 3.67 \times 10^{-6} y \quad (5-28)$$

Equation (5-25) is made up of two terms, the first due to copper losses (α_c) and the second due to dielectric losses (α_d). If equation (5-28) is solved for α_c^{nep} and the result equated to the first term in equation (5-25) the desired solution for K_1 results. It is:

$$K_1 = \frac{2 y' \sqrt{\epsilon_r} R_o}{\sqrt{\pi} b} \quad (5-29)$$

The expression we wish to examine to determine the validity of equation (5-22) is

$$\frac{K_1}{\sqrt{\omega} L \infty} << 1 \quad (5-30)$$

Let us examine equation (5-30) for a "worst" case.

Take:

$$y = 1.7 \times 10^{-3} \text{ (maximum ordinate on Fig 4-7)}$$

$$R_o = 98.5$$

$$b = 0.125 \text{ inch}$$

$$\epsilon_r = 2.6$$

$$C = 0.553 \mu\mu\text{fd/in.}$$

These values were obtained from the Table of Characteristic Impedance Measurements given in Chapter I. If these values are used in equation (5-28) and (5-29) we find that $K_1 = 8.91 \times 10^{-8}$.

The value of L_∞ can be found by realizing that

$$R_o = \sqrt{\frac{L_\infty}{C}} \quad (5-31)$$

or

$$L_\infty = R_o^2 C \quad (5-32)$$

Inserting the given values of Characteristic Impedance and Capacitance per unit length, we find that $L_\infty = 5.37 \times 10^{-9}$ henries. If a frequency of 3 Kmc is assumed

$$\frac{K_1}{\sqrt{\omega} L \infty} = 1.22 \times 10^{-4} << 1 \quad (5-33)$$

Then the assumptions required for the binomial expansion are justified and we may proceed with the development.

C. Stripline Transfer Functions.

The transfer function to be investigated can now be written from equation (5-3), (5-25) and (5-26). It is

$$F(\omega) = e^{-\frac{K_2 R_o}{2} \frac{1}{\omega}} e^{-\frac{K_1}{2\sqrt{2} R_o} \sqrt{\omega}} e^{-\frac{j K_1}{2\sqrt{2} R_o} \sqrt{\omega}} \quad (5-34)$$

In our investigation of equation (5-36), it would be desirable to be able to apply the physical realizability conditions given for transfer functions of lumped constant systems to transmission line transfer functions. Bode⁴² shows that provided the delay of propagation term in the expression for the propagation constant (equation 5-24) is subtracted out, the analogy is valid. Since the first term of equation (5-24) has already been removed in the derivation of equation (5-34), $F(\omega)$ must satisfy the realizability conditions for lumped constant transfer functions. These conditions are given by Bode⁴³ and Balbanian⁴⁴ and are:

- (1) Zeroes and Poles are either real or occur in complex conjugate pairs.
- (2) The real and imaginary components are respectively even and odd functions on the real frequency axis.
- (3) None of the poles can be found in the right hand plane.
- (4) Poles on the real frequency axis must be simple with imaginary residues.
- (5) No Poles of the voltage transfer function $F(\omega)$ can lie at 0 or ∞ .
- (6) The Zeroes of $F(\omega)$ may be multiple and can lie anywhere in the s plane.
- (7) From physical reasoning, it is obvious that $F(\omega) \rightarrow 0$ as $\omega \rightarrow \pm \infty$ and $|F(\omega)| \leq 1$ for all ω .

For those who may be unfamiliar with the pole zero concept the following definitions are given:

- (1) A Zero is that value of frequency which causes $F(\omega)$ to go to zero.
- (2) A Pole is that value of frequency which causes $F(\omega)$ to go to ∞ .

If condition (7) is met, the other conditions will be met. Examination of equation (5-3⁴) shows that for $\omega \geq 0$, condition (7) is met but for $\omega < 0$ this condition is not satisfied.

Let $F(\omega)$ be broken into two parts such that:

$$F(\omega) = F_1(\omega) + F_2(\omega) \quad (5-35)$$

where

$$F_1(\omega) = \text{term due to dielectric loss}$$

$$F_2(\omega) = \text{term due to skin effect}$$

Consider first the dielectric term

$$F_1(\omega) = e^{-\frac{K_2 R_o l \omega}{2}} \quad (\omega \geq 0) \quad (5-36)$$

Since the attenuating case is wanted for both positive and negative frequencies, it seems obvious that for all ω , $F_1(\omega)$ should be

$$F_1(\omega) = e^{-\frac{K_2 R_o l |\omega|}{2}} \quad (\text{for all } \omega) \quad (5-37)$$

Now let us consider the skin effect terms

$$F_2(\omega) = e^{-\frac{K_1 \sqrt{\omega} l}{2\sqrt{2} R_o}} \quad e^{-\frac{j K_1 \sqrt{\omega} l}{2\sqrt{2} R_o}} \quad (5-38)$$

For simplicity, define

$$K = \frac{K_1}{2\sqrt{2} R_o} \quad (5-39)$$

With equation (5-39) inserted, equation (5-38) becomes:

$$F_2(\omega) = e^{-K\sqrt{\omega}} e^{-j K \sqrt{\omega}} \quad (5-40)$$

$$= e^{-K\sqrt{\omega}} (1 + j)$$

Equation (5-40) must hold for negative as well as positive frequencies. Bode⁴⁵ states: "In any real physical circuit, the real component of the impedance is an even function of frequency and the imaginary component is an odd function. In other words, the real component of the impedance at a negative frequency is equal to its value at the corresponding positive frequency, while the imaginary component at a negative frequency is the negative of the imaginary component at the corresponding positive frequency". Let us then postulate

$$\begin{aligned} F_2(-\omega) &= e^{-K\sqrt{-|\omega|}} (1 + j) \\ &= e^{-K\sqrt{|\omega|}} (1 - j) \end{aligned} \quad (5-41)$$

and examine the validity of equations (5-40) and (5-41) under Bode's conditions. From equation (5-40)

$$\begin{aligned} \text{Re} [F_2(\omega)] &= \text{Re} [e^{-K\sqrt{\omega}(1+j)}] \\ &= e^{-K\sqrt{\omega}} \cos K\sqrt{\omega} \end{aligned} \quad (5-42)$$

and from equation (5-41)

$$\begin{aligned} \text{Re} [F_2(-\omega)] &= \text{Re} [e^{-K\sqrt{|-\omega|}(1-j)}] \\ &= e^{-K\sqrt{|-\omega|}} \cos K\sqrt{|-\omega|} \end{aligned} \quad (5-43)$$

Therefore

$$\text{Re} [F_2(\omega)] = \text{Re} [F_2(-\omega)] \quad (5-44)$$

and Bode's first condition is fulfilled. Also from equation (5-40)

$$\begin{aligned} \text{Im} [F_2(\omega)] &= \text{Im} [e^{-K\sqrt{\omega}(1+j)}] \\ &= -e^{-K\sqrt{\omega}} \sin K\sqrt{\omega} \end{aligned} \quad (5-45)$$

and from equation (5-41)

$$I_m \left[F_2(-\omega) \right] = I_m \left[e^{-K\sqrt{|\omega|}} (1 - j) \right]$$

$$= e^{-K\sqrt{|\omega|}} \sin K\sqrt{|\omega|} \quad (5-46)$$

As a result of equation (5-45) and equation (5-46)

$$I_m \left[F_2(-\omega) \right] = -I_m \left[F_2(\omega) \right] \quad (5-47)$$

and Bode's second condition is fulfilled. Our postulation is therefore valid. In summary then

$$\begin{aligned} F_2(\omega) &= e^{-K\sqrt{\omega}} (1 + j) \quad \omega \geq 0 \\ &= e^{-K\sqrt{|\omega|}} (1 - j) \quad \omega < 0 \end{aligned} \quad (5-48)$$

It is desirable to express $F_2(\omega)$ as a function of $j\omega$.

We therefore make the following transformations:

$$F_2(\omega) = e^{-K\sqrt{\omega}(1+j)} = e^{-K\sqrt{\omega}(1+j)} \frac{(\sqrt{2}, 1)}{(\sqrt{2} j)}$$

$$= e^{-K\sqrt{2j\omega}} \quad (5-49)$$

and

$$F_2(-\omega) = e^{-K\sqrt{|\omega|}(1-j)} = e^{-K\sqrt{|\omega|}(1-j)} \frac{(1+j)}{(1-j)}$$

$$= e^{-K\sqrt{-2j|\omega|}} \quad (5-50)$$

Comparison of equations (5-49) and (5-50) shows that for $\omega < 0$

$$F_2(\omega) = F_2(-\omega) \quad (5-51)$$

Now if we let $s = j\omega$ and use analytic continuation, we obtain the final result which is

$$F_2(s) = e^{-K\sqrt{2s}} = e^{\frac{-K_1 1 \sqrt{s}}{2 R_o}} \quad (5-52)$$

D. Skin Effect Transient.

Equation (5-52) has been solved by Wigington and Nahman.⁴⁶

This paper is included as Appendix VII. From this analysis, the impulse response is found to be

$$f_2(t) = \alpha t^{-3/2} e^{-\beta/t} \quad t \geq 0 \\ = 0 \quad t < 0 \quad (5-53)$$

where

$$\alpha = \frac{K_1}{4 R_o} \frac{1}{\sqrt{\pi}}$$

and

$$\beta = \left[\frac{K_1}{4 R_o} \right]^2$$

In a similar manner, the stop response was found to be

$$g_2(t) = \operatorname{erfc} \sqrt{\beta/t} \quad t \geq 0 \\ = 0 \quad t < 0 \quad (5-54)$$

and the ramp response is

$$h_2(t) = 1/a \int_w^t \operatorname{erfc} \sqrt{\beta/\tau} d\tau \quad \tau \geq 0 \\ = 0 \quad \tau < 0 \quad (5-55)$$

where:

$$w = t - a \text{ for } t \geq a$$

$$w = 0 \text{ for } t < a$$

$$a = 0-100\% \text{ rise time of a unit ramp.}$$

Equation (5-53) is shown graphically in normalized form as Fig 2 of Appendix VII whereas equation (5-55) is shown graphically in normalized form as Fig 3, 4 and 5 of that Appendix having normalized ramp rise time as a running parameter. The curve for $a = 0$ corresponds to the step response (equation 5-54). Use of these curves will be discussed later.

E. Transient Due to Dielectric loss.

The transfer function for the dielectric was given as:

$$F_1(\omega) = e^{-\frac{K_2 R_o}{2} \frac{1}{|\omega|}}$$

$$= e^{-K_o |\omega|} \quad (5-37)$$

where:

$$K_o = \frac{K_2 R_o}{2}$$

The transform of equation (5-37) is given by Cambell and Foster⁴⁷ as

$$f_1(t) = \frac{K_o}{\pi (t_o^2 + K_o^2)} \quad (5-56)$$

Equation (5-56) is the dielectric impulse response and is shown in normalized graphical form as Fig 5-1.

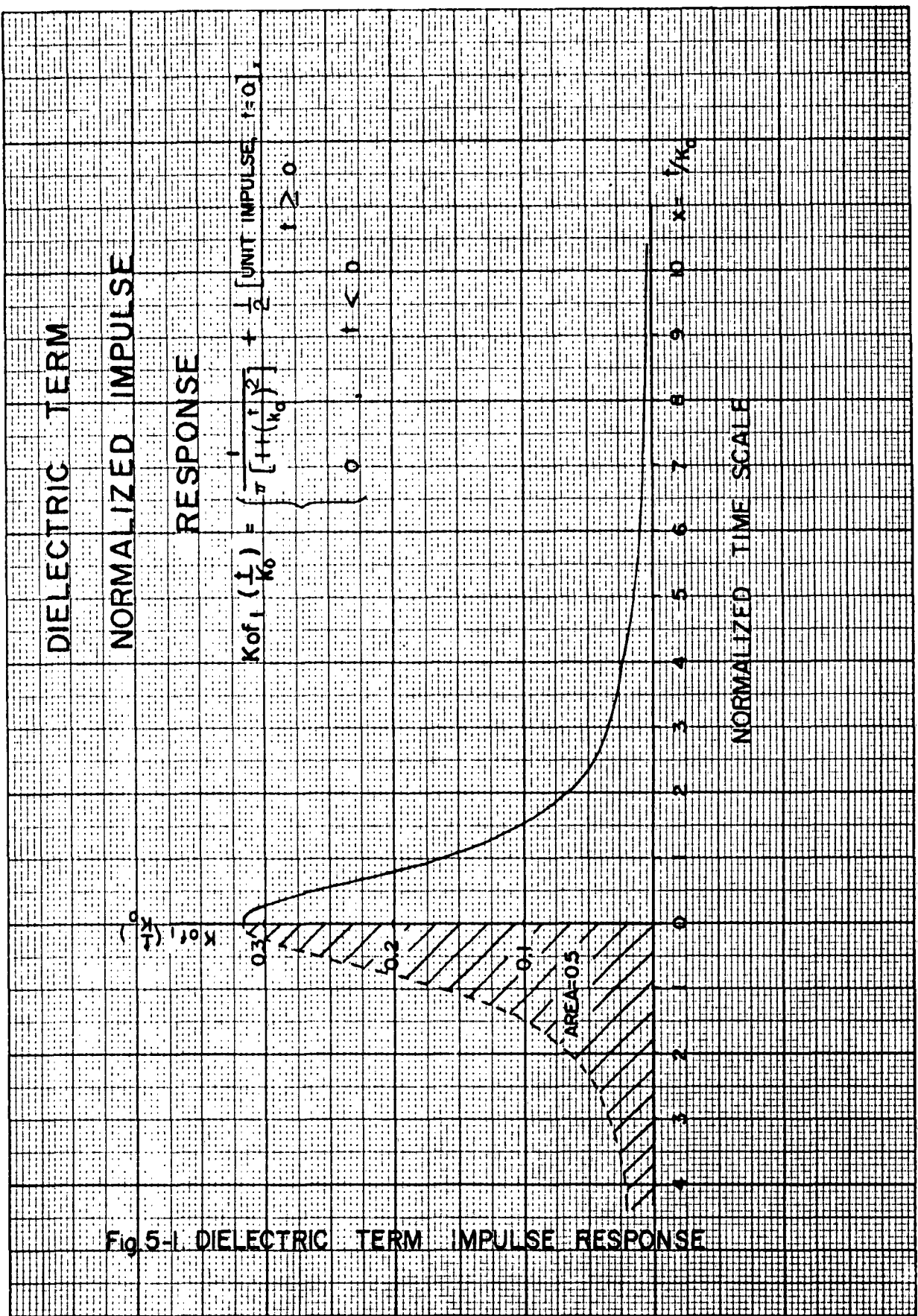
The dielectric step response can be obtained from the impulse response (equation 5-56) by the following manipulation:

$$G_1(s) = 1/s F_1(s)$$

$$\begin{aligned} g_1(t) &= \int_{-\infty}^t f_1(\tau) d\tau \\ &= \int_{-\infty}^t \frac{K_0}{\pi(\tau^2 + K_0^2)} d\tau \\ &= 1/2 + 1/\pi \tan^{-1}(t/K_0) \end{aligned} \quad (5-57)$$

Let us now examine equation (5-37), (5-56) and (5-57). The following observations may be made:

- (1) For the analysis performed the mathematics holds for all time, both positive and negative, according to the transform Tables.
- (2) Equation (5-37) is supposedly a network transfer function, yet it is not analytic.
- (3) The time response is from a transfer function which has no phase time and no delay, yet it seems to satisfy the requirements as a network function, except for analyticity.



- (4) Physical reasoning would require that there be no response prior to an excitation, i.e., the response should be zero for $t < 0$ and for $t \rightarrow \infty$, $g(t) \rightarrow 1$. Equation (5-57) fulfills the condition $g_1(t) \rightarrow 1$ as $t \rightarrow \infty$, but for $t < 0$ $g_1(t) \rightarrow 0$ only as $t \rightarrow -\infty$ i.e. $g_1(t) \neq 0$ for $t < 0$.
- (5) If equation (5-56) is assumed to be true for $t \geq 0$ only (with $f(t) = 0$ for $t < 0$), then the constant $1/2$, in equation (5-57) is not obtained in the step response and $\zeta_1(t) \rightarrow 1/2$ as $t \rightarrow \infty$ rather than a value of unity as it should.
- (6) The dielectric step response was obtained from the impulse response by integrating in the time domain. Let us find the step response in the frequency domain, then transform it to the time domain. The dielectric impulse response was

$$F_1(\omega) = e^{-K_o |\omega|} = e^{-K_o |s|} \quad (5-57)$$

The step response in the following domain would then be

$$G_1(\omega) = \frac{e^{-K_o |s|}}{s} \quad (5-58)$$

From Table 1 of Campbell and Foster⁴⁸

$$\text{Pair 633: } \frac{e^{-K_o |s|}}{s} - \frac{1}{s} \xrightarrow{\quad} -\frac{1}{\pi} \tan^{-1}\left(\frac{K_o}{t}\right) \quad (5-59)$$

$$\text{Pair 107: } \frac{1}{s} \xrightarrow{\quad} 1 \quad t > 0 \quad (5-60)$$

$$\text{Pair 201: } F_1 \pm F_2 \xrightarrow{\quad} G_1 \pm G_2 \quad (5-61)$$

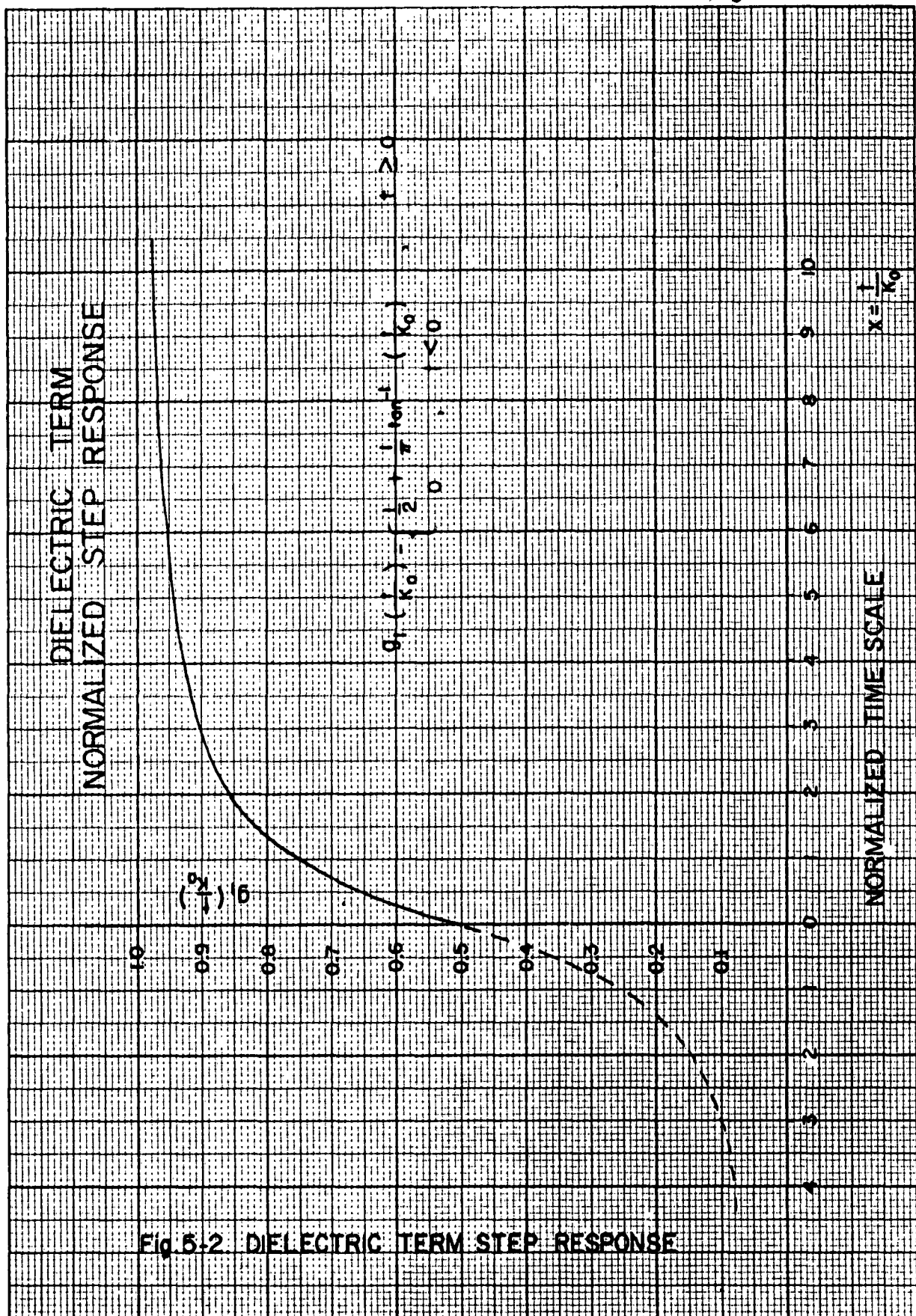
Equations (5-58) through (5-61) may be manipulated to yield the transform mate of equation (5-58) as follows:

$$\begin{aligned} F_1 + F_2 &= \left(\frac{e^{-K_o |s|}}{s} - \frac{1}{s} \right) + \frac{1}{s} \xrightarrow{\quad} \\ &\quad 1 - \frac{1}{\pi} \tan^{-1}\left(\frac{K_o}{t}\right) \\ &= G_1 + G_2 = g_1(t) \quad \tau > 0 \quad (5-62) \end{aligned}$$

Equation (5-62) may be further manipulated to yield the same result as that given by equation (5-57)

$$\begin{aligned}
 g_1(t) &= 1 - 1/\pi \tan^{-1}(K_o/t) \\
 &= 1/\pi \left[\pi/2 + \pi/2 - \tan^{-1}(K_o/t) \right] \\
 &= 1/\pi \left[\pi/2 + \tan^{-1}(t/K_o) \right] \\
 &= 1/2 + 1/\pi \tan^{-1}(t/K_o) \quad t > 0 \quad (5-63)
 \end{aligned}$$

Note that equation (5-63) is valid only for $t > 0$ whereas equation (5-57) is valid for both positive and negative time. Physical reasoning tells us that for $t < 0$, $g_2(t)$ should be zero while for $t \rightarrow \infty$ $g_2(t) \rightarrow 1$. Equation (5-63) therefore is the result required. Let the mathematics be true in detail for $t > 0$. In order to overcome the objection resulting from (5), observe that the DC value of a step excitation over all time (from $-\infty$ to $+\infty$) is $1/2$. Since there is no delay and the transfer function at zero frequency is unity, this appears as a step of value $1/2$ at the output. The response due to frequency components greater than zero is described by the arctangent function and is added to the step due to the DC term. In addition, to preserve the integral relationship between the impulse and step response the requirement that the area under impulse response for all time is unity, an impulse of value $1/2$ at $t = 0$ must be postulated. Figure 5-2 shows equation (5-56) in graphical form.



We now have the impulse and step response for the dielectric.

Finally, the response to an arbitrary ramp will be considered.

It is shown in Gardner and Barnes⁴⁹ that if the impulse response is known, the response to any arbitrary driving function may be found by convolving the driving function and the impulse response in the time domain. This principle has already been used in finding the ramp response to skin effect in Appendix VII.

Let us postulate the following normalized unit ramp:

$$r(x) = \begin{cases} 0 & x < 0 \\ x/\alpha & 0 \leq x \leq \alpha \\ 1 & x > \alpha \end{cases} \quad \alpha = a/K_0$$

where:

$a = 0\text{-}100\%$ rise time of a finite ramp.

Equation (5-56) modified as described above consists of two parts; the initial impulse and the part due to the rest of the impulse. Each part will be dealt with separately and the results added. In normalized form equation (5-53) is:

$$K_0 f_1(t/K_0) = \frac{1}{2} + \frac{1}{\pi \left[1 + (t/K_0)^2 \right]} \quad t \geq 0$$

$$(= 0 \quad t < 0 \quad (5-65)$$

The response to a unit ramp $r(x)$ will be of the form:

$$h_1(y) = 1/2 r(x) + \int_0^y f(x) r(y-x) dx \quad (5-66)$$

$$h_{1a}(y) + h_{1b}(y)$$

Considering the second term of equation (5-66) in conjunction with equation (5-65) and letting $x = t/K_o$ there results

$$h_{1b}(y) = \int_0^y \frac{1}{\pi(1+x^2)} r(y-x) dx \quad (5-67)$$

Observe that when the scale change $x = t/K_o$ is made in equation (5-65), $f_1(t/K_o) = f_1(x)$, preserving the area under to impulse response to be unity. Equation (5-67) must be considered in three parts corresponding to the three parts of $r(x)$ (equation 5-64)

$$\text{Case I: } y < 0 \quad h_{1b} = 0 \quad (5-68)$$

$$\text{Case II: } 0 \leq y \leq \alpha$$

$$h_{1b}(y) = 1/\pi \int_0^y \left(\frac{y-x}{\alpha} \right) \frac{dx}{(1+x^2)}$$

$$= \frac{1}{\alpha \pi} \left[y \tan^{-1} y - 1/2 \ln(1+y^2) \right] \quad (5-69)$$

Case III: $y > \alpha$

$$h_{1b}(y) = 1/\pi \int_0^{y-\alpha} \frac{dx}{(1+x^2)} + 1/\pi \int_{y-\alpha}^y \left(\frac{y-x}{\alpha} \right) \frac{dx}{1+x^2}$$

$$= 1/\pi \tan^{-1}(y-\alpha) + 1/\alpha \pi \quad x$$

$$\left[y \left(\tan^{-1} y - \tan^{-1}(y-\alpha) \right) - 1/2 \ln \left(\frac{1+y^2}{1+(y-\alpha)^2} \right) \right] \quad (5-70)$$

If the appropriate ramp responses are included in $h_{1a}(y)$
the required equations are obtained:

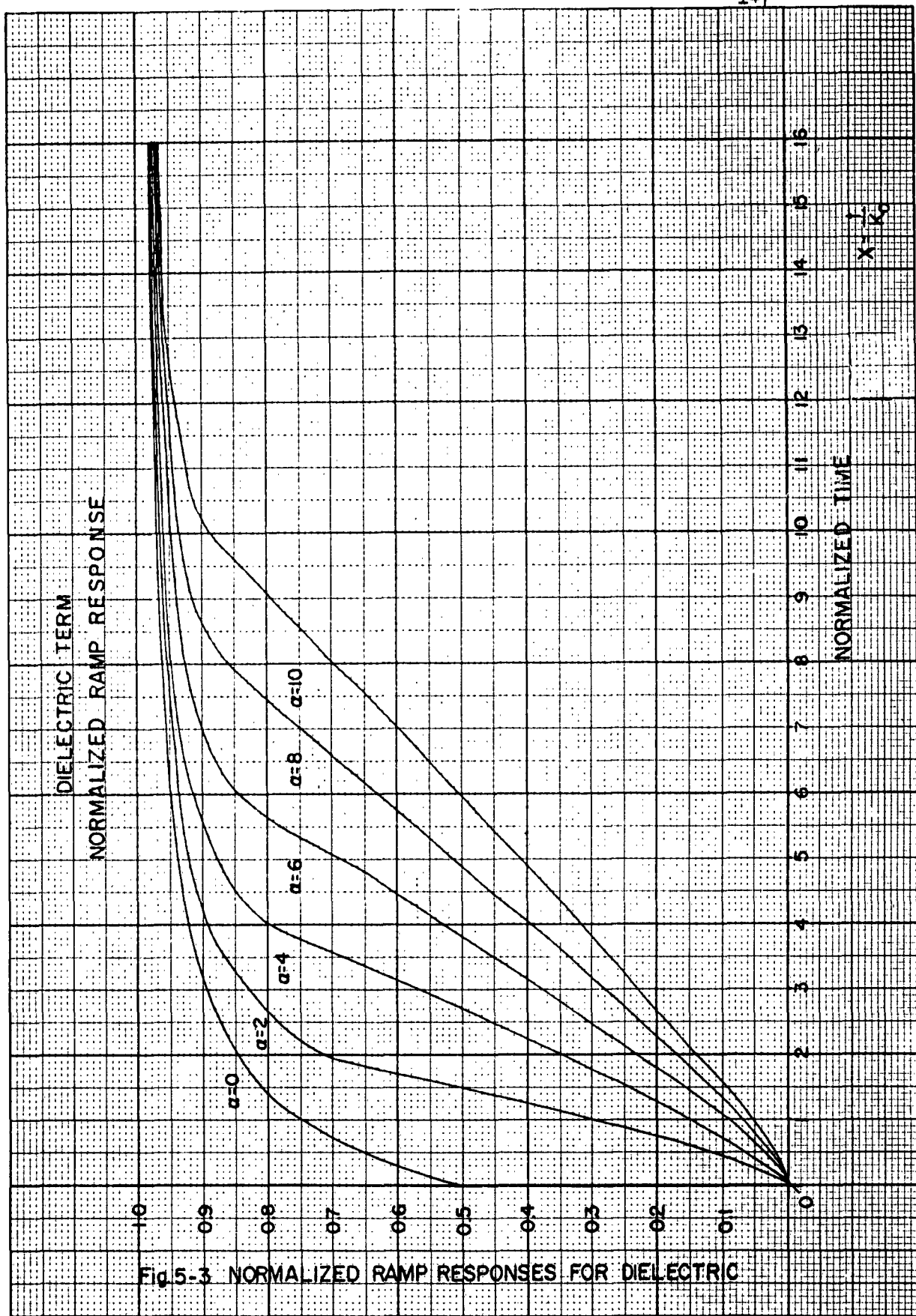
$$h_1(y) = 0 \quad y < 0$$

$$h_1(y) = y/2\alpha + 1/\alpha\pi \left[y \tan^{-1} y - 1/2 \ln(1+y^2) \right] \quad 0 \leq y \leq \alpha$$

$$h_1(y) = 1/2 + 1/\pi \tan^{-1}(y-\alpha) + 1/\alpha\pi \left[y \left(\tan^{-1} y - \tan^{-1}(y-\alpha) \right) \right.$$

$$\left. - 1/2 \ln \left(\frac{1+y^2}{1+(y-\alpha)^2} \right) \right] \quad y > \alpha \quad (5-71)$$

The behavior of equations (5-73) is correct in that
 $h_1(0) = 0$; $h_1(\alpha)$ in Case III reduces to that of Case II;
For large y , $h_1(y) \rightarrow g_1(y) \rightarrow 1$; and for $\alpha \rightarrow 0$, $h_1(y) \rightarrow g_1(y)$.
For ease in working practical problems, equations (5-71) have
been put in graphical form and are shown as Fig. 5-3. The
practical use of Fig. 5-3 in conjunction with the curves of
Appendix VII will now be shown in a practical example.



F. Experimental Verification:

1. Measurement Procedure:

A theoretical analysis is only as valid as its agreement with actual results. Let us proceed then to an experimental verification of Stripline transient behavior.

At the time that the transient analysis was begun, it was thought to be desirable to be able to record the input and output waveforms from a Stripline configuration on graph paper. Consequently, a study was undertaken resulting in a report included as Appendix VIII. This report compares oscilloscope and graphical results and imposes limitations on the speed of the recording sweep. The procedure employs a Lumatron sampling attachment and a Ballantine peak reading voltmeter. As can be seen from Fig. 2 of Appendix VIII, the observed pulses were those of an SKL pulse generator. To observe the transient response of a Stripline configuration then, it is only necessary to; (a) record the output pulse of the SKL generator, (b) break the signal line between the generator and the Lumatron delay unit and insert the device and (c) record the resulting output pulse of the device. Since the system is assumed linear, any degradation of the SKL pulse must be due to the Stripline device (the degradation due to the rest of the system is included in the measurement of the SKL pulse).

2. Transient Response Example:

In order to use the theory described in the preceding sections, it is first necessary to approximate the input pulse to the stripline device by a series of ramps. Rather than use a graphical recording of the input pulse, it was decided to use the equivalent oscilloscope photograph. Consequently, Fig. 3b of Appendix VIII was decided on and blown up to 8 X 10 inch size. It was overlayed with graph paper and approximated by a series of ramps. The result is shown as Fig. 5-4. The reader may wonder why the essentially straight line from (0, 0) to (1.0, 0.834) was broken into the three sections, (0, 0) to (0.35, 0.283), (0.35, 0.283) to (0.715, 0.583) and (0.715, 0.583) to (1.0, 0.834). This was done in order that the individual ramps would fall in the range of the tabulated curves of Fig. 5-3 and Appendix VII.

The stripline device under investigation was the spiral used for attenuation measurements in Chapter IV. We must therefore first find the values of K_o and β which respectively describe the dielectric and skin effect responses of the spiral. These constants can be found from equation (5-25) which was

$$\alpha(\omega) = \frac{K_1 \sqrt{\omega}}{2 \sqrt{2} R_o} + \frac{K_2 R_o \omega}{2} \text{ nepers/unit length } (5-25)$$

$$\text{Define } K_o = \frac{K_2 R_o}{2} \frac{1}{\omega}$$

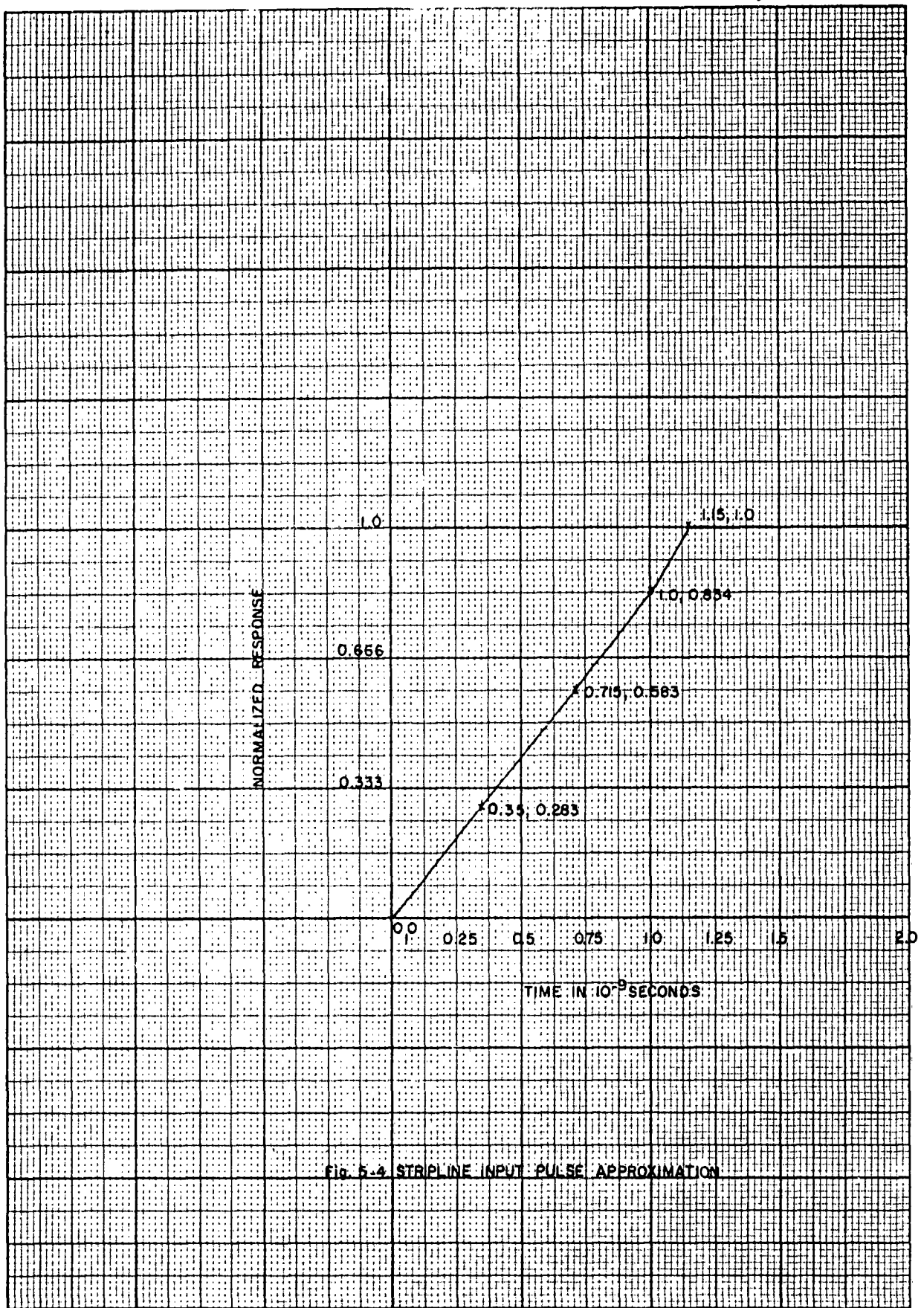
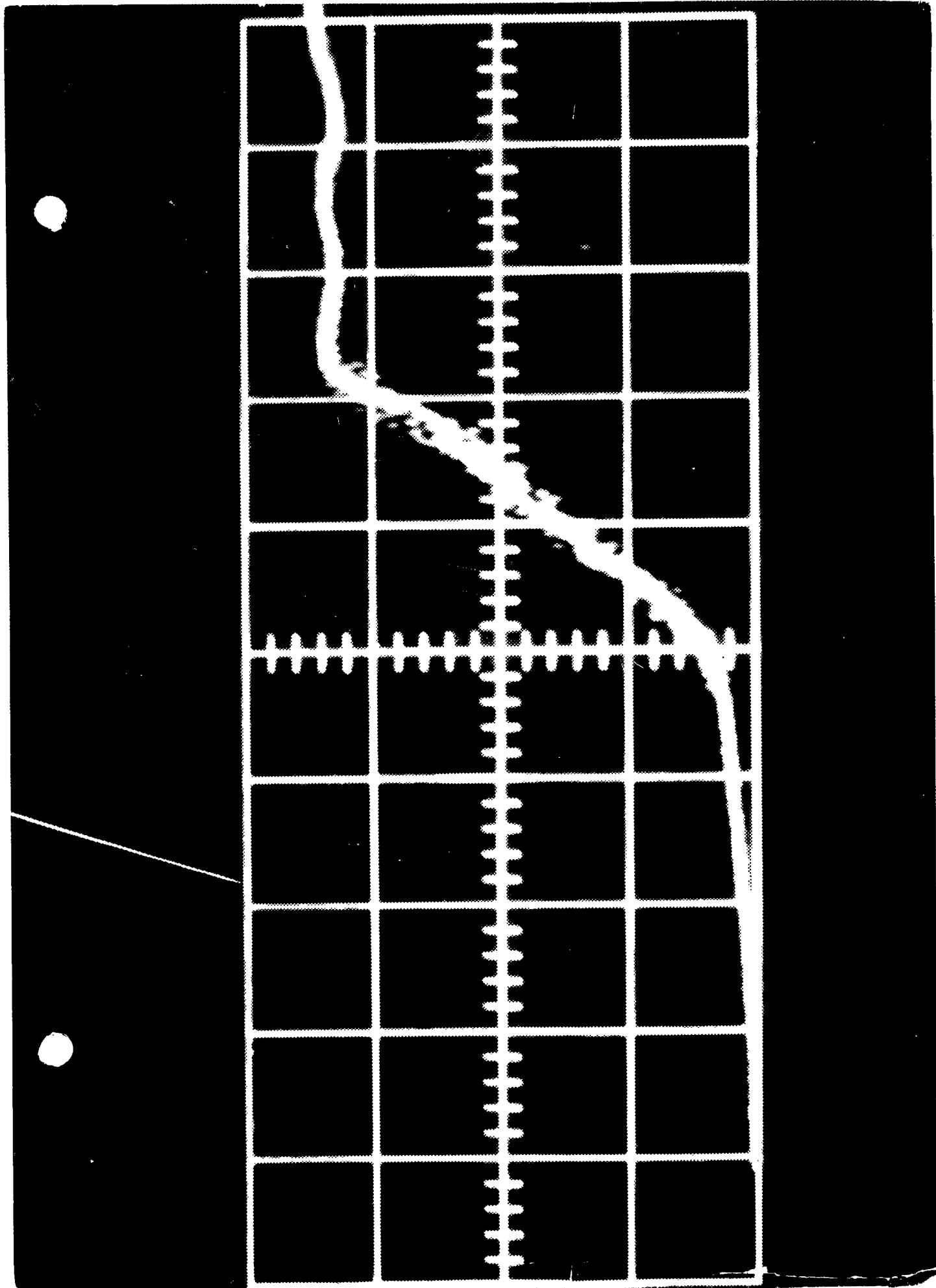


Fig. 5-4 STRIPLINE INPUT PULSE APPROXIMATION



and

$$\beta = \left[\frac{K_1}{4R_o} \right]^2$$

then

$$\alpha(\omega) = K_o \omega + \sqrt{2\beta\omega} \text{ nepers} \quad (5-72)$$

Now

$$1 \text{ neper} = 8.68 \text{ db.}$$

so

$$\alpha(\omega) = 8.68 (K_o \omega + \sqrt{2\beta\omega}) \text{ db.} \quad (5-73)$$

From Table 4-1 in the chapter on Stripline attenuation,
we see that

frequency	α theoretical	α measured
400 mc	2.45 db	2.4 db
3500 mc	11.67 db	11.6 db

Using these values of frequency and theoretical attenuation
(determined from the graph of Fig. 4-7), we can obtain from
equation (5-73)

$$0.282 = 25.2 K_o \times 10^8 + 7.1 \times 10^4 \sqrt{\beta}$$

and

$$1.35 = 220 K_o \times 10^8 + 21 \times 10^4 \sqrt{\beta}$$

Solving equation (5-74) and (5-75) simultaneously, we find
that

$$\beta = 7.3 \times 10^{-12}$$

and

$$K_o = 3.57 \times 10^{-11}$$

a. Dielectric Response:

Now that the constants K_o and β have been obtained, we can use Fig. 5-3 to obtain the dielectric response of the Stripline Spiral. The four ramps obtained from Fig. 5-4 will be considered individually. The total dielectric response is then obtained by adding the individual responses (superposition).

al. First Ramp:

$$\text{Amplitude} = 0.283$$

$$\text{Rise Time} = a = 0.35 \times 10^{-9} \text{ sec.}$$

$$\alpha = \frac{a}{K_o} = \frac{3.5 \times 10^{-10}}{0.357 \times 10^{-10}} = 9.82$$

$$x = \frac{t}{K_o} = \frac{t}{3.57 \times 10^{-11}} = 28 t \quad (t \text{ in } 10^{-9} \text{ sec.})$$

From Fig. 5-3

<u>$t (10^{-9} \text{ sec.})$</u>	<u>$x = 28 t$</u>	<u>Response</u>	<u>0.283 Response</u>
0.05	1.40	0.09	0.025
0.10	2.8	0.22	0.062
0.15	4.2	0.36	0.102
0.20	5.6	0.48	0.136
0.25	7.0	0.62	0.176
0.30	8.4	0.75	0.212
0.35	9.8	0.88	0.249
0.40	11.2	0.93	0.263
0.45	12.6	0.96	0.272

<u>t (10⁻⁹ sec.)</u>	<u>X = 28 t</u>	<u>Response</u>	<u>0.283 Response</u>
0.50	14.0	0.97	0.275
0.55	15.4	0.98	0.276
0.60	16.8	1.0	0.283
0.65	18.2	1.0	0.283
0.70	19.6	1.0	0.283
0.75	21.0	1.0	0.283
0.80	22.4	1.0	0.283
0.85	23.8	1.0	0.283
0.90	25.2	1.0	0.283
0.95	26.6	1.0	0.283
1.0	28.0	1.0	0.283
1.05	29.4	1.0	0.283
1.10	30.8	1.0	0.283
1.15	32.2	1.0	0.283
1.20	33.6	1.0	0.283
1.25	35.0	1.0	0.283

The last column may be somewhat confusing. The response of Fig. 5-3 is based on a ramp of amplitude unity. Since the first ramp has only an amplitude of 0.283, the response of Fig. 5-3 must be adjusted accordingly.

a2. Second Ramp:

$$\text{Amplitude} = 0.583 - 0.283 = 3.00$$

$$\text{Rise Time} = (0.715 - 0.350) \times 10^{-9} = 0.365 \times 10^{-9}$$

$$\alpha = \frac{0.365 \times 10^{-9}}{3.57 \times 10^{-11}} = 10.2$$

<u>t (10⁻⁹ sec.)</u>	<u>x = 28 t</u>	<u>Response</u>	<u>0.30 Response</u>
0.05 - 0.35	0	0	0
0.10 - 0.35	0	0	0
0.15 - 0.35	0	0	0
0.20 - 0.35	0	0	0
0.25 - 0.35	0	0	0
0.30 - 0.35	0	0	0
0.35 - 0.35	0	0	0
0.40 - 0.35 = 0.05	1.4	0.09	0.027
0.45 - 0.35 = 0.10	2.8	0.21	0.063
0.50 - 0.35 = 0.15	4.2	0.34	0.102
0.55 - 0.35 = 0.20	5.6	0.46	0.138
0.60 - 0.35 = 0.25	7.0	0.58	0.178
0.65 - 0.35 = 0.30	8.4	0.73	0.214
0.70 - 0.35 = 0.35	9.8	0.87	0.261
0.75 - 0.35 = 0.40	11.2	0.93	0.279
0.80 - 0.35 = 0.45	12.6	0.95	0.285
0.85 - 0.35 = 0.50	14.0	0.96	0.288
0.90 - 0.35 = 0.55	15.4	0.97	0.291
0.95 - 0.35 = 0.60	16.8	1.0	0.30
1.00 - 0.35 = 0.65	18.2	1.0	0.30
1.05 - 0.35 = 0.70	19.6	1.0	0.30
1.10 - 0.35 = 0.75	21.0	1.0	0.30
1.15 - 0.35 = 0.80	22.4	1.0	0.30
1.20 - 0.35 = 0.85	23.8	1.0	0.30
1.25 - 0.35 = 0.90	25.2	1.0	0.30

The value of 0.35×10^{-9} seconds subtracted from the time in column one may cause some confusion. It must be remembered that we are interested in the superposition of the contribution of a number of ramps. If ramp one starts at time $t = 0$, then ramp two does not start until time $t = 0.35 \times 10^{-9}$ seconds. In a similar manner ramp three begins at time $t = 0.715 \times 10^{-9}$ seconds and ramp four begins at time $t = 1.0$ seconds.

a3. Third Ramp:

$$\text{Amplitude} = 0.834 - 0.583 = 0.251$$

$$\begin{aligned}\text{Rise Time} &= (1.000 - 0.715) \times 10^{-9} \\ &= 0.285 \times 10^{-9} \text{ sec.}\end{aligned}$$

$$\alpha = \frac{0.285 \times 10^{-9}}{3.57 \times 10^{-11}} = 8.0$$

<u>$t (10^{-9} \text{ sec.})$</u>	<u>$x = 28 t$</u>	<u>Response</u>	<u>0.251 Response</u>
0.05 - 0.715	0	0	0
0.10 - 0.715	0	0	0
0.15 - 0.715	0	0	0
0.20 - 0.715	0	0	0
0.25 - 0.715	0	0	0
0.30 - 0.715	0	0	0
0.35 - 0.715	0	0	0
0.40 - 0.715	0	0	0
0.45 - 0.715	0	0	0
0.50 - 0.715	0	0	0

<u>t (10⁻⁹ sec.)</u>	<u>x = 28 t</u>	<u>Response</u>	<u>0.251 Response</u>
0.55 - 0.715	0	0	0
0.60 - 0.715	0	0	0
0.65 - 0.715	0	0	0
0.70 - 0.715	0	0	0
0.75 - 0.715 = 0.035	0.98	0.076	0.019
0.80 - 0.715 = 0.085	2.38	0.215	0.054
0.85 - 0.715 = 0.135	3.78	0.38	0.095
0.90 - 0.715 = 0.185	5.18	0.538	0.138
0.95 - 0.715 = 0.235	6.58	0.71	0.178
1.00 - 0.715 = 0.285	7.98	0.862	0.216
1.05 - 0.715 = 0.335	9.38	0.925	0.232
1.10 - 0.715 = 0.385	10.78	0.950	0.238
1.15 - 0.715 = 0.435	12.18	0.96	0.240
1.20 - 0.715 = 0.485	13.58	0.97	0.243
1.25 - 0.715 = 0.535	14.98	0.97	0.243

a4. Fourth Ramp:

$$\text{Amplitude} = 1.00 - 0.834 = 0.166$$

$$\begin{aligned}\text{Rise Time} &= (1.15 - 1.00) \times 10^{-9} \\ &= 0.15 \times 10^{-9} \text{ sec.}\end{aligned}$$

$$\alpha = \frac{0.15 \times 10^{-9}}{3.57 \times 10^{-11}} = 4.2$$

<u>t (10⁻⁹ sec.)</u>	<u>x = 28 t</u>	<u>Response</u>	<u>0.166 Response</u>
0.05 - 1.0	0	0	0
0.10 - 1.0	0	0	0

<u>t (10⁻⁹ sec.)</u>	<u>x = 28 t</u>	<u>Response</u>	<u>0.166 Response</u>
0.15 - 1.0	0	0	0
0.20 - 1.0	0	0	0
0.25 - 1.0	0	0	0
0.30 - 1.0	0	0	0
0.35 - 1.0	0	0	0
0.40 - 1.0	0	0	0
0.45 - 1.0	0	0	0
0.50 - 1.0	0	0	0
0.55 - 1.0	0	0	0
0.60 - 1.0	0	0	0
0.65 - 1.0	0	0	0
0.70 - 1.0	0	0	0
0.75 - 1.0	0	0	0
0.80 - 1.0	0	0	0
0.85 - 1.0	0	0	0
0.90 - 1.0	0	0	0
0.95 - 1.0	0	0	0
1.0 - 1.0	0	0	0
1.05 - 1.0 = 0.05	1.4	0.24	0.039
1.10 - 1.0 = 0.10	2.8	0.534	0.089
1.15 - 1.0 = 0.15	4.2	0.830	0.138
1.20 - 1.0 = 0.20	5.6	0.905	0.150
1.25 - 1.0 = 0.25	7.0	0.930	0.154

a5. Total Dielectric Response:

The total dielectric response is found by adding the response of the individual ramps at a given time. For instance, the total response at time $t = 1.25 \times 10^{-9}$ seconds is

$$(0.283 + 0.30 + 0.243 + 0.154) = 0.98$$

<u>$t (10^{-9} \text{ sec.})$</u>	<u>Total Dielectric Response</u>
0.05	0.026
0.10	0.062
0.15	0.102
0.20	0.136
0.25	0.176
0.30	0.212
0.35	0.249
0.40	0.290
0.45	0.335
0.50	0.377
0.55	0.414
0.60	0.461
0.65	0.497
0.70	0.544
0.75	0.581
0.80	0.622
0.85	0.666
0.90	0.712

<u>t (10⁻⁹ sec.)</u>	<u>Total Dielectric Response</u>
0.95	0.761
1.0	0.799
1.05	0.854
1.10	0.907
1.15	0.962
1.20	0.967
1.25	0.980

Total dielectric response is shown in graphical form as Fig. 5-5. For comparison, the input pulse approximation has also been included. As can be seen, the dielectric causes the rise time of the input pulse to deteriorate somewhat.

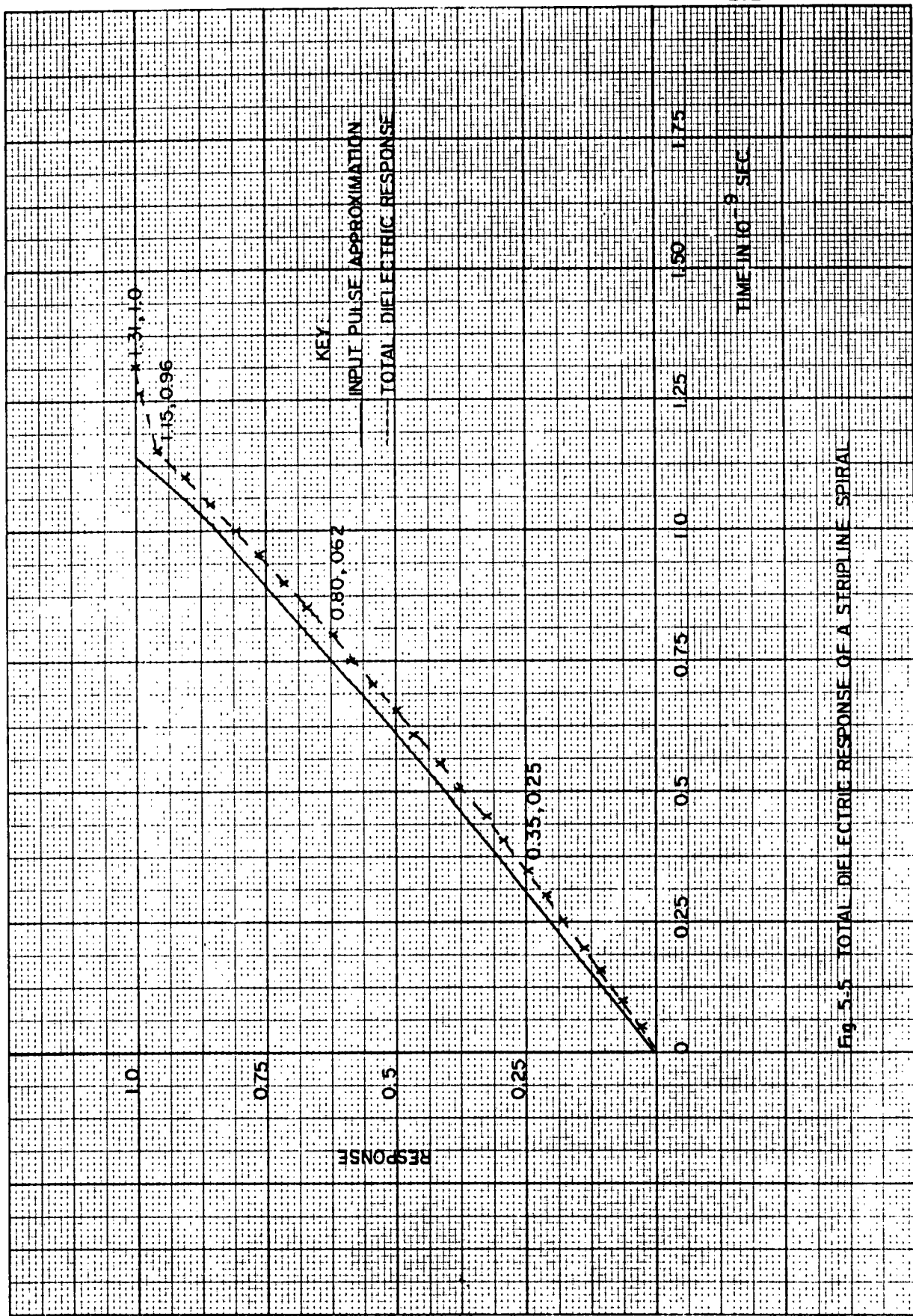
b. Skin Effect Response:

Now that the degradation of the input pulse rise time due to the dielectric has been taken into account, we wish to examine the degradation of rise time due to skin effect. This is done by approximating the dielectric response shown in Fig. 5-5 by a series of ramps and applying these ramps to the graphs of Appendix VII. As in the dielectric response analysis, the ramps were chosen so that they fell in the range of the graphs.

bl. First Ramp:

Amplitude = 0.25

Rise Time = a = 0.35 X 10⁻⁹ sec.



$$\rho = t/\beta = \frac{t \times 10^{-9}}{7.3 \times 10^{-12}} = 137 t \quad (t \text{ in } 10^{-9} \text{ sec.})$$

($\beta = 7.3 \times 10^{-12}$ was determined in section F 2)

$$\alpha = a/\beta = \frac{0.35 \times 10^{-9}}{7.3 \times 10^{-12}} = 48$$

For this value of α , use Fig. 4 of Appendix VII.

<u>t (10^{-9} sec.)</u>	<u>$\rho = 137 t$</u>	<u>Response</u>	<u>0.25 Response</u>
0.05	6.85	0.04	0.01
0.10	13.7	0.13	0.03
0.15	20.6	0.25	0.06
0.20	27.4	0.35	0.09
0.25	34.3	0.44	0.11
0.30	41.1	0.56	0.14
0.35	48	0.70	0.18
0.40	54.8	0.76	0.19
0.45	61.7	0.80	0.20
0.50	68.5	0.81	0.20
0.55	75.4	0.84	0.21
0.60	82.2	0.85	0.21
0.65	89.1	0.86	0.22
0.70	96.0	0.87	0.22
0.75	102.8	0.88	0.22
0.80	109.5	0.89	0.22
0.85	116.5	0.89	0.22

<u>t (10⁻⁹ sec.)</u>	<u>$\rho = 137 t$</u>	<u>Response</u>	<u>0.25 Response</u>
0.90	123.3	0.89	0.22
0.95	130.1	0.89	0.22
1.0	137.0	0.90	0.23
1.05	143.9	0.90	0.23
1.10	151.0	0.90	0.23
1.15	157.5	0.90	0.23
1.20	164.5	0.90	0.23
1.25	171.2	0.90	0.235

As was the case in the dielectric response analysis, the graphs assume a ramp of unit amplitude. Column four of the above table adjusts the amplitude of the graph to the ramp under discussion.

b2. Second Ramp:

$$\text{Amplitude} = 0.62 - 0.25 = 0.37$$

$$\begin{aligned}\text{Rise Time} &= (0.80 - 0.35) \times 10^{-9} \\ &= 0.45 \times 10^{-9} \text{ sec.}\end{aligned}$$

$$\alpha = \frac{0.45 \times 10^{-9}}{7.3 \times 10^{-12}} = 61.7$$

Using Fig. 4 of Appendix VII, we obtain the following table.

<u>t (10⁻⁹ sec.)</u>	<u>$\rho = 137 t$</u>	<u>Response</u>	<u>0.37 Response</u>
0.05 - 0.35	0	0	0
0.10 - 0.35	0	0	0
0.15 - 0.35	0	0	0
0.20 - 0.35	0	0	0

<u>t (10⁻⁹ sec.)</u>	<u>p = 137 t</u>	<u>Response</u>	<u>0.37 Response</u>
0.25 - 0.35	0	0	0
0.30 - 0.35	0	0	0
0.35 - 0.35	0	0	0
0.40 - 0.35 = 0.05	6.85	0.04	0.02
0.45 - 0.35 = 0.10	13.7	0.08	0.03
0.50 - 0.35 = 0.15	20.6	0.23	0.09
0.55 - 0.35 = 0.20	27.4	0.32	0.12
0.60 - 0.35 = 0.25	34.3	0.36	0.13
0.65 - 0.35 = 0.30	41.1	0.47	0.17
0.70 - 0.35 = 0.35	48.0	0.58	0.22
0.75 - 0.35 = 0.40	54.8	0.64	0.24
0.80 - 0.35 = 0.45	61.7	0.73	0.27
0.85 - 0.35 = 0.50	68.5	0.77	0.29
0.90 - 0.35 = 0.55	75.4	0.80	0.29
0.95 - 0.35 = 0.60	82.2	0.83	0.31
0.0 - 0.35 = 0.65	89.1	0.85	0.32
1.05 - 0.35 = 0.70	91.0	0.86	0.32
1.10 - 0.35 = 0.75	102.8	0.86	0.32
1.15 - 0.35 = 0.80	109.5	0.87	0.32
1.20 - 0.35 = 0.85	116.5	0.87	0.32
1.25 - 0.35 = 0.90	123.3	0.88	0.33

It will be noted that 0.35×10^{-9} seconds is subtracted from all values of time in column one. The reasoning is the same as that used in the dielectric response, i.e., the

second ramp does not begin until ramp one has been on for
 0.35×10^{-9} seconds.

b3. Third Ramp:

$$\text{Amplitude} = 0.96 - 0.62 = 0.34$$

$$\begin{aligned}\text{Rise Time} &= (1.15 - 0.80) \times 10^{-9} \\ &= 0.35 \times 10^{-9} \text{ sec.}\end{aligned}$$

$$\alpha = \frac{0.35 \times 10^{-9}}{7.3 \times 10^{-12}} = 48$$

Using Appendix VII, Fig. 4

<u>t (10⁻⁹ sec.)</u>	<u>p = .137 t</u>	<u>Response</u>	<u>0.34 Response</u>
0.05 - 0.80	0	0	0
0.10 - 0.80	0	0	0
0.15 - 0.80	0	0	0
0.20 - 0.80	0	0	0
0.25 - 0.80	0	0	0
0.30 - 0.80	0	0	0
0.35 - 0.80	0	0	0
0.40 - 0.80	0	0	0
0.45 - 0.80	0	0	0
0.50 - 0.80	0	0	0
0.55 - 0.80	0	0	0
0.60 - 0.80	0	0	0
0.65 - 0.80	0	0	0
0.70 - 0.80	0	0	0
0.75 - 0.80	0	0	0
0.80 - 0.80	0	0	0

<u>t (10⁻⁹ sec.)</u>	<u>$\rho = 137 t$</u>	<u>Response</u>	<u>0.34 Response</u>
0.85 - 0.80 = 0.05	6.85	0.04	0.01
0.90 - 0.80 = 0.10	13.7	0.14	0.05
0.95 - 0.80 = 0.15	20.6	0.25	0.09
1.0 - 0.80 = 0.20	27.4	0.35	0.12
1.05 - 0.80 = 0.25	34.2	0.44	0.15
1.10 - 0.80 = 0.30	41.1	0.58	0.20
1.15 - 0.80 = 0.35	48.0	0.70	0.24
1.20 - 0.80 = 0.40	54.8	0.73	0.25
1.25 - 0.80 = 0.45	61.7	0.80	0.27

b4. Fourth Ramp:

$$\text{Amplitude} = 1.0 - 0.96 = 0.04$$

$$\begin{aligned}\text{Rise Time} &= (1.31 - 1.15) \times 10^{-9} \\ &= 0.16 \times 10^{-9} \text{ sec.}\end{aligned}$$

$$\alpha = \frac{0.16 \times 10^{-9}}{7.3 \times 10^{-12}} = 21.9$$

For an α of 21.9, Fig. 3 of Appendix VII was used to determine the table for the fourth ramp.

<u>t (10⁻⁹ sec.)</u>	<u>$\rho = 137 t$</u>	<u>Response</u>	<u>0.04 Response</u>
0.05 - 1.15	0	0	0
0.10 - 1.15	0	0	0
0.15 - 1.15	0	0	0
0.20 - 1.15	0	0	0
0.25 - 1.15	0	0	0
0.30 - 1.15	0	0	0

<u>t (10⁻⁹ sec.)</u>	<u>p = 137 t</u>	<u>Response</u>	<u>0.04 Response</u>
0.35 - 1.15	0	0	0
0.40 - 1.15	0	0	0
0.45 - 1.15	0	0	0
0.50 - 1.15	0	0	0
0.55 - 1.15	0	0	0
0.60 - 1.15	0	0	0
0.65 - 1.15	0	0	0
0.70 - 1.15	0	0	0
0.75 - 1.15	0	0	0
0.80 - 1.15	0	0	0
0.85 - 1.15	0	0	0
0.90 - 1.15	0	0	0
0.95 - 1.15	0	0	0
1.0 - 1.15	0	0	0
1.05 - 1.15	0	0	0
1.10 - 1.15	0	0	0
1.15 - 1.15	0	0	0
1.20 - 1.15	6.85	0.12	0.005
1.25 - 1.15	13.7	0.33	0.013

b5. Total Skin Effect Response:

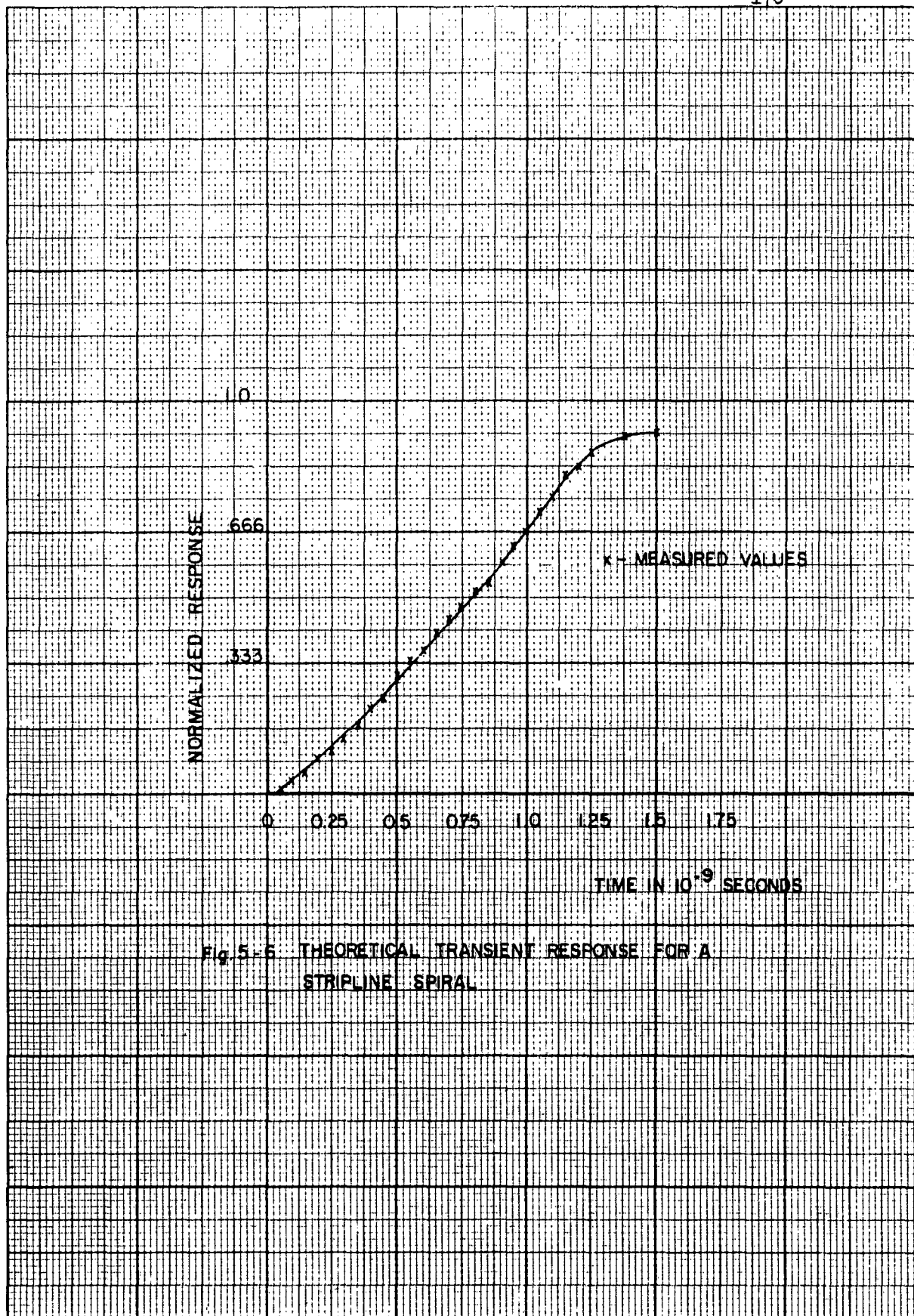
Total skin effect response is found by adding up the contributions of the individual ramps at a given time. Thus, for $t = 1.25 \times 10^{-9}$ seconds the total response is $(0.235 + 0.33 + 0.27 + 0.013) = 0.84$

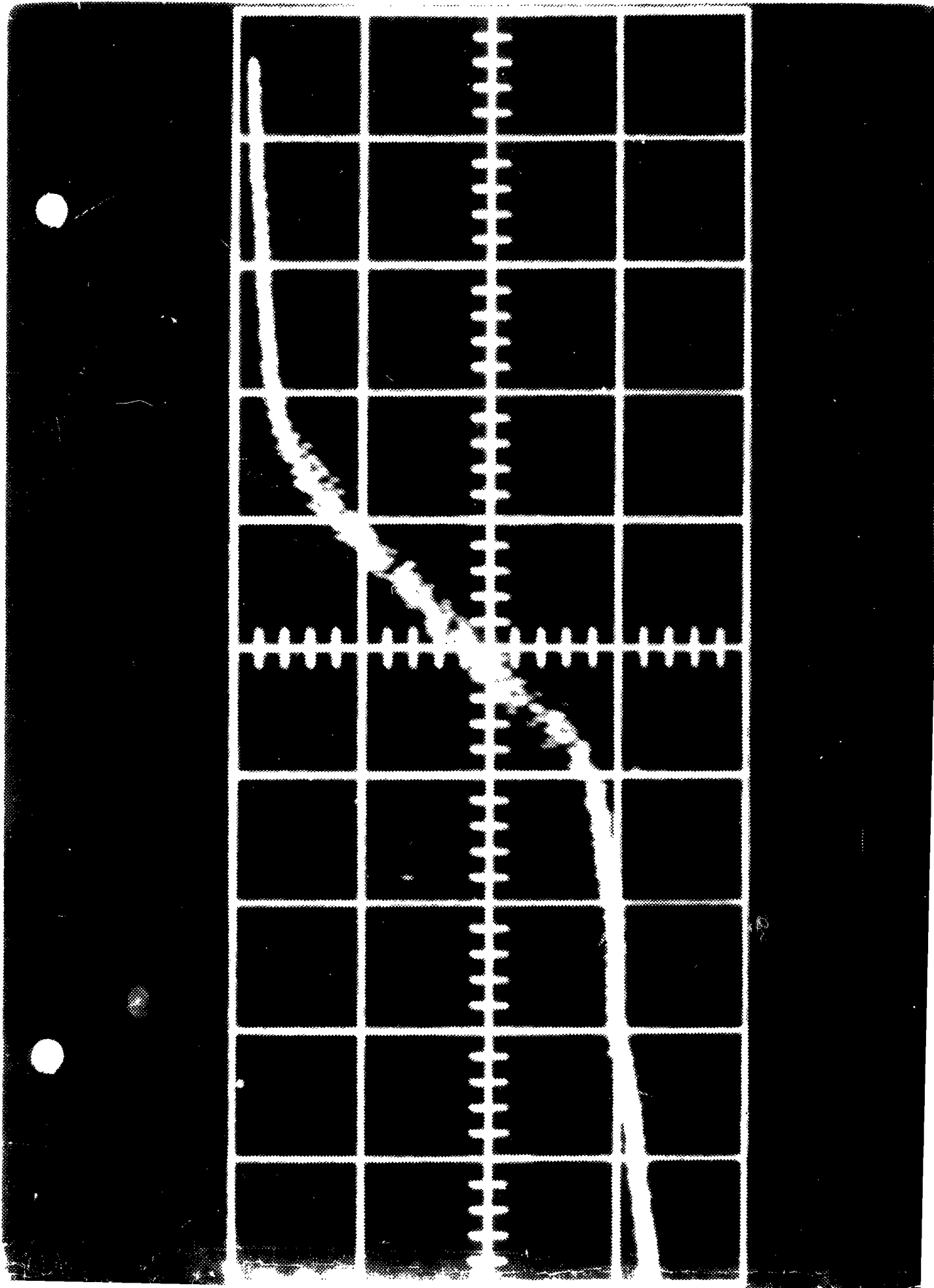
<u>t (10⁻⁹ sec.)</u>	<u>Total Response</u>
0.05	0.01
0.10	0.03
0.15	0.06
0.20	0.09
0.25	0.11
0.30	0.14
0.35	0.18
0.40	0.21
0.45	0.23
0.50	0.29
0.55	0.33
0.60	0.35
0.65	0.39
0.70	0.43
0.75	0.46
0.80	0.49
0.85	0.52
0.90	0.57
0.95	0.62
1.0	0.65
1.05	0.70
1.10	0.74
1.15	0.78
1.20	0.80
1.25	0.84

Now the total skin effect response is really the transient response of the Spiral, since we started by approximating the dielectric response. Figure 5-6 presents the results in graphic form.

A photograph of the transient response of the stripline Spiral was made utilizing the method described in section F 1. The signal line between the pulse generator and the Lumatron delay unit was broken and the Spiral inserted. The resulting waveform was photographed and blown up to 8" X 10" size. This picture is included for comparison and follows Fig. 5-6. Correlation between the theoretical transient response given by Fig. 5-6 and measured transient response given by the picture following Fig. 5-6 is quite good. Both have rise times of about 1.25×10^{-9} seconds.

Wigington⁴⁰ also did an example of his paper although his calculations were not included. His input pulse is shown as Fig. 5-7. The theoretical vs. measured response of his Spirals are shown as Fig. 5-8. A summary of the characteristics of these Spirals are included as Appendix IX.





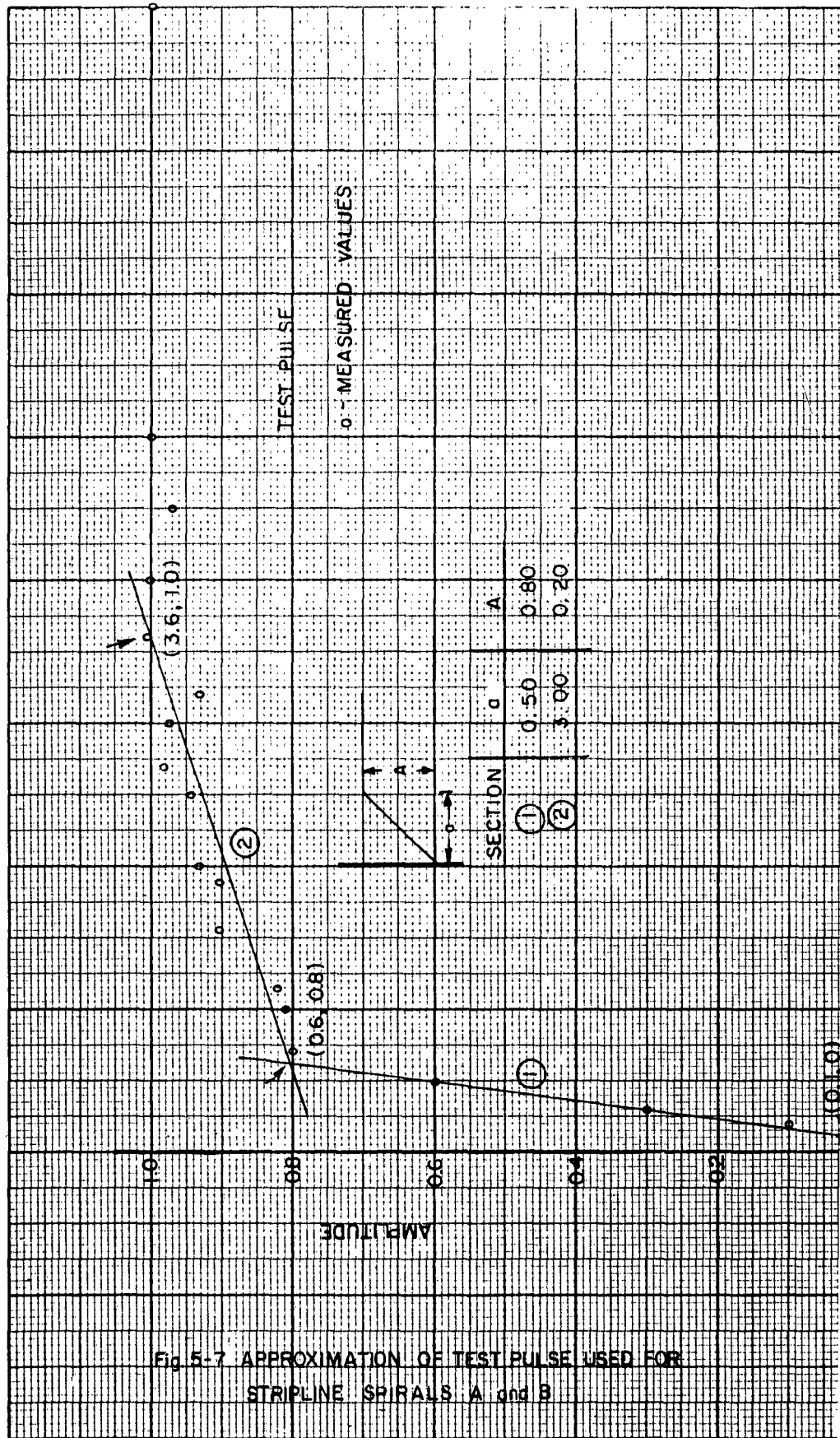


Fig. 5-7 APPROXIMATION OF TEST PULSE USED FOR
STRIPLINE SPIRALES A and B

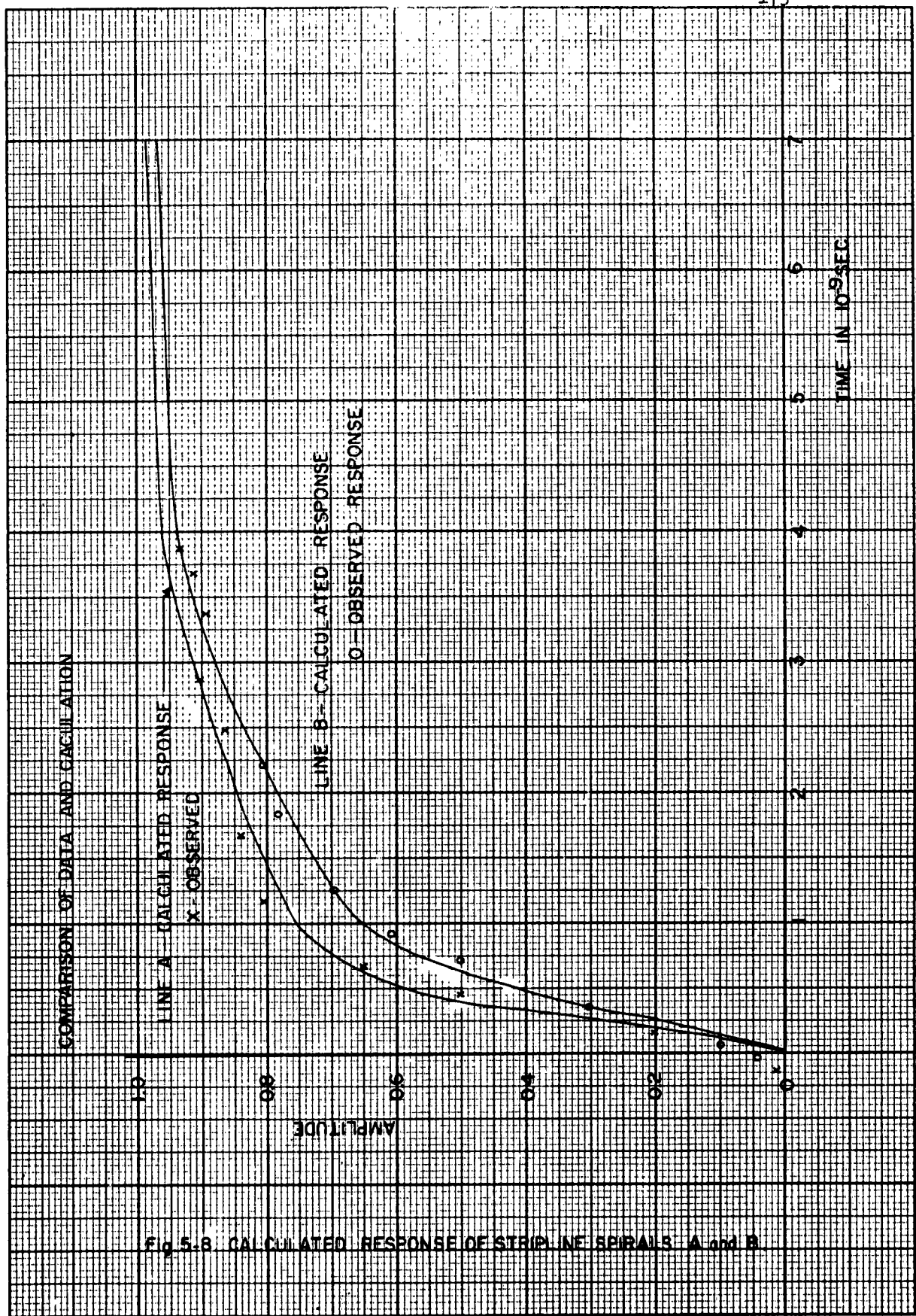


Fig. 5.8. CALCULATED RESPONSE OF STRIP-IN SPIRALS A and B.

G. Summary

We have seen that knowing copper and dielectric thickness, dielectric constant, loss tangent and desired characteristic impedance, we can find the transient response of a stripline device. The analysis proceeds in the following steps: (1) approximate the input pulse by a series of ramps, (2) apply these ramps to the graph of Fig. 5-3 and add the contribution of the individual ramps to obtain the dielectric response, (3) approximate the dielectric response by a series of ramps, and (4) apply these ramps to the graphs of Appendix VII and add the individual contributions to obtain the skin effect response. This response is the transient response since we have taken dielectric degradation into account by considering dielectric response as the input pulse to the skin effect analysis.

BIBLIOGRAPHY

40. R. L. Wigington, "The Transient Response of Strip Line", Master's Thesis, University of Maryland, College Park, Maryland, 1959.
41. Ramo and Whinnery, "Fields and Waves in Modern Radio", pp 213-214, Second Edition, John Wiley and Sons, New York, 1953.
42. H. W. Bode, "Network Analysis and Feedback Amplifier Design", pp 298-299, Van Nostrand, Princeton, N. J., 1945.
43. H. W. Bode, "Network Analysis and Feedback Amplifier Design", pp 120-121, Van Nostrand, Princeton, N. J., 1945.
44. N. Balabanian, "Network Synthesis", p 143, Prentice-Hall Inc., Englewood Cliffs, N. J., 1958.
45. H. W. Bode, "Network Analysis and Feedback Amplifier Design", p 24, Van Nostrand, Princeton, N. J., 1945.
46. R. L. Wigington and N. S. Nahman, "Transient Analysis of Coaxial Cables Considering Skin Effect", Proc. IRE, Feb 1957, pp 166-174.
47. G. A. Campbell and R. M. Foster, "Fourier Integrals for Practical Applications", Table 1, Formula 632, D. Van Nostrand Co., Princeton, N. J.
48. G. A. Campbell and R. M. Foster, "Fourier Integrals for Practical Applications", Table 1, Formulas 107, 201 and 633, D. Van Nostrand Co., Princeton, N. J.
49. M. F. Gardner and J. L. Barnes, "Transients in Linear Systems", Vol 1, p 234, John Wiley and Son, Inc., New York, 1942.

APPENDIX VII

Transient Analysis of Coaxial Cables Considering Skin Effect*

R. L. WIGINGTON† AND N. S. NAHMAN‡, ASSOCIATE MEMBER, IRE

Summary—A transient analysis of coaxial cables is made by considering the skin effect of the center conductor as the distorting element. Generalized curves are presented by which the response of any length of coaxial cable can be predicted if one point on the attenuation vs frequency curve is known. An experimental check on the analysis is made by comparing measurements and prediction of the responses of several different coaxial cables.

INTRODUCTION

IN A STUDY of oscilloscope systems for use in observing voltage waveforms of the duration of a few millimicroseconds ($1 \mu\text{s} = 10^{-9}$ sec), the problem of the distortion of waveforms by the high frequency loss of coaxial cable was encountered. Elementary consideration of the problem indicated a degradation of fast rise times ($1 \mu\text{s}$ or less) due to greater attenuation of the high-frequency components of the signal.

In polyethylene dielectric coaxial cables, the conductance loss is extremely small. Polyethylene has a dissipation factor of 0.0031 at 3000 mc¹ and less at lower frequencies. Likewise, in air dielectric cables the conductance loss is even less. Therefore, the major portion of high-frequency loss could not be blamed on leakage conductance. The other source of loss in coaxial cable is the series resistance of the center conductor. For analysis the skin effect of the outer conductor was considered to be lumped with the skin effect of the center conductor increasing it slightly. Using empirical data to evaluate the skin effect constant achieves this directly. Ordinary analysis of transmission lines ignore this resistance as being negligible. However, at frequencies at which the skin effect of conductors becomes significant, the analysis must include its effects, both as series resistance and inductance.

In this analysis, a transmission line is treated as a four-pole network. With the aid of an approximation which is good at high frequencies, an analysis including skin effect and neglecting dielectric effects can be made. All calculations are in mks units.

POSSIBLE APPLICATIONS

Before proceeding with the analytical details of the problem, a few words about the engineering applications would be indicative of the role which skin effect distortion in coaxial cables may play in contemplated and future systems using fast transients.

* Original manuscript received by the IRE, August 20, 1956; revised manuscript received, October 18, 1956.

† Natl. Security Agency, Washington, D. C.

‡ Univ. of Kansas, Lawrence, Kan. Formerly with Natl. Security Agency, Washington, D. C.

¹ "Reference Data for Radio Engineers," Federal Telephone and Radio Corp., 3rd ed., p. 51.

The origination of this problem was in the design of an oscilloscope system for observing very fast rise times, $1 \mu\text{s}$ or less. In triggered oscilloscope systems a signal delay path (usually a simulated line or a coaxial cable) is necessary to allow time for the trigger circuits to detect the pulse to be observed and to start the sweep. The delay of this path is $50 \mu\text{s}$ or longer in present systems. As shown in this paper, the distortion in this amount of coaxial cable is very serious for millimicrosecond transients. Therefore, along with the other limitations of oscilloscope systems (such as rise time of the signal amplifiers, writing speed, and vertical sensitivity), the distortion due to the signal delay cable must be considered. Perhaps a knowledge of the form of this distortion will enable the extension of the range of oscilloscope systems which are limited by the signal delay distortion.

If preserving the rise times in fast pulse circuits is in any way critical to the proper operation of the circuitry, one must begin to consider the skin effect distortion in 10-mc prf circuits for long cable runs, and in 100-mc prf circuits, the distortion would be troublesome even in short cable lengths. The practice of using special small size coaxial cable to conserve space results in greater attenuation per unit length than for larger cable of the same characteristic impedance, and thus, also makes the skin effect distortion greater.

Another example of a problem in which the analysis may be very useful is in the analysis of regenerative pulse generators, a circuit which is essentially a loop consisting of an amplifier and a delay circuit.² For practical, high rep-rate pulse generation, the delay circuit is usually a coaxial cable. The pulse shape obtained is a composite of the characteristics of the cable and of the amplifier.

In short, for any electronic circuit application using coaxial cables as transmission media to provide either time delay or transmission of millimicrosecond pulses, the effects of skin effect distortion must be considered.

ANALYSIS

For a transmission line of length, l , terminated in its characteristic impedance, Z_0 , and with propagation constant, γ , the following relation exists between input (E_i) and the output (E_o) voltages as functions of complex frequency:³

² C. C. Cutler, "The regenerative pulse generator," Proc. IRE, vol. 43, pp. 140-148; February, 1955.

³ The complex variable is the Laplace Transform variable p . Eqs. (1) and (2) comprise the Laplace Transform equations of the system differential equations.

$$E_2 = e^{-\gamma t} E_1 \quad (1)$$

where in general

$$\gamma = \sqrt{(R + pL)(G + pC)} \quad (2a)$$

$$Z_0 = \sqrt{\frac{R + pL}{G + pC}}. \quad (2b)$$

For high frequencies (skin depth small with respect to conductor radius), the skin effect impedance of a round wire is:⁴

$$Z_s = K\sqrt{p} \quad (3a)$$

and

$$K = \frac{1}{2\pi r} \sqrt{\frac{\mu}{\sigma}} \quad (3b)$$

where r is conductor radius, μ is the permeability and σ is the conductivity of the wire.

At high frequencies the series resistance of a wire is expressed by the skin effect equation. Since an increase in inductance is also caused by skin effect, it is treated as an impedance rather than as a resistance. Therefore, replacing R in (2) by Z_s , and neglecting dielectric leakage ($G=0$), (2) becomes

$$\gamma = \sqrt{(K\sqrt{p} + pL)pC} \quad (4a)$$

$$Z_0 = \sqrt{\frac{K\sqrt{p} + pL}{pC}}. \quad (4b)$$

The transfer function of a length of line is then:

$$\frac{E_2}{E_1} = e^{-\gamma t} = e^{-t\sqrt{p^2LC + p^2CK\sqrt{p}}}. \quad (5)$$

The inverse Laplace Transform of the transfer function (5) is the impulse response of the section of line. For simplification, the following approximation was made. Expanding the square root in the exponent of (5) by the binomial expansion, one obtains

$$\begin{aligned} \gamma(p) &= (p^2LC + p^{3/2}CK)^{1/2} \\ &= p\sqrt{LC} + \frac{Kp^{1/2}}{2} \sqrt{\frac{C}{L}} + \frac{1}{2} \sum_{n=1}^{\infty} (-1)^{n-1} \\ &\quad \left(\frac{1 \cdot 3 \cdots (2n-3)}{2^{n-1} n!} \right) \frac{K^n}{L^{n-1}} \sqrt{\frac{C}{L}} p^{1-n/2}. \end{aligned} \quad (6)$$

The first term of (6) is the delay term and the remaining terms describe the waveform distortion. The series is an alternating convergent series (for $p^2LC > p^{3/2}CK$). Approximating it by the second term of (6), the p^0 term, results in an error less than the next term, the $p^{1/2}$ term. The ratio of these two terms will be used as a measure of validity of applying this approximation to specific examples.

⁴S. Ramo and J. R. Whinnery, "Fields and Waves in Modern Radio," John Wiley and Sons, Inc., New York, N. Y.; 1945.

$$\begin{aligned} A &= \left| \frac{p^0 \text{ term}}{p^{1/2} \text{ term}} \right| = \left| \frac{\frac{K^2}{8L} \sqrt{\frac{C}{L}}}{\frac{Kp^{1/2}}{2} \sqrt{\frac{C}{L}}} \right| = \left| \frac{K}{4Lp^{1/2}} \right| \\ &= \frac{K}{4L\sqrt{2\pi f}}. \end{aligned} \quad (7)$$

Using the first two terms of (6) in (5) and letting $R_0 = \sqrt{L/C}$, $T = \sqrt{LC}$, results in

$$\frac{E_2}{E_1} = e^{-t(pT + (K/2R_0)p^{1/2})}. \quad (8)$$

The $\exp(-lt)$ is simply a delay term so that the inverse transform of (8) is the inverse transform of $\exp(-lkp^{1/2}/2R_0)$ delayed an amount lT . The latter exponential is a common transform and is listed in ordinary Laplace Transform tables.⁵ Its inverse giving the impulse response is:

$$\begin{aligned} g(t) &= \alpha x^{-1/2} e^{-\beta/x} & x \geq 0 \\ &= 0 & x < 0 \end{aligned} \quad (9)$$

where

$$\alpha = \frac{lK}{4R_0\sqrt{\pi}}, \quad \beta = \left(\frac{lK}{4R_0} \right)^2, \quad \text{and } x = t - lT.$$

Of greater utility in studying the distortion of fast rise times by skin effect are the step response and the response to a linear rise. The step response can be obtained by finding the inverse transform of $1/p$ times the transfer function. As before, the transform $1/p \exp(-lkp^{1/2}/2R_0)$ is listed in tables.⁶ Therefore in terms of x and β as defined above, the step response is:

$$\begin{aligned} h(t) &= \text{cerf} \sqrt{\frac{\beta}{x}} & x \geq 0 \\ &= 0 & x < 0. \end{aligned} \quad (10)$$

cerf (y) is the "complementary error function of y ."

The linear rise referred to previously is defined specifically as the following, and it will be referred to as a ramp input.

$$\begin{aligned} F(t) &= 0 & t < 0 \\ &= t/a & 0 \leq t \leq a \\ &= 1 & t > a. \end{aligned}$$

The response to $F(t)$, called $f(t)$, is given by the convolution of $F(t)$ with the impulse response of the line, $g(t)$.

$$f(t) = \int_0^t F(t-\tau)g(\tau)d\tau.$$

This integral reduces to the following special cases:

⁵S. Goldman, "Transformation Calculus and Electrical Transients," Prentice-Hall, Inc., New York, N. Y., p. 423; 1949.

Case I: $0 < t \leq Tl$ $f(t) = 0$ since $g(\tau) = 0$ for $\tau < Tl$

Case II: $Tl \leq t \leq Tl+a$

$$f(t) = \int_0^x \left(\frac{x-\tau}{a} \right) \tau^{-3/2} e^{-\beta/\tau} d\tau, \quad x = t - Tl$$

Case III: $t > Tl+a$

$$f(t) = \int_0^{x-a} \tau^{-3/2} e^{-\beta/\tau} d\tau + \int_{x-a}^x \left(\frac{x-\tau}{a} \right) \tau^{-3/2} e^{-\beta/\tau} d\tau, \quad x = t - Tl.$$

Note that Case II is contained in Case III providing that the integrands are limited to positive values of τ only for Case II.

Considering Case III only and evaluating with the aid of the identity derived in Appendix I, one obtains

$$f(t) = \text{cerf } \sqrt{\frac{\beta}{x-a}} + \frac{x}{a} \left(\text{cerf } \sqrt{\frac{\beta}{x}} - \text{cerf } \sqrt{\frac{\beta}{x-a}} \right) \quad (11)$$

$$- \frac{1}{a} \int_{x-a}^x \tau \alpha \tau^{-3/2} e^{-\beta/\tau} d\tau.$$

Integrating the last term of (11) by parts one obtains

$$\frac{1}{a} \int_{x-a}^x \tau \alpha \tau^{-3/2} e^{-\beta/\tau} d\tau$$

$$= \frac{x}{a} \text{cerf } \sqrt{\frac{\beta}{x}} - \frac{x-a}{a} \text{cerf } \sqrt{\frac{\beta}{x-a}}$$

$$- \frac{1}{a} \int_{x-a}^x \text{cerf } \sqrt{\frac{\beta}{\tau}} d\tau. \quad (12)$$

Observing that the first two terms of (12) cancel the corresponding terms of (11), the function $f(t)$ is simply,

$$f(t) = \frac{1}{a} \int_{x-a}^x \text{cerf } \sqrt{\frac{\beta}{\tau}} d\tau \quad x \geq 0$$

$$x = t - Tl \quad (13)$$

with the understanding that for $x < a$ the lower limit is zero.

As verification, one may note that the limit of the ramp response as "a" approaches zero is simply the step response. Also, as x gets large, the function approaches unity; physical interpretation of the function required that this be true.

EVALUATION OF CONSTANTS

Using the first two terms of (6), the propagation constant is approximately

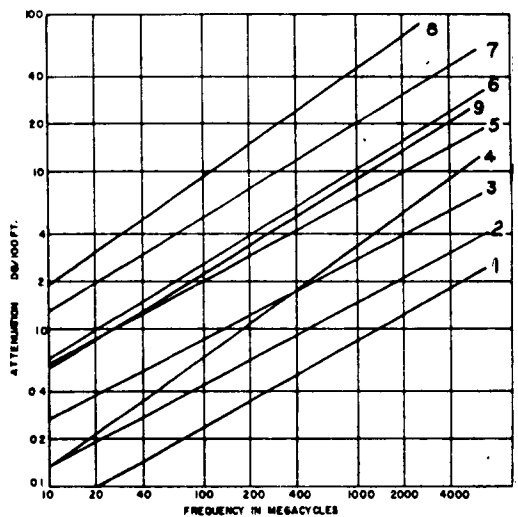
$$\gamma(p) = \rho T + \frac{K}{2R_0} p^{1/2}$$

$$\gamma(j\omega) = \frac{K}{2R_0} \sqrt{\frac{\omega}{2}} + j \left(\omega T + \frac{K}{2R_0} \sqrt{\frac{\omega}{2}} \right).$$

The real part of $\gamma(j\omega)$ is the attenuation constant of the transmission line, for the purposes of the analysis, called $C(f)$.

$$C(f) = \frac{K\sqrt{\pi f}}{2R_0} \text{ nepers/meter.} \quad (14)$$

Any coaxial cable whose attenuation constant obeys the above law will have a straight line relation of slope one-half between the logarithm of the attenuation constant and the logarithm of the frequency. The majority of types of coaxial cable have very nearly this characteristic (see Fig. 1). The ratio of $C(f)$ to \sqrt{f} from (14) is therefore a constant for each type of cable and can be calculated from the attenuation characteristic of the cable.



- | | |
|-------------------------|------------------------|
| 1) Styroflex 1/8 inches | 6) General Radio—874A2 |
| 2) Styroflex 1/4 inch | 7) RG—58 A/u |
| 3) Styroflex 1/2 inch | 8) RG—38, 39, 40/u |
| 4) RG—19, 20/u | 9) RG—8/u |
| 5) RG—63/u | |

References:

- 1), 2), 3)—Brochure of Phelps-Dodge Copper Products Corp.
- 4), 5), 7), 8), 9)—"Reference Data for Radio Engineers," Federal Telephone and Radio Corp., 3rd ed.
- 6)—Catalog N, General Radio Co.

Fig. 1—Attenuation vs frequency characteristics for common coaxial cables.

In this way, the value of K , and subsequently of β , can be evaluated for each case as follows:

$$\beta = \left(\frac{K}{4R_0} \right)^2 = \left(\frac{l}{4R_0} \frac{2R_0 C(f_0)}{\sqrt{\pi f_0}} \right)^2 = \left(\frac{l C(f_0)}{2\sqrt{\pi f_0}} \right)^2 \quad (15)$$

where f_0 is the frequency chosen to evaluate β . For convenience in calculation let $l = T_l/T$ where T_l is the time length of the cable and $T = \sqrt{LC}$ is the delay per unit length.

$$\beta = \left(\frac{T_l C(f_0)}{2T \sqrt{\pi f_0}} \right)^2. \quad (16)$$

RESISTIVE TERMINATION

The analysis assumes that the transmission line is terminated in its characteristic impedance which is given in (4b). However, in the ordinary circuit, a purely resistive termination of value $R_0 = \sqrt{L/C}$ would be used. To see at what frequencies Z_0 would be a good approximation for Z_0 , the following comparison of actual Z_0 with R_0 is made.

From (4b)

$$\begin{aligned} Z_0 &= \sqrt{\frac{pL + K\sqrt{p}}{pC}} = \left(R_0^2 + \frac{K}{C\sqrt{p}} \right)^{1/2} \\ &= R_0 + \frac{K}{2R_0 C \sqrt{p}} - \frac{K^2}{8R_0^2 C^2 p} + \dots \end{aligned} \quad (17)$$

The fractional deviation of Z_0 from R_0 as a function of p is less than the second term of (17) divided by R_0 . The smallness of the magnitude of this fraction indicates the closeness of approximation.

$$\left| \frac{Z_0(p) - R_0}{R_0} \right| < \left| \frac{K}{4R_0^2 C \sqrt{p}} \right| = \frac{K}{4R_0^2 C \sqrt{2\pi f}}. \quad (18)$$

Since $R_0^2 C = L$ then (18) is the same as (7). Thus, A , the validity constant calculated previously is also an expression of the departure of Z_0 from R_0 .

GENERALIZATION OF THEORY

In order to present curves with which any transient problem involving skin effect distortion of rise times could be solved, the theory is generalized. First, the assumption is made that any rising function can be approximated sufficiently closely for engineering analysis by a series of a few straight line segments. The response to any function can then be obtained from the sum of the responses to the ramp functions used for approximation. A generalized ramp response is then the function to be plotted.

Recalling from the analysis the three basic functions,

Impulse response $\equiv g(t)$

$$= g(x + Tl) = \sqrt{\frac{\beta}{\pi}} x^{-1/2} e^{-\beta x} \quad (9)$$

$$\text{Step response } \equiv f(t) = f(x + Tl) = \text{cerf } \sqrt{\frac{\beta}{x}} \quad (10)$$

Ramp response $\equiv h(t)$

$$= h(x + Tl) = \frac{1}{a} \int_{x-a}^x \text{cerf } \sqrt{\frac{\beta}{\tau}} d\tau \quad (13)$$

$x \geq 0, \text{ all cases,}$

the problem is to generalize them so that β , the constant which is determined by the specific case, does not appear in the functions, but only in the scales to which the responses are plotted.

As the first step, the transformation $x = \beta\rho$ is used in (9). The resulting function of ρ is⁶

$$g_0(\rho) = \frac{\rho^{-1/2} e^{-1/\rho}}{\beta \sqrt{\pi}} \quad \rho \geq 0 \quad (19)$$

or

$$\beta g_0(\rho) = \frac{\rho^{-1/2} e^{-1/\rho}}{\sqrt{\pi}} \quad \rho \geq 0. \quad (20)$$

To apply the normalized impulse response (20) as plotted in Fig. 2 to a specific case, the β is calculated from (15) or (16) using physical data. The horizontal scale is then multiplied by β and the vertical scale divided by β to obtain the impulse response $g(x + Tl)$ vs x .

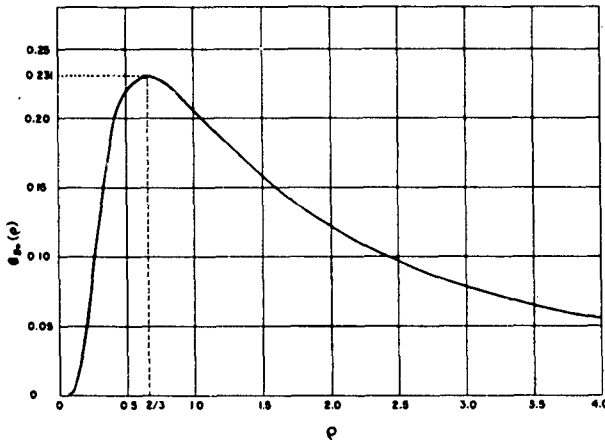


Fig. 2—Normalized impulse response,

$$\beta g_0(\rho) = \frac{\rho^{-1/2} e^{-1/\rho}}{\sqrt{\pi}}.$$

Performing the same transformation in (10), a normalized step response is obtained.

$$h_0(\rho) = \text{cerf } \sqrt{\frac{1}{\rho}} \quad \rho \geq 0. \quad (21)$$

To obtain $h(x + Tl)$ vs x the horizontal scale is multiplied by the proper β .

Likewise, performing the same operation on (13), the normalized ramp response is obtained.

$$f_0(\rho) = \frac{1}{a'} \int_{\rho-a'}^{\rho} \text{cerf } \sqrt{\frac{1}{\rho'}} d\rho' \quad \rho \geq 0 \quad (22)$$

where $a' = a/\beta$.

This represents a family of curves (Figs. 3, 4, and 5) with a' as the parameter. Practical utilization of them again requires only a time scale multiplication of magnitude β . Thus, the response of a particular piece of coaxial cable is obtained for a series of ramp inputs with 0-100 per cent rise times of $a'\beta$. For $a' = 0$ the step re-

⁶ This transformation is simple; however much confusion can arise if one does not state and visualize the problem. This is particularly true with respect to obtaining (22). See Appendix II for details.

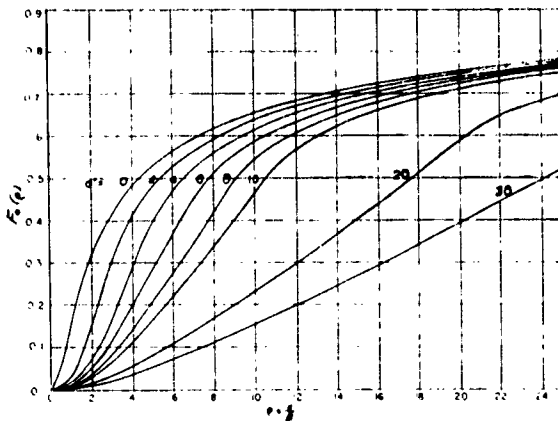


Fig. 3—Normalized ramp responses,

$$f_0(p) = \frac{1}{a'} \int_{p-a'}^p \operatorname{cerf} \sqrt{\frac{T}{p}} dp.$$

$$a' = \frac{a}{\beta}.$$

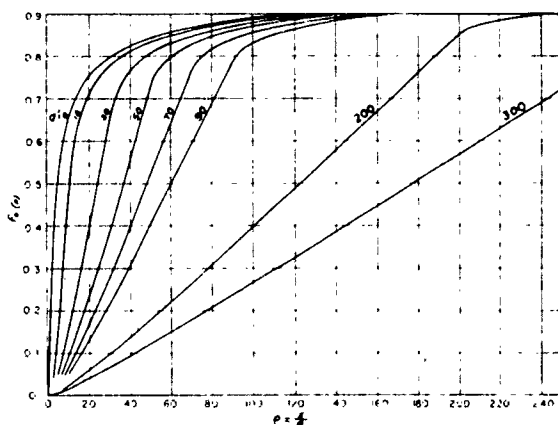


Fig. 4—Normalized ramp responses,

$$f_0(p) = \frac{1}{a'} \int_{p-a'}^p \operatorname{cerf} \sqrt{\frac{T}{p}} dp.$$

$$a' = \frac{a}{\beta}.$$

sponse (21) is obtained. The ramps corresponding to a' larger than the largest one plotted are relatively undistorted.

EXPERIMENTAL VERIFICATION

The experimental verification of the analysis which has been presented required the use of an extremely wide-band oscilloscope. Facilities which were available at the Naval Research Laboratory were used to obtain the transient response of eight pieces of coaxial cable.⁷ Two time lengths of each of four types of cable, namely, RG-8/U, RG-58/AU, General Radio-874A2, and $\frac{1}{2}$ -inch-diameter Styroflex, were tested. The signal applied to

⁷ See Acknowledgment.

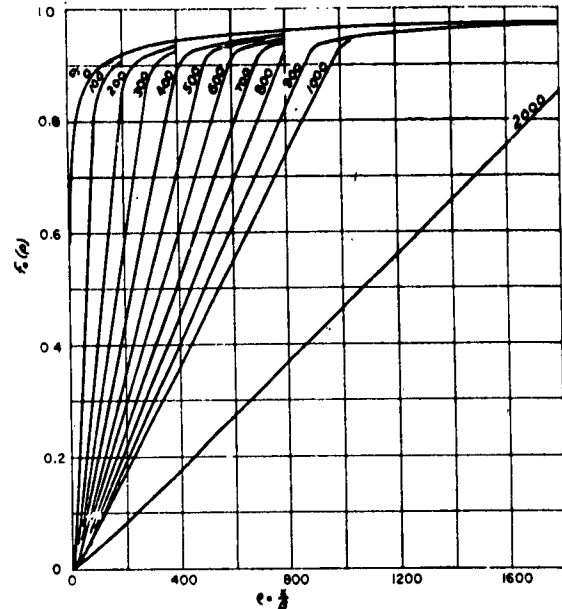


Fig. 5—Normalized ramp responses,

$$f_0(p) = \frac{1}{a'} \int_{p-a'}^p \operatorname{cerf} \sqrt{\frac{T}{p}} dp.$$

$$a' = \frac{a}{\beta}.$$

the cables was approximated by five ramp functions, and the response was calculated and compared with the observed response for each case.

EXPERIMENTAL SYSTEM

Fig. 6 shows the cable comparison test circuit employing the NRL TW-10 traveling-wave cathode-ray tubes as the indicating instrument. The TW-10 has a bandwidth well in excess of 2000 mc, which should be sufficient for displaying rise times of the order of 0.1 m μ s.

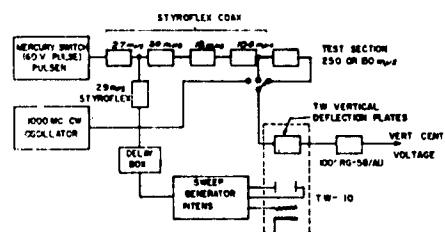


Fig. 6—Cable comparison test circuit.

The test pulse was generated by a mercury contact relay pulser giving a 60-volt pulse, 45 m μ s wide and having a rise time of 0.25 m μ s. Some signal delay (179 m μ s of $\frac{1}{2}$ -inch Styroflex) was required to allow time for operation of the sweep and intensifier circuits of the crt. The pulse observed at the end of the 179-m μ s delay was called the standard pulse. Cable test sections of either 150 or 250 m μ s were added, and the response

of the added sections to the standard pulse, as well as the standard pulse itself, were recorded photographically. Time reference was added to each photograph by applying a 1000-mc sine wave to the crt and taking double exposures.

ANALYSIS OF DATA

Data was taken from the photographs using the sine wave as the time reference and the maximum amplitude of the standard pulse as the amplitude reference.

The rise of the standard pulse (Fig. 7) was approx-

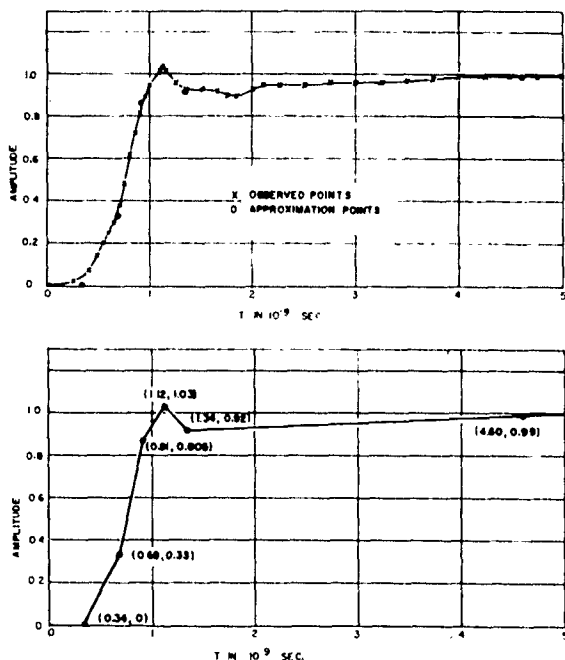


Fig. 7—Standard pulse and linear approximation.

imated by five straight line-segments as specified in the following Table I.

TABLE I
ANALYSIS OF STANDARD PULSE

Line Segment	End Points of Segments (10^{-9} second, Amplitude)	Amplitude	0-100 Per Cent Rise Time	t_0
1	(0.34, 0); (0.68, 0.33)	0.330	0.34×10^{-9} second	0
2	(0.68, 0.33); (0.91, 0.805)	0.535	0.23	0.34×10^{-9} second
3	(0.91, 0.805); (1.12, 1.03)	0.165	0.21	0.57
4	(1.12, 1.03); (1.34, 0.92)	-0.110	0.22	0.78
5	(1.34, 0.92); (5.00, 1.00)	0.080	3.66	1.00

The approximation to the standard pulse is then a succession of ramp functions having rise times and amplitudes as specified above and each starting at the appropriate t_0 .

The β and appropriate values for a' for each case were calculated from (16) and $a' = a/\beta$ [see (22)]. Considering now each example (*i.e.*, 150-m μ s delay of $\frac{1}{2}$ -inch Styroflex), five ramp responses, one for each approximation

segment, were calculated from the general curves in Figs. 3, 4, and 5.

The general curves consider ramp responses for ramps of amplitude unity; therefore, it was necessary to correct the amplitudes as listed in Table I. Points (in time) for calculation were preselected so that when the ramp responses were shifted according to the correct t_0 (listed in Table I) addition of ordinates would give the response to the standard pulse. The calculated responses as compared to the observed responses are given in Figs. 8-11 (next page).

In all cases no attempt was made to keep track of the zero time position of the transients. No information as to the time at which the transient first departed from zero amplitude after passing through a test section with respect to the time at which the transient "entered" the test section could be obtained. This difficulty is the same as is always met in relating physical transient data to mathematical prediction. The mathematician can define exactly a time before which the system is quiescent. However, the engineer must define the beginning of a transient as the time at which the waveform reaches same measurable value.

For comparison of calculation and observation, therefore, the curves were shifted in time relative to each other so the leading edges most nearly coincided at the region of steepest slope.

EXPERIMENTAL RESULTS AND DEPARTURES FROM THEORY

From the comparisons of Figs. 8-11, one may conclude that in the coaxial cables considered the major cause of distortion of fact rise time transients is the skin effect. Each type of cable seems to have its own characteristic departure from the predicted response. During this study the causes of some of the departure has become apparent.

First, the analysis involves an approximation in taking the inverse transform of the transfer function as

expressed in the validity constant A (7). The A for each case is indicated on the graphs (Figs. 8-11). As yet no quantitative measure has been developed to determine limits of error due to a particular value of A . However, the values of A in the examples considered are believed to be sufficiently small as to cause negligible error in the time range plotted. One may note that in the propagation constant $\gamma(p)$ (6) the first term ignored is a con-

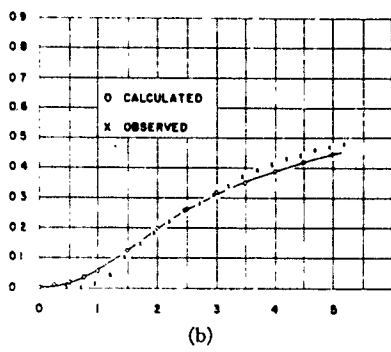
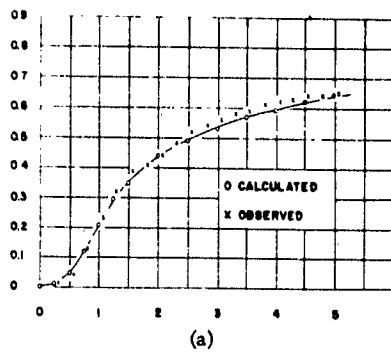


Fig. 8—Response of RG-58 A/u; $A(100 \text{ mc}) = 0.056$.
 (a) 150 m μ s of cable— $\beta = 4.50 \times 10^{-10}$ second.
 (b) 250 m μ s of cable— $\beta = 1.25 \times 10^{-10}$ second.

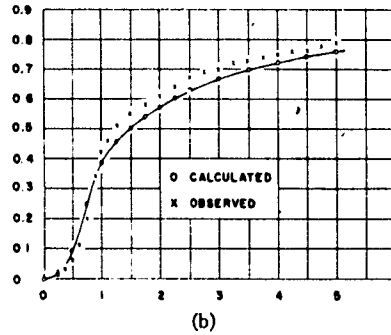
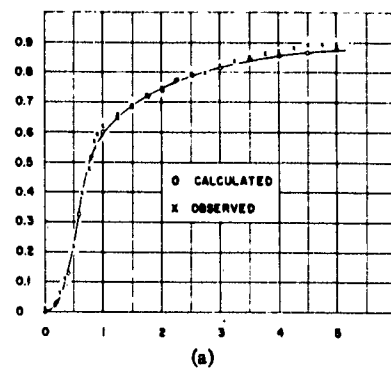


Fig. 10—Response of RG-8/u; $A(100 \text{ mc}) = 0.0024$.
 (a) 150 m μ s of cable— $\beta = 8.14 \times 10^{-11}$ second.
 (b) 250 m μ s of cable— $\beta = 2.26 \times 10^{-10}$ second.

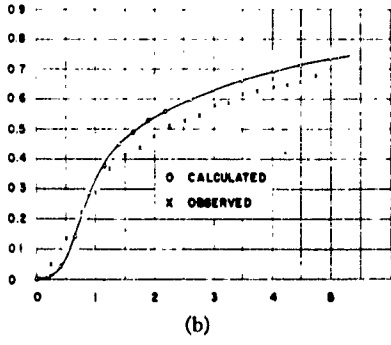
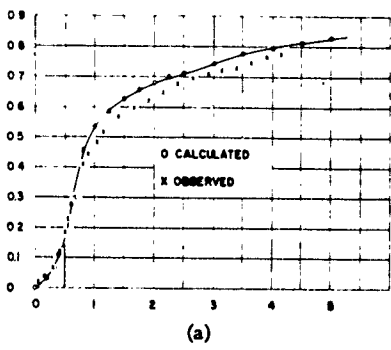


Fig. 9—Response of GR-874A2. $A(100 \text{ mc}) = 0.0027$.
 (a) 150 m μ s of cable— $\beta = 1.02 \times 10^{-10}$ second.
 (b) 250 m μ s of cable— $\beta = 2.83 \times 10^{-10}$ second.

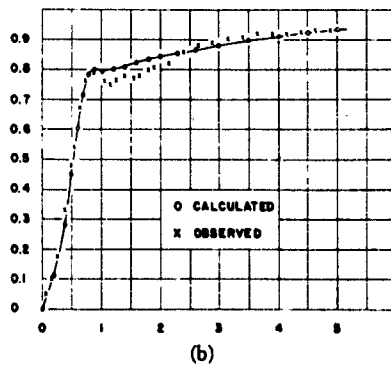
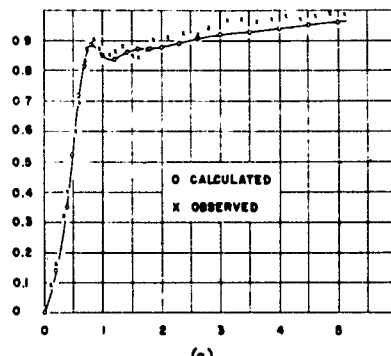


Fig. 11—Response of 1/2 inch Styroflex. $A(100 \text{ mc}) = 0.00057$.
 (a) 150 m μ s of cable— $\beta = 4.57 \times 10^{-12}$ second.
 (b) 250 m μ s of cable— $\beta = 1.27 \times 10^{-11}$ second.

stant (ρ^0 term) which adds nothing to the distortion and only insignificantly affects the amplitude.

The analysis assumes a $f^{0.4}$ law for the variation of attenuation with frequency [see (3) and (4)]. This is very nearly true for Styroflex cable. However, other cables have a somewhat greater exponent, GR-874 being as high as 0.6. A more elaborate analysis using f^m , $0 \leq m \leq 0.5$, has been made; however its usefulness is questionable since it cannot be directly related to the real physical problem. A realistic approach is to search for a second distorting factor such as dielectric loss which in this study was assumed to be negligible. Dielectric loss should be greater for GR-874 and other polyethylene dielectric cables than for Styroflex, although still it should not be the major distorting mechanism. Work on this phase of the problem is continuing.

Useful engineering results may be obtained even though the $f^{0.4}$ law is not followed exactly by the cable. The choice of the frequency at which β is evaluated (16) then becomes important. The frequency chosen in this study was $f_0 = 1000$ mc because the components of most importance were in the region of 1000 mc (considering a logarithmic frequency scale).

The bandwidth of the TW-10 was considered to be sufficient not to distort appreciably the response. The 10-90 per cent rise time of the standard pulse is 0.5 μ s. Approximately 700-900 mc of bandwidth (to the 3-db points) is needed to pass such a rise. The designers of the TW-10 oscilloscope system have established that the 3-db point of the deflection structure is well in excess of 2000 mc although no detailed data of deflection as a function of frequency is available. The ringing which is evident in some of the responses is probably due to the slight impedance discontinuities in the system.

Another possible source of error is in the nonlinearity of the crt deflection as a function of input amplitude. Checking this possibility showed that the crt deflection was within approximately 2 per cent of being linear. A slight curvature of the field of view (sometimes called "pin-cushion effect") made transcription of amplitude data difficult for time values of 3 to 5 μ s after the beginning of each response. Errors of up to 4 per cent (positive) may arise from this cause.

The RG-8 flexible connection between the TW-10 and the waveform to be observed (not explicitly shown in Fig. 6) does introduce appreciable distortion in the crt display; however, it does not invalidate the technique used to check the analysis.

Referring to Fig. 6, let the waveform entering the test section be represented by $F_1(p)$. Let the transfer function of the 15- μ s RG-8 connecting cable be $G_1(p)$. Also let $F'_1(p)$ represent the waveform observed on the CRT (the standard pulse) when the test section is not included. Then, $F'_1(p) = F_1(p)G_1(p)$. Now let $G_2(p)$ be the transfer function of the test section of cable. Then,

$F_2(p)$ which represents the waveform observed on the CRT when the test section is included is given by

$$\begin{aligned} F_2(p) &= F_1(p)G_1(p)G_2(p) \\ &= F_1(p)G_1(p)G_2(p) = F'_1(p)G(p) \end{aligned}$$

since transfer functions of passive networks are commutative.

In words, what this means is that the distorting element, $G_1(p)$ having been present both in observation of the input and output of the test section allows isolation of the characteristics of the test section alone. This is the basis for all comparison type measurement techniques. For accuracy, the distortion due to $G_1(p)$ must be of the same order of magnitude or preferably less than that due to $G_2(p)$. It is less in all cases.

CONCLUSION

The analysis as described is a first order theory for the transient response of coaxial cables. As presented, it is useful in engineering problems involving millimicrosecond transients, however, later refinements in the theory may permit greater accuracy for cables in which dielectric loss is an appreciable factor.

APPENDIX I

The following identity was useful in the analysis.

$$I(x) = \int_0^x \sqrt{\frac{\beta}{\pi}} r^{-3/2} e^{-\beta/r} dr = \text{erf } \sqrt{\frac{\beta}{x}}$$

It may be verified by using Laplace Transformation operational theorems.⁹ Letting L indicate the operation of taking the Laplace Transform and L^{-1} the inverse,

$$L[I(x)] = \frac{1}{p} L\left[\sqrt{\frac{\beta}{x}} r^{-3/2} e^{-\beta/r}\right] = \frac{1}{p} e^{-2\sqrt{\beta p}}$$

$$I(x) = L^{-1}[L[I(x)]] = L^{-1}\left[\frac{1}{p} e^{-2\sqrt{\beta p}}\right] = \text{erf } \sqrt{\frac{\beta}{x}}$$

This inverse has been listed.⁸

Since a function which is expressed as a definite integral with a variable in the limits is a function only of the limits, then

$$I(x-a) = \int_0^{x-a} \sqrt{\frac{\beta}{\pi}} r^{-3/2} e^{-\beta/r} dr = \text{erf } \sqrt{\frac{\beta}{x-a}}$$

APPENDIX II

The normalization of (9), (10), and (13) to obtain (19), (21), and (22) is performed as follows. Consider first (9) and (10).

$$g(x+Tl) = \sqrt{\frac{\beta}{\pi}} x^{-3/2} e^{-\beta/x} \quad x \geq 0 \quad (9)$$

$$h(x+Tl) = \text{erf } \sqrt{\frac{\beta}{x}} \quad x \geq 0. \quad (10)$$

⁸ These expressions are given in complex variable form as Laplace transforms of the time functions.

⁹ C. R. Wylie, "Advanced Engineering Mathematics," McGraw-Hill Book Co., Inc., New York, N. Y.; 1951.

Let $x = \beta\rho$

$$g(\beta\rho + Tl) = \sqrt{\frac{\beta}{\pi}} (\beta\rho)^{-3/2} e^{-1/\rho} = \frac{\rho^{-3/2} e^{-1/\rho}}{\beta\sqrt{\pi}}$$

$$h(\beta\rho + Tl) = \text{cerf } \sqrt{\frac{1}{\rho}}.$$

As written above, the functions g and h are still plotted on the x time scale although x does not appear in the expressions. Changing the time scale to the dimensionless ρ (β has the dimensions of time) new functions $g_0(\rho)$ and $h_0(\rho)$ are obtained.

$$g_0(\rho) = \frac{\rho^{-3/2} e^{-1/\rho}}{\beta\sqrt{\pi}} \quad \rho \geq 0 \quad (19)$$

$$h_0(\rho) = \text{cerf } \sqrt{\frac{1}{\rho}} \quad \rho \geq 0. \quad (21)$$

For plotting, (19) is changed to

$$\beta g_0(\rho) = \frac{\rho^{-3/2} e^{-1/\rho}}{\sqrt{\pi}} \quad \rho \geq 0. \quad (20)$$

Note that in the transformation the shape of the functions were preserved, and in order to plot the functions $g(x+Tl)$ and $h(x+Tl)$ for any particular physical case the horizontal scale is altered by the factor β for that case. In (20) the vertical scale must also be altered by the factor β .

Considering (13), more care must be used in the change of time scales.

$$f(x+Tl) = \frac{1}{a} \int_{x-a}^x \text{cerf } \sqrt{\frac{\beta}{\tau}} d\tau \quad x \geq 0. \quad (13)$$

In the above, change the scale on the dummy variable

by the substitution $t = \beta\rho$. A corresponding change of scale must be made in the limits by dividing by β

$$f(x+Tl) = \frac{1}{a} \int_{(x-a)/\beta}^{x/\beta} \text{cerf } \sqrt{\frac{1}{\rho}} \beta d\rho.$$

The function is now set up for normalization by letting $x = \beta\rho$ and plotting the resulting function $f_0(\rho) \equiv f(\beta\rho + Tl)$ vs ρ

$$f_0(\rho) = f(\beta\rho + Tl) = \frac{\beta}{a} \int_{(\beta\rho-a)/\beta}^{\beta\rho/\beta} \text{cerf } \sqrt{\frac{1}{\rho}} d\rho.$$

Finally, letting $a' = a/\beta$,

$$f_0(\rho) = \frac{1}{a'} \int_{\rho-a'}^{\rho} \text{cerf } \sqrt{\frac{1}{\rho}} d\rho \quad \rho \geq 0. \quad (22)$$

ACKNOWLEDGMENT

The cooperation of the Naval Research Laboratory, specifically, the group under G. F. Wall, was vital in securing the experimental data. The experiment was set up and the photographs were taken by them. Also, the same analytical conclusions concerning the role of skin effect in coaxial cables have been reached independently by R. V. Talbot, F. E. Huggin, and C. B. Dobbie of NRL.

Others who have contributed significant amounts are G. W. Kimball of the Department of Defense, who supplied the rigorous mathematical steps to verify (22) which had originally been deduced by physical reasoning and E. D. Reilly of the Department of Defense who did the computer programming for the calculation of the curves in Fig. 3, 4, and 5. Drafting for the figures was done by Paul Peters and Cletus Isbell of the University of Kansas.

APPENDIX VIII

CONTENTS

Abstract	1
I. Introduction	1
II. Statement of the Problem	2
III. Operation of the Sampling Oscilloscope	4
IV. Recording of Waveforms having low repetition rates . .	6
V. Recording of Waveforms having high repetition rates .	21

FIGURES

NUMBER	PAGE
1 Block Diagram Model 222 Sampling Unit	5
2 Block Diagram of Test Setup for Graphically Recording Low Repetition Rate Signals	7
3 Photographic record of Pulse Rise Times for varying time scales	8-9
4 Rise Time of SKL Pulse	10-13
5 Photographic record of Pulse Fall Times for varying time scales	14-15
6 Fall Time of SKL Pulse	16-19
7 Photographic Record of 10 mc and 300 mc sine waves	22
8a 10 mc Sine Wave	23
b 300 mc Sine Wave	24

USE OF AN X-Y RECORDER WITH A SAMPLING OSCILLOSCOPE

Abstract:

A method has been described for using an X-Y recorder to record waveforms having both low and high repetition rates. Pictorial and graphical recordings were made and limiting sweep rates established for accurate graphical recording of waveforms having repetition rates in the order of 100 cps (assuming the use of the specified equipment). It was also shown experimentally that the inertia of the X-Y recorder was sufficient to integrate waveforms having a repetition rate of over 10 megacycles per second. Finally a 300 megacycle sine wave is recorded and a statement is made about observation of waveforms having higher repetition rates.

I. Introduction:

During a recent investigation into the transient properties of strip transmission line, it became desirable to use an X-Y recorder to record graphically a fast rise time pulse before and after passing through a length of strip transmission line. Considerable difficulty was encountered in actually implementing the recording of these pulses. Since interest has been shown in the solution of this problem it was felt that the problem and its solution should be reported.

II Statement of the Problem:

Any X-Y recorder has two independent inputs, one for the X axis, the other for the Y axis. If it is desired to plot voltage vs. time, a linear sawtooth is placed on the X axis and the voltage of interest is placed on the Y axis. These voltages must of course be of sufficient amplitude to drive the vertical and horizontal amplifiers of the recorder and must vary slowly enough so that the recorder can follow them. The recorder used was a Mosely Autograph X-Y Recorder, which has a basic sensitivity of 5 millivolts for full scale deflection both on the X and Y axis. Through the use of step attenuators, this sensitivity can be reduced to 100 volts for full scale deflection. Both X and Y axes require a minimum of one second for full scale travel. These figures are felt to be representative of most commercially available X-Y recorders.

Now that the signal requirements have been specified, let us see how these requirements were met. The linear sawtooth required for the X axis deflection was easily obtained from the Tektronix 545 Oscilloscope by setting the sweep on 100 milliseconds per centimeter or slower and taking the output from the "Sawtooth - Main Sweep" terminals. This voltage has a peak value of 150 volts whereas the maximum voltage the recorder will take is 100 volts. This problem was easily solved through the use of a one megohm potentiometer as a voltage divider. The axis zero is set through the use of a zeroing control on the recorder and the maximum deflection was set by varying the setting of the one megohm potentiometer.

The voltage requirements for the Y axis were not so easily met as those of the X axis. The principle waveform of interest was a pulse having a rise time of 0.5 nanosecond and a pulse length of 50 nanoseconds. Clearly a recorder requiring a full second for full scale deflection cannot respond to a rise time of 0.5 nanosecond! How then are we to meet the requirements of the recorder for the Y axis deflection? The answer to this problem lies in the use of an oscilloscope sampling attachment, whose operation will be described below.

The output of the sampling attachment is a series of negative pulses which are amplitude modulated to correspond to the shape of the waveform under observation. The sweeping rate is set by the attachment and not by the sawtooth from the oscilloscope. Sweep speed is a function of the slope of the sawtooth but not of the repetition rate. To provide a slowly varying voltage for the recorder input, the peaks of the negative pulses must be integrated. If the number of pulses per unit time is great enough, the inertia of the recorder will provide the desired integration. Since there is one pulse for each cycle of the input waveform, a high pulse rate depends on a high repetition rate. For low repetition rates, an integrating network is required. Fast rise time pulses such as the output from the SKL Pulse Generator have low repetition rates of the order of 100 cycles per second. For such pulses an integrating network will be required. It will be shown below that since the slowest sweep rate of the sampling unit used (Lumatron Model 222) was 100 nanoseconds for full scale deflection (assuming that it is desirable to see at least one cycle of the waveform), a minimum repetition rate of 10 megacycles is of

interest. For this frequency the inertia of the recorder will integrate the negative pulses quite satisfactorily.

III Operation of the Sampling Oscilloscope:

The sampling attachment used was the Lumatron Model 222. The principles of operation described below as well as Fig. 1 are taken from the specification sheet for this unit. "The sampling unit produces a very narrow strobe pulse which samples the signal wave form under investigation. The sum of the sampling pulse and the instantaneous level of the signal at the moment of sampling is applied to the sampling diode. The output of the sampling diode is a narrow pulse, which varies in amplitude in proportion to the signal at the instant of sampling. This voltage is amplified in a linear amplifier of only moderate band width, stretched and applied to the vertical plates of the oscilloscope. Therefore, vertical deflection at any instant is proportional the amplitude of signal at the instant of the strobing. In order to take successive samples of the signal, the moment of sampling is advanced progressively, relative to the start of the signal. This is done by a fast ramp which is started by a trigger signal. When the ramp reaches a preset voltage, it fires an avalanche transistor. The instant of firing is delayed by a slowly increasing voltage on which the fast ramp rides. The slow ramp provides reset of the sweep to zero, so that the sampling process may be repeated. The slow ramp is derived from the oscilloscope sweep sawtooth output.

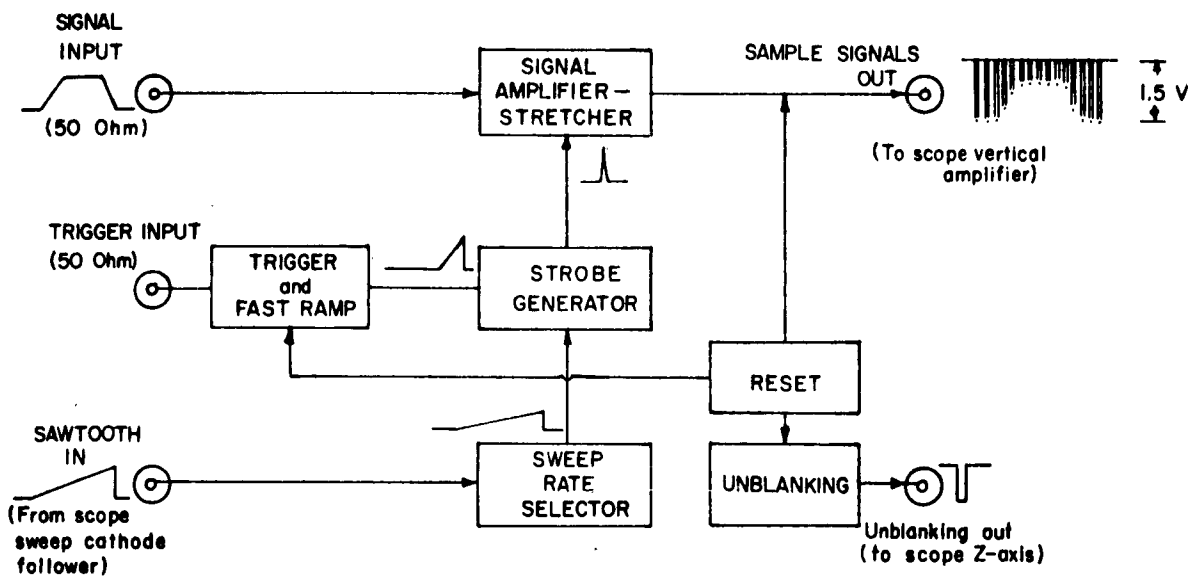


Fig. I. BLOCK DIAGRAM MODEL 222 SAMPLING UNIT

It should be noted that the apparent sweep speed of the sampling oscilloscope is only a function of the slope of the ramp, and not of the actual sweep speed of the oscilloscope.

The Model 22ST sync trigger circuit locks to very high rep rate signal pulses to provide a 50 kc output to trigger the sampling unit".

IV Recording of Waveforms having low repetition rates:

As mentioned above, fast rise time pulses normally have low repetition rates. The repetition rate of the Model 305 SKL Pulse Generator for instance is continuously variable up to about 150 cps. Since one negative amplitude modulated spike is produced for each cycle of the input waveform, it can be seen that even at slow sweep speeds, the number of spikes per sweep will be relatively small. Since a slowly varying voltage is required to drive the Y axis of the X-Y recorder, it is necessary to integrate these negative spikes.

Of course an integrating network could be built to do the job, but it would certainly be more attractive to be able to use a commercially available instrument. Such an instrument is a peak reading voltmeter. A peak reading volt meter incorporates circuitry that responds quite rapidly to fast rising positive or negative pulses but whose response decays slowly in order to hold the peak value of the waveform between pulses. This rise and fall time of the circuitry will vary with the meter used. For purposes of this work a Ballantine Model 305 peak reading voltmeter was used and the minimum rise and fall times were determined experimentally. The test setup is shown as Figure 2.

Using the experimental setup shown in Figure 2, the rise and fall times of an output pulse from the SKL Pulse generator were observed. The results were recorded both photographically and graphically for comparison purposes and are shown as Figures 3-6. Several comments

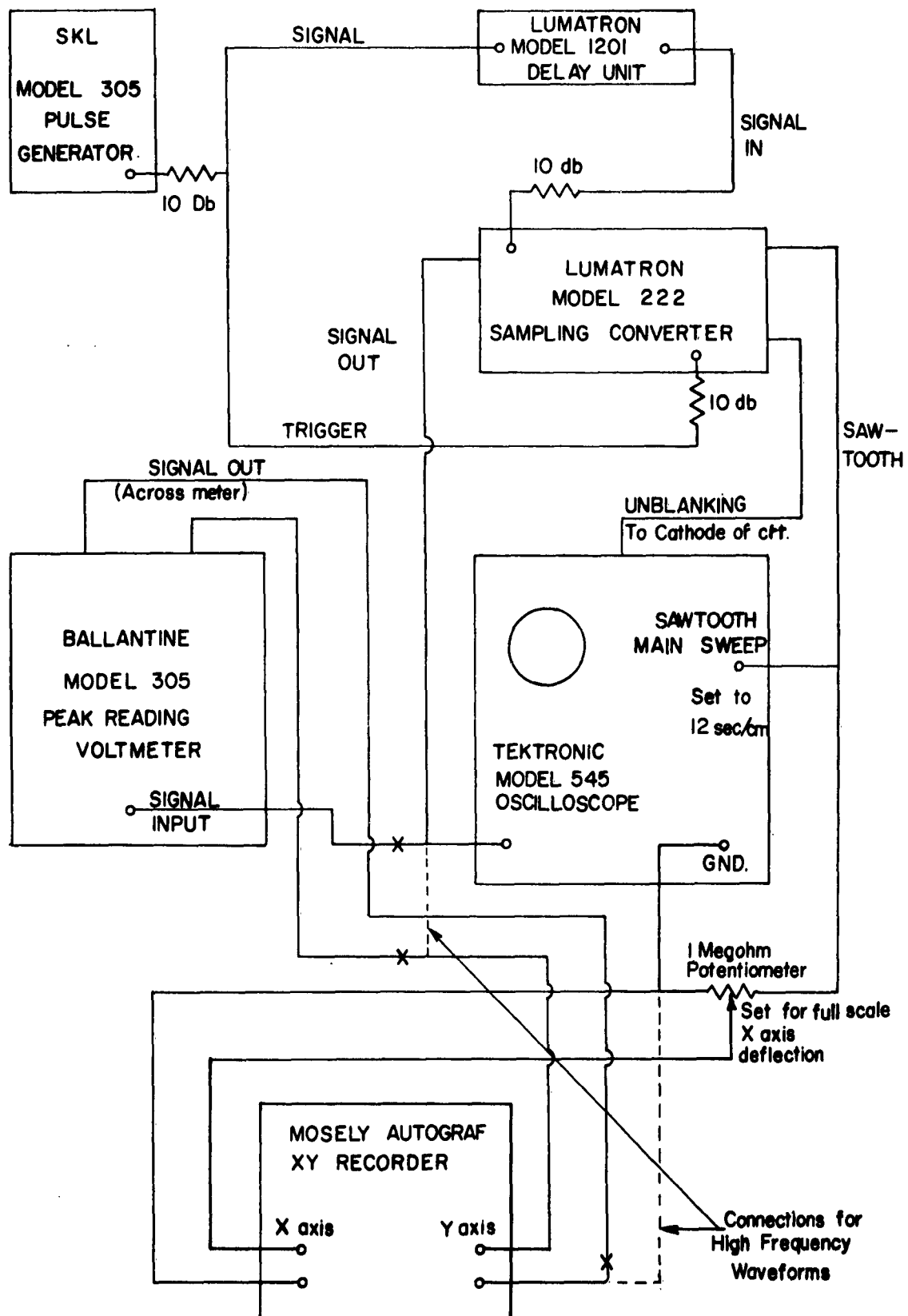
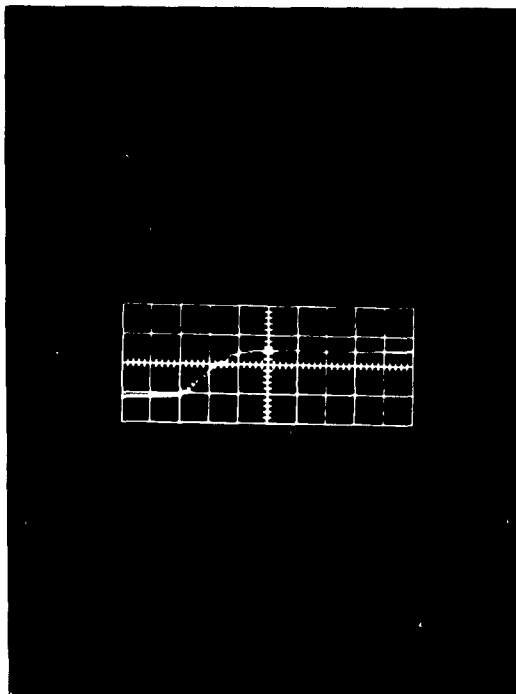
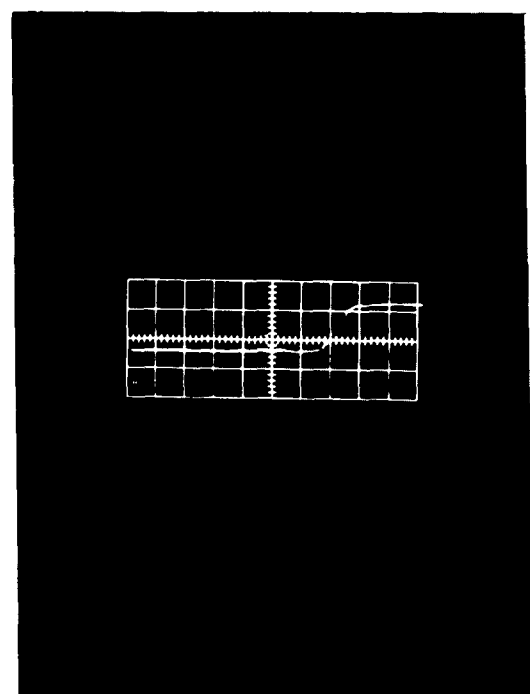


Fig. 2. BLOCK DIAGRAM OF TEST SETUP FOR GRAPHICALLY RECORDING LOW REPETITION RATE SIGNALS



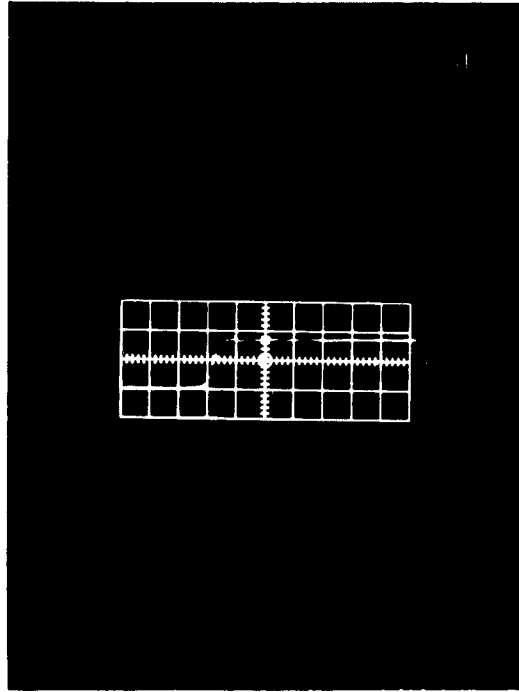
a. Vertical: 1v/cm
Horizontal: 0.5×10^{-9} sec/cm



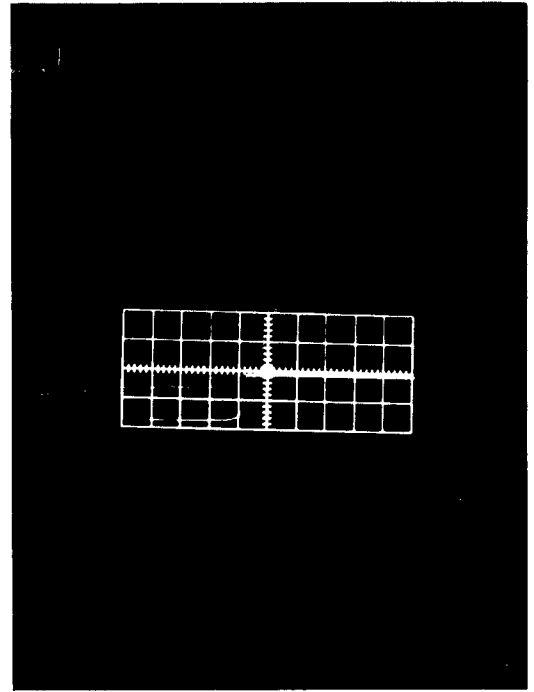
b. Vertical: 1v/cm
Horizontal: 0.5×10^{-9} sec/cm

FIGURE 3

Photographic record of Pulse Rise Times
for varying time scales



c. Vertical: $1v/cm$
Horizontal: $2 \times 10^{-9} \text{ sec}/\text{cm}$



d. Vertical: $2v/cm$
Horizontal: $5 \times 10^{-9} \text{ sec}/\text{cm}$

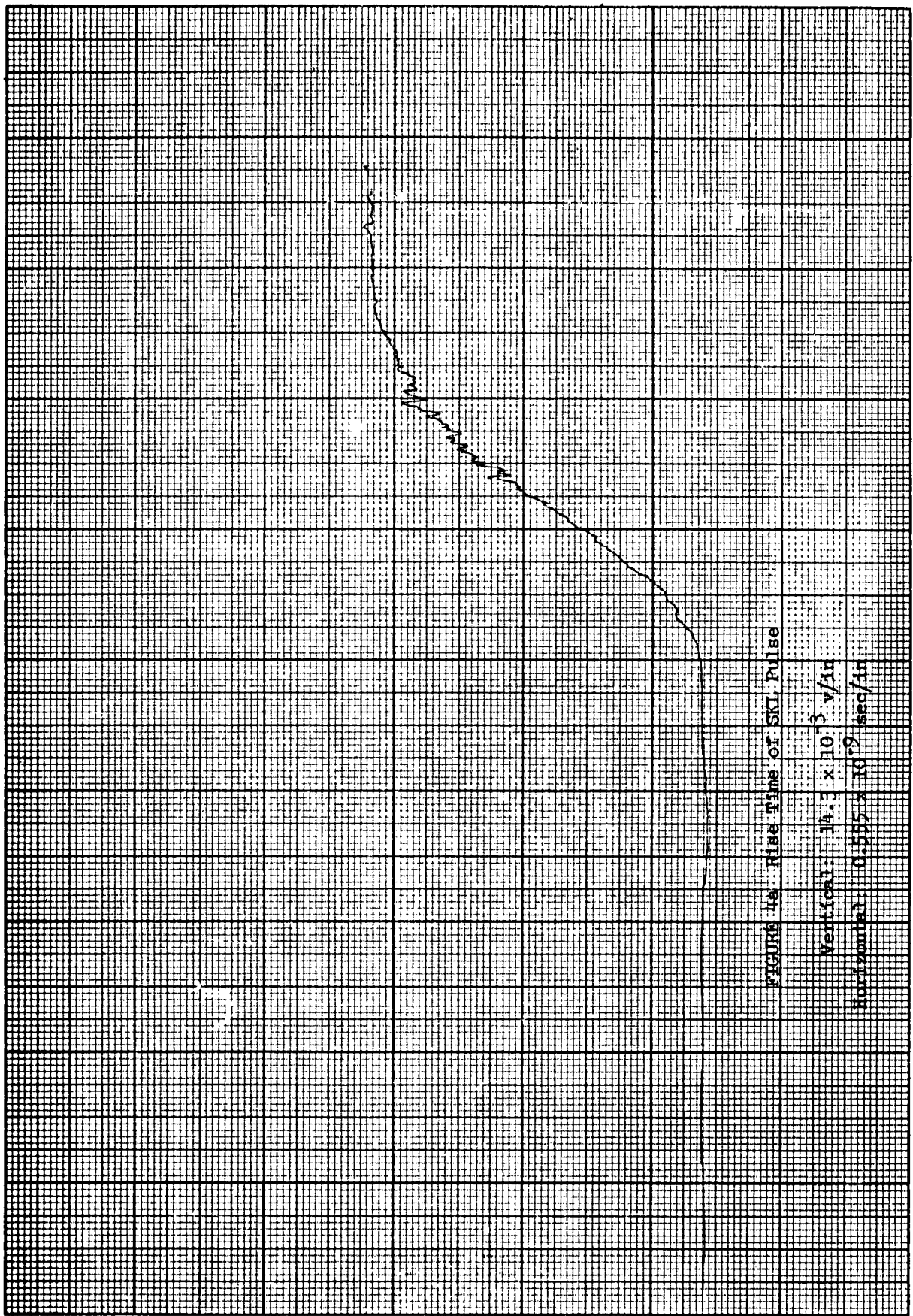
FIGURE 3

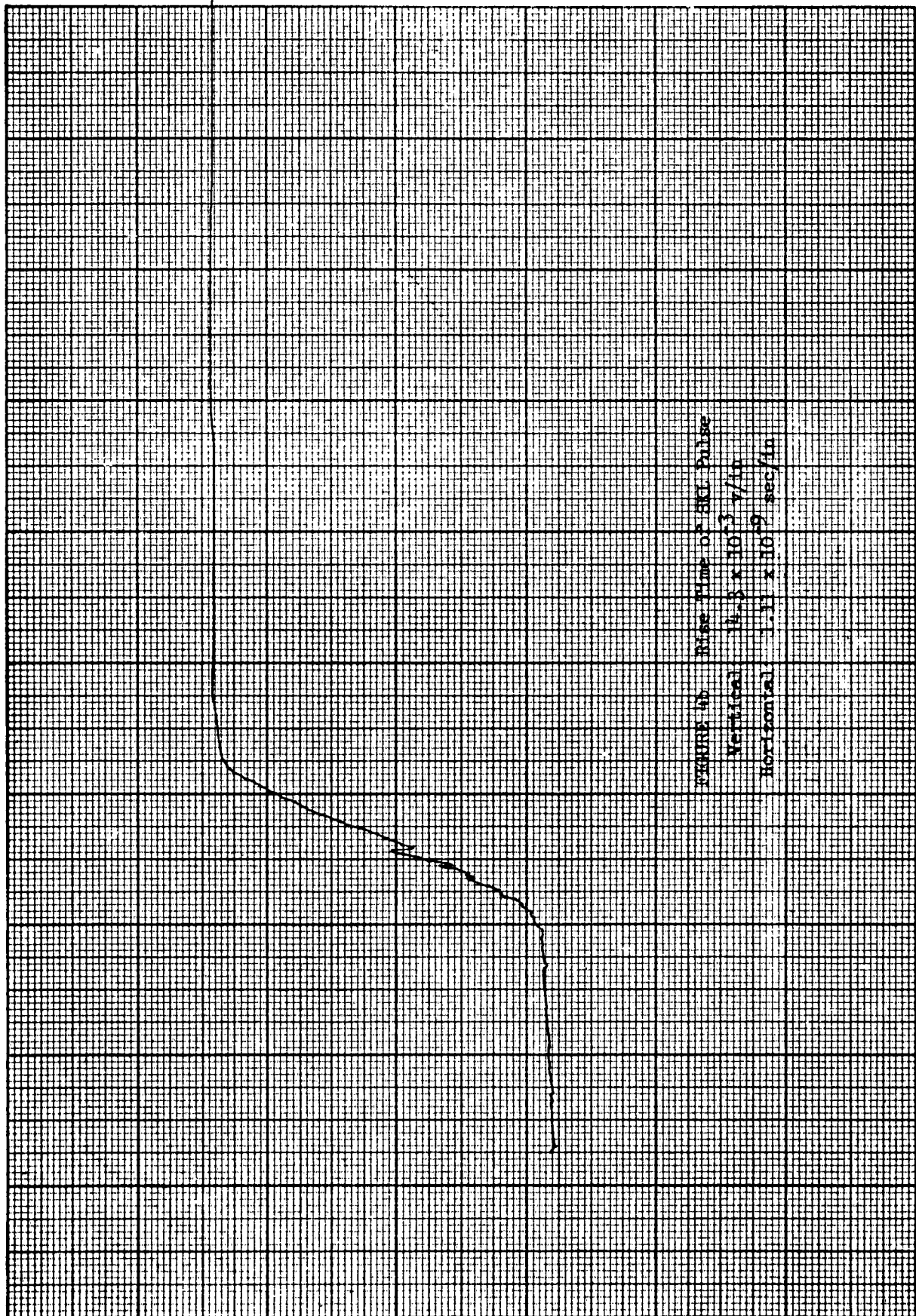
Photographic record of Pulse Rise Times
for varying time scales

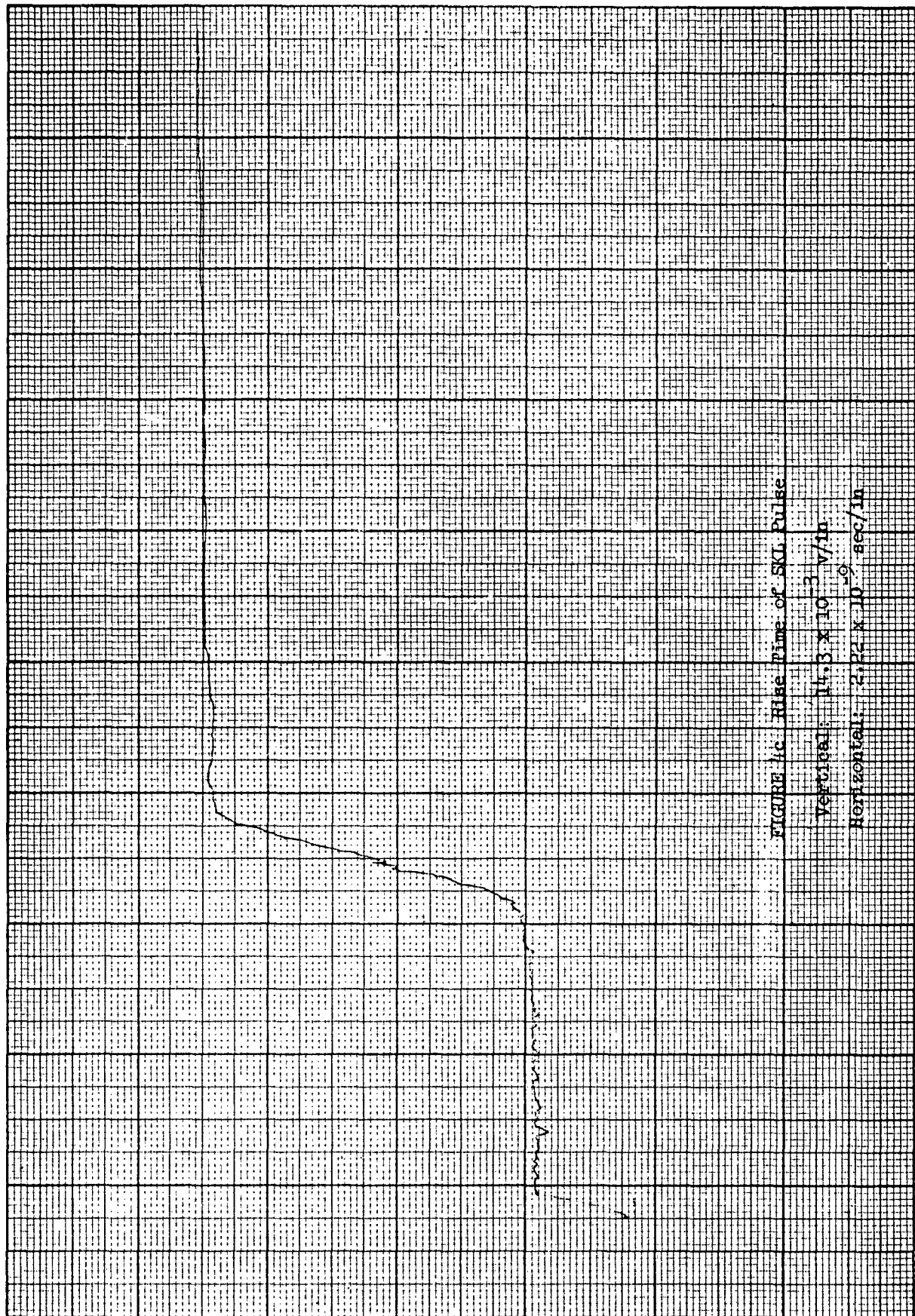
FIGURE 4a. Rise Time of SK1 Pulse

Vertical: $1.4 \times 10^{-3} \text{ V/m}$

Horizontal: $0.555 \times 10^{-9} \text{ sec/15 mm}$







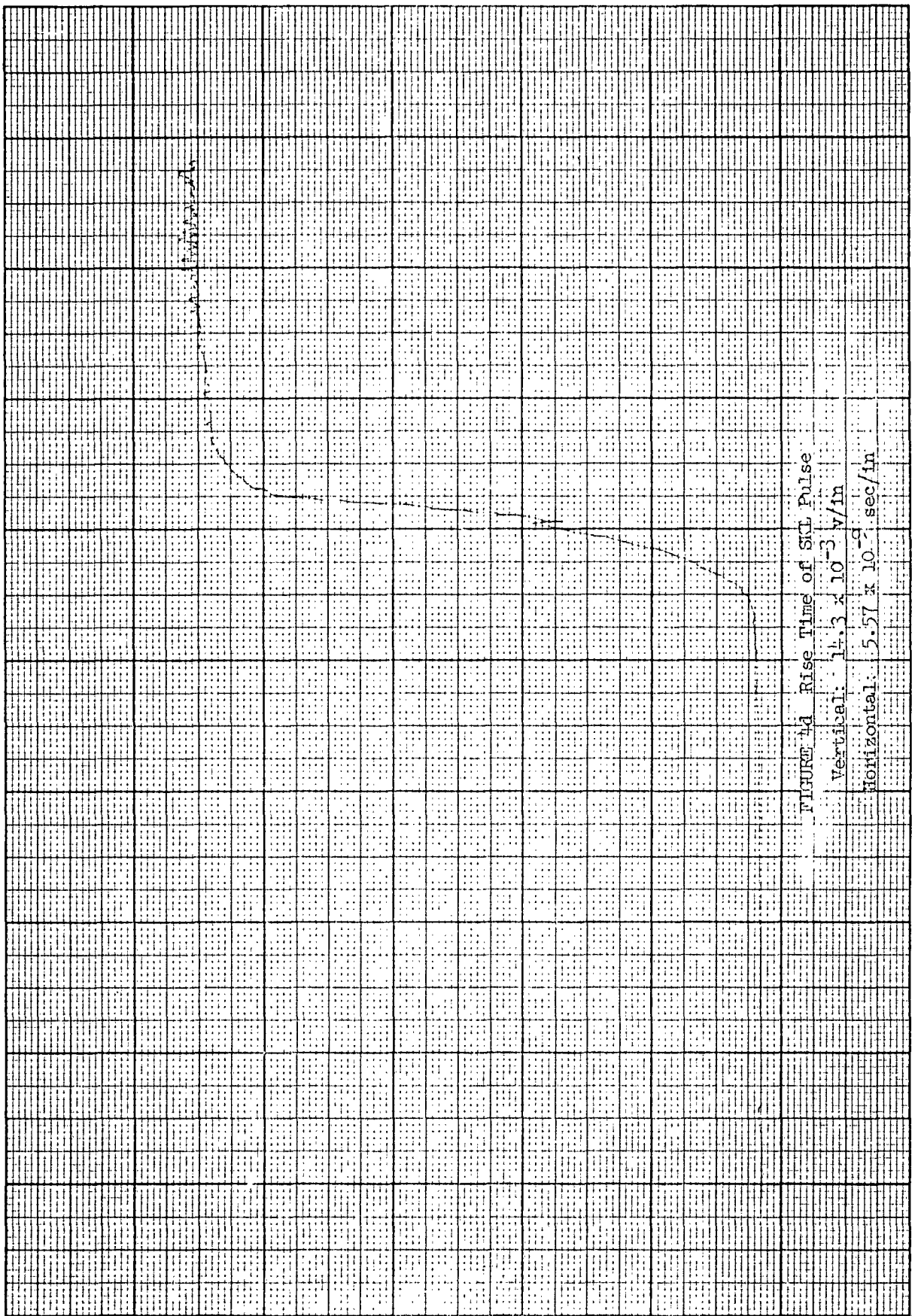
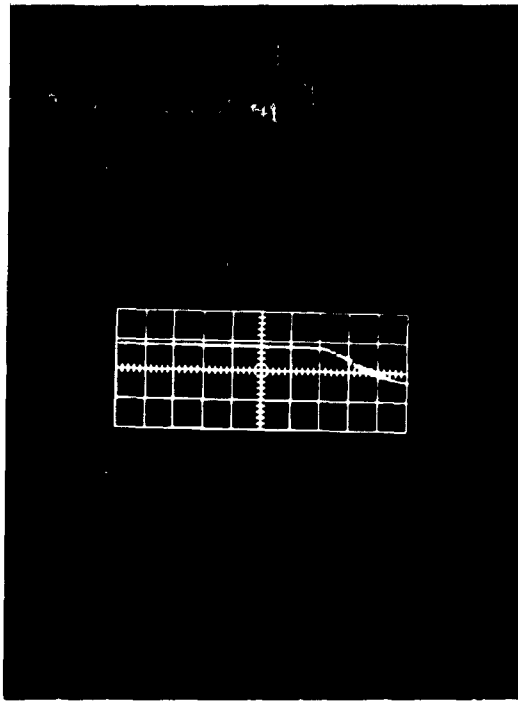


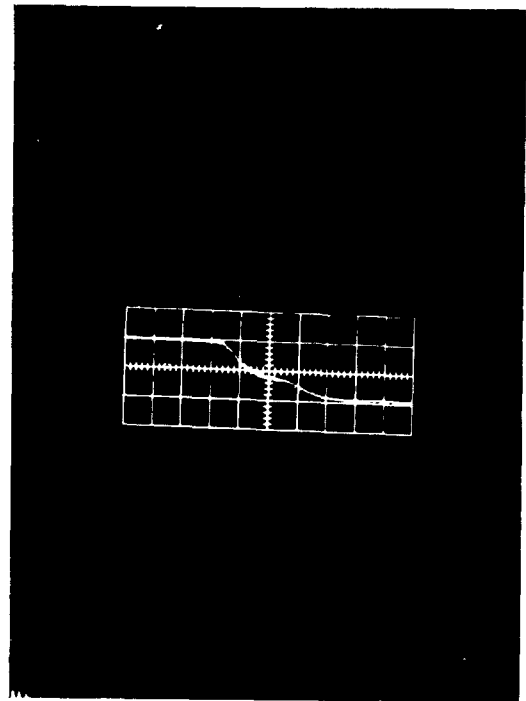
FIGURE 4a Rise Time of SCR Pulse

Vertical: 1.4×10^{-3} v/in

Horizontal: 5.57×10^{-9} sec/in



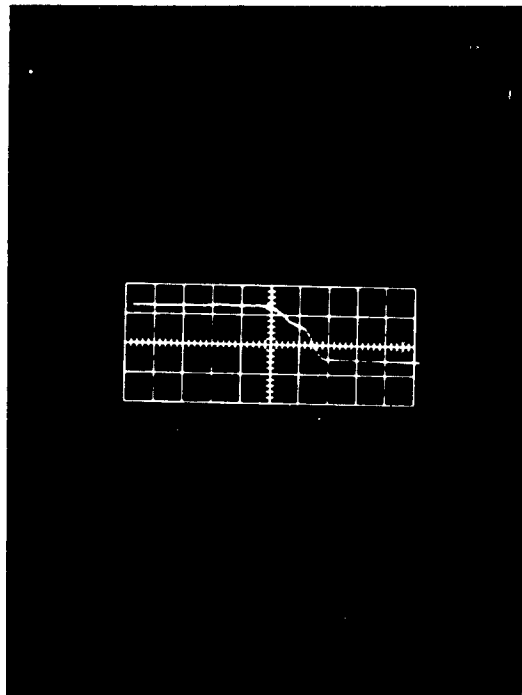
a. Vertical: 1v/cm
Horizontal: 0.5×10^{-9} sec/cm



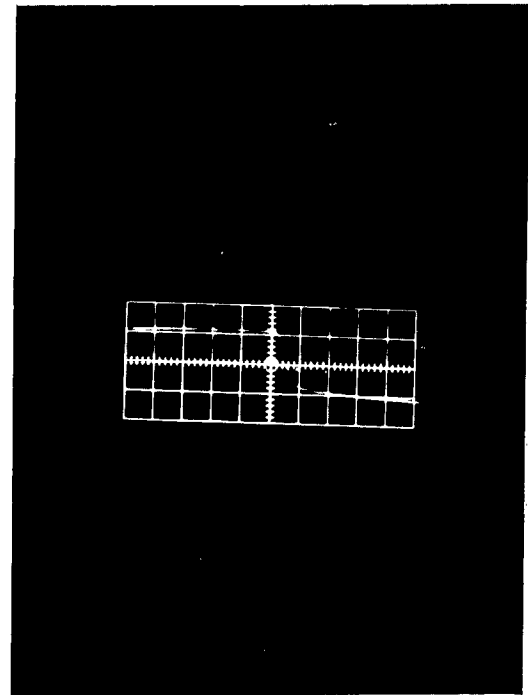
b. Vertical: 1v/cm
Horizontal: 1×10^{-9} sec/cm

FIGURE 5

Photographic record of Pulse Fall Times
for varying time scales



c. Vertical: 1v/cm
Horizontal: 2×10^{-9} sec/cm



d. Vertical: 1v/cm
Horizontal: 5×10^{-9} sec/cm

FIGURE 5

Photographic record of Pulse Fall Times
for varying time scales

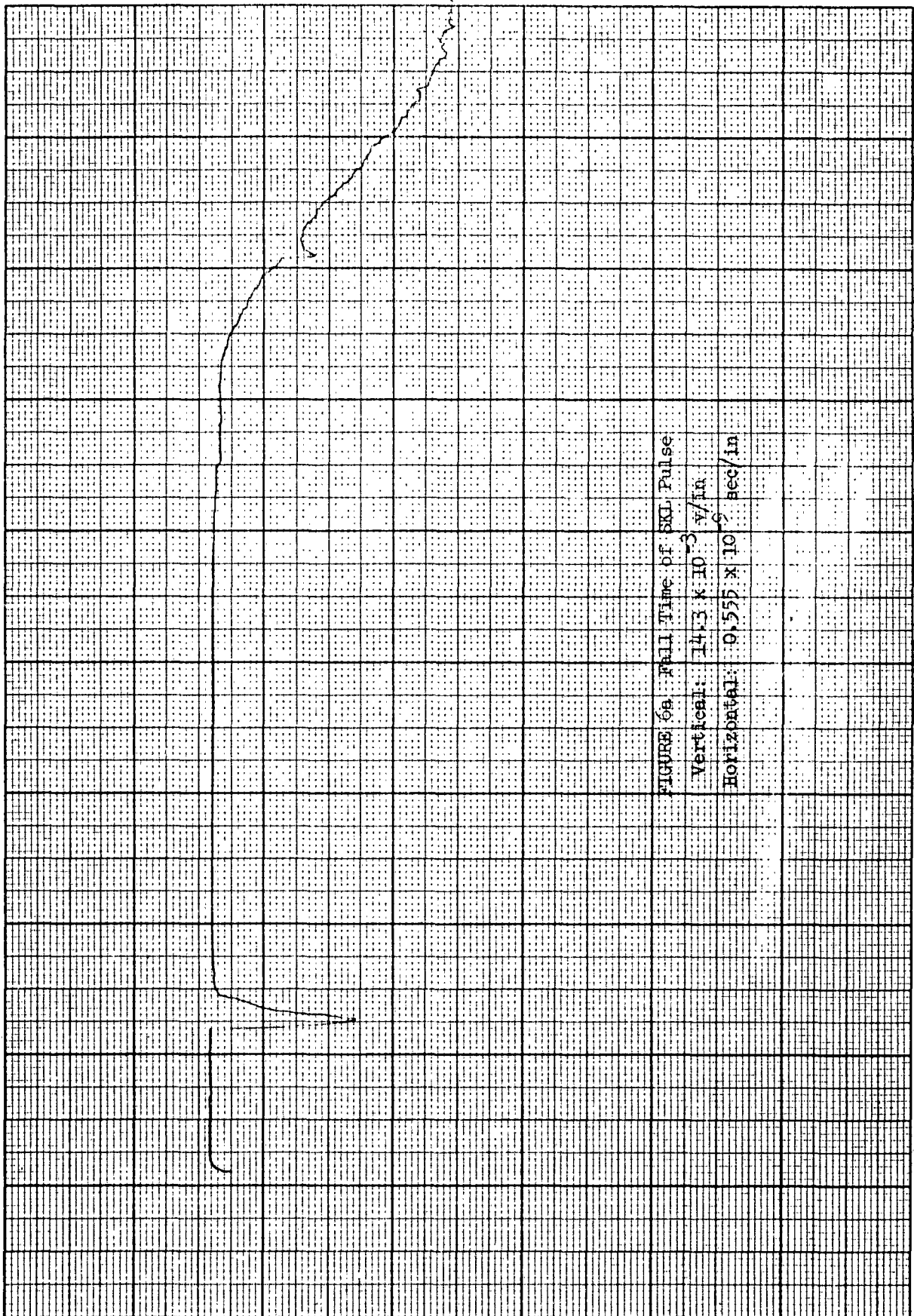
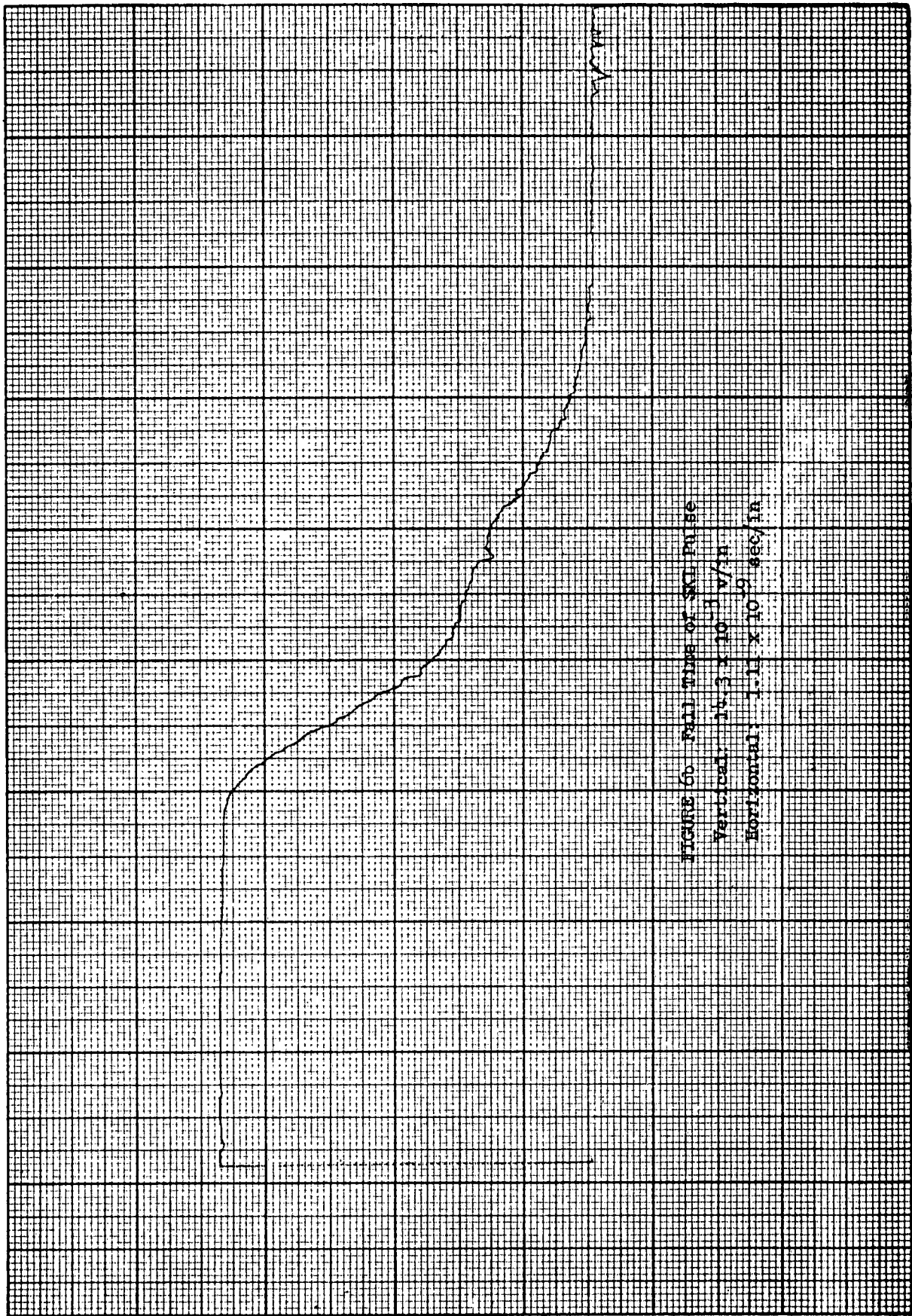
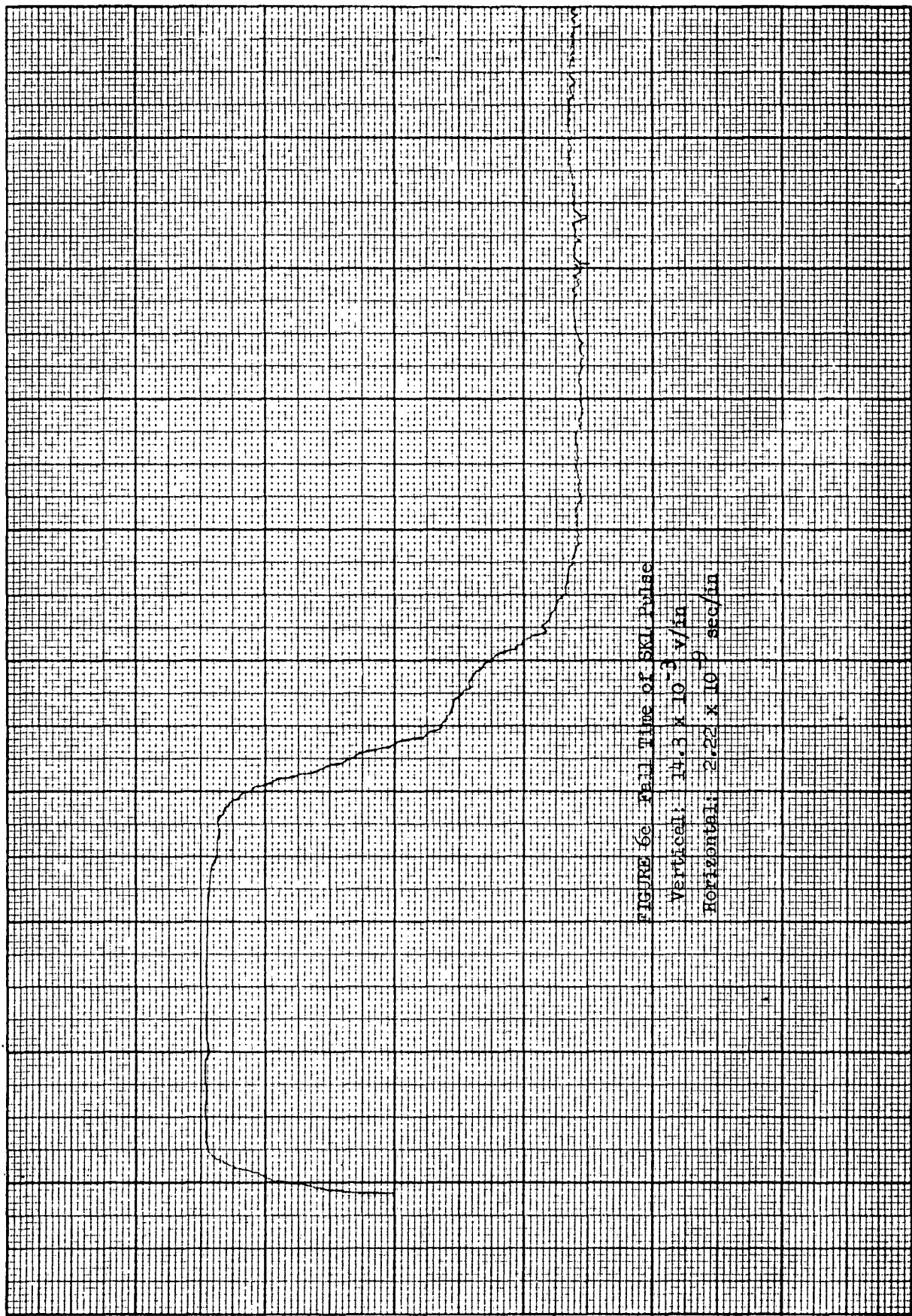
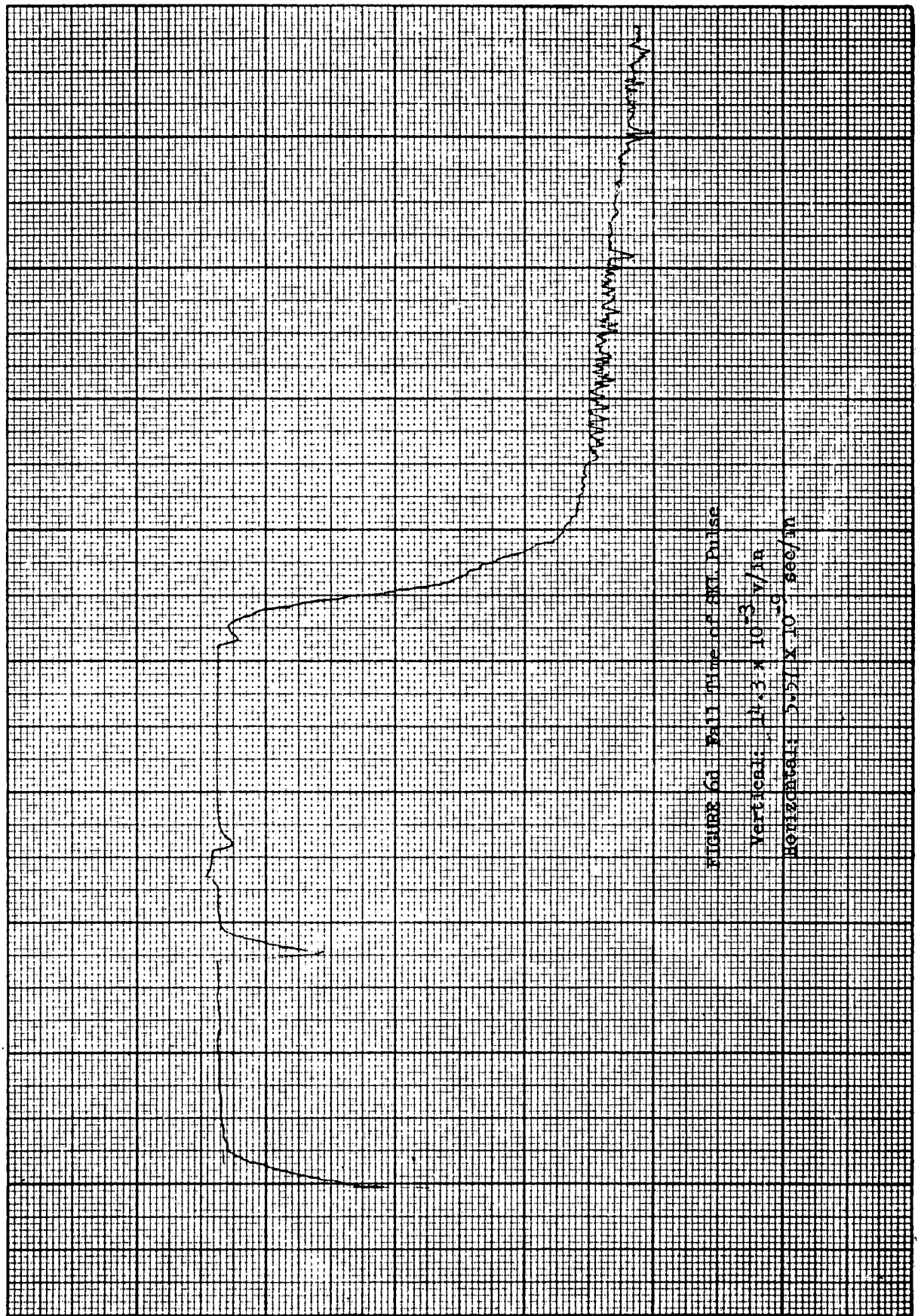


FIGURE 6a. Fall time of SCC profile
Vertical: $10^{-3} \times 10^{-3}$ sec/m
Horizontal: $10^{-3} \times 10^{-3}$ sec/m





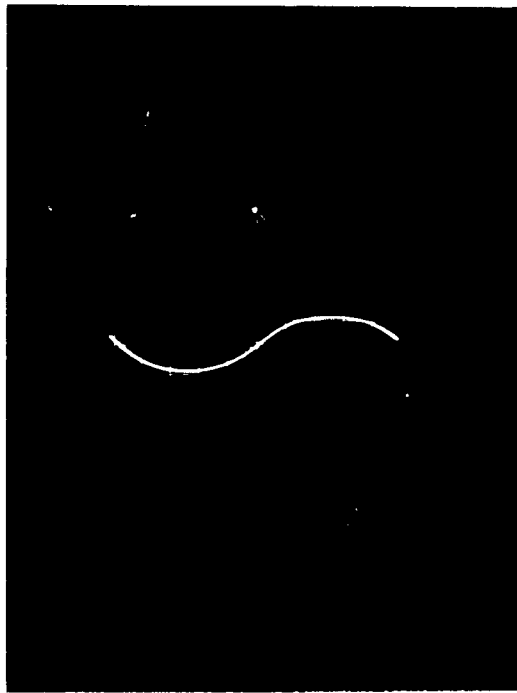


regarding the pictures and graphs should be made. First, the waveform as observed on the oscilloscope is usually thought of as a series of dots. The continuous trace shown in the pictures was produced by the 100 millisecond/cm sweep and taking a time exposure with the camera. For the graphic recording, a sweep of twelve seconds per centimeter was used to allow for the time constants of the peak reading voltmeter. Sweep calibration showed the sweep to actually take 170 seconds rather than the 120 seconds expected.

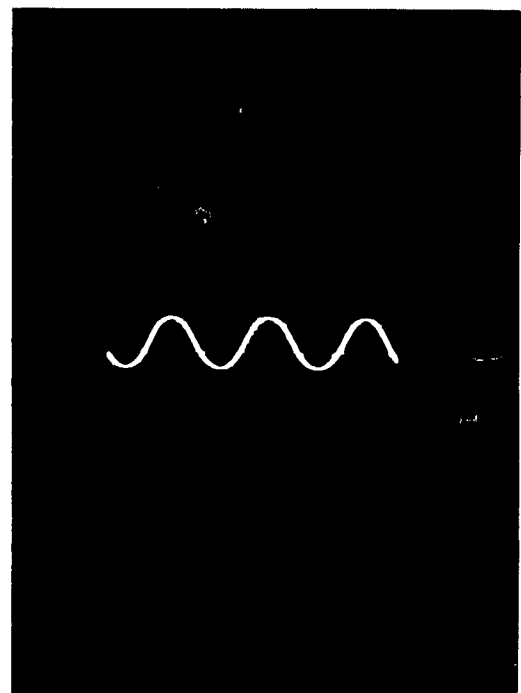
It was stated above that the peak reading voltmeter will follow quite well a voltage swinging from ground to a plus or minus value but it will not follow as well as voltage swinging from a plus or minus value to ground. The voltage swinging from ground to a negative value corresponds to the fall time of the SKL Pulse. Comparison of the fall times shown by the photographs and the graphs shows good correlation for all sweep rates. We may therefore conclude by a simple calculation that if 14 seconds are allowed for full scale vertical deflection, pulse fall time as shown by the recorder can be expected to agree with the value shown by the oscilloscope. If the pulse rise time is compared in a similar manner, it is found that disagreement between picture and graph rise times begins with Figures 5c and 6c. For this sweeping rate, the time constants of the peak reading voltmeter do not allow the recorder to follow the pulse rise time correctly. If the sweeping rate shown by Figure 5b and 6b is taken as the maximum allowable a simple calculation shows that 50 seconds should be allowed for full scale vertical deflection of the recorder in order to obtain agreement between oscilloscope and recorder.

V. Recording of Waveforms having High repetition rates:

As previously stated, for higher repetition rates, the inertia of the recorder serves to integrate the pulse without the use of the peak reading voltmeter. If it is desired to see at least one cycle of the waveform, then the lowest frequency of interest will be 10 megacycles since the slowest sweep rate, as determined by the sampling attachment, is 10 nanoseconds per centimeter. If the connections marked "X" in Figure 2 are broken and the dotted wiring inserted, the equipment will be set up for high frequency waveforms. Essentially all that is done is to by-pass the peak reading voltmeter. Figure 7 shows pictorial recordings of 10 and 300 megacycle sine waves while Figure 8 shows graphical recordings of the same two waves. Examination of these figures shows good correlation. Three hundred megacycles is the upper frequency limit of the Lumatron Sampling Attachment. It is felt that if some type of count down unit could be used, much higher frequencies could be recorded.



a. 10 megacycle sine wave
Vertical: 2v/cm
Horizontal: 10×10^{-9} sec/cm



b. 300 megacycle sine wave
Vertical: 2v/in
Horizontal: 1×10^{-9} sec/cm

FIGURE 7

Photographic Record
of 10 mc and 300 mc sine waves

FIGURE 8a 10-m Sine Wave
Vertical: 0.535 $\sqrt{1n}$
Horizontal: 5.57×10^{-9} sed/ln

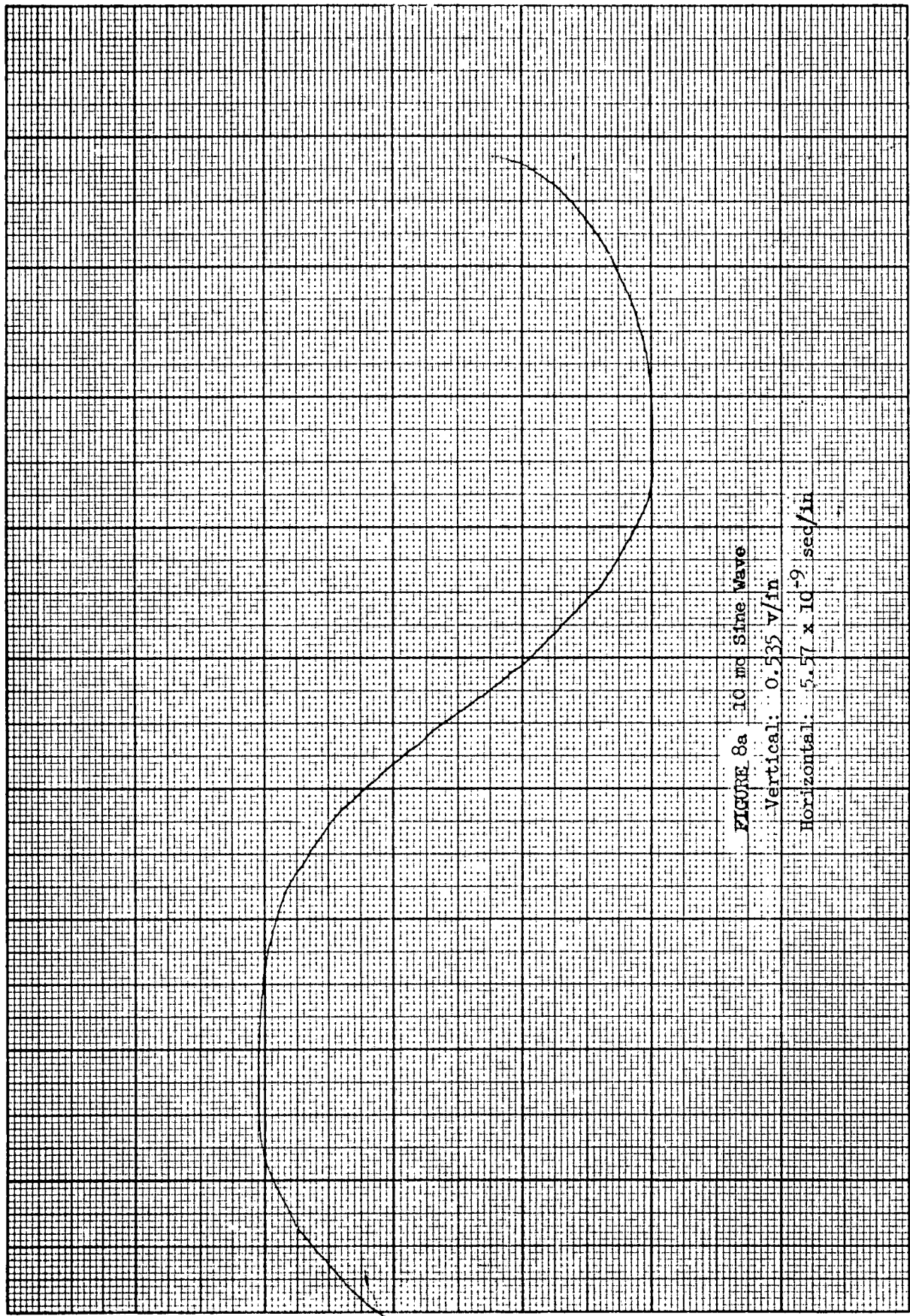
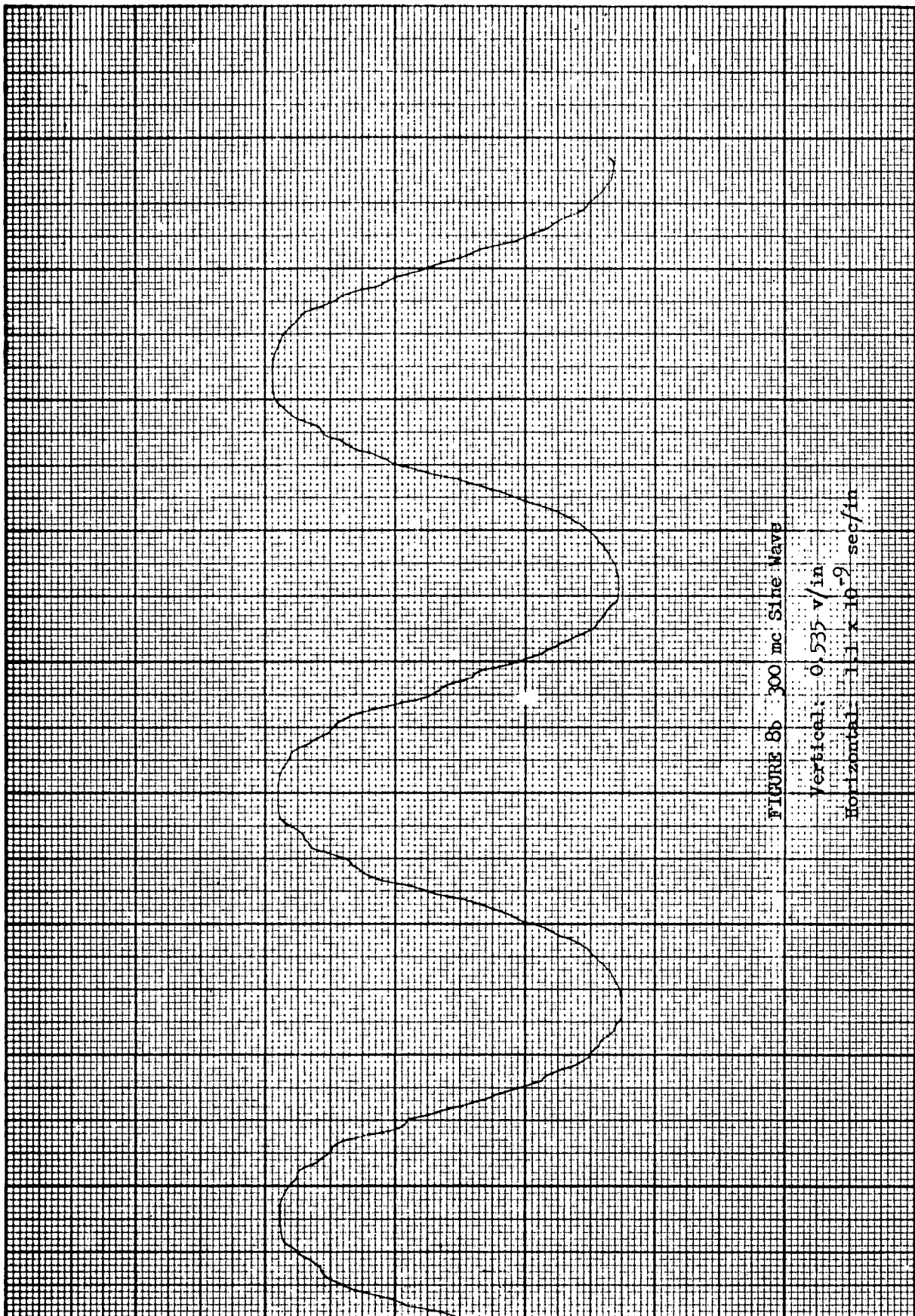


FIGURE 8b 300 mc Sine Wave

Vertical - 0.535 v/in
Horizontal - 1.1×10^{-9} sec/in



APPENDIX IX

APPENDIX IX

PROPERTIES OF MATERIALS, MEASUREMENT RESULTS,

CALCULATION OF LINE PARAMETERS

Nominal values for the Stripline delay lines are as follows:

<u>Item</u>	<u>Line A</u>	<u>Line B</u>
Dielectric Material	Glass-Teflon	Glass-Epoxy Resin
Dielectric Constant (meas.)	2.73	5.27
Dielectric Loss Tangent (adv.)	0.003	0.03
Dielectric Loss Tangent (calc.)	0.00256	0.0133
Ground Plane Spacing, b (meas.)	0.113 in.	0.116 in.
Copper Thickness, t (meas.)	0.003 in.	0.003 in.
Characteristic Impedance, R_o	50 ohms	50 ohms
Strip Width, w (calc.)	0.070 in.	0.035 in.
Length (calc. from spiral design)	7.40 m., 24.3 ft.	3.68 m., 12.1 ft.
Total Delay (calc.)	4.15×10^{-9} sec.	28.2×10^{-9} sec.
Delay/unit length, T (calc.)	5.59×10^{-9} sec.	7.65×10^{-9} sec.
Inductance/unit length, L_∞ (calc.)	279×10^{-9} h/m	382×10^{-9} h/m
Capacitance/unit length, C (calc.)	112×10^{-12} f/m	153×10^{-12} f/m
Value of the convergence factor, $K_1 \sqrt{2 \pi f_c L_\infty}$ at 10 Mc (For accuracy this should be $\ll 1$.)	2.18×10^{-2}	5.14×10^{-2}
α_c at 1 Kmc (calc. from meas.)	0.0716 db/ft.	0.232 db/ft.
α_c at 1 Kmc (calc. from curves)	0.113 db/ft.	0.185 db/ft.
β (calc. from meas.)	3.21×10^{-12} sec.	8.29×10^{-12} sec.
K_o (calc. from meas.)	5.25×10^{-11} sec.	1.88×10^{-10} sec.

ABSTRACT

A general review of matrix network analysis is considered first. Simplifications are made for the case where the networks involved are real, lossless and symmetrical. Theoretical equivalent circuits are derived using an approximate model of stripline, a stored power small aperture procedure and a Babinet Equivalence or duality procedure. Through the use of these procedures, the discontinuities can be identified with waveguide discontinuity expressive which are well established in the literature. Experimental verification was performed by building physical discontinuities and measuring them via the tangent relation method. In some cases measurements could be made directly; in others, it was necessary to measure a cascade of discontinuities and abstract data for a single discontinuity through matrix inversion procedures. Finally comparisons of theoretical and experimental data is made. In general, correlation is good within the specified range of validity.

TABLE OF CONTENTS

Chapter	Page
VIII Stripline Discontinuities	1
A. Introduction	1
B. General Discussion of Stripline Discontinuities	1
C. Microwave Network Theory	3
1. Microwave Network Representations	3
2. Transfer Matrix Formulation	4
a. Definition of the Matrix	4
b. Restrictions Imposed on the Transfer Matrix	5
c. Consequences of Restrictions	7
d. Cascaded Sections	8
(1) Repeated Multiplication of Cascaded Unit Cells, t	9
(2) Raising t to the n^{th} power . .	10
e. Inversion of Cascaded Matrix	12
f. Representations for the Unit Cell, t	15
g. Unit Cell, t	19
(1) Transformer Network Representation	19
(2) Symmetric Tee (Π)	22
(3) Transmission Line Parameters in Terms of Tee Parameters . .	24
(4) Length of Transmission Line Connected in Tandem	25

TABLE OF CONTENTS

	Page
h. Representation of the Unit Cell at Shifted Reference Planes	27
(1) Symmetric Shift at Both Reference Planes	27
(2) Shift of One Reference Plane by a Half Wavelength	28
i. Inversion of "N" Identical Unit Cells	30
D. Theoretical Determination of Equivalent Circuits for Stripline Discontinuities	31
1. The Approximate Model	31
a. Gap Discontinuity in the Center Strip	33
b. Slot Discontinuity in the Center Strip	35
2. Small Aperture Procedure	37
a. Round Hole in the Center Conductor .	41
b. Vertical Post in Stripline	42
3. Babinet Equivalence Procedure	44
a. Right Angle Bend	44
b. Sharp Bend of Any Angle	47
c. Uniform Circular Bend	48
d. Junction of a Straight and a Tapered Centered Conductor	48
e. 120° Junction	50
f. Sudden Change in Width	51
g. Symmetric Tee Junction	52

TABLE OF CONTENTS

	Page
4. Parameter d_{wgh} Reference Plane Shift in Stub Arm	55
5. Parameter n---Transformer Turns Ratio	59
6. Parameter d---Reference Plane Shift in Main Arm	59
7. The Abruptly Ended Center Conductor	60
 E. Experimental Verification of Discontinuity Equivalent Circuits	 63
1. Experimental Setup	63
a. Auxiliary Equipment	63
b. The Measurement Apparatus	64
2. Measurement Procedure Based on the Tangent Network Relations	68
3. Theoretical Relations for Determining Discontinuity Equivalent Circuits from D_o , S_o and γ	75
4. Gap and Slot in the Center Conductor . .	78
5. Round Hole in the Center Conductor . . .	82
6. Abruptly Ended Center Conductor	82
7. Relationship Between Series Reactance Network and Tangent Network	82
8. Step Change in Width of the Center Conductor	87

TABLE OF CONTENTS

	Page
9. Sharp Angle Bends in the Center Conductor	89
a. Right Angle Bends	91
b. Sharp Bend of Any Angle ($\theta \neq 90^\circ$)	94
F. Conclusions	114
Bibliography	116
Appendix XI	117
Appendix XII	123
Appendix XIII	125

LIST OF FIGURES

Figure	Page
8-1 Transfer Coefficient Matrix Representation of a Two-Port Network	5
8-2 Center Line of Symmetry for Two Cascaded Sections	9
8-3 Model of a Lossless Transmission Line	17
8-4 Model of a Pure Shunt Susceptance	17
8-5 Model of a Pure Series Reactance	18
8-6 Model of a Lossless Transformer	18
8-7 Arbitrary Lossless Transformer Network	19
8-8 Tangent Relation Network	21
8-9 Symmetric Tee Network	23
8-10 Symmetric Pi Network	23
8-11 Determination of Stripline Characteristic Impedance	32
8-12 Approximate Model of Stripline	33
8-13 Gap in Inner Conductor of Stripline	34
8-14 Centerline Representations for a Gap in the Center Conductor of Stripline	34
8-15 Slot in Center Conductor (a) Physical Structure . .	36
8-16 Functions Employed in Slot Formulas	38
8-17 Functions Employed in Slot Formulas	39
8-18 Centerline Representation of a Round Hole in the Center Conductor of Stripline	41

Figure	Page
8-19 Centerline Representation for a Round Centered Conducting Vertical Post in stripline	43
8-20 The stripline Approximate Model and Its Babinet Equivalent	44
8-21 Approximate Model of a Right Angle Bend in stripline	45
8-22 Babinet Equivalent of a Right Angle Bend and its Equivalent Circuit	45
8-23 A Right Angle Bend in stripline and its Equivalent Circuit	46
8-24 Equivalent Circuit for a Sharp Bend of Any Angle in stripline	47
8-25 Equivalent Circuit for a Uniform Circular Bend . .	48
8-26 Equivalent Circuit for the Junction of a Straight and a Tapered Center Conductor	49
8-27 Equivalent Circuit for a 120° Y Junction in the Center Conductor	50
8-28 Equivalent Circuit for a Sudden Change in Center Strip Width	52
8-29 Symmetric Tee Junction	53
8-29a Recommended Equivalent Circuit for stripline Tee Junction	55
8-29b Location of Terminal Plane T_1' for Open E-Plane T	56
8-29c Transformer Ratio for Open E-Plane T at Terminals T_1, T_1'	57
8-29d Comparison Between Available Experimental Data and Theory for Parameter d, the Reference Plane Shift in the Main Arms	58

Figure		Page
8-29e	Comparison Between Available Experimental Data and a Semi-Empirical Procedure for B_s , the Susceptance Element	61
8-29f	Abruptly Ended Center Conductor	62
8-30	Block Diagram of Measurement Equipment	65
8-31	Measurement Apparatus, Sketch of Front View	66
8-32	Tangent Relation Network	69
8-33	Procedure for Choosing Reference Planes in the Two Regions, (a) the network is perfectly terminated, (b) region II is shorted.	69
8-34	Distribution of Electric Field on the Two Sides of the Coupling Network due to the Shorting Plunger in Region II.	71
8-35	$D + S$ vs. S Curve	72
8-36	First Error Curve	74
8-37	Final Error Curve	74
8-38	Typical Data Curve and Associated Residual Scatter	76
8-39	Generalized Equivalent Pi Network	77
8-40	Circuit Parameters of Slots and Gaps	79
8-41	Circuit Parameters of Slots and Gaps	80
8-42	Normalized Susceptance of Hole in 50-Ohm Strip Transmission Line (B_a/Y_o)	83
8-43	Normalized Susceptance of Hole in 50-Ohm Transmission Line (B_b/Y_o)	84
8-44	Location of Equivalent Open Circuit for Abruptly-Ended Center Conductor	85

Figure		Page
8-45	Tangent and Series Reactance Networks	86
8-46	Sudden Change in Width of the Center Strip . . .	87
8-47	Step in Center Conductor	90
8-48	Right Angle Bend in Center Conductor	91
8-49a	Reactance Tee Network Parameters for Right Angle Bends	95
8-49b	Reactance Tee Network Parameters for Right Angle Bends	96
8-50a	Tangent Network Parameters for Right Angle Bends	97
8-50b	Tangent Network Parameters for Right Angle Bends	98
8-51a	Four-Cornered Sharp Angle Bend in the Center Conductor	99
8-51b	Distances to be Measured for Four Cornered Bend Measurement ($\theta \pm 90^\circ$)	100
8-51c	Definition of D_R for Four Cornered Bend Measurement ($\theta \pm 90^\circ$)	100
8-52a	Three Cornered Bend in the Center Conductor ($\theta = 90^\circ$)	101
8-52 b&c	Definitions of D_R ; g for Three Cornered Bend Measurements ($\theta = 90^\circ$)	101
8-53	Sharp Angle Bend in Center Conductor (Obtuse Angle, $\theta > 90^\circ$) Series Reactance Network at Specified Reference Planes from D_o , S_o , $-Y$. . .	104
8-54	Definition of D_R , d_k , g_k for Three Cornered Bend Measurement	105

Figure		Page
8-53a	Reactance Tee Network Parameters for Sharp Angle Bends	109
8-53b	Reactance Tee Network Parameters for Sharp Angle Bends	110
8-54a	Tangent Network Parameters for Sharp Angle Bends	111
8-54b	Tangent Network Parameters for Sharp Angle Bends	112
A11-1	Tangent and Series Reactance Networks	117
A11-2	Equivalent Tangent and Reactance Network Representation	119
A12-1	Discontinuity Structure for Study of Acute Angle Bends	123
A13-3	Discontinuity Structure for the Study of Obtuse Angle Bends	125

CHAPTER VIII

Stripline Discontinuities

A. Introduction:

The lumped circuit parameters of Resistance, Capacitance and Inductance are quite familiar. While lumped parameters are quite valid at low frequencies, at the higher frequencies lumped concepts become invalid and it is necessary to consider distributed parameters. In this chapter, the problem of realizing the equivalent circuits of a number of Stripline discontinuities will be considered. Since the operating frequencies of interest are in the microwave range, these discontinuities will have equivalent circuits consisting of a number of elements rather than a single lumped element. By knowing the equivalent circuits of the various discontinuities, one is able to synthesize a lumped constant circuit in the standard fashion, then through the use of discontinuity equivalent circuits, realize the proper combination of holes, slots and bends to achieve the desired results in Stripline.

B. General Discussion of Stripline Discontinuities:

A number of points common to all Stripline discontinuities should be discussed at this point.

1. Discontinuities in balanced Stripline will possess purely reactive equivalent circuits if (a) the discontinuity is balanced, (b) the ground plane spacing is less than a half wavelength in Stripline and, obviously, (c) the discontinuity structure contains no dissipative elements. If the discontinuity structure is unbalanced (unsymmetrical with respect to

the ground planes) the discontinuity will excite the dominant mode in radial transmission line (the pillbox mode). Since the pillbox mode radiates, radiation resistance then has to be included in the equivalent circuit. While any practical discontinuity structure may be slightly asymmetrical due to constructional difficulties, propagation of higher order modes may be discouraged by making sure the ground plane spacing is less than a half wavelength in stripline.

2. Most of the transverse discontinuity structures (those occupying a section of the cross sectional plane) in coaxial line or waveguide have no stripline counterpart due to construction problems. As a result it is difficult to obtain a shunt capacitive discontinuity in stripline; a shunt inductance can be obtained through the use of a vertical post. Series inductances and capacitances are quite easily obtained.

3. Since the dominant mode in stripline is the TEM mode, field distribution can be obtained by conformal mapping as has already been seen in previous chapters. Conformal mapping is not valid for higher order modes however. Their solution requires the Green's function for the region. Since stripline does not have a separable geometry the rigorous determination of this function becomes a major job in itself. It therefore becomes advantageous to seek solutions for discontinuity structures by approximate means.

C. Microwave Network Theory:

1. Microwave Network Representations:

A symmetric Stripline structure in which only the dominate TEM transmission line mode is assumed propagating may be represented by an equivalent microwave network. Transmission lines may be used to characterize the dominant mode propagating along continuous uniform sections, while lumped constant networks characterize the fields due to the nonpropagating higher order modes which are generated in the vicinity of the discontinuity. A variety of combinations of lines and lumped circuits may be chosen to represent a particular discontinuity structure at specified reference planes. If a number of discontinuities are considered along the line, their overall effect is completely determined when the network parameters characterizing each of the regions is specified. An expression relating an output "quantity" to an input "quantity," then follows on a basis similar to that used in lumped parameter network analysis.

Such quantities as voltages and currents (related to the E and H fields in the region) may be spoken of at points along the line with the result that techniques using low frequency impedance parameters, admittance parameters and matrix theory may be used. It is with this fundamental premise that discontinuity structures in Stripline may be directly characterized by different network or corresponding matrix representations, which allow us to analyze, and eventually perform measurements on, complex overall Stripline structures.

2. Transfer Matrix Formulation:

a. Definition of the Matrix:

A linear two-port network may be used to represent a particular transmission line structure at certain specified reference planes. The voltages and currents defined at the two reference planes may be linearly related by four complex coefficients which completely express the network behavior. The voltages and currents may be grouped arbitrarily at each reference plane, so that several different combinations of the coefficients are possible. A variety of network representations corresponding to each choice of the coefficients then follows. Thus, it is possible to represent the structure either by these coefficients or by the corresponding network representations. If the coefficients are chosen as the representation, they are conveniently written as the elements of a square (2 X 2) matrix. One fundamental set of coefficients called the "transfer coefficients" A, B, C, D serve to relate the voltage V_1 and current I_1 at the terminal $z = T_1$ to the voltage V_2 and current I_2 , at the terminal plane $z = T_2$ by the relations

$$V_1 = A V_2 - B I_2 \quad (8-1)$$

and

$$I_1 = C V_2 - D I_2 \quad (8-2)$$

where

$$\begin{array}{l} A = \frac{V_1}{V_2} \mid I_2 = 0 \quad G = \frac{I_1}{V_2} \mid I_2 = 0 \\ B = \frac{-V_1}{I_2} \mid V_2 = 0 \quad D = \frac{-I_1}{I_2} \mid V_2 = 0 \end{array}$$

In matrix notation, equations 8-1 and 8-2 may be expressed

as

$$\begin{pmatrix} v_1 \\ i_1 \end{pmatrix} = \begin{pmatrix} A & B \\ C & D \end{pmatrix} \begin{pmatrix} v_2 \\ -i_2 \end{pmatrix} = t \begin{pmatrix} v_2 \\ -i_2 \end{pmatrix} \quad (8-3)$$

where

$$t = \begin{pmatrix} A & B \\ C & D \end{pmatrix}$$

The voltages and currents referred to in equations 8-3 are shown in Fig. 8-1.

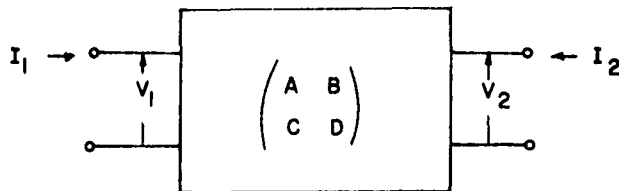


Fig. 8-1: Transfer Coefficient Matrix Representation of a Two-port Network.

b. Restrictions Imposed on the Transfer Matrix:

Several restrictions may be placed on the "transfer coefficients" when transmission line structures with specific physical properties are considered. These restrictions limit the arbitrariness of the functional form of each matrix coefficient, so that, once the structural nature is specified (regardless of the choice of physical network) the

matrix follows directly. For a single frequency situation, the coefficients are constants.

Several restrictions are of interest in the present analysis.

The first of these is that the network be reciprocal.

Reciprocity imposes the condition

$$\Delta = \begin{vmatrix} A & B \\ C & D \end{vmatrix} = AD - BC = 1 \quad (8-4)$$

We further require that the network be lossless and symmetric.

These conditions require A and D to be real quantities. It further restricts B and C to be pure imaginary quantities. For a reciprocal, lossless, symmetrical (hereafter abbreviated r.l.s.) matrix, the matrix t becomes

$$t = \begin{pmatrix} a & jb \\ jc & d \end{pmatrix} \quad (8-5)$$

where; a, b, c, d are real numbers.

Then

$$\Delta = ad + bc = 1 \quad (8-6)$$

If the transfer matrix is non-singular ($\Delta \neq 0$), it may be inverted so that the voltage and current at terminals T_2 now depend on the voltages and currents at terminals T_1 .

The inverse of t is t^{-1} where

$$tt^{-1} = t^{-1}t = I = \begin{pmatrix} 1 & 0 \\ 0 & 1 \end{pmatrix} \quad (8-7)$$

t^{-1} can be obtained from t by using the relation

$$t^{-1} = \frac{1}{\Delta} \begin{pmatrix} d & -jb \\ -jc & a \end{pmatrix} \quad \Delta \neq 0 \quad (8-8)$$

But from equation 8-6, for the r.l.s. network $\Delta = 1$.

Equation 8-8 then becomes

$$t^{-1} = \begin{pmatrix} d & -jb \\ -jc & c \end{pmatrix} \quad (8-9)$$

The inversive of equation 8-3 is then

$$\begin{pmatrix} v_2 \\ I_2 \end{pmatrix} = t^{-1} \begin{pmatrix} v_1 \\ -I_1 \end{pmatrix} \quad (8-10)$$

Finally, the symmetry condition requires that $a = d$.

The above restrictions and their consequences will appear later in the development.

c. Consequences of Restrictions:

The restrictions imposed on the matrix elements by the structural nature reduces the number of independent complex quantities necessary for a complete network description. These reductions occur when (a) physical symmetries exist; (b) the structure is lossless and (c) when the structure is reciprocal. The most general two-port descriptive structure is described by four independent complex matrix elements, a total of eight real numbers. If it is reciprocal, three elements are independent and six real numbers result. When, in addition, physical symmetry exists, the diagonal elements are equal ($a = d$),

and only two independent elements, consisting of four real numbers, remain. If, furthermore, the structure is lossless, these two independent elements are real and they serve to completely describe the structure.

All of the structures considered in this chapter are r.l.s. so that only two real elements are sufficient for a complete network description.

d. Cascaded Sections:

When a number of dissimilar two-ports are connected in tandem, the resulting structure may be represented by an overall transfer matrix T , or by one of several equivalent networks. For "n" cascaded two-ports, the overall matrix is the matrix product (taken in the order of connection) of the individual matrices. Thus, in general,

$$T_n = t_1 \ t_2 \ \dots \ t_{n-1} \ t_n = \prod_{k=1}^n t_k \quad (8-11)$$

If the cascaded r.l.s. two-ports are similar, the overall matrix is the n^{th} iteration of "unit cell" transfer matrices, t . For this case

$$t_1 = t_2 = t_3 = \dots = t_n \quad (8-12)$$

so that

$$t_n = t_1 \ t_1 \ t_1 \ \dots \ t_1 = t^n$$

Obviously, the overall matrix may also consist of a combination of "n" matrices, connected in arbitrary order, some of which are similar, while those remaining are all different.

If the individual unit cells are r.l.s., the resultant matrix T_n will be r.l.s. For an even number of cascaded unit structures, it can be seen that the resulting overall matrix is even. For "n" even, the physical symmetry plane will be located halfway between the physical reference planes of the overall structure and at the junction between two unit cell structures. Fig. 8-2 illustrates this idea. In the remaining discussions only the cascading of an even number of unit

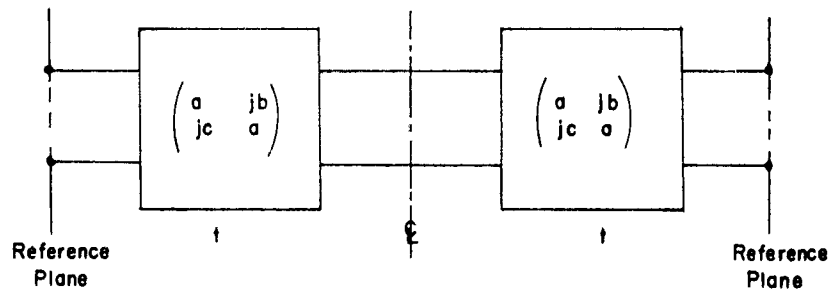


Fig. 8-2: Center Line of Symmetry
for Two Cascaded Sections.

structures will be considered. Each structure will be represented by its corresponding r.l.s. unit cell matrix t .

Once the elements of the unit cell t are known, those of the overall matrix are obtained either by "n" repeated matrix multiplications (dissimilar structures) or by raising t to the n^{th} power. An example will illustrate the procedure.

(1) Repeated Multiplication of Cascaded Unit Cells, t :

For $n = 2$, and t the r.l.s. unit cell, the

overall matrix T_2 becomes

$$T_2 = \begin{pmatrix} a & jb \\ jc & a \end{pmatrix} \begin{pmatrix} a & jb \\ jc & a \end{pmatrix} = \begin{pmatrix} A_2 & jB_2 \\ jC_2 & A_2 \end{pmatrix} \quad (8-13)$$

where

$$A_2 = a^2 - bc = 2a^2 - 1 \quad (\text{using eq. 8-4})$$

$$B_2 = 2ab$$

$$C_2 = 2ac$$

It can be observed, on continuing this process, that A_n and B_n are polynomials in a and b of degree "n." A_n is purely a function of a ; B_n is linearly related to b , but is a function of a and b .

(2) Raising t to the n^{th} power:

To raise a matrix t to the n^{th} power,

it must be reduced to the diagonal form

$$t = P \begin{pmatrix} s_1 & 0 \\ 0 & s_2 \end{pmatrix} P^{-1} \quad (8-14)$$

where:

P is a matrix used to reduce t to diagonal form.

P^{-1} = Inverse matrix to P .

s_1, s_2 = Eigenvalues of the characteristic determinant.

Upon being raised to the n^{th} power, equation 8-14 takes the form

$$t^n = P \begin{pmatrix} s_1^n & 0 \\ 0 & s_2^n \end{pmatrix} P^{-1} \quad (8-15)$$

The characteristic determinant from which the eigenvalues S_1 and S_2 are determined is

$$\begin{vmatrix} (a-s) & jb \\ jc & (a-s) \end{vmatrix} = s^2 - 2as + 1 = 0 \quad (\text{using eq. 8-4}) \quad (8-16)$$

The r.l.s. unit cell t can be expressed in parametric form for convenience in its n^{th} power representation. The result is expressed as

$$\begin{aligned} t^n &= \begin{pmatrix} \cosh nx & j b \frac{\sinh nx}{\sinh x} \\ -j/b \sinh nx \sinh x & \cosh nx \end{pmatrix} \\ &= \begin{pmatrix} A_n & j B_n \\ j C_n & A_n \end{pmatrix} = T_n \end{aligned} \quad (8-17)$$

where:

$$A_n = \cosh nx = \cosh(n \cosh^{-1} a)$$

$$B_n = \frac{b \sinh nx}{\sinh x} = \frac{b \sinh(n \cosh^{-1} a)}{\sinh(\cosh^{-1} a)}$$

$$C_n = -1/b \sinh nx \sinh x = -1/b \sinh(n \cosh^{-1} a) \\ \times \sinh(\cosh^{-1} a)$$

Obviously $x = (\cosh^{-1} a)$ in eq. 8-17. The hyperbolic trigonometric functions of this equation are for the case $|a| \geq 1$. For $|a| \leq 1$, the circular trigonometric functions are used. Using the trigonometric identity

$$\cosh^2 x - \sinh^2 x = 1 \quad (8-18)$$

it can be seen from eq. 8-17 that

$$A_n^2 + B_n C_n = 1 \quad (8-19)$$

A_n is directly related to the Tschebyscheff polynomial of the first kind $T_n(a)$, i.e.,

$$T_n(a) \equiv \cosh(n \cosh^{-1} a) = A_n \quad |a| \geq 1 \quad (8-20)$$

B_n is related to the rationalized Tschebyscheff polynomial of the second kind $U_n(a)$:

$$U_n(a) = \frac{\sinh(n \cosh^{-1} a)}{\sqrt{a^2 - 1}} = \frac{B_n}{b} \quad (8-21)$$

The denominator of eq. 8-21 can be identified with B_n of eq. 8-17 by using the identity of eq. 8-18 and realizing that in the parametric representation of the r.l.s. unit cell, the element a was replaced with $\cosh x$. For any value of "n" we now have A_n and B_n in easily manipulable closed forms. Table 8-1 gives the specific polynomial expansions of $T_n(a)$ and $U_n(a)$ for "n" = 2, 4, 6 along with the general recurrence formula to be used when higher values of "n" are desired.

e. Inversion of Cascaded Matrix:

In the previous section an overall two-port structure, represented by a transfer matrix T_n , is stated as consisting of "n" cascaded "simpler" structures, each with the associated matrix t . It is assumed that the elements of t are known, whereupon the elements of the overall matrix are shown to be polynomials of degree equal to the number "n" of cascaded sections. However, here it is assumed that the elements of t are unknown but may be obtained by solving the n^{th} degree polynomial equations contained in the known elements A_n , B_n , C_n and

TABLE 8-1
Tschebyscheff Polynomial Expansions. For Transfer Matrix Elements

$$T_n(a) = A_n(a) = \cosh(n \cosh^{-1} a)$$

$$U_n(a) = \frac{B_n(a)}{\sqrt{a^2 - 1}} = \frac{\sinh(n \cosh^{-1} a)}{\sqrt{a^2 - 1}}$$

$$x_{n+1}(a) = 2a x_n(a) - x_{n-1}(a)$$

$$T_1(a) = a$$

$$U_1(a) = 1$$

$$T_2(a) = 2a^2 - 1$$

$$U_2(a) = 2a$$

$$T_4(a) = 8a^4 - 8a^2 + 1$$

$$U_4(a) = 8a^3 - 4a$$

$$T_6(a) = 32a^6 - 48a^4 + 18a^2 - 1 \quad U_6(a) = 32a^5 - 32a^3 + 6a$$

D_n of the specified overall matrix, T_n . The number of cascaded sections, where unknown elements can be solved for by inverting the elements of T_n , depends upon the assumed nature of each section. Furthermore, if T_n is r.l.s., it is not possible to solve for the elements of more than one ($n = 1$) cascaded section unless these sections are all assumed to be similar structures (unit cells).

Here the inversion problem is one of finding solutions of an algebraic, or transcendental form n^{th} degree polynomial. If the r.l.s. structure is assumed to consist of four cascaded similar unit cells, then:

$$T_4 = \begin{pmatrix} A_4 & j B_4 \\ j C_4 & A_4 \end{pmatrix} \quad (8-22)$$

In polynomial form

$$A_4 = 8 a^4 - 8 a^2 + 1 \quad (8-23)$$

$$B_4 = b (8 a^3 - 4 a) \quad (8-24)$$

Solving eq. 8-23 for a , we obtain

$$a = \pm \left(\frac{1}{2} \pm \sqrt{\frac{1 + A_4}{2}} \right)^{1/2} \quad (8-25)$$

and from eq. 8-24 there results

$$b = \frac{B_4}{4 a (2 a^2 - 1)} \quad (8-26)$$

The solution of the polynomials of eqs. 8-23 and 8-24 leads to four different values as can be seen from the multiplicity of

signs in eqs. 8-25 and 8-26. The situation is further complicated by the fact that A_4 and B_4 may be negative. This multiplicity increases the number of possible solutions, for each element of t , to eight.

In transcendental form:

$$A_4 = T_4(a) = \cosh(4 \cosh^{-1} a) \quad (8-27)$$

$$B_4 = b U_4(a) = \frac{b \sinh(4 \cosh^{-1} a)}{\sinh(\cosh^{-1} a)} \quad (8-28)$$

from eq. 8-27

$$a = \pm \cosh(1/4 \cosh^{-1} A_4)$$

and, from eq. 8-28

$$b = \pm \frac{B_4 \sinh(\cosh^{-1} a)}{\sinh(4 \cosh^{-1} a)} \quad (8-29)$$

This form of solution similarly displays the multiplicity of values, but is more useful than the previous one, in that the transcendental functions involved are well tabulated.

f. Representations for the Unit Cell, t:

In this section we shall establish relationships between several useful network representatives of the unit cell and their corresponding elements of the transfer matrix t . In each case the dependence of these elements on the measured parameters D_o , S_o and $-v$ will be emphasized. D_o , S_o and $-v$ will be defined at a later point in the chapter.

The general unit cell may always be considered to consist of cascaded basic circuit matrices to be written as t_c . These are the transfer matrices corresponding to

- (1) A length of lossless transmission line.
- (2) A pure shunt susceptance.
- (3) A pure series reactance.
- (4) An ideal transformer.

In a lossless line the voltages and currents at any point may be related as:

$$V_1 = V_2 \cos \beta (z_2 - z_1) + j Z_o I_2 \sin \beta (z_2 - z_1) \quad (8-30)$$

and

$$I_1 = j V_2 Y_o \sin \beta (z_2 - z_1) + I_2 \cos \beta (z_2 - z_1) \quad (8-31)$$

where

$$\beta = \frac{2\pi}{\lambda_g}$$

λ_g = transmission line wavelength

In matrix notation eqs. 8-30 and 8-31 are represented as

$$\begin{pmatrix} V_1 \\ I_1 \end{pmatrix} = \begin{pmatrix} \cos \beta (z_2 - z_1) & j Z_o \sin \beta (z_2 - z_1) \\ j Y_o \sin \beta (z_2 - z_1) & \cos \beta (z_2 - z_1) \end{pmatrix} \begin{pmatrix} V_2 \\ I_2 \end{pmatrix} \quad (8-32)$$

Therefore the transfer matrix for a lossless line (Fig. 8-3)

is

$$t_t = \begin{pmatrix} \cos \theta & j Z_o \sin \theta \\ j Y_o \sin \theta & \cos \theta \end{pmatrix} \quad (8-33)$$

where

$$\theta = \beta l = \beta (z_2 - z_1)$$

$$Y_o = 1/Z_o$$

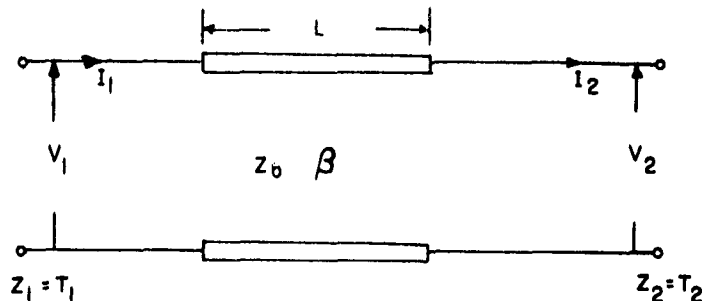


Fig. 8-3: Model of a Lossless Transmission Line.

The transfer matrix for a pure shunt susceptance may be obtained by writing the circuit equation for the model of Fig. 8-4. The result in matrix form is

$$\begin{pmatrix} v_1 \\ I_1 \end{pmatrix} = \begin{pmatrix} 1 & 0 \\ jb & 1 \end{pmatrix} \begin{pmatrix} v_2 \\ I_2 \end{pmatrix} \quad (8-34)$$

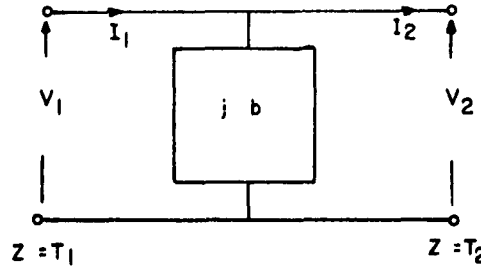


Fig. 8-4: Model of a Pure Shunt Susceptance.

By inspection of eq. 8-34, the transfer matrix of the shunt susceptance can be seen to be

$$t_s = \begin{pmatrix} 1 & 0 \\ jb & 1 \end{pmatrix} \quad (8-35)$$

The pure series reactance can be represented by the model of Fig. 8-5. Inspection of this model shows the circuit equations in matrix form to be

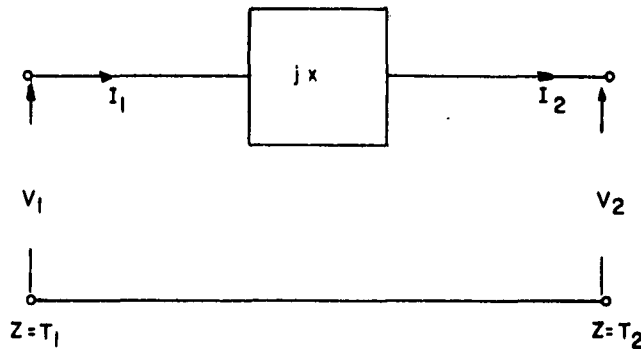


Fig. 8-5: Model of a Pure Series Reactance.

$$\begin{pmatrix} V_1 \\ I_1 \end{pmatrix} = \begin{pmatrix} 1 & jx \\ 0 & 1 \end{pmatrix} \begin{pmatrix} V_2 \\ I_2 \end{pmatrix} \quad (8-36)$$

The transfer matrix eq. the pure series reactance is
then

$$T_t = \begin{pmatrix} 1 & jx \\ 0 & 1 \end{pmatrix} \quad (8-37)$$

Finally we consider the lossless transformer. Fig. 8-6 depicts its theoretical model. Straightforward circuit

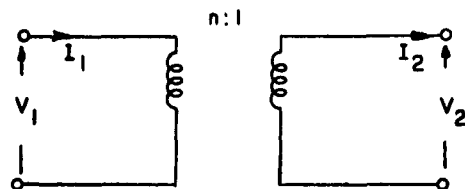


Fig. 8-6: Model of a Lossless Transformer.

analysis yields the matrices

$$\begin{pmatrix} V_1 \\ I_1 \end{pmatrix} = \begin{pmatrix} n & 0 \\ 0 & 1/n \end{pmatrix} \begin{pmatrix} V_2 \\ I_2 \end{pmatrix} \quad (8-38)$$

We then have for the transfer matrix of the lossless transformer

$$t_t = \begin{pmatrix} n & 0 \\ 0 & 1/n \end{pmatrix} \quad (8-39)$$

g. Unit Cell, t:

(1) Transformer Network Representation:

Making use of the basic circuit matrices

for two lengths of transmission line connected by a transformer

Fig. 8-7 we have

$$T = t_1 \quad t_t \quad t_1$$

$$= \begin{pmatrix} \cos \theta_1 & jZ_o \sin \theta_1 \\ jY_o \sin \theta_1 & \cos \theta_1 \end{pmatrix} \begin{pmatrix} n & 0 \\ 0 & n^{-1} \end{pmatrix} \begin{pmatrix} \cos \theta_2 & jZ_o \sin \theta_2 \\ jY_o \sin \theta_2 & \cos \theta_2 \end{pmatrix} \quad (8-40)$$

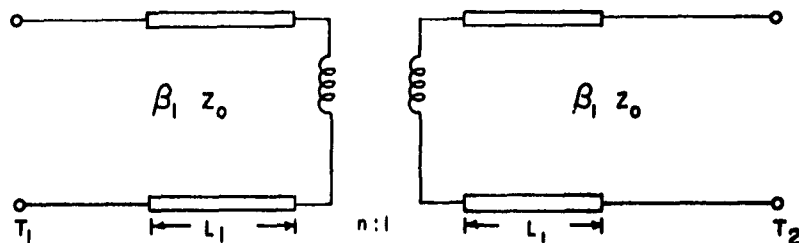


Fig. 8-7: Arbitrary Lossless Transformer Network.

If standard matrix multiplication is applied to the matrices of eq. 8-40, it can be seen that

$$T = \begin{pmatrix} A & B \\ C & D \end{pmatrix} \quad (8-41)$$

where:

$$A = n \cos \theta_1 \cos \theta_2 - n^{-1} \sin \theta_1 \sin \theta_2$$

$$B = j Z_o (n \cos \theta_1 \sin \theta_2 + n^{-1} \sin \theta_1 \cos \theta_2)$$

$$C = j Y_o (n \sin \theta_1 \cos \theta_2 + n^{-1} \sin \theta_2 \cos \theta_1)$$

$$D = n^{-1} \cos \theta_1 \cos \theta_2 - n \sin \theta_1 \sin \theta_2$$

If the assumed symmetry conditions ($A = D$) are applied to the above matrix, the following equality results:

$$\begin{aligned} n \cos \theta_1 \cos \theta_2 - n^{-1} \sin \theta_1 \sin \theta_2 &= \\ n^{-1} \cos \theta_1 \cos \theta_2 - n \sin \theta_1 \sin \theta_2 & \end{aligned} \quad (8-42)$$

Equating the coefficients of n , we see that

$$\cos \theta_1 \cos \theta_2 = - \sin \theta_1 \sin \theta_2 \quad (8-43)$$

or

$$-\tan \theta_1 = \cot \theta_2 \quad (8-44)$$

Relation 8-44 implies

$$\begin{aligned} \theta_2 &= \theta_1 \pm (2n + 1) \pi/2 \\ n &= 0, 1, 2, \dots \end{aligned} \quad (8-45)$$

and

$$\sin \theta_2 = \pm \cos \theta_1 \quad (8-46)$$

$$\cos \theta_2 = \mp \sin \theta_1 \quad (8-47)$$

Using eqs. 8-46 and 8-47, the general matrix expression for T can be solved for the symmetry condition $a = d$. The resulting matrix is

$$T_s = \begin{pmatrix} A & B \\ C & D \end{pmatrix} \quad (8-48)$$

where

$$A = \mp (n + n^{-1}) \cos \theta_1 \sin \theta_1$$

$$B = j Z_0 (\pm n \cos^2 \theta_1 \mp n^{-1} \sin^2 \theta_1)$$

$$C = j Y_0 (\mp n \sin^2 \theta_1 \pm n^{-1} \cos^2 \theta_1)$$

$$D = \mp (n + n^{-1}) \cos \theta_1 \sin \theta_1$$

Let the following quantities be defined:

$$l_1 = -D_0 \quad (8-49)$$

$$l_2 = -S_0 \quad (8-50)$$

$$\theta_1 = -\beta D_0 \quad (8-51)$$

$$\theta_2 = -\beta S_0 \quad (8-52)$$

$$n = \sqrt{-\gamma} \quad (8-53)$$

Under the transformations of eqs. 8-49 - 8-53, Fig. 8-7 becomes Fig. 8-8. In the literature this representation of a microwave network is known as the Tangent Relation equivalent network. The generalized matrix t can be put

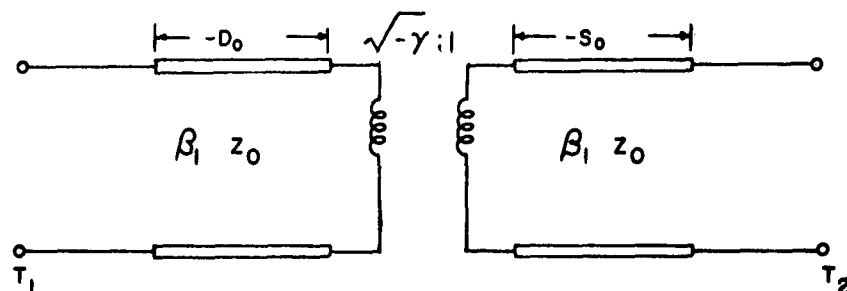


Fig. 8-8: Tangent Relation Network

into the Tangent Relation form through the substitution of eqs. 8-49 - 8-53 resulting in

$$T_E = \begin{pmatrix} A & B \\ C & D \end{pmatrix} \quad (8-54)$$

$$A = (\sqrt{-\gamma} \cos \beta D_o \cos \beta S_o - \sqrt{-\gamma}^{-1} \sin \beta D_o \sin \beta S_o)$$

$$B = -jZ_o (\sqrt{-\gamma} \cos \beta D_o \sin \beta S_o + \sqrt{-\gamma}^{-1} \sin \beta D_o \cos \beta S_o)$$

$$C = -jY_o (\sqrt{-\gamma} \sin \beta D_o \cos \beta S_o + \sqrt{-\gamma}^{-1} \sin \beta S_o \cos \beta D_o)$$

$$D = (-\sqrt{-\gamma} \sin \beta D_o \sin \beta S_o + \sqrt{-\gamma}^{-1} \cos \beta D_o \cos \beta S_o)$$

In a similar manner, eqs. 8-49 through 8-53 transform

the symmetric matrix of eq. 8-48 to

$$T_S = \begin{pmatrix} E & F \\ G & H \end{pmatrix} \quad (8-55)$$

$$E = \mp \left(\frac{1}{2} \frac{-\gamma}{\sqrt{-\gamma}} \right) \sin 2 \beta D_o$$

$$F = jZ_o \left(\pm \sqrt{-\gamma} \cos^2 \beta D_o \mp \frac{1}{\sqrt{-\gamma}} \sin^2 \beta D_o \right)$$

$$G = jY_o \left(\mp \sqrt{-\gamma} \sin^2 \beta D_o \pm \frac{1}{\sqrt{-\gamma}} \cos^2 \beta D_o \right)$$

$$H = \mp \left(\frac{1}{2} \frac{-\gamma}{\sqrt{-\gamma}} \right) \sin 2 \beta D_o$$

(2) Symmetric Tee (Pi):

The unit cell may be represented, alternatively, by a Symmetric Impedance (Admittance) Tee (Pi) network. The physically symmetric structure is characterized as having two equal reactance (susceptance) series (shunt) arms.

For the Symmetric Tee network representation, the unit

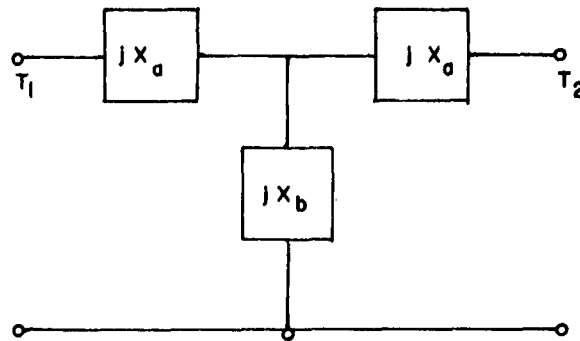


Fig. 8-9: Symmetric Tee Network

cell matrices of eq. 8-35 and 8-37 can be put together in the following form:

$$T_T = t_r \ t_s \ t_r = \begin{pmatrix} 1 & jX_a \\ 0 & 1 \end{pmatrix} \begin{pmatrix} 1 & 0 \\ \frac{1}{jX_b} & 1 \end{pmatrix} \begin{pmatrix} 1 & jX_a \\ 0 & 1 \end{pmatrix}$$

$$= \begin{pmatrix} 1 + \frac{X_a}{X_b} & j X_a \left(2 + \frac{X_a}{X_b} \right) \\ -j & 1 + \frac{X_a}{X_b} \end{pmatrix} \quad (8-56)$$

Figure 8-9 illustrates the form of the Symmetric Tee network. In a similar manner, the unit matrices can be

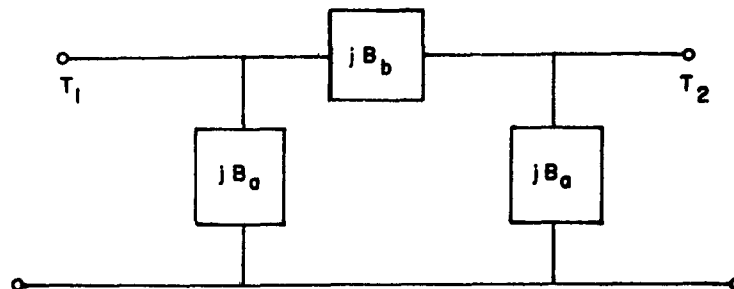


Fig. 8-10: Symmetric Pi Network

manipulated to give the transfer matrix for the Symmetric Pi network of Fig. 8-10. The result takes the form:

$$\begin{aligned}
 T_{\pi} = t_s \ t_r \ t_s &= \begin{pmatrix} 1 & 0 \\ jB_a & 1 \end{pmatrix} \begin{pmatrix} 1 & \frac{1}{jB_b} \\ 0 & 1 \end{pmatrix} \begin{pmatrix} 1 & 0 \\ jB_a & 1 \end{pmatrix} \\
 &= \begin{pmatrix} 1 + \frac{B_a}{B_b} & \frac{-j}{B_b} \\ jB_a (2 + \frac{B_a}{B_b}) & 1 + \frac{B_a}{B_b} \end{pmatrix} \tag{8-57}
 \end{aligned}$$

(3) Transmission Line Parameters in Terms of Tee Parameters:

It was previously shown in eq. 8-33 that a length of lossless transmission line could be represented by the matrix

$$t_1 = \begin{pmatrix} \cos \theta & jZ_o \sin \theta \\ jY_o \sin \theta & \cos \theta \end{pmatrix} \tag{8-33}$$

where $\theta = \beta l$ and $Y_o = 1/Z_o$. If the elements of this matrix are equated to the corresponding elements of the Symmetric Tee matrix, relations for Z_o and θ can be obtained in terms of the Symmetric Tee network reactances. The required equivalences are

$$\cos \theta = 1 + \frac{x_a}{x_b} \tag{8-58}$$

$$jZ_o \sin \theta = j \frac{x_a}{x_b} (x_a + 2 x_b) \tag{8-59}$$

and

$$j Y_o \sin \theta = - j/X_b \quad (8-60)$$

Now

$$\tan \theta/2 = \sqrt{\frac{1 - \cos \theta}{1 + \cos \theta}} \quad (8-61)$$

Substituting eq. 8-58 into eq. 8-61 we get

$$\tan \theta/2 = \sqrt{\frac{x_a^2}{-x_a(x_a + 2x_b)}} \quad (8-62)$$

In a like manner, the substitution of eq. (8-59) in eq. (8-60) give the relation

$$z_o^2 = -x_a(x_a + 2x_b) \quad (8-63)$$

(4) Length of Transmission Line Connected in Tandem:

If "n" identical r.l.s. structures "t"

are connected in tandem and each is represented by a transmission line of length $\theta = \beta l$ and Characteristic Impedance Z_o , they form an overall structure "T" which has the same Characteristic Impedance, but a new length $\theta_n = n\theta = n\beta l$. Now the matrix representative for the unit cell was shown in eq.

8-33 to be

$$t_1 = \begin{pmatrix} \cos \theta & j Z_o \sin \theta \\ j Y_o \sin \theta & \cos \theta \end{pmatrix} = \begin{pmatrix} a & jb \\ jc & a \end{pmatrix} \quad (8-33)$$

For "n" unit cells in tandem, eq. 8-33 then becomes

$$\begin{aligned}
 T &= \begin{pmatrix} \cos n\theta & jZ_0 \sin n\theta \\ jY_0 \sin n\theta & \cos n\theta \end{pmatrix} \\
 &= \begin{pmatrix} A_n & B_n \\ C_n & A_n \end{pmatrix} \tag{8-64}
 \end{aligned}$$

Matching elements in matrix 8-64 we have

$$A_n = \cos n\theta = \cos(n \cos^{-1} a) = T_n(a)$$

where

$$a = \cos \theta \text{ (from eq. 8-33)}$$

$T_n(a)$ = Tschebyscheff Polynomial of the first kind.

and

$$B_n = Z_0 \sin n\theta = Z_0 \sin(n \cos^{-1} a)$$

$$= \frac{b \sin(n \cos^{-1} a)}{\sqrt{1 - a^2}} = b U_n(a)$$

where

$$Z_0 = \frac{b}{\sin \theta} = \frac{b}{\sqrt{1 - a^2}}$$

a, b = elements from matrix 8-33

$U_n(a)$ = Tschebyscheff Polynomial of the Second kind.

These last relationships, derived on a network basis, are similar to the equations resulting from raising the unit cell matrix to the n^{th} power. Hence, the cascading of " n " identical r.l.s. structures follow immediately from the transmission line

representation once the characteristics of the basic unit are known.

h. Representation of the Unit Cell at Shifted Reference Planes:

(1) Symmetric Shift at Both Reference Planes:

In first formulating the "T" matrix for the transformer network at reference planes T_1, T_2 a turns ratio $n:1$ and two arbitrary lengths of line l_1, l_2 were chosen.

It follows that the representation for this network at shifted reference planes is brought about merely by adding the lengths of each shift to the original lengths of transmission line, and evaluating the new matrix elements. Thus, if we wish to evaluate the new matrix, as a result of a symmetric shift of reference planes, we have at T_1, T_2

$$T = \begin{pmatrix} A & jB \\ jC & A \end{pmatrix} \quad (8-55)$$

where A, B, C are the elements of the matrix of eq. 8-55 and at T_1', T_2'

$$\begin{aligned} T' &= t_1 T t_1 \\ &= \begin{pmatrix} \cos \theta & jZ_o \sin \theta \\ jY_o \sin \theta & \cos \theta \end{pmatrix} \begin{pmatrix} A & jB \\ jC & A \end{pmatrix} \begin{pmatrix} \cos \theta & jZ_o \sin \theta \\ jY_o \sin \theta & \cos \theta \end{pmatrix} \\ &= \begin{pmatrix} A' & jB' \\ jC' & A' \end{pmatrix} \quad (8-65) \end{aligned}$$

where

$$\begin{aligned}
 A' &= A \cos 2\theta - \left(\frac{B Y_o + C Z_o}{2} \right) \sin 2\theta \\
 &= A \cos 2\theta - 1/2 \left(B Y_o + \frac{1 - A^2}{B Y_o} \right) \sin 2\theta \\
 B' &= B \cos^2 \theta + Z_o A \sin 2\theta - Z_o^2 \left(\frac{1 - A^2}{B Y_o} \right) \sin^2 \theta \\
 C' &= A Y_o \sin 2\theta + C \cos^2 \theta - B Y_o^2 \sin^2 \theta \\
 \theta &= \beta d \\
 d &= \text{length of shift.}
 \end{aligned}$$

Alternatively, using a Symmetric Tee representation, it may be shown that if X_a and X_b of Fig. 8-9 are known at T_1 , T_2 , then after a symmetric shift of length d , the new network parameters at T_1' , T_2' are

$$\begin{aligned}
 X_a' &= \frac{D X_a + 1}{D - X_a} \\
 2 X_b' &= \frac{D X_c + 1}{D - X_c} - X_a
 \end{aligned} \tag{8-66}$$

where

$$D = \cot \beta d = \cot \theta$$

$$X_c = X_a + 2 X_b$$

(2) Shift of One Reference Plane by a Half

Wavelength:

If a half wavelength of line is added at one reference plane of a symmetric impedance Tee network, the

network at the new reference planes may be expressed in terms of the original parameters. In matrix form we have

$$\begin{aligned} T_1' &= \begin{pmatrix} \cos \pi & jZ_o \sin \pi \\ jY_o \sin \pi & \cos \pi \end{pmatrix} \begin{pmatrix} 1 + x_a/x_b & jx_a (2 + x_a/x_b) \\ -j/x_b & 1 + x_a/x_b \end{pmatrix} \quad (8-67) \\ &= \begin{pmatrix} - (1 + x_a/x_b) & - jx_a (2 + x_a/x_b) \\ j/x_b & - (1 + x_a/x_b) \end{pmatrix} \end{aligned}$$

Equating like elements of the equivalent matrices the following equivalences can be obtained:

$$\begin{aligned} \bar{x}_a &= x_a + 2 x_b \\ \bar{x}_b &= -x_b \end{aligned} \quad (8-68)$$

Also

$$\begin{aligned} x_a &= \bar{x}_a - 2 \bar{x}_b \\ x_b &= -\bar{x}_b \end{aligned} \quad (8-69)$$

We note that although only one of the two structures is physically symmetric, the representation for both is symmetric.

If we assume that a measured structure with physical reference planes corresponding to T_1 and T_2 is represented by the Reactance Tee network, the input impedance at T_1 is related to the output impedance at T_2 by:

$$z_{in} = x_{11} - \frac{|x_{12}|^2}{x_{11} + z_{out}} \quad (8-70)$$

where

$$X_a = X_{11} - X_{12}$$

$$X_b = X_{12}$$

X_{11}, X_{12} = elements of an impedance matrix

at the reference planes T_1, T_2 .

We can obtain only $|X_{12}|^2$ from a measurement. The sign of X_{12} is therefore left in doubt. If X_b is chosen as $+|X_{12}|$, the representation must be taken at T_1, T_2 . However, if $X_b = -|X_{12}|$ the representation must be taken at T_1, T_2' . Only one of these representations is theoretically correct, whereas both give the correct input-output relationship. As will be seen under the discussion of the measurement procedure, the ambiguity of the sign of the mutual element is due to the inability of the probing arrangement to distinguish between two voltages whose phases are 180° apart.

i. Inversion of "N" Identical Unit Cells:

If "N" structures "t" are connected in tandem, the resulting overall structure "T" may be represented directly by a transmission line having parameters β_1, Z_o ; such a line consisting of "N" unit cell transmission lines. When "T" is measured it can be represented by β_1, Z_o or by $\bar{\beta}_1, Z_o$. These two lengths occur due to the half wavelength probing ambiguity. These lengths are related as

$$\bar{\beta}_1 = \beta_1 \pm \pi$$

so that "T" can be represented (including the half wavelength ambiguity) by $Z_o, \beta_1 \pm \epsilon \pi$. From this one can determine the

representation for "t" which, in view of the n^{th} order multiplicity is given by:

$$z_o, \frac{(\beta 1 + \epsilon \pi) + 2 \pi n}{N} \quad n = 0, 1, \dots, N-1 \quad (8-72)$$

$$\epsilon = 0, 1$$

or

$$z_o, \frac{(\beta 1 + m \pi)}{N} \quad m = 0, 1, \dots, 2N-1 \quad (8-73)$$

There are $2N$ solutions; given any of these, the others may be found. By solving eq. (8-58), (8-62) and (8-63) for the general case, the equations for the corresponding impedance network can be found. These equations are

$$x_{am} = z_o \tan \frac{(\beta 1 + m \pi)}{N} \quad m = 0, 1, \dots, 2N-1 \quad (8-74)$$

and

$$x_{bm} = -z_o \csc \frac{(\beta 1 + m \pi)}{N} \quad m = 0, 1, \dots, 2N-1 \quad (8-75)$$

Although $2N$ pairs of parameters are found by using this procedure, only one set rigorously represents the unit cell. This pair cannot be experimentally distinguished from the other pairs; it can be identified only after a comparison with the theoretically derived parameters.

D. Theoretical Determination of Equivalent Circuits for
Stripline Discontinuities:

1. The Approximate Model:

In Chapter II of this report a rigorous conformal mapping of Stripline was performed. It was the purpose of

this mapping to obtain the capacitance and thus the Characteristic Impedance of Stripline. Through the use of a conformal



Fig. 8-11: Determination of Stripline

Characteristic Impedance.

mapping an equivalent strip width D was found (Fig. 8-11) to take into account fringing capacitance from the actual strip of width w . For the case of a zero thickness center strip a rigorous expression for D has been derived by Oberhettinger and Magnus⁴ and is

$$D = b \frac{K(k)}{K(k')}$$

where

$K(k)$ is a complete elliptic integral of the first kind.

$$k = \tanh(\pi w/2 b)$$

$$k' = \sqrt{1 - k^2}$$

When $w/b > 0.5$, corresponding roughly to Characteristic Impedances less than 100 ohms, D is given to an excellent approximation by

$$D = w + \frac{2}{\pi} b \ln 2. \quad (8-77)$$

The structure of Fig. 8-11 may be viewed as two identical portions of parallel plate transmission placed back to back and any incident wave will divide equally into both portions. Since any geometrically balanced discontinuity in the line will reflect the same proportion of the incident wave in both top and bottom portions, and since this proportion is also that for the total wave, it is not necessary when dealing with normalized quantities to retain both halves in the line. Thus, in the analysis of balanced discontinuities which are described in terms of normalized quantities, one need only consider one half of the structure and may thus employ the approximate model of Fig. 8-12.

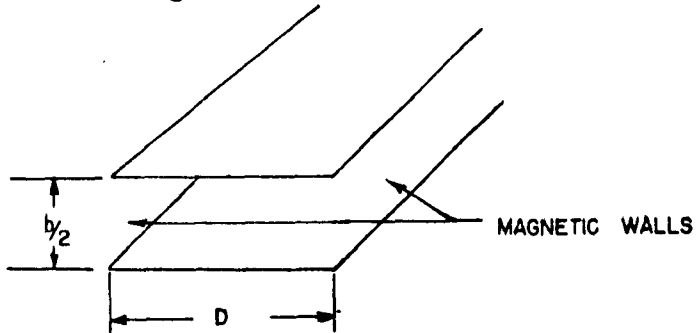


Fig. 8-12: Approximate Model of Stripline.

a. Gap Discontinuity in the Center Strip:

Once the approximate model has been obtained, the equivalent circuit for a slot in the center conductor of stripline can easily be found.⁵⁹ Fig. 8-13 illustrates the gap discontinuity. Since the gap extends completely across the width of the inner conductor, the discontinuity can be approximated by a gap extending completely across the bottom of the approximate model.

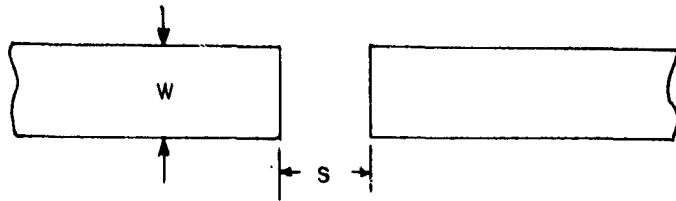
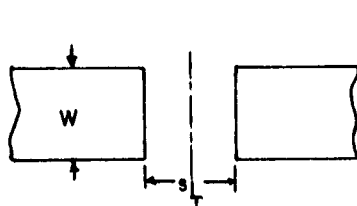
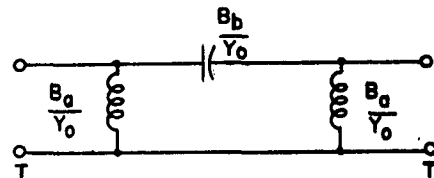


Fig. 8-13: Gap in Inner Conductor of Stripline.

But this configuration is the same as a gap of infinite width in a parallel plate waveguide of infinite width. The solution for the latter configuration is obtainable from the already available solution for the E plane slot coupling of rectangular waveguides given on pp. 373-375 of the Waveguide Handbook.³⁹ (It should be noted that parameter B_b of the equivalent circuit of Fig. 7.1-1 on p. 374 should be a capacitance rather than an inductance as given there.) Fig. 8-14 shows the Stripline gap with its centerline reference plane in part a and the Pi equivalent circuit for the enterline representation in part b. The values of B_a and B_b may be found from the relations given on page 374 of the Waveguide Handbook.



(a) CENTER CONDUCTOR



(b) EQUIVALENT CIRCUIT

Fig. 8-14: Centerline Representations for a Gap
in the Center Conductor of Stripline.

Equation 1-b of that page becomes with the appropriate Stripline notation

$$\frac{B_a}{Y_0} = -\frac{2b}{\lambda} \ln \cosh \frac{\pi s}{2b} \quad \frac{b}{\lambda} \ll 1 \quad (8-78)$$

Equation 2-b of p. 374 is

$$\frac{B_b}{Y_0} - \frac{B_a}{Y_0} = \frac{2b}{\lambda} \ln \operatorname{csch} \frac{\pi s}{2b} \quad \frac{b}{\lambda} \ll 1 \quad (8-79)$$

If eq. (8-78) is used in eq. 8-79 and the hyperbolic trigonometric identities are used, we obtain

$$\frac{B_b}{Y_0} = \frac{b}{\lambda} \ln \coth \frac{\pi s}{2b} \quad (8-80)$$

where

$$Y_0 = \frac{1}{Z_0} = \frac{D}{30 \pi b}$$

λ = Stripline wavelength

b = Distance between ground planes

$$D = \frac{b}{K(k)} \quad \frac{w}{b} < 0.5 \quad (8-76)$$

$$= w + \frac{2b}{\pi} \ln 2 \quad \frac{w}{b} > 0.5 \quad (8-77)$$

b. Slot Discontinuity in the Center Strip:

Using the approximate model Suzuki⁶⁰ has

obtained expressions for a slot in the center conductor of Stripline. The slot is considered to be cut in one face of the approximate model. By duality considerations, the geometry is then related to a flat metal rectangle located

parallel to the electric field in a parallel plate waveguide of width equal to the height of the original Stripline. The equivalent circuit for the metal rectangle in parallel plate guide is then obtained approximately from an accurately derived result for a tuned post in rectangular guide.

The formulas for the slot are given below. In the limit as the slot runs completely across the center conductor, these complicated formulas reduce to eqs. 8-78 and 8-80 for the gap. Fig. 8-15 illustrates the slot discontinuity in part a and the centerline equivalent circuit in part b.

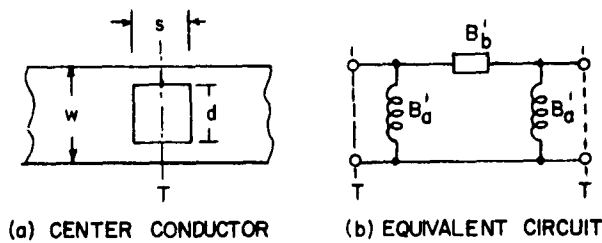


Fig. 8-15: Slot in Center Conductor (a) Physical Structure
(b) Equivalent Circuit at Centerline Reference Plane.

The parameters B_a' and B_b' are given by

$$B_a' = \frac{-\frac{2b}{\lambda} \ln \cosh \frac{w\tau}{b}}{1+P} \quad (8-81)$$

and

$$B_b' = -\frac{b}{\lambda} \ln \sinh \frac{w\tau}{b} - \frac{B_a'}{2} - \frac{b\lambda}{w^2} (1 + \frac{2b}{\pi w} \ln 2) Q \quad (8-82)$$

where

$$Q \approx \frac{1}{4\tau} \left[\frac{-1}{\ln B} - \left(\frac{1-B^2}{\ln B} \right)^2 \sum_{n=1}^N f(2n\tau) \frac{x_n^2}{n} \right]$$

N is the integer nearest the quantity

$$(0.7/\tau - 1)$$

$$P = 1/4 \left(\frac{1-B^2}{\ln B} \right)^2 \sum_{n=1}^5 g(2n\tau) \frac{x_n^2}{n^2} + \tau^2 Q$$

and where

$$\tau = \frac{\pi s}{2w} \quad B = \cos \frac{\pi d}{2w}$$

The quantity x_n is given by

$$x_1 = 1, \quad x_2 = -1 + 3B^2, \quad x_3 = 1 - 8B^2 + 10B^4$$

$$x_4 = -1 + 15B^2 - 45B^4 + 35B^6$$

$$x_5 = 1 - 24B^2 + 126B^4 - 226B^6 + 126B^8$$

The functions $f(x)$ and $g(x)$ are plotted in Fig. 8-16 and 8-17. The formulas for B_a' and B_b' are applicable only when $\tau \geq 0.15$ and $d/w \geq 0.25$.

2. Small Aperture Procedure:

One very useful procedure for obtaining reasonably accurate approximate values for the circuit parameters of a discontinuity structure employs well-known "small aperture" or stored power considerations together with a variational expression. In general terms a variational expression for series elements can be written as

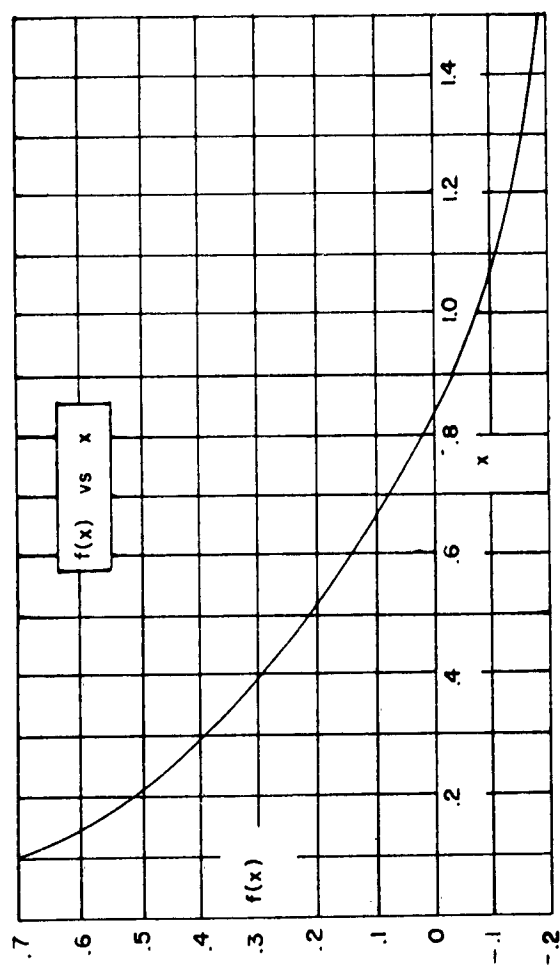


Fig. 8-16. FUNCTIONS EMPLOYED IN SLOT FORMULAS.

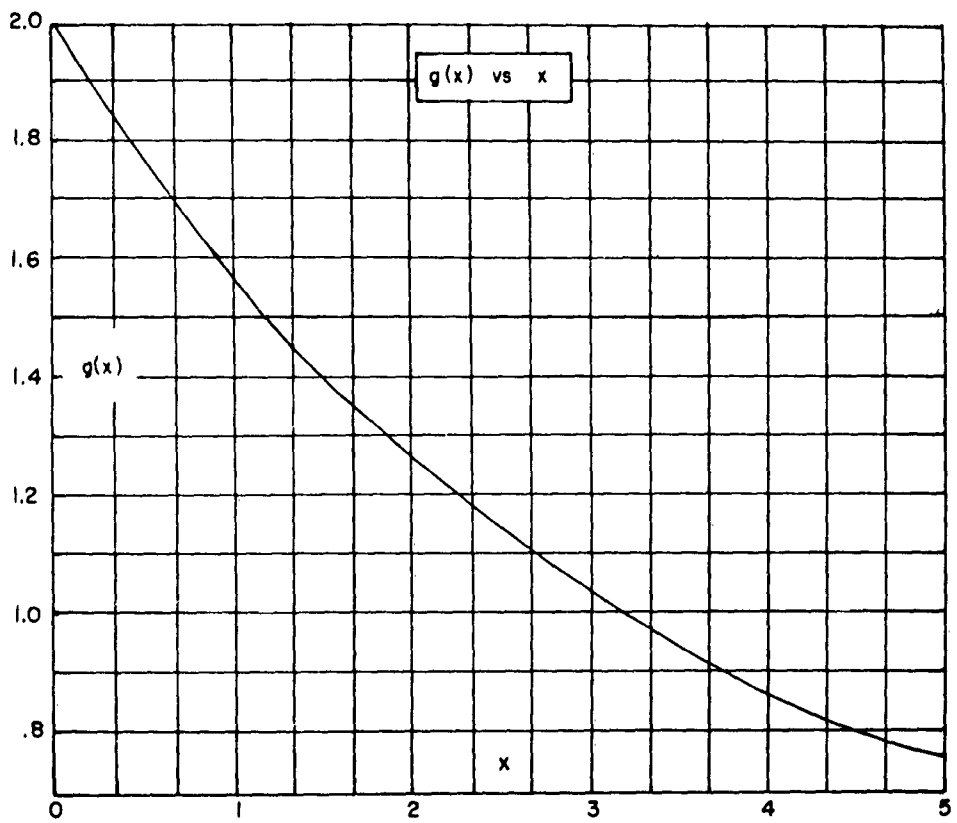


Fig. 8-17. FUNCTIONS EMPLOYED IN SLOT FORMULAS

$$\frac{B}{Y_0} = \frac{\text{Stored Power}}{Y_0 (\text{voltage})^2} \quad (8-83)$$

where a trial aperture electric field E must be inserted into both numerator and denominator. The voltage term is then of the form

$$\text{Voltage} = \iint_{\text{aperture}} n \times E \cdot H \, ds$$

where

n = unit vector normal to aperture

E = electric field vector

H = magnetic field vector

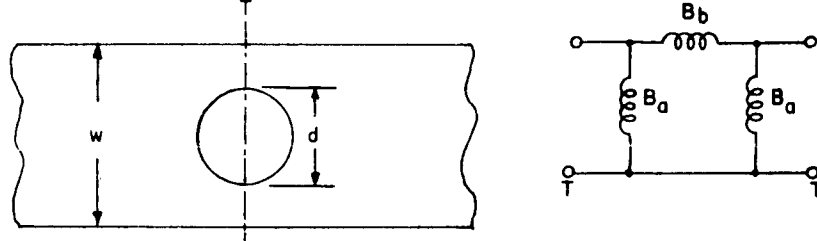
H is an appropriate mode function which depends on the nature of the excitation of the discontinuity and on the type of waveguide. The determination of the stored power is always the formidable portion of any such integration, since it involves integrations over all the higher modes of the waveguide.

The use of the "small apertures" or "stored power" considerations avoids the necessity for a separate evaluation of the numerator of eq. (8-83). Instead one seeks the already available solution for a similar problem in a different waveguide cross section. If the guide walls, which are different in the two problems, do not substantially influence the stored power (i.e., speaking loosely the distortion of the field lines) in the neighborhood of the discontinuity, the stored powers for the two problems may be taken to be equal. For

"small apertures," the assumption that the guide walls do not substantially influence the stored power is a valid one. The stored power expression is extracted from this similar problem by setting it up in the variational form of eq. 8-83. This similar problem must, of course, involve a discontinuity of the same shape and with the same manner of excitation as in the original problem. The desired susceptance value is then equal to the already known susceptance value multiplied by the ratio of the pertinent dominators.

a. Round Hole in the Center Conductor:

Fig. 8-18 illustrates a round hole in the center conductor of Stripline along with its equivalent circuit. The



(a) CENTER CONDUCTOR

(b) EQUIVALENT CIRCUIT

Fig. 8-18: Centerline Representation of a Round Hole in the Center Conductor of Stripline.

equivalent circuit for this discontinuity can be found from p. 376 of the Waveguide Handbook.³⁹ Through the use of the "small aperture" procedure, the susceptance expressions for small aperture coupling of rectangular waveguides excited in the TM_{10} mode can be related to the equivalent circuit susceptance for a round hole in the center conductor of Stripline.

Equation (3b) of p. 376 becomes with the correct Stripline

equivalences inserted

$$\frac{B_b}{Y_o} = -\frac{3}{4\pi} \frac{\lambda b D}{d^3} \quad d \ll \lambda \quad (8-85)$$

where

λ , b , D = same as those of eq. 8-80

d = diameter of round hole

In a similar manner, eq. (2b) of p. 376 reduces to

$$\frac{B_a}{Y_o} = \frac{1}{4(B_b/Y_o)} \quad d/\lambda \ll 1 \quad (8-86)$$

The above development has been for the round hole. The case of the elliptic hole can be solved through the use of the general relations on p. 375 - 376 of the Waveguide Handbook.³⁹ The general ellipse is specified by its major and minor axes d_1 and d_2 . The round hole is, of course, just the special case where $d_1 = d_2 = d$.

b. Vertical Post in Stripline:

Through the use of the small aperture procedure, equivalent circuits can be obtained for a vertical post in Stripline. The post may be of conducting or dielectric material, may be centered or off centered and may be of round, elliptical or rectangular cross section. The case for the round centered conducting post will be considered here. Other cases mentioned above follow using the formulas of p. 257 - 267 of the Waveguide Handbook.³⁹

Fig. 8-19 illustrates the round centered conducting post as well as its equivalent circuit.

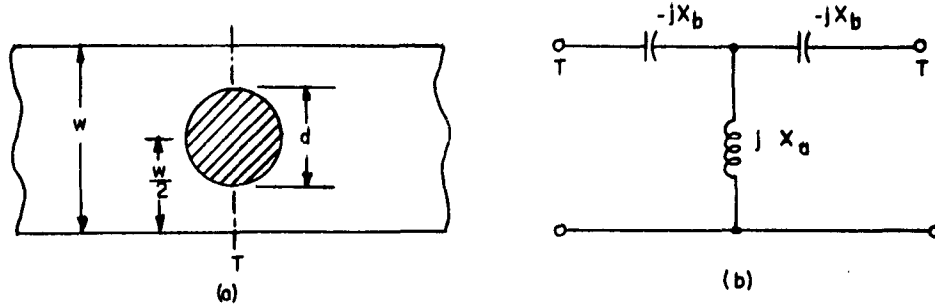


Fig. 8-19: Centerline Representation for a Round Centered Conducting Vertical Post in Stripline.

The parameters X_a and X_b are found by inserting the appropriate Stripline parameters in eq. 3-4 a and b p. 258 of the Waveguide Handbook.³⁹ They are

$$\frac{X_a}{Z_0} - \frac{X_b}{2Z_0} = \frac{D}{2\lambda} \left[s_0 - \left(\frac{\pi d}{2\lambda} \right)^2 - \frac{5}{8} \left(\frac{\pi d}{2\lambda} \right)^4 - 2 \left(\frac{\pi d}{2\lambda} \right)^4 (s_2 - 2s_0)^2 \right] \quad (8-87)$$

eqs. 8-87 and 8-88 are valid

$$\frac{X_b}{Z_0} = \frac{D}{\lambda} \frac{\left(\frac{\pi d}{D} \right)^2}{1 + \frac{11}{24} \left(\frac{\pi d}{D} \right)^2} \quad \text{for } (2D > \lambda > 2D/3) \quad (8-88)$$

$d/D < 0.20$

where

$$s_0 = \ln \frac{4D}{\pi d} - 2 + 2 \sum_{n=3, 5, \dots}^{\infty} \left[\frac{1}{\sqrt{n^2 - \left(\frac{2D}{\lambda} \right)^2}} - \frac{1}{n} \right]$$

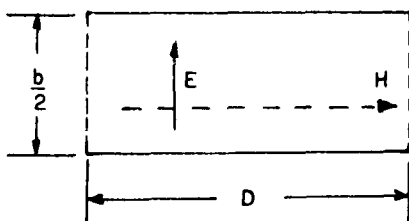
$$s_2 = \ln \frac{4D}{\pi d} - \frac{5}{2} + \frac{11}{3} \left(\frac{\lambda}{2D} \right)^2$$

$$- \left(\frac{\lambda}{D} \right)^2 \sum_{n=3, 5, \dots}^{\infty} \left[\sqrt{n^2 - \left(\frac{2D}{\lambda} \right)^2} - n + 2/n (D/\lambda)^2 \right]$$

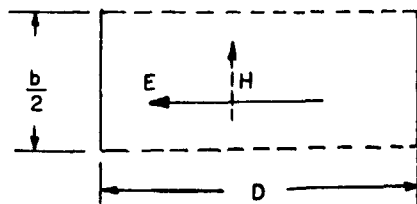
3. Babinet Equivalence Procedure:

The Babinet principle is simply an extension of the principle of duality found in standard network theory. It states that if the E field is replaced by an H field and the H field by a - E field, then the equivalent circuit resulting from the transformed discontinuity structure is simply the dual of the equivalent circuit of the original discontinuity structure. The numerical values of the corresponding dual elements are identical. The dual model of Stripline turns out to be very useful.

Fig. 8-20a shows a cross sectional view of the Stripline approximate model. Part b of Fig. 8-20 shows the Babinet equivalent of the approximate model.



(a) APPROXIMATE MODEL



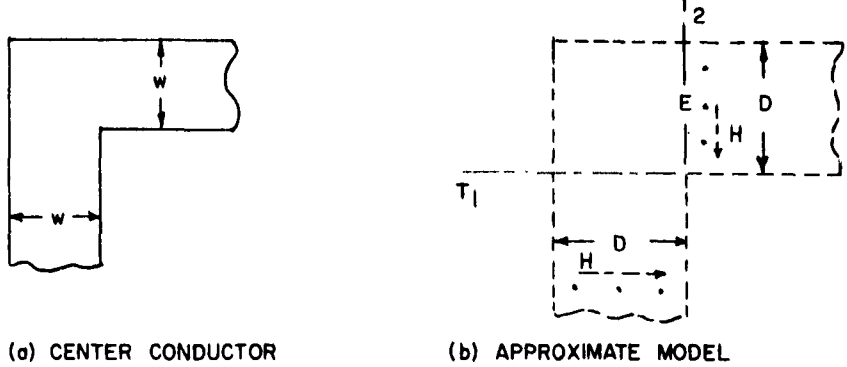
(b) BABELT EQUIVALENT

Fig. 8-20: The Stripline Approximate Model

and Its Babinet Equivalent.

a. Right Angle Bend:

The plan view of a right angle bend in Stripline is shown in part a of Fig. 8-21. The approximate model equivalent is shown in part b of Fig. 8-21. With

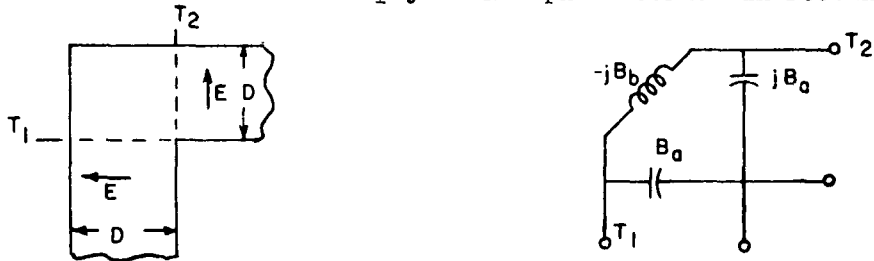


(a) CENTER CONDUCTOR (b) APPROXIMATE MODEL

Fig. 8-21: Approximate Model of a Right

Angle Bend in stripline.

electric and magnetic walls interchanged as well as lines of E with H and H with $-E$, the Babinet equivalent model of Fig. 8-22a results. However a close look at this equivalent model shows it to be simply an E - plane corner in rectangular



(a) Babinet Equivalent

(b) EQUIVALENT CIRCUIT

Fig. 8-22: Babinet Equivalent of a Right Angle

Bend and its Equivalent Circuit.

waveguide. Turning to page 313 of the Waveguide Handbook,³⁹ we find the equivalent circuit of Fig. 8-22b as well as formulas for the parameter B_a and B_b . With the correct Stripline parameters inserted these equations (3b and 4b) become,

$$\frac{B_a}{Y_o} = \frac{2 D}{\lambda} \left[0.878 + 0.498 \left(\frac{2 D}{\lambda} \right)^2 \right] \quad \frac{2 D}{\lambda} < < 1 \quad (8-89)$$

and

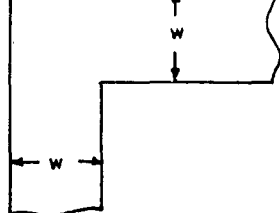
$$\frac{B_b}{Y_o} = \frac{\lambda}{2\pi D} \left[1 - 0.114 \left(\frac{2D}{\lambda} \right)^2 \right] \quad \frac{2D}{\lambda} \ll 1 \quad (8-90)$$

Now let us remember that the equivalent circuit we have obtained is the dual of the circuit we are seeking. We obtain the desired circuit by a simple duality transformation. The equivalent circuit of Fig. 8-22b has the dual shown in Fig. 8-23b. The parameter X_a and X_b may be obtained from eq. 8-89 and 8-90 by replacing B_a/Y_o and B_b/Y_o by their duals X_a/Z_o and X_b/Z_o . We then have

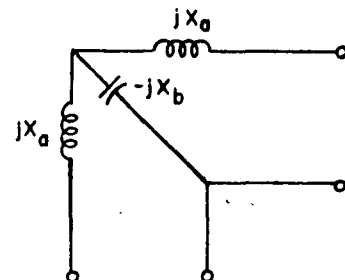
$$\frac{X_a}{Z_o} = \frac{2D}{\lambda} \left[0.878 + 0.498 \left(\frac{2D}{\lambda} \right)^2 \right] \quad \frac{2D}{\lambda} \ll 1 \quad (8-91)$$

and

$$\frac{X_b}{Z_o} = \frac{\lambda}{2\pi D} \left[1 - 0.114 \left(\frac{2D}{\lambda} \right)^2 \right] \quad \frac{2D}{\lambda} \ll 1 \quad (8-92)$$



(a) CENTER CONDUCTOR



(b) EQUIVALENT CIRCUIT

Fig. 8-23: A Right Angle Bend in Stripline

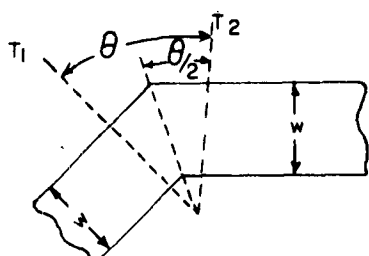
and its Equivalent Circuit.

Equations 8-91 and 8-92 are simplified asymptotic expressions that agree with the exact solutions within eight per cent for $2D/\lambda < 0.6$.

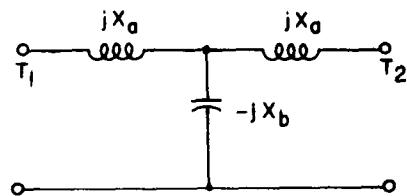
b. Sharp Bend of Any Angle:

The detailed procedure for the sharp bend of any angle is just a repetition of that used for the 90° bend. The equivalent approximate model is found from the physical situation. The Babinet equivalent is then found and identified with eqs. 1 and 2 of p. 316 in the Waveguide Handbook.³⁹ Using duality, the desired results are obtained.

Fig. 8-24a shows the physical configuration while part b of



(a) CENTER CONDUCTOR



(b) EQUIVALENT CIRCUIT

Fig. 8-24: Equivalent Circuit for a Sharp Bend of Any Angle in Stripline.

that figure shows the equivalent circuit for a sharp bend of any angle. The parameter X_a and X_b are given by

$$\frac{X_b}{Z_0} = -\frac{\lambda}{2 \pi D} \cot \theta/2 \quad (8-93)$$

and

$$\frac{X_a}{Z_0} = \frac{2 D}{\lambda} \left[\Psi(x) + 1.9635 - \frac{1}{x} \right] \quad (8-94)$$

where, with θ in degrees,

$$x = 1/2 (1 + \theta/180) \quad 1/2 < x < 1$$

The function $\Psi(x)$ is tabulated.⁶¹

c. Uniform Circular Bend:

In a manner similar to that used in part a and b of this section, the equivalent circuit of a uniform circular bend can be determined. The physical configuration is shown in part a of Fig. 8-25. The equivalent circuit at

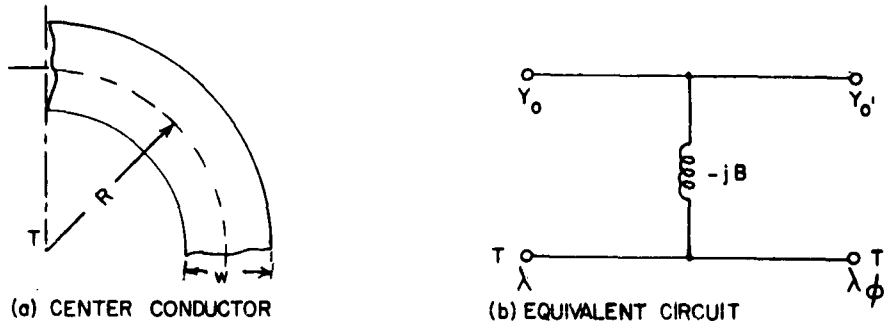


Fig. 8-25: Equivalent Circuit for

a Uniform Circular Bend.

the reference plane T is shown as part b. The parameter B is given by

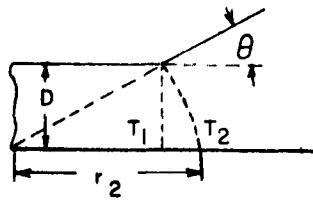
$$\frac{B}{Y_0} = \frac{32}{\pi^7} \left(\frac{2\pi D}{\lambda} \right) \left(\frac{D}{R} \right)^2 \sum_{n=1, 3, \dots}^{\infty} \frac{1}{n^7} \sqrt{1 + \left(\frac{2D}{n\lambda} \right)^2} \quad (8-95)$$

The equivalent circuit is applicable in the wavelength range $2D/\lambda < 1$. The circuit parameters have been evaluated to order $(D/R)^2$, but no estimate of the range of accuracy is available.

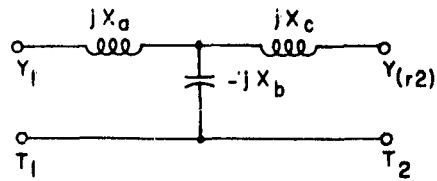
d. Junction of a Straight and a Tapered Centered

Conductor:

The equivalent circuit for the function of a straight and a tapered center conductor may also be determined through the use of a Babinet equivalence. The center conductor configuration is shown as part a of Figure 8-26. Its



(a) CENTER CONDUCTOR



(b) EQUIPMENT CIRCUIT

Fig. 8-26: Equivalent Circuit for the Junction of a Straight and a Tapered Center Conductor.

equivalent circuit is the dual of that given for the E plane junction of a rectangular and a radial waveguide on page 322 of the Waveguide Handbook.³⁹ The parameters of this dual equivalent circuit are found by taking the duals of the relations for the junction of the rectangular and radial guides.

Inserting the correct Stripline parameters we get

$$\frac{Z(r_2)}{Z_1} = \frac{\sin \theta}{\theta} \quad (8-96)$$

$$\frac{X_a}{Z_1} = \frac{2 \pi D}{\lambda \theta} \ln \frac{\theta}{\sin \theta} \quad (8-97)$$

$$\frac{X_c}{Z_1} = \frac{2 D}{\lambda} \left[0.577 + \psi \left(\frac{\theta}{\pi} \right) \right]$$

$$\frac{X_b}{Z_1} = \frac{\lambda}{\pi D} \frac{\sin \theta}{\theta} \frac{\sin \theta}{1 - \frac{\sin 2\theta}{2\theta}} \quad (8-98)$$

where

$\psi(x)$ is the logarithmic derivative⁶¹ of $x!$ and θ is measured in radians. Formulas (8-96) - (8-98) also apply for the case where θ is negative, i.e., the taper is downward.

The equivalent circuit is applicable in the wavelength range $2D/\lambda < 1$. The circuit parameters have been obtained by a simple equivalent static method and are valid only in the range $2D/\lambda << 1$. The error is estimated to lie within a few per cent for $2D/\lambda < 0.1$.

e. 120° Junction:

The case of three center conductors coming together at angles of 120° can also be treated using the approximate model and the dual of its Babinet equivalent circuit. A plan view of the physical configuration is shown in Fig. 8-27a. The equivalent circuit shown is the dual to that given under

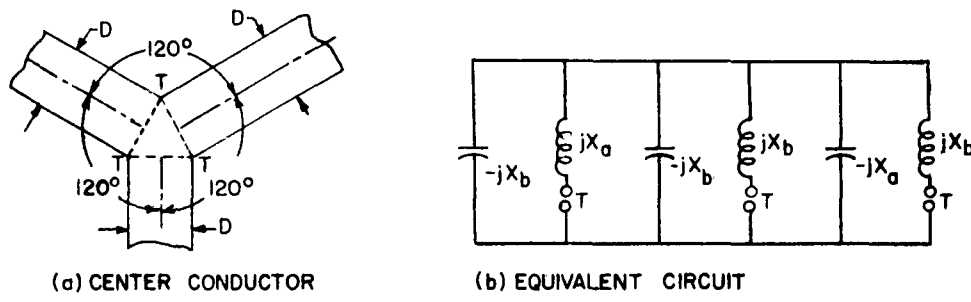


Fig. 8-27: Equivalent Circuit for a 120° Y

Junction in the Center Conductor.

the discussion of the 120° E plane Y waveguide junction in the Waveguide Handbook³⁹ on page 352. The parameters X_a and X_b are given by

$$\frac{X_a}{Z_0} = \frac{2D}{\lambda} \cdot 0.6455 \quad (8-99)$$

and

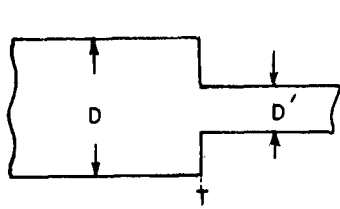
$$\frac{X_b}{Z_0} = \frac{\lambda}{D} \cdot \frac{2\sqrt{3}}{\pi} \quad (8-100)$$

The equivalent circuit is applicable in the wavelength range $2 D/\lambda < 1$. Equation 8-99 and 8-100 are static approximations and have been obtained by conformal mapping methods. They are estimated to be accurate to within a few per cent in the range $D/\lambda < 0.1$.

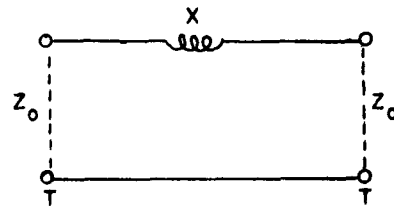
f. Sudden Change in Width:

A sudden change in width of the center conductor can be dealt with using the above principles. This example is not quite as obvious as those previously given. The obvious thing to do for the case under consideration is to look up the E plane change in rectangular height in the Waveguide Handbook.³⁹ This expression is found on p. 307 of the above reference and is extremely nasty; too nasty in fact to be easily useful.

A simple result for the change in stripline center conductor width is given by Oliner.⁵⁹ A number of previously derived equivalent circuits for center strip discontinuities are also given in this paper. Private communication with Dr. Oliner revealed that the following rule of thumb was used to derive the expression for sudden change in center strip width: "The dual expression for the parameter of the equivalent circuit of a sudden change in center strip width is given by $1/2$ the dominant term in the expression for the E plane slit in waveguide." The expression for the E plane slit is given on page 218 of the Waveguide Handbook.³⁹ Fig. 8-28 illustrates the physical configuration and its equivalent circuit. As usual,



(a) CENTER CONDUCTOR



(b) EQUIVALENT CIRCUIT

Fig. 8-28: Equivalent Circuit for a Sudden
Change in Center Strip Width.

D refers to the equivalent center strip width of the approximate model. The parameter X of the equivalent circuit is given by

$$\frac{X}{Z_0} = \frac{2D}{\lambda} \ln \csc \frac{\pi D'}{2D} \quad (8-101)$$

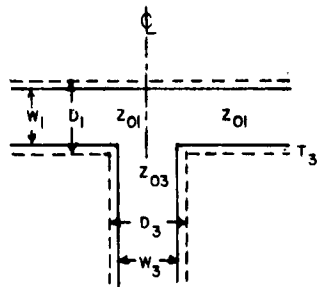
where

$$\frac{D}{D'} = \frac{Z_0'}{Z_0} \quad (8-102)$$

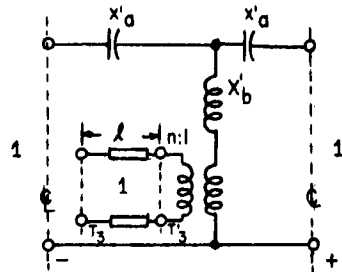
Equation 8-101 is derived by taking one half of the dual of eq. 2a p. 218 for the E plane slit. Equation 8-102 is gotten by taking the dual of eq. 1 p. 307 for the change in height of rectangular guide.

e. Symmetric Tee Junction:

The final discontinuity whose equivalent circuit is based on the Babinet equivalent circuit is that of the Symmetric Tee and is due to Oliner.⁶² The physical structure of the Tee and its equivalent circuit are shown as Fig. 8-29. The symmetric arms of the Tee are represented at the center



(a) Physical Structure



(b) Equivalent Circuit

Fig. 8-29: Symmetric Tee Junction

line and the reactances x'_a and x'_b are normalized to z_{01} .

In Fig. 8-29, "l" represents the length of transmission line connecting reference planes T_3 and T_3' . The approximate theory employed in the derivation predicts, however, that l has a zero value. In consequence, the measured value of l expresses any error in choosing T_3 as the plane at which the representation includes only the parameters x'_a , x'_b and n .

The values of the parameters x'_a , x'_b and n are found via the Babinet equivalence procedure using known results of the E-plane rectangular waveguide Tee as a basis. They are

$$n' = \frac{\sin(\pi D_3/\lambda)}{(\pi D_3/\lambda)} \quad (8-103)$$

$$n = n' \sqrt{\frac{D_3}{D_1}} \quad (8-104)$$

$$x_a' = -\frac{D_3}{\lambda} (0.785 n)^2 \quad (8-105)$$

$$l = 0 \quad (8-106)$$

$$x_b' = -\frac{x_a'}{2} + \frac{1}{(n')^2} \left\{ \frac{B_t}{2 Y_o} + \left(\frac{2 D_1}{\lambda} \right) x \right. \\ \left[\ln 2 + \frac{\pi D_3}{6 D_1} + 3/2 \left(\frac{D_1}{\lambda} \right)^2 \right] \} \quad (8-107)$$

Eq. (8-107) is valid for $\frac{D_3}{D_1} < 0.5$

where

$$\frac{B_t}{2 Y_o} = \left(\frac{2 D_1}{\lambda} \right) \left[\ln \csc \left(\frac{\pi D_3}{2 D_1} \right) \right. \\ \left. + 1/2 \left(\frac{D_1}{\lambda} \right)^2 \cos^4 \left(\frac{\pi D_3}{2 D_1} \right) \right] \quad (8-108)$$

$$x_b' = -\frac{x_a'}{2} + \frac{2 D_1}{(n')^2 \lambda} \left[\ln \left(\frac{1.43 D_1}{D_3} \right) + 2 \left(\frac{D_1}{\lambda} \right)^2 \right] \quad (8-109)$$

Eq. (8-109) is valid for $\frac{D_3}{D_1} > 0.5$

More recently Franco and Oliner⁶⁶ have modified the equivalent circuit for the Symmetric Tee Junction. The new equivalent circuit is shown as Fig. 8-29a and is derived as a result of work done at IBM, Stanford and Brooklyn Polytechnic Institute.

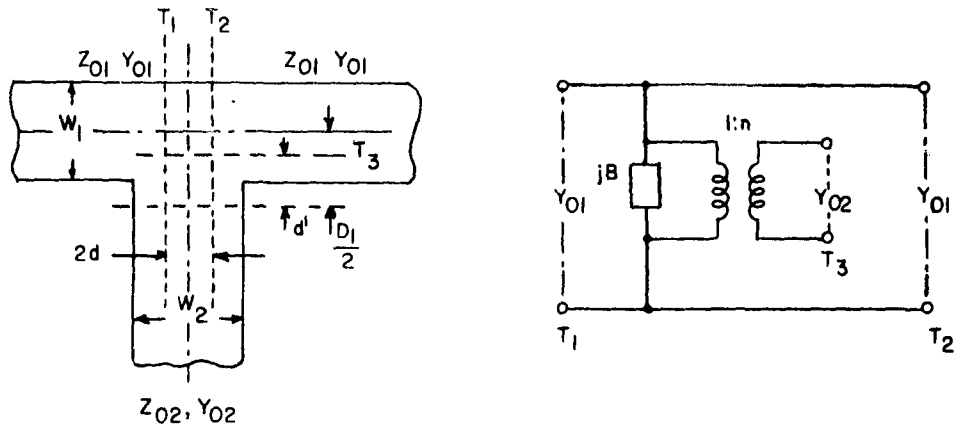


Fig. 8-29a: Recommended Equivalent Circuit for Stripline Tee Junction.

The equivalent circuit parameters are given by the following equations:

$$n^2 = \frac{n'^2 \cos^2 \left(\frac{2\pi}{\lambda} [d'_{wgh}] \right)}{\cos^2 \left(\frac{2\pi}{\lambda} d \right)} \quad (8-103A)$$

$$\frac{B}{Y_{01}} = 2 \tan \left(\frac{2\pi}{\lambda} d \right) - n^2 \frac{Y_{02}}{Y_{01}} \tan \left(\frac{2\pi}{\lambda} [d'_{wgh}] \right) \quad (8-104A)$$

$$\tan \left(\frac{2\pi}{\lambda} d \right) = -0.7 \frac{X_a}{Z_{01}} \quad (8-105A)$$

4. Parameter d'_{wgh} Reference Plane Shift in Stub Arm:

Measurements taken at Stanford Research Institute and IBM indicate that the best results for d'_{wgh} are gotten by using Fig. 6.1-9 of the Waveguide Handbook³⁹ with appropriate

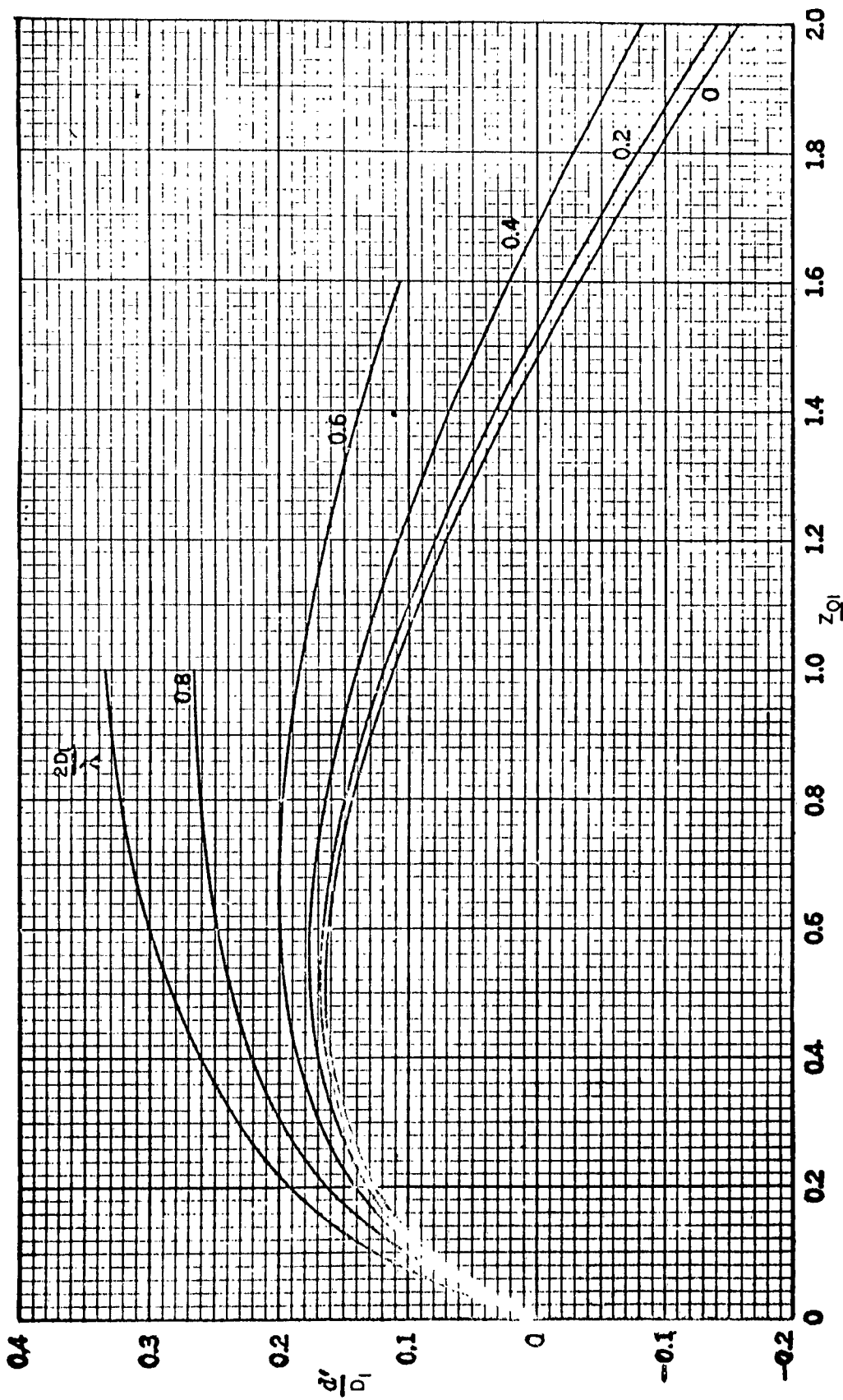


FIG. 8-29b -Location of terminal plane T' , for open E -plane T .

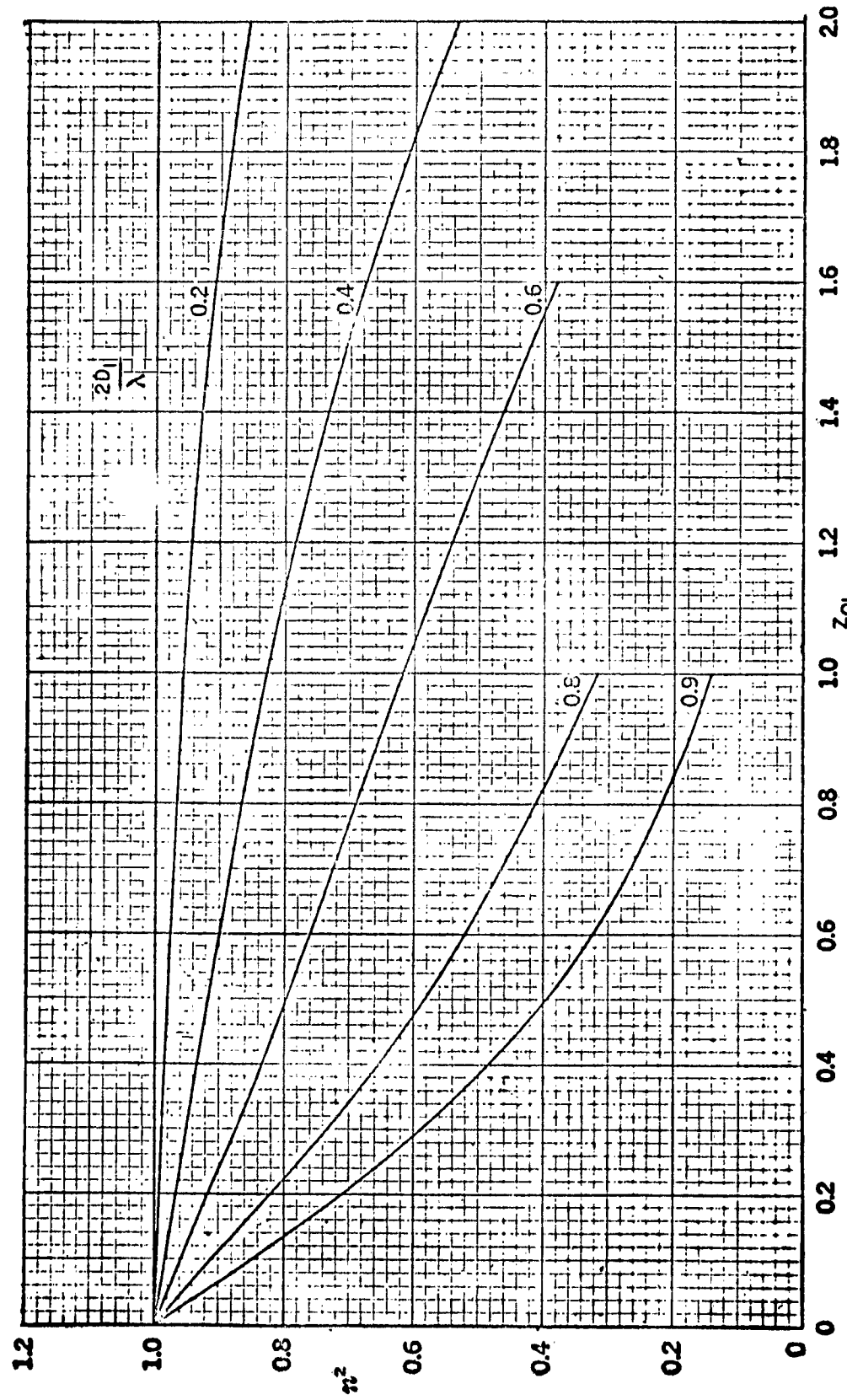


Fig. 8-29c — Transformer ratio for open E-plane T at terminals T_1 , T_2 .

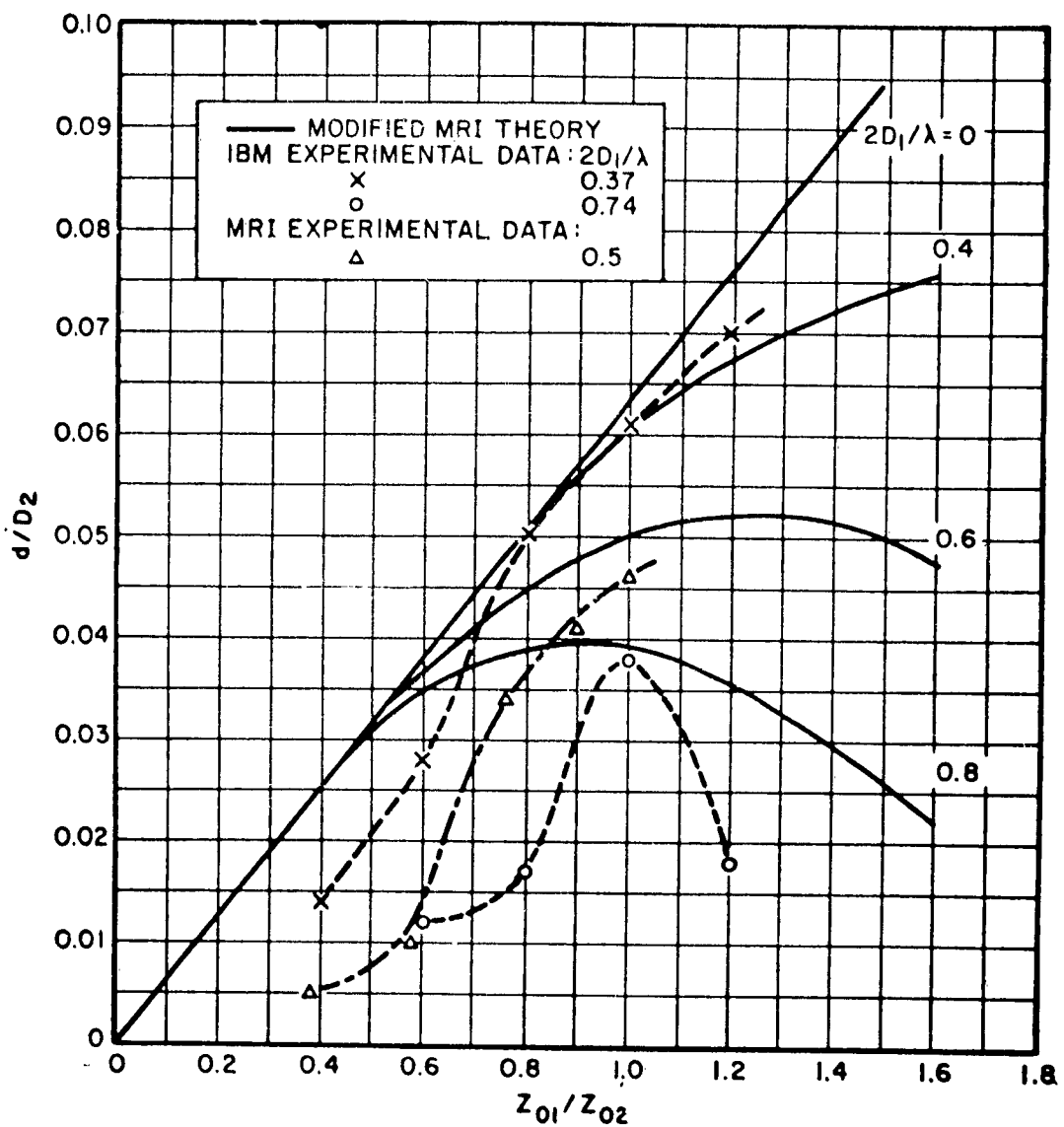


Fig.8-29d Comparison between available experimental data and theory for parameter d , the reference plane shift in the main arms.

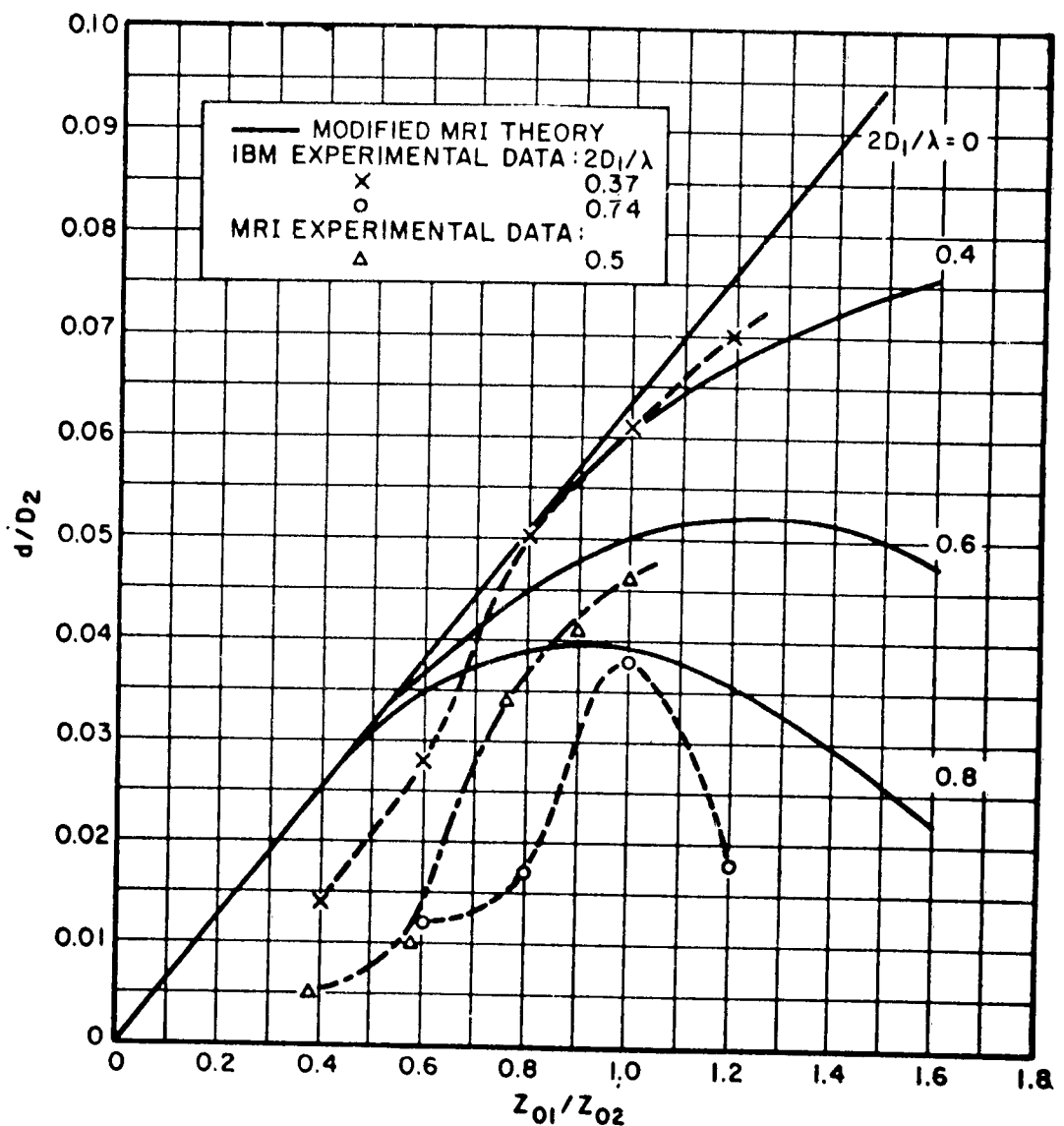


Fig. 8-29d Comparison between available experimental data and theory for parameter d , the reference plane shift in the main arms.

changes of notation. The use of E plane waveguide junction curves is justified through duality and Babinet equivalence. Fig. 8-29d is Fig. 6.1-9 with appropriate changes of notation. For values of $2 D_1/\lambda$ for which curves do not exist, one can either interpolate between curves or use (a) on page 338 of the Waveguide Handbook.³⁹

5. Parameter n--Transformer Turns Ratio:

Depending on the accuracy desired, several recommendations are possible, (a) Fig. 6.1-10 of the Waveguide Handbook³⁹ may be modified for Stripline use. This modified version is shown as Fig. 8-29c. For values of $2 D_1/\lambda$ not given on Fig. 8-29c and for $Z_{01}/Z_{02} \leq 1.0$, one can interpolate between the curves or use eq. 8-103A. In that equation, n' is given by eq. 8-103, d'_{wgh} has been discussed above, d is given by eq. 8-105A and X_a/Z_{01} is given by eq. 8-105. For values of $Z_{01}/Z_{02} > 1$ Franco and Oliner⁶⁶ recommend use of Fig. 8-29c.

6. Parameter d--Reference Plane Shift in Main Arm:

Comparison of measurements made by IBM, Stanford and the Microwave Research Institute shows that for $Z_{01}/Z_{02} < 1.0$, the IBM data should be used, while for $Z_{01}/Z_{02} \geq 1.0$, the MRI data is recommended. Fig. 8-29d displays these data in graphical form. The value of d is given by equation 8-105A and X_a/Z_{01} is

given by equation 8-106A:

$$\tan \left(\frac{2 \pi d}{\lambda} \right) = - \frac{x_a}{z_{01}} \quad (8-106A)$$

While a fair prediction of the parameter d may be obtained by the above described procedure except possibly in the particular region where $2 D_1/\lambda > 0.7$ and $z_{01}/z_{02} > 1.0$. In this region only a helpful upper bound is available.

Parameter B--Shunt Susceptance:

The parameter B should be determined from Fig. 8-29e. These curves are semi-empirical, having been determined from a combination of the MRI theory and the IBM measurements for d below $z_{01}/z_{02} < 1.0$. The MRI theory requires the computation of B via equation 8-104A. The curves are to be taken as fairly reliable except for $2 D_1/\lambda > 0.7$ and $z_{01}/z_{02} > 1.0$, where the experimental drop-off in d would indicate a lower value for B.

7. The Abruptly Ended Center Conductor:

An equivalent circuit for an abruptly ended center conductor has been developed by Altschuler and Oliner.⁶² The physical circuit and its equivalent network are shown as Fig. 8-29f. Since, to a crude approximation, an open circuit can be

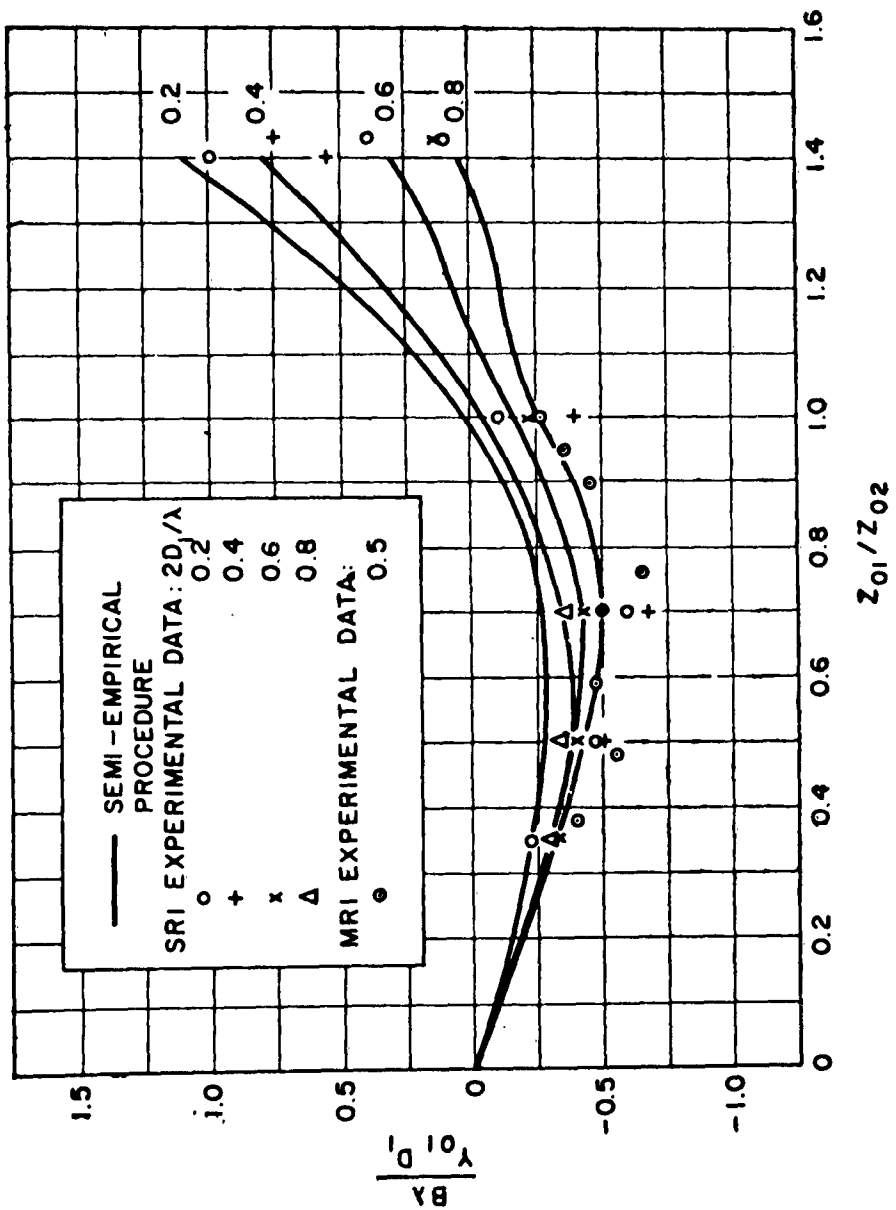
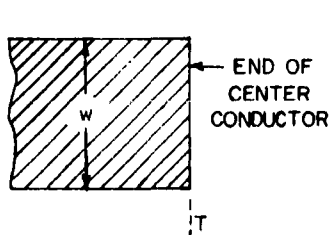
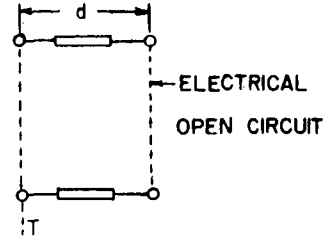


Fig. 8-29e—Comparison between available experimental data and a semi-empirical procedure for B , the susceptance element.



(a) PHYSICAL STRUCTURE



(b) EQUIVALENT CIRCUIT

Fig. 8-29f: Abruptly Ended Center Conductor

expected to occur at the plane T , the length of the transmission line d is quite small for practical transmission lines.

There is only one rigorous theoretical result that is applicable to this discontinuity; that of the static fringing capacitance of a conductor of infinite width. For this case $d = c$ where

$$c = \frac{b \ln 2}{\pi} \quad (8-110)$$

As usual b is the distance between ground planes. For the case in which the center conductor is not infinite, Oliner⁶² has developed a theoretical expression based on corner and edge fringing. The edge contribution is based on equation (8-110), while the corner expression was developed empirically from measured data. The resulting equation is

$$d = 1/k \cot^{-1} \left[\frac{4c + 2w}{c + 2w} \cot(kc) \right] \quad (8-111)$$

where

$$k = \frac{2\pi}{\lambda}$$

c defined by eq. (8-110)

w = width of the center strip

λ = wavelength in stripline

For most practical dimensions (kc small), eq. (8-111) can be approximated by eq. 8-112 which is

$$d = c \left(\frac{c + 2w}{4c + 2w} \right) \quad (8-112)$$

Inspection of eq. 8-112 shows it to be independent of both frequency and dielectric constant of the transmission line.

For $kc \leq 0.3$, eq. 8-112 approximates eq. 8-111 to 3%.

Equations 8-111 and 8-112 hold implicit the value of the empirically obtained corner fringing capacitance C_{cf} . Cohn⁶³ has independently derived an expression for d/b which includes the corner fringing capacitance as a parameter. Cohn's expression is for the case of two parallel coupled strips, one of which is open ended. In the limit as the strips become completely uncoupled, Cohn's expression reduces exactly to eq. 8-112.

The symbol C_f'' employed by these authors⁶³ is defined as one half of C_{cf} ; their empirical value for $2C_f''$ in micromicrofarads for a zero-thickness center strip is $0.019 \epsilon_r b$ where b is in inches and ϵ_r is the relative dielectric constant. The corresponding value of C_{cf} implicit in eq. 8-112 is $0.011 \epsilon_r b$.

E. Experimental Verification of Discontinuity Equivalent Circuits:

1. Experimental Setup:

a. Auxiliary Equipment:

Experimental verification of a number of the above derived formulas for various stripline discontinuities

was done by Stillman.⁶⁴ A block diagram of Stillman's measurement apparatus is shown as Fig. 8-30. Microwave power is obtained from a P.R.D. type 707 Klystron Oscillator which is powered and square-wave modulated by a P.R.D. 801-A power supply. For frequency monitoring, a small amount of output power is abstracted through a coaxial tee and fed into a high Q cavity. After detection and amplification, the signal drives a meter which gives a maximum indication at the resonant frequency of the cavity. A low pass filter is used to prevent any of the spurious modes generated by the oscillator from reaching the test apparatus. In the test apparatus, field amplitude in the presence of the discontinuity of interest is measured as a function of position. Measurements were made at 1500 mc with 1000 cycle square wave modulation.

b. The Measurement Apparatus:

The measuring apparatus is essentially a standard impedance measuring setup consisting of a standing wave indicator followed by the discontinuity, which in turn is terminated in a variable short circuit. Fig. 8-31 is a blown-up view of the apparatus under consideration. The upper ground plane is shown in an exploded view. The carefully machined ground planes are supported by cylindrical spacers. The center conductor is supported at the input end by a clamp which is made as small as possible to keep the associated discontinuity reasonably low. A number of interchangeable center

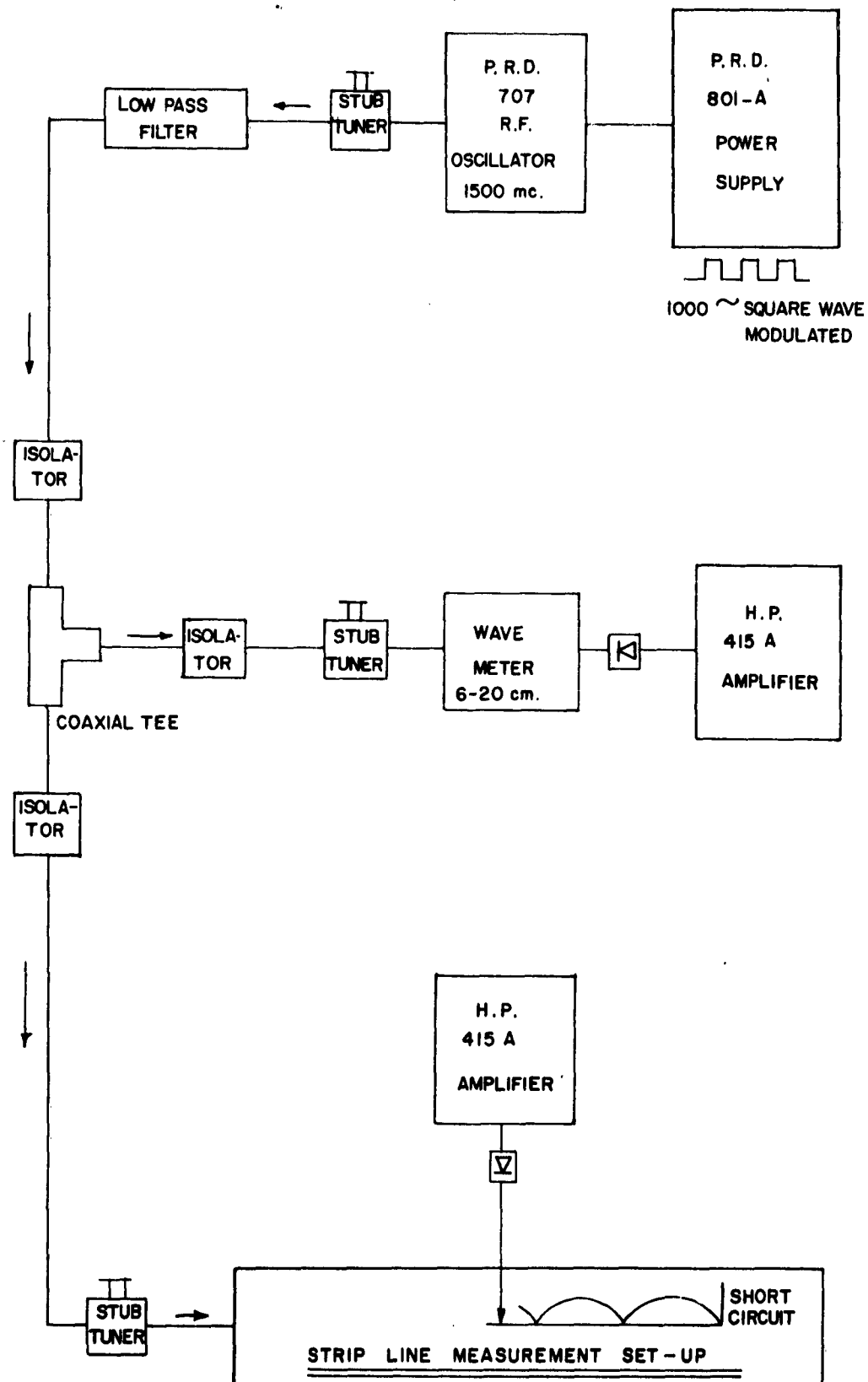
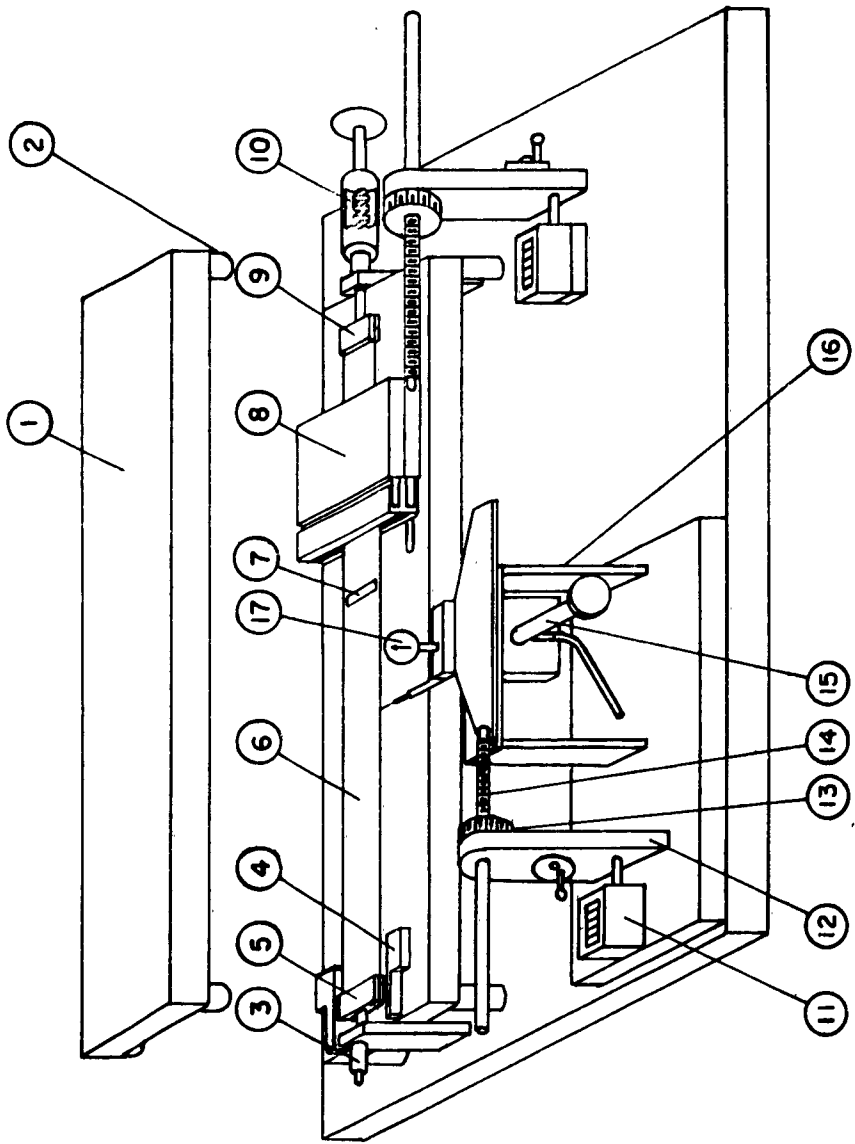


Fig. 8-30 BLOCK DIAGRAM OF MEASUREMENT EQUIPMENT



1	UPPER GROUND PLATE	5	INPUT CLAMP	9	END CLAMP	13	VERNIER	17	DIAL GAUGE
2	SUPPORT	6	STRIP	10	TENSION SPRING	14	DRIVING SCREW		
3	INPUT CONNECTOR	7	DISCONTINUITY	11	REVOLUTION COUNTER	15	PROBE		
4	MODE SUPPRESSOR	8	CHOKE SHORT CIRCUIT	12	GEAR TRAIN	16	STANDING WAVE METER		

FIG. 8-3I. MEASUREMENT APPARATUS, SKETCH OF FRONT VIEW.

strips were made, each one containing a different discontinuity. Two mode suppressor plates are placed near the input in order to discriminate strongly against the radiating (parallel plate) TEM mode. A side probing arrangement is used in order to distract the field pattern as little as possible. This probe is driven by a set of gears having a revolution counter with an accuracy of ± 0.0001 inch readability. The probe itself is a standard arrangement modified by adding a sleeve to prevent droop. Vertical as well as horizontal movement of the probe is possible, the distance from the bottom ground plane being indicated by a dial. An adjustment is also provided to bring the probe travel into parallelism with the center strip. A movable choke-type short circuit is employed. Movement is guided by a groove in the bottom ground plane and its magnitude is measured by a counter arrangement similar to that used on the probe carriage. A "sandwich" type of construction is used in the short circuit in order that the center conductor can be easily changed. A clamp holds the end of the center strip behind the variable short circuit. This end clamp also transmits the force of a variable tension spring to the center strip.

Construction of the center strip proved to be a considerable problem. A flat thin strip supported by end clamps and surrounded by air was used since it came nearest to meeting the assumptions of the theoretical derivation of Characteristic Impedance. A Characteristic Impedance of 50 ohms was chosen resulting in a center strip of 1.5 inches in width and a ground plane spacing of 1.051

inches. These large dimensions helped reduce mechanical problems and increase accuracy. Tension in the center strip tended to cause undesirable deformations in the neighborhood of the center strip discontinuities. A satisfactory construction was finally arrived at by using a 0.001 inch "Mylar" polyester film sandwiched between two 0.001 inch copper strips. The discontinuity was cut in both copper strips but not in the "Mylar." After assembly with teflon cement, a thickness of 0.0035 inch resulted. Deformation was further minimized by making cuts in the copper strips perpendicular to the direction of tension and placing the strips in tension for several hours for stress relief.

2. Measurement Procedure Based on the Tangent Network

Relations:

In section C-2-g of this chapter relations are developed for the tangent network equivalent circuit.

In review, the tangent relation network consists of three real parameters, depicted in Fig. 8-32 as two lengths of transmission line of length $-D_o$ and $-S_o$ coupled by a transformer having a turns-ratio of

$$n = \sqrt{-\gamma} : 1$$

The three parameters of this lossless network relate, at T_1 ($= D_R$) and T_2 ($= S_R$), the input quantities D (similar to Z_{in} , Y_{in} , etc.) to the output quantities S (corresponding to Z_{out} , Y_{out} , etc.).

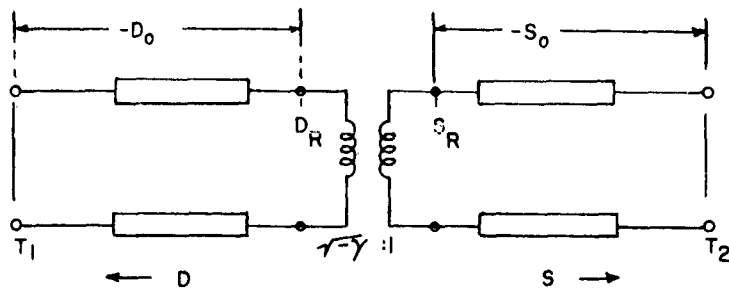


Fig. 8-32: Tangent Relation Network

The tangent relation network is based on the nodal shift method. Let us consider the circuit of Fig. 8-33. Suppose, as illustrated in Fig. 8-33, that the transmission line in region II is terminated in its own Characteristic Impedance. As a rule, standing waves will occur in region I. The position of the voltage maximum in region I defines the position of the terminals 1 - 1. The resultant VSWR in region I is defined by the symbol γ . If Z_1 is the Characteristic Impedance of region I, then

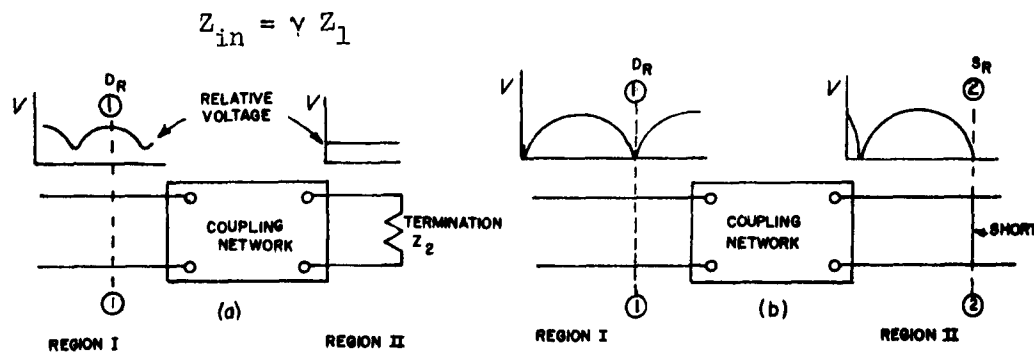


Fig. 8-33: Procedure for choosing reference planes in the two regions, (a) the network is perfectly terminated, (b) region II is shorted.

Now, suppose region II is shorted. As shown in Fig. 8-33b, the voltage mode will appear somewhere in region I, its position being controlled by the position of the short in region II. If the short in region II is moved until a voltage mode appears at the terminals 1 - 1 ($Z_{in} = 0$), then the position of the short is defined as the terminals 2 - 2.

In general four-terminal network theory, there is a theorem which states that input and output impedances, Z_{in} and Z_{out} respectively of a linear passive network can be related through the expression

$$Z_{in} = \frac{A Z_{out} + B}{C Z_{out} + D} \quad (8-114)$$

Using eq. 8-113 and defining Z_2 as the Characteristic Impedance in region II, eq. 8-114 becomes

$$\gamma Z_1 = \frac{A Z_2 + B}{C Z_2 + D} \quad (8-115)$$

To evaluate the constants A, B, C, and D consider the shorted condition. For this case $Z_{out} = 0$ and $Z_{in} = 0$; hence $B/D = 0$. Consequently, $B = 0$. The four-terminal network under consideration is assumed to be lossless. A lossless network implies that the constants A and D of eq. 8-114 be real and the constants B and C of that equation be imaginary. Since rZ_1 and Z_2 are real, eq. 8-115 requires that $C = 0$. Thus, with the terminals 1 - 1 and 2 - 2 chosen as discussed above, $A/D = \gamma Z_1/Z_2$, transforming eq. 8-114 to read

$$Z_{in} = \gamma \left(\frac{Z_1}{Z_2} \right) Z_{out} \quad (8-116)$$

To determine the parameters of the coupling network, place a short circuit a distance S_2 ($= |S - S_R|$) to the right of the terminal 2 - 2 as illustrated in Fig. 8-34. The impedance Z_{out} will be

$$Z_{out} = j Z_2 \tan \beta_s S_2 \quad (8-117)$$

where

β_s = propagation constant in region II

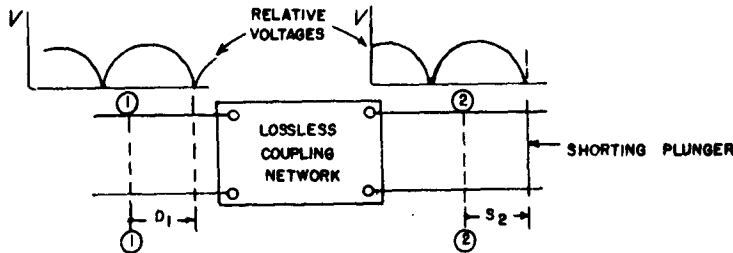


Fig. 8-34: Distribution of electric field on the two sides of the coupling network due to the shorting plunger in region II.

As indicated in Fig. 8-34, this short circuit creates a voltage node to the right of the terminal 1 - 1. The impedance Z_{in} is then

$$Z_{in} = j Z_1 \tan \beta_d D_1 \quad (8-118)$$

where

β_d = propagation constant in region I

If now eq. 8-116 is substituted in eq. 8-118 and the result is substituted in eq. 8-117, there is obtained

$$\tan \beta_d D_1 = \gamma \tan \beta_s S_2 \quad (8-119)$$

If arbitrary lengths of transmission line ($-D_o$ and $-S_o$) are added at the 1 - 1 and 2 - 2 terminals respectively, as indicated by Fig. 8-32, the terminals 1 - 1 and 2 - 2 are shifted to $D' = D_R + (-D_o)$ and $S' = S_R + (-S_o)$. Eq. 8-119 then becomes

$$\tan \beta_d | D - D' | = \gamma \tan \beta_s | S - S' | \quad (8-120)$$

If a short circuit in region II is allowed to assume various positions S , the sum of S and the corresponding voltage mode positions D in region I may be plotted vs. S to yield the tangent parameters. Fig. 8-35 illustrates a typical plot. This plot represents a graphical averaging of the data points. Two lines are then drawn through the peaks of the curve bounding

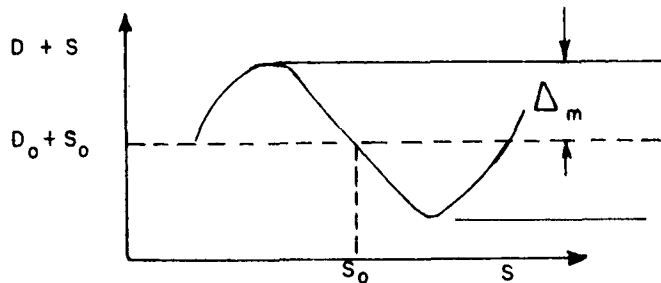


Fig. 8-35: $D + S$ vs. S Curve

it from above and below. These boundary lines are not always parallel to the abscissa (or to each other) and correction of the slope is necessary. Correction is achieved by taking the average slope of the boundary lines and using it in the relation

$$D_{\text{corrected}} = D_{\text{measured}} (1 + \text{slope}) \quad (8-121)$$

to obtain new values of D . These values of D are then used to plot a new $D + S$ curve. The process is repeated until no slope

is observable. A line is then constructed perpendicular to the two boundary lines and bisected. A new line is drawn through the bisecting line parallel to the boundary lines. Intersection of this "bisecting" line with the D + S curve at a point of negative slope gives S_o directly. The construction is illustrated in Fig. 8-35. Stillman⁶⁴ states that if Δ_m is defined as the maximum distance between the "bisecting line" and the D + S curve, $-\gamma$ may be calculated from the relation

$$-\gamma = 1 + 2 \tan \delta (\tan \delta + \sec \delta) \quad (8-122)$$

where

$$\delta = \frac{2\pi}{\lambda_g} \Delta_m \quad (8-123)$$

$$\tan \delta = \frac{1 + \delta}{2\sqrt{-\delta}} \quad (8-124)$$

In expression 8-123, λ_g is guide wavelength. For $\delta < < 1$, the approximation may be made

$$-\gamma = 1 + 2\delta \quad (8-125)$$

The above procedure results in semi-precision values for the parameters. However, these first approximations for D_o , S_o and $-\gamma$ may be used as a starting point for a precision analysis where accuracies are limited to the random errors of measurement. To obtain more precise values for D_o , S_o and $-\gamma$, the tabulated values of S (obtained by moving the short in region II) are used in the equation

$$D_{comp} = D_o + \frac{\lambda_g}{2\pi} \tan^{-1} \left[\gamma \tan \frac{2\pi}{\lambda_g} (S - S_o) \right] \quad (8-126)$$

together with the semi-precision values of D_0 , S_0 and γ to obtain new values of D . If there were no errors, the values of D computed would be equal to the actual values of D measured. If an error curve is plotted with $\Delta D = D_{\text{comp}} - D_{\text{measured}}$ as ordinate and S as abscissa, a figure like that of Fig. 8-36 results.

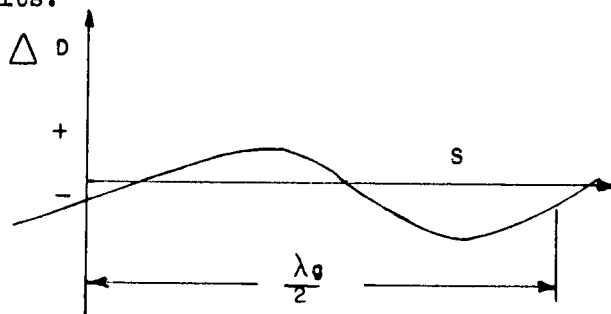


Fig. 8-36: First Error Curve

If the error curve exhibits some regularity (say periodicity in $\lambda_g/2$ etc.) due to some systematic error in one of the first order parameters, further analysis may be performed by comparing the ΔD curve with a ΔD_{comp} curve (total differential of eq. 8-126). This process is repeated until the error curve no longer displays regularity but results in ΔD 's which are scattered in random fashion as shown in Fig. 8-37. The average

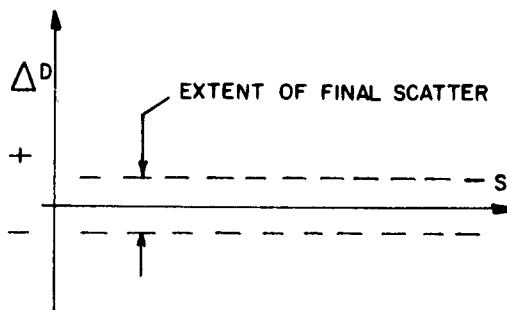


Fig. 8-37: Final Error Curve

deviation of the final error curve leads to the tolerances that may be placed on the corrected parameters. These errors represent "electrical" errors. In addition the "mechanical" errors due to physically located D_o and S_o must be taken into account.

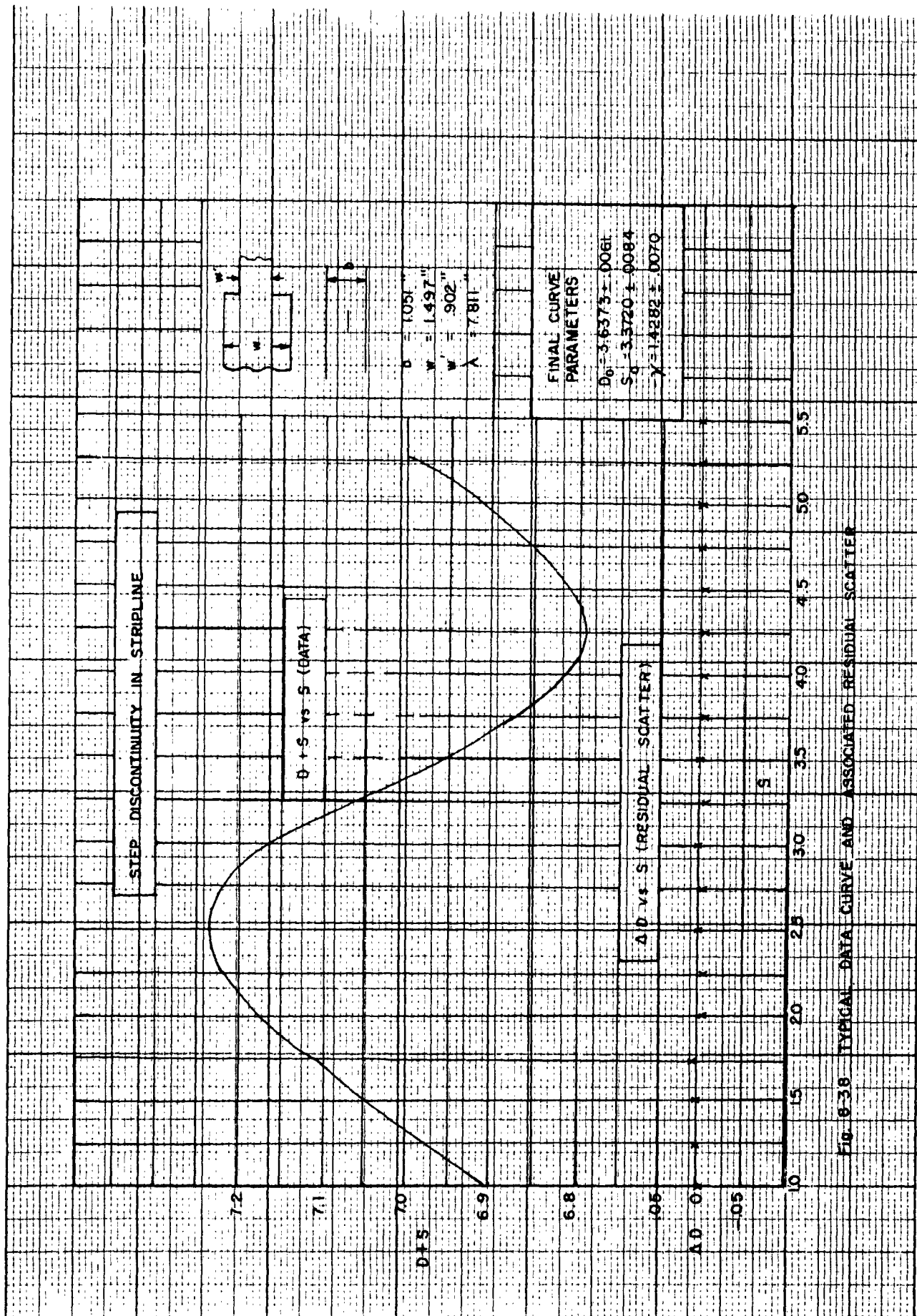
The quality of Stillman's measurements can be seen by looking at several values of γ as reported in his thesis. They were $|\gamma| = 1.167 \pm 0.006$, $|\gamma| = 1.422 \pm 0.008$, and $|\gamma| = 1.48 \pm 1.5$. If a comparison is made with measurements made in precision waveguide having a $- \gamma$ of 1.5, it is seen that typical tolerances range from 0.002 to 0.007 while Stillman's Stripline measurements tolerances for the same $- \gamma$ were 0.006 to 0.010.

An application of $D + S$ vs. S curve to obtain the parameters D_o , S_o and $- \gamma$ for a step discontinuity in Stripline is shown as Fig. 8-38. The sinusoidal curve represents the $D + S$ vs. S plot, while the error curve is shown in the bottom of the figure.

3. Theoretical Relations for Determining Discontinuity

Equivalent Circuits from D_o , S_o and $- \gamma$:

In order that a comparison may be made between equivalent circuits determined experimentally and those determined through measurement, it is necessary to develop a set of relations that will determine a four terminal equivalent network from the tangent relation parameters. Such a set of relations can be found in the Waveguide Handbook³⁹ on page 121.



Through appropriate manipulation, these equations can be modified to fit the case under discussion.

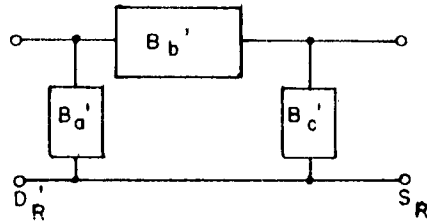


Fig. 8-39: Generalized Equivalent Pi Network.

Fig. 8-39 illustrates the generalized Pi equivalent network. Its parameters β_a' , β_b' , β_c' are given by the following development.

Given

$$D_o, S_o, -\gamma, D_R, \lambda_g$$

Find

$$\beta_{11}', \beta_{22}', \beta_{12}', \beta_{11}' - \beta_{22}' - \beta_{12}'^2$$

Define

$$\alpha = -\cot \frac{2\pi}{\lambda_{g1}} (D_o - D_R) \quad (8-127)$$

$$\beta = -\cot \frac{2\pi}{\lambda_{g2}} (S_o - S_R) \quad (8-128)$$

$$a = -\left(\frac{\alpha \beta + \gamma}{\beta - \alpha \gamma}\right) \quad (8-129)$$

$$b = \left(\frac{\alpha - \beta \gamma}{\beta - \alpha \gamma}\right) \quad (8-130)$$

$$c = \frac{1 + \alpha \beta \gamma}{\beta - \alpha \gamma} \quad (8-131)$$

$$d = \frac{\gamma (1 + \alpha^2) (1 + \beta^2)}{(\beta - \alpha \gamma)^2} \quad (8-132)$$

then

$$\begin{aligned} B_{11}' &= a; B_{22}' = c; B_{11}' B_{22}' - B_{12}'^2 = -b; \\ B_{12}'^2 &= -d; B_{12}' = \pm j(d)^{1/2} \end{aligned} \quad (8-133)$$

and

$$B_b' = B_{12}'; B_a' = B_{11}' - B_{12}'; B_c' = B_{22}' - B_{12}' \quad (8-134)$$

4. Gap and Slot in the Center Conductor:

A theoretical derivation for the slot is given in section D-1-a of this chapter along with its range of validity.

Similarly the theoretical derivation for the slot is given in section D-1 b. Stillman obtained experimental values of the tangent relation parameters D_o , $-y$ and S_o . Through the use of equations 8-127 through 8-134 he obtained values of B_a , B_b and B_c . Since the assumed discontinuity structure is symmetrical, B_a and B_c are averaged. Table 8-1 summarizes the data. The parameters d and s are those referred to Fig. 8-14 and Fig. 8-15.

For conciseness define

$$B_a' = \frac{B_a}{Y_o} \quad (8-135)$$

$$B_b' = \frac{B_b}{Y_o} \quad (8-136)$$

as determined from the theoretical formulas. Figs. 8-40 and 8-41 graphically illustrate the correlation between the theoretically and experimentally determined parameters B_a' and B_b' .

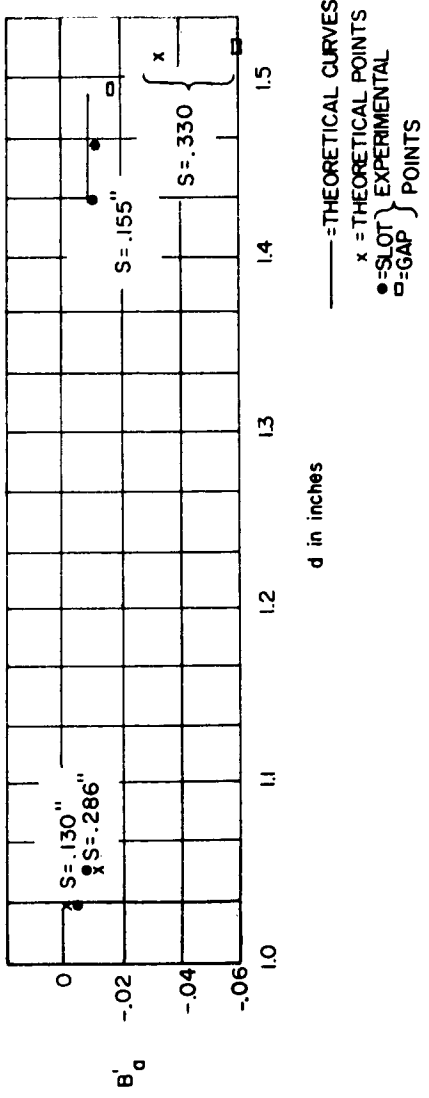


Fig. 8-40. CIRCUIT PARAMETERS OF SLOTS AND GAPS

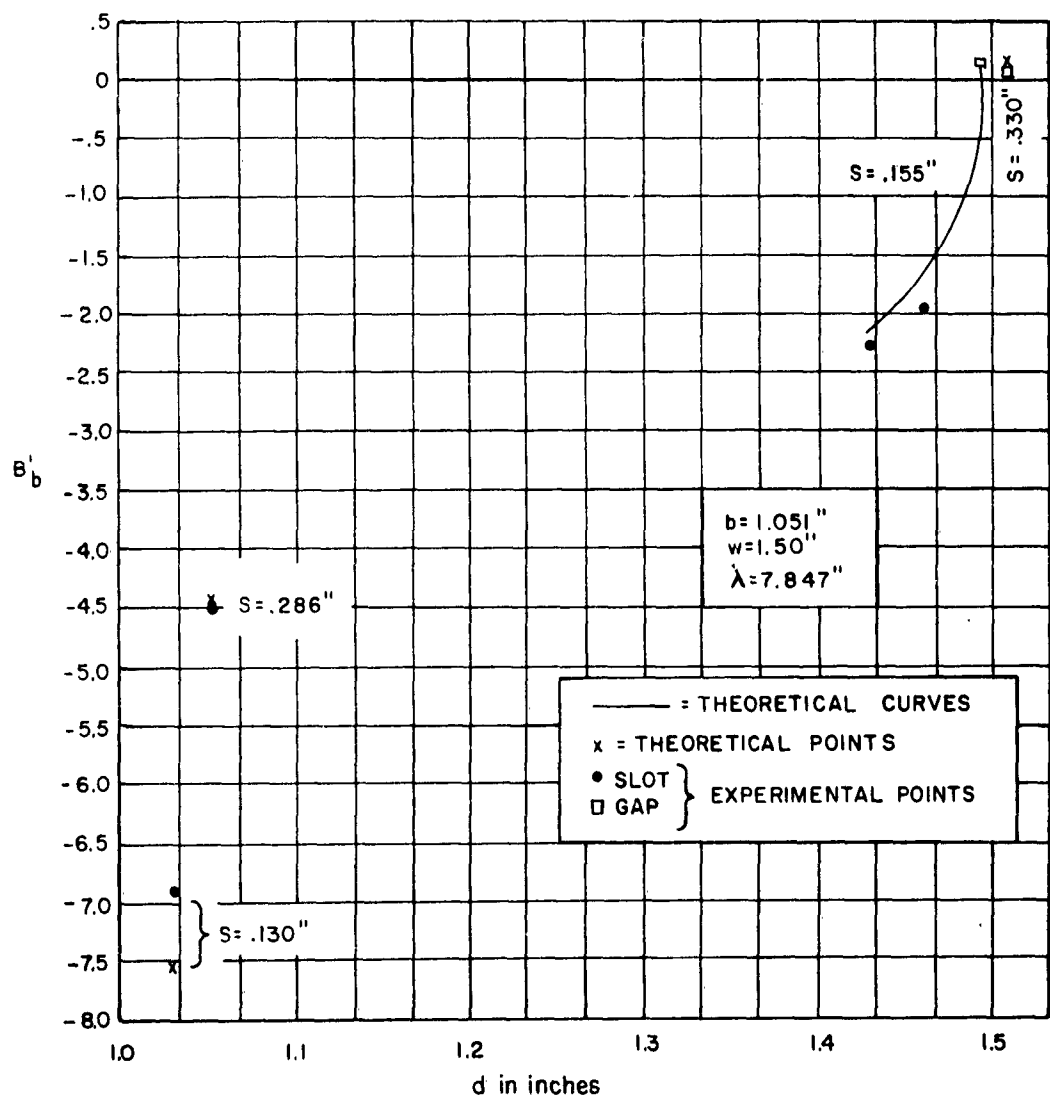


Fig.8-41.CIRCUIT PARAMETERS OF SLOTS AND GAPS

TABLE 8-1
Gap and Slot in Center Conductor

$$b = 1.051" \lambda = 7.874"$$

d	S	-γ	B_a'		B_b'	
			Theo.	Exp.	Theo.	Exp.
1.030	0.130	1.1665	-0.0032	-0.0044	-7.5575	-6.8805
1.050	0.286	1.2738	-0.0154	-0.0103	-4.4188	-4.4832
1.430	0.155	1.5815	-0.0066	-0.0085	-2.1266	-2.2451
1.460	0.155	1.7053	-0.0068	-0.0104	-1.717	-1.9256
1.490	0.155	41.000	-0.0072	-0.0147	0.1991	0.1594
1.513	0.330	148.00	-0.0318	-0.0598	0.0918	0.0825

The range of validity of the gap formulas is $b/2\lambda < < 1$, while those for the slot are valid for the range $\tau \geq 0.15$ and $d/w \geq 0.25$. In the measurement $b/2\lambda = 0.067$, while $\tau_{min.} = 0.136 < 0.15$, $d/w_{min.} = 0.87$. It can be seen that for $S = 0.130$, τ falls somewhat below the stated range of validity of the theoretical formulas. Reference to Fig. 8-41 shows that it is only for $S = 0.13$ that a considerable discrepancy exists between measured and theoretically determined parameters. Of special interest is the value of d for which the curve ($S = 0.155$) of B_b' passes through zero. It is at this value of d (1.49") that the slot is series resonant. The slot is seen to be very sensitive to its dimensions making it impractical as a resonant structure. The value of B_a' , shown in Fig. 8-39 is much smaller than B_b' . A consistent error seems to exist between measured and theoretical points.

5. Round Hole in the Center Conductor:

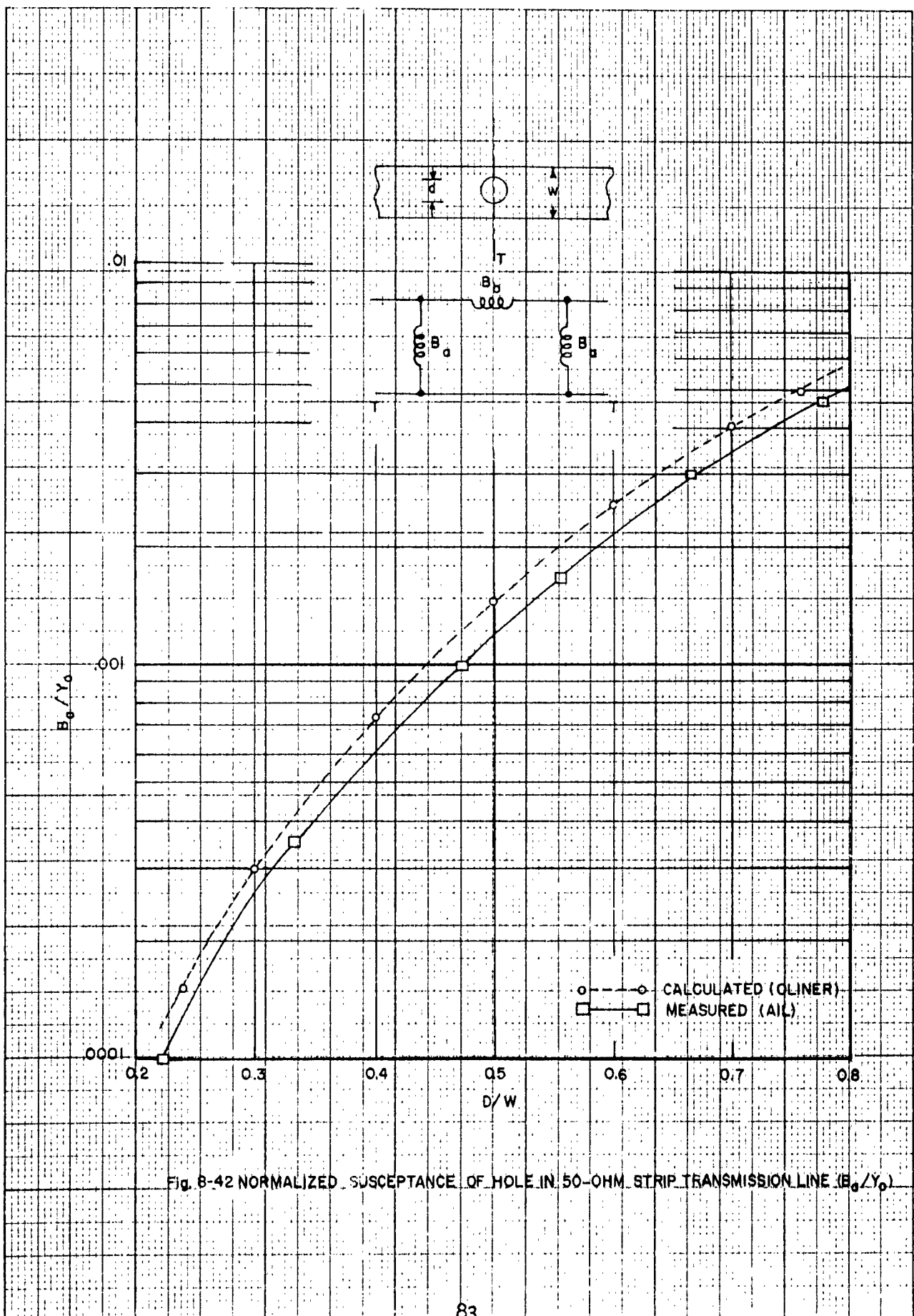
A theoretically determined equivalent circuit for a round hole in the center conductor is given in section D-2-a of this chapter. Component values are given by equations (8-85) and (8-86). Measurements were made on this discontinuity by the Airborne Instruments Laboratory.⁶⁵ Their results are shown as Fig. 8-42 and Fig. 8-43. In both cases a consistent error seems to result.

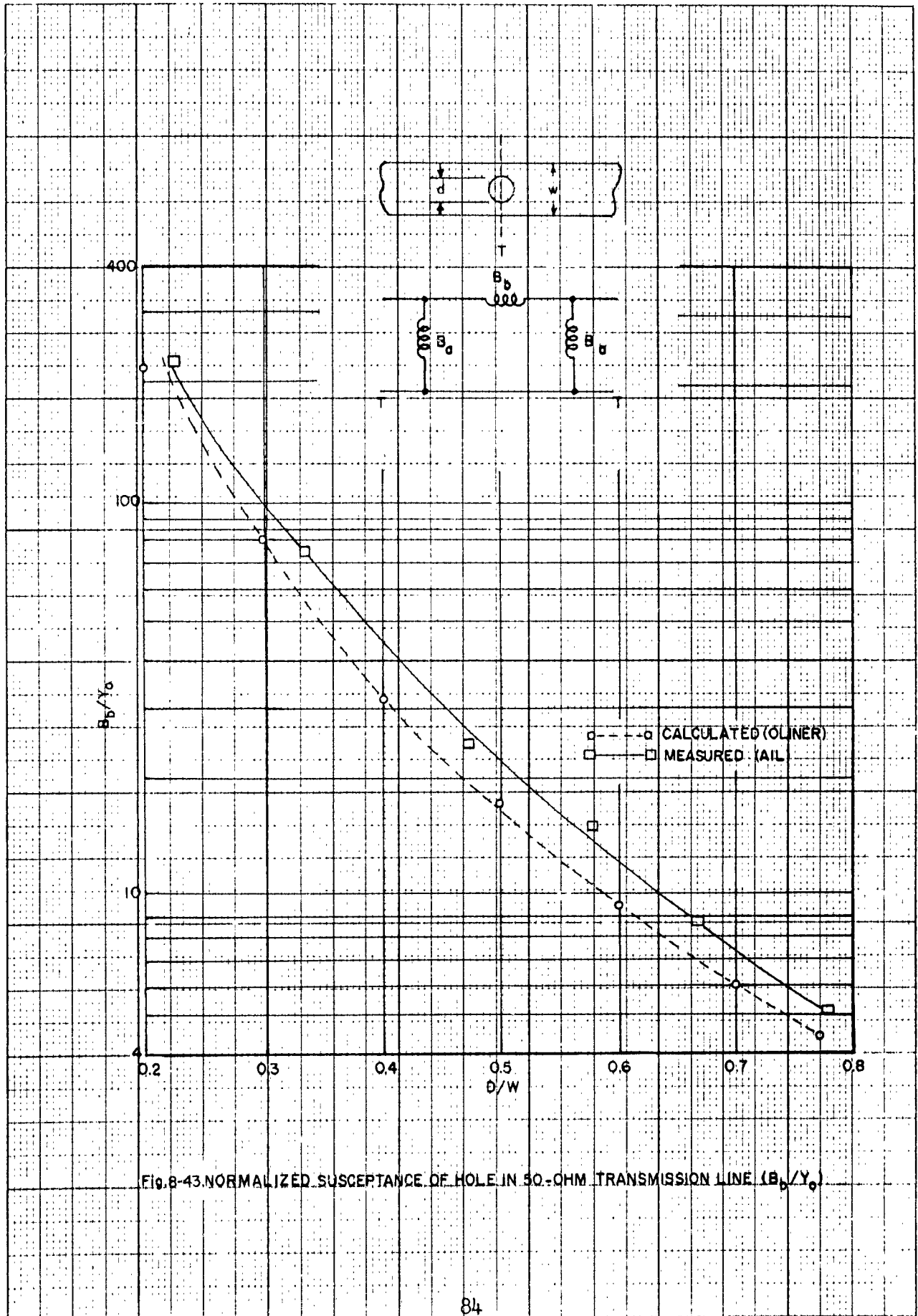
6. Abruptly Ended Center Conductor:

The equivalent circuit for the abruptly ended center conductor is discussed in section D-4. Altshuler and Oliner⁶² did some experimental work with this discontinuity resulting in Fig. 8-44. Measurements were made at six different wavelengths ranging from $\lambda = 5.4"$ to $\lambda = 11.8"$. The "bars" crossing the theoretical curves result from both scatter and the small variation of d/b with frequency. The theoretical curve is based on eq. 8-112.

7. Relationship Between Series Reactance Network and Tangent Network:

Before a comparison can be made between measured and theoretically determined equivalent circuits for a step in the center conductor, a set of relations between the tangent equivalent network and the series reactance equivalent network must be derived. The results are stated in the literature in the form of a series reactance network or can be seen by referring to Fig. 8-28. On the other hand, the measurements give the





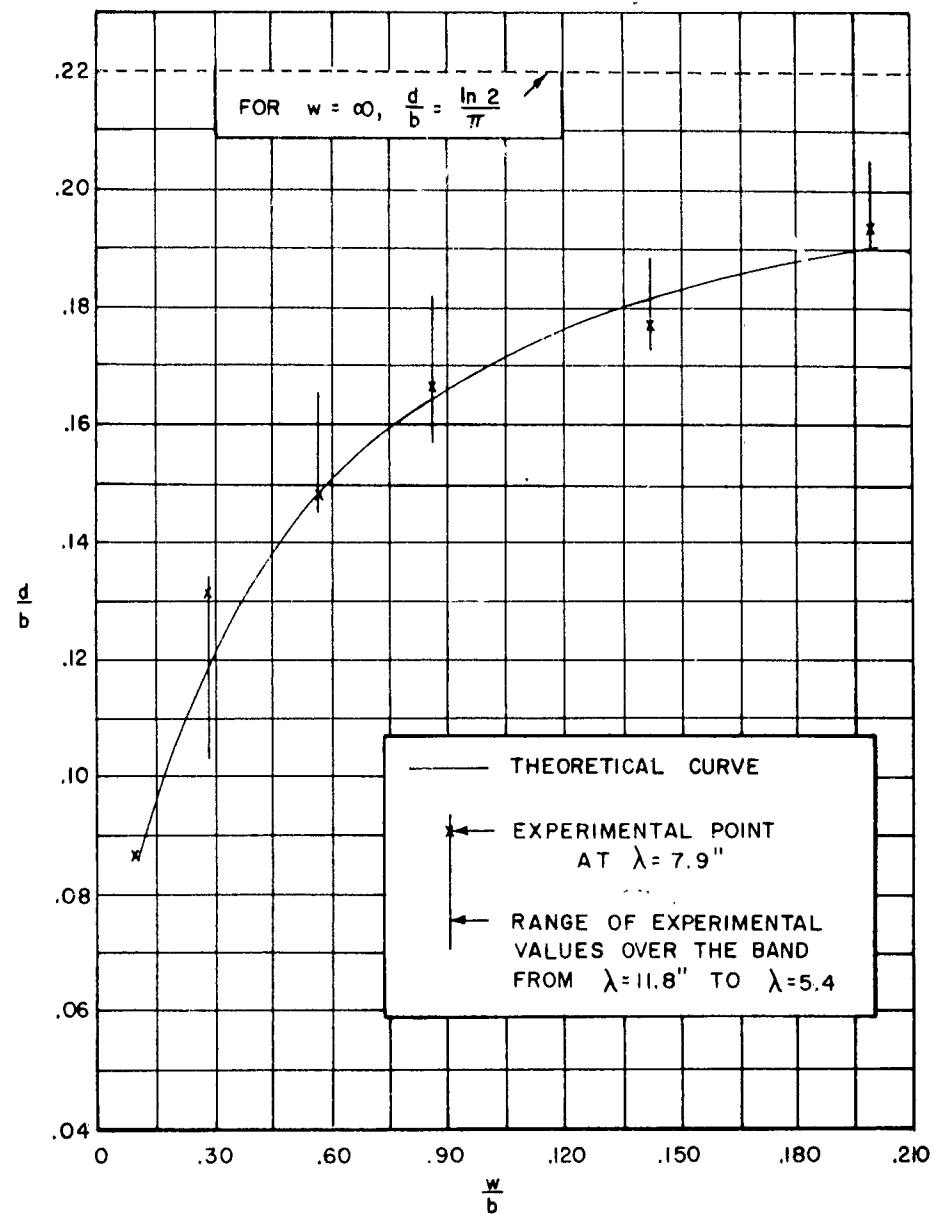


Fig. 8-44. LOCATION OF EQUIVALENT OPEN CIRCUIT FOR ABRUPTLY-ENDED CENTER CONDUCTOR

parameters D_o , S_o and γ . The tangent relation equivalent network is developed through the transformations of section E-3. The series reactance network is then derived from the relations to be developed in this section.

In order to spare the casual reader the trouble of wading through the derivation, only the results are stated here. The more careful reader will find the complete derivation in Appendix XI. Fig. 8-45 illustrates the two equivalent circuits referred to in the transformation.

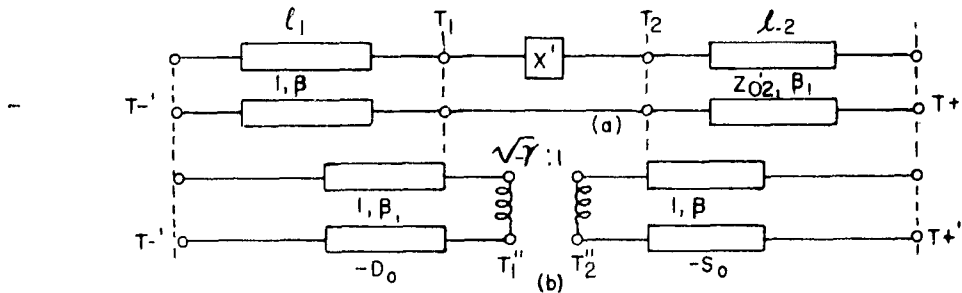


Fig. 8-45: Tangent and Series Reactance Networks.

Given

$$D_o, S_o, -\gamma$$

Find

$$X', l_1, l_2$$

$$x' = \left[\frac{z_{02}'}{|\gamma|} (\gamma^2 + 1) - (z_{02}'^2 + 1) \right]^{1/2} \quad (8-137)$$

where

$$z_{02}' = \frac{z_{02}}{z_{01}} \text{ and } X' = \frac{X}{z_{01}}$$

Z_{01} and Z_{02} are the Characteristic Impedance of the input and output transmission lines respectively,

$$l_2 = 1/\beta \left[\cot^{-1} (\xi \pm \sqrt{\xi^2 + 1}) \right] \cdot s_o \quad (8-138)$$

where

$$\xi = \left(\frac{1 + X'^2}{2 X'} - \frac{Z_{02}'}{Z_{02}} \right)$$

$$l_1 = 1/\beta \cot^{-1} \left[X' + Z_{02}' \cot \beta (l_2 + s_o) \right] - D_o \quad (8-139)$$

The plus sign in eq. (8-138) is used if $Z_{02}' > 1$. The minus sign is used when $Z_{02}' < 1$.

8. Step Change in Width of the Center Conductor:

Fig. 8-46 shows the physical configuration for a sudden change in width in the center conductor. In section D-3-f of this chapter a theoretically determined series

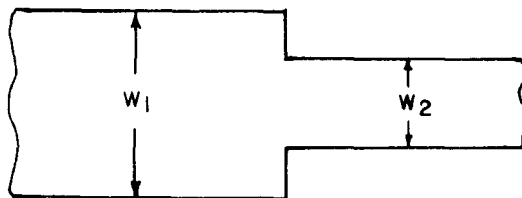


Fig. 8-46: Sudden Change in Width of the Center Strip. reactance equivalent circuit is given for a sudden change of width. The parameter of this equivalent circuit is given by eq. 8-101.

Measurements of this discontinuity were made by Stillman.⁶⁴

Theoretical and experimental values for some circuit parameters are given in the table below. The values given assume various wavelengths very close to 7.8 inches strip widths w_1 nearly equal

to 1.5 inches and a ground plane spacing maintained at $b > 1.05$ inches. Theoretical values of γ are found by solving eq. 8-137 for γ , resulting in

$$\gamma = a + \sqrt{a^2 - 1} \quad (8-140)$$

where

$$a = \frac{x'^2 + Z_{02}' + 1}{2 Z_{02}} \quad (8-141)$$

Table 8-2: Sudden Change in Width of Center Conductor.

w_2 inches	Theoretical Z_{02}'	γ	x'	Exp'l. γ
.152	3.375	3.429	.408	$3.348 \pm .035$
.310	2.577	2.614	.287	$2.614 \pm .025$
.600	1.842	1.857	.142	$1.825 \pm .013$
.902	1.436	1.440	.059	$1.428 \pm .007$
1.205	1.174	1.175	.014	$1.204 \pm .018$

It should be noted, in Table 8-2, that the theoretical values for Z_{02}' and γ and the experimental values of γ , all fall very close to one another, differences between corresponding values being roughly of the order of one per cent. It is immediately possible to conclude that changes in Z_{02}' dominate by far over changes in x' in eq. 8-140. Since experimental values of x' are obtained from eq. 8-137, it follows that x' is extremely sensitive to even the smallest errors in both Z_{02}' and γ . This is indeed the case, in fact so much so that the experimentally determined value of x' were completely

unreliable and are not included. Theoretical values, however, have been tabulated. While the experiments performed have not verified these theoretical values, they do indicate that the magnitudes of X' are correct.

Consideration of Table 8-2 then leads to the conclusion that the step in width of the center conductor is well approximated at the step by only the transformer ($\sqrt{Z_{02}} : 1$) (Fig. 8-45b with $- \gamma = Z_{02}'$). Also the series reactance X' is negligible for most practical purposes.

The data in Table 8-2 are used to plot the graph of Fig. 8-47. It can be seen from this figure that a straight line drawn through the nominal values of $|\gamma|$ measured differs from the theoretical value of $|\gamma|$, by an amount almost accountable for by the neglected series reactance. This difference is emphasized especially where the tolerances, which bound the nominal $|\gamma|$ measured, almost include the theoretical values.

9. Sharp Angle Bends in the Center Conductor:

Because of an inability to mount discontinuities not beginning and ending on the same longitudinal axis in the measuring apparatus, it was necessary to construct a composite discontinuity consisting of a number of bends in succession. Each composite discontinuity was made symmetrical about a center line normal to the strip axis and at the geometric center of the discontinuity. This, to measure a single right angle bend, a discontinuity structure of four identical bends had to be measured. The data for a single bend was then abstracted through matrix

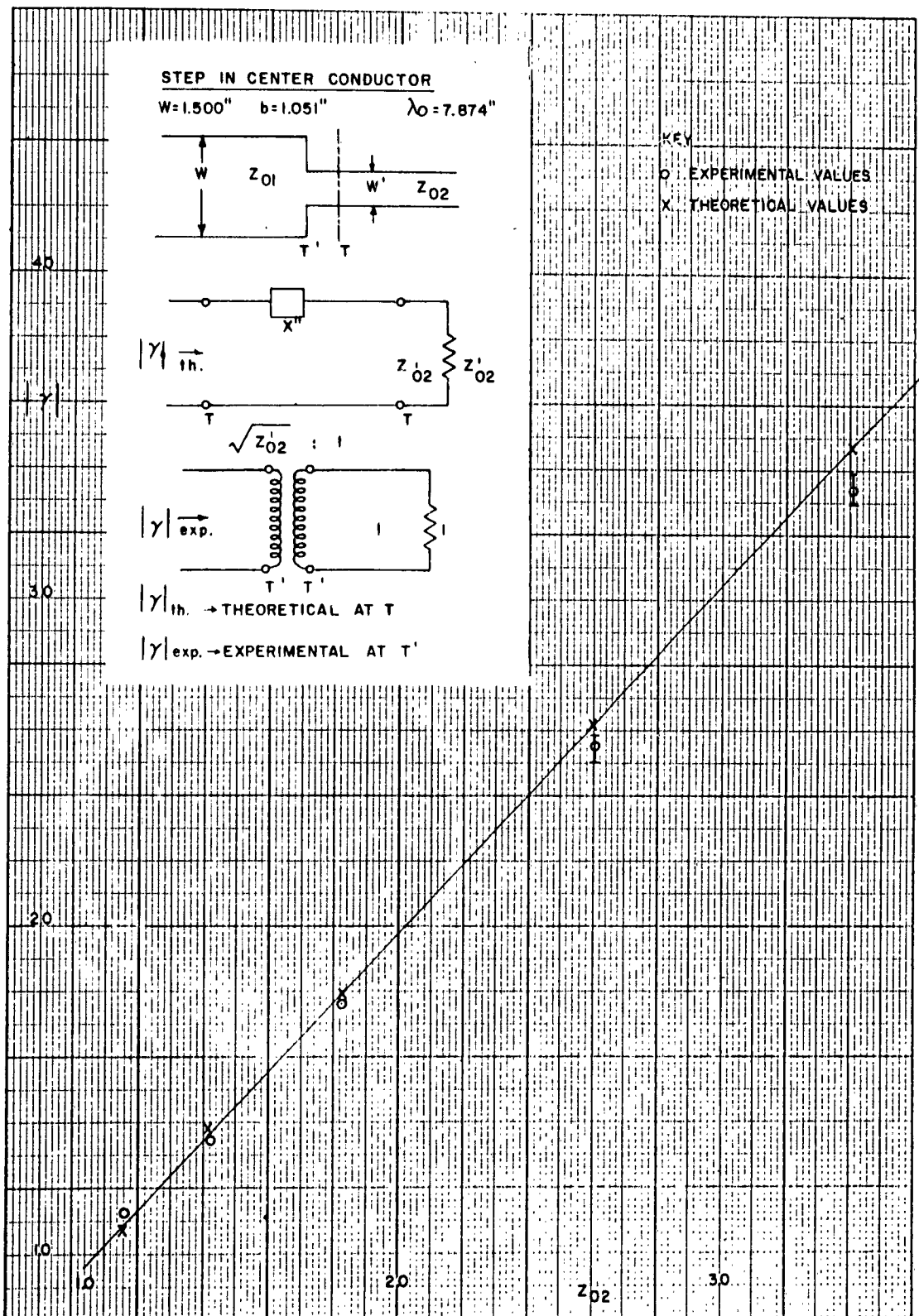


Fig. 8-47 STEP IN CENTER CONDUCTOR

analysis. A similar procedure produced parameters for the 60 and 100 degree bends. Alternative schemes were used to measure bends of 15, 30, 45 and 120 degrees. Here, each structure consisted of three cascaded bends, some of which were known from previous measurements. For measurement of acute angles, the bends were unknown-known-unknown, where for obtuse angles the bends were known-unknown-known.

a. Right Angle Bends:

In section D-3a the theoretically determined equivalent circuit for the Right Angle Bend is discussed. It should be noted the the equivalent network is given at reference planes T_1 , T_2 , each at a distance of $b/\pi \ln 2$ away from the physical junction of the two strips.

As discussed in the previous section, it was not possible to measure the Right Angle Bend as a single discontinuity, so a cascade of four identical bends was used. Measurements were made with respect to reference planes T_1'' and T_2'' shown in Fig. 8-48. The sequence of operations necessary to the determination of the parameters X_{al} and X_{bl} are discussed in the

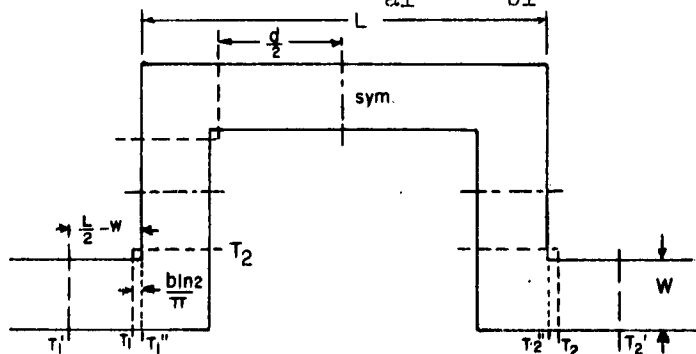


Fig. 8-48: Right Angle Bend in Center Conductor

following paragraph.

Given:

$$D_o, -\gamma, D_r, \lambda_g \text{ (wavelength in stripline)}$$

Find:

$$x_a', x_b'$$

We first wish to shift the reference plane from T_1'' to T_1' :

$$D_o' = D_o - D_r - (L/2 - v) \quad (8-142)$$

$$\theta = \frac{2\pi D_o'}{\lambda_g} \quad (8-143)$$

The parameters of the reactance tee are then calculated using results of previous sections of the chapter.

Now

$$E = \mp \left(\frac{1 - \gamma}{2\sqrt{-\gamma}} \right) \sin 2\theta \quad (8-55)$$

$$F = \mp Z_o \left(\sqrt{-\gamma} \cos^2 \theta \mp \frac{1}{\sqrt{-\gamma}} \sin^2 \theta \right)$$

and

$$a = \pm \left(\frac{1}{2} + \sqrt{\frac{1+E}{2}} \right)^{1/2} \quad (8-25)$$

$$b = \pm \frac{F}{4a(2a^2 - 1)}$$

In normalized form then,

$$x_a' = \frac{b}{Z_o(1+a)}$$

and

$$x_b' = \frac{x_a'}{a-1}$$

Finally, we shift the reference planes to those used in the theoretical derivations, namely T_1 and T_2 .

Since,

$$d = L - 2w - \frac{2b}{\pi} \ln 2$$

$$D = \cot \theta \quad (8-66)$$

$$x_c' = x_a' + 2x_b'$$

then

$$x_{al}' = \frac{D x_a' + 1}{D - x_a'}$$

$$x_{bl}' = 1/2 \left[\frac{D x_c' + 1}{D - x_c'} - x_a' \right]$$

Experimental results on the right angle bend are compiled in Table 8-3. w and L are defined in Fig. 8-48, x_{al} and x_{bl} by eq. 8-66 and γ and βD_o are the parameters of the tangent network.

Table 8-3: Right Angle Bend in the Center Conductor.

w''	L''	x_{al}	x_{bl}	γ	βD_o				
Theo.	Exp.	Theo.	Exp.	Theo.	Exp.				
0.5	4	0.2217	0.2393	-1.2933	-1.3535	1.4419	1.3519	2.0472	2.0463
0.5	5	0.2217	0.2596	-1.2933	-1.3307	1.4419	1.3257	2.0472	2.1219
1.0	5	0.3539	0.3936	-0.8381	-0.8636	1.8673	1.7218	1.8623	1.8469
1.5	5	0.5032	0.5481	-0.6160	0.6197	2.6838	2.6234	1.6526	1.6208

Figure 8-49 and 8-50 offer a graphical comparison of theoretical and experimental results. Solid lines represent theoretical data and points indicate measured data. While the measured data is for a single right angle bend, it must be remembered that it was extracted from a measurement made on four cascaded bends. As can be seen from observation of Fig. 8-49 and 8-50, correlation between measured and theoretical parameters is good. A special test was made at $w = 0.5"$ to determine whether there was higher mode propagation and interaction between the four cascaded bends. The results are conflicting in that for $w = 0.5$; $L = 4"$, the shunt reactance labeled \bullet on the graph is closer to the theoretical value, while for $w = 0.5"$, $L = 5"$, the series reactance label $d \square$ on Figs. 8-49 and 8-50 is in better agreement. It can only be concluded from the above measurements that there is a small but detectable difference in the magnitudes of the parameters for different spacings between discontinuity junctions.

b. Sharp Bend of any Angle ($\theta \neq 90^\circ$):

The theoretical formulas for the sharp bend of any angle are discussed in section D-3b. The theoretical discontinuity structure is represented as a Reactance Tee with reference planes $b/\pi \ln 2$ away from the physical discontinuity.

Three measurement schemes were used to abstract the parameters for sharp angle bends. In the first scheme, four cascaded discontinuities are constructed as in the case of the Right

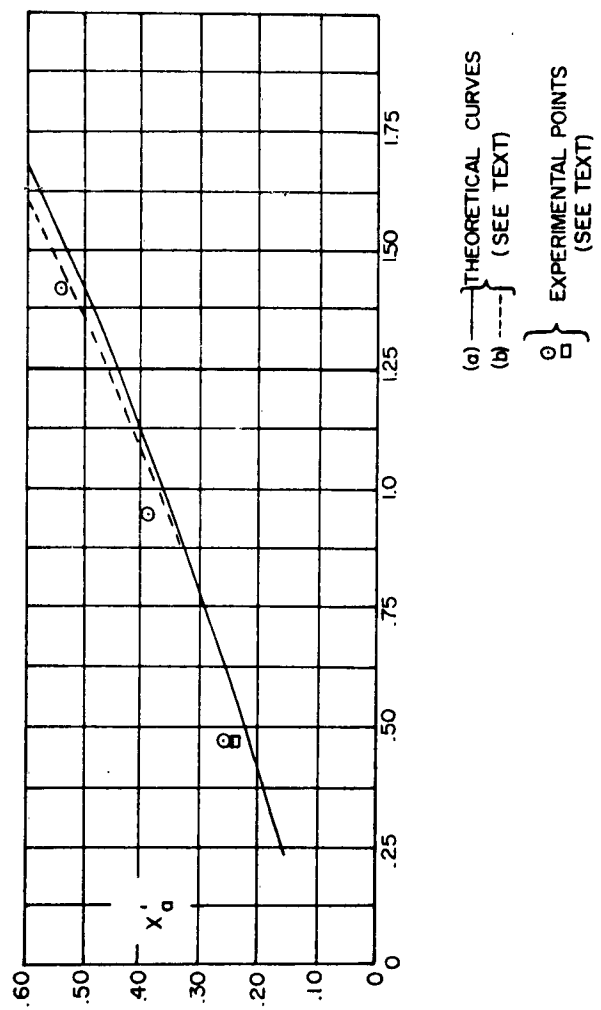


Fig. 8-49 a. REACTANCE TEE NETWORK PARAMETERS FOR RIGHT ANGLE BENDS

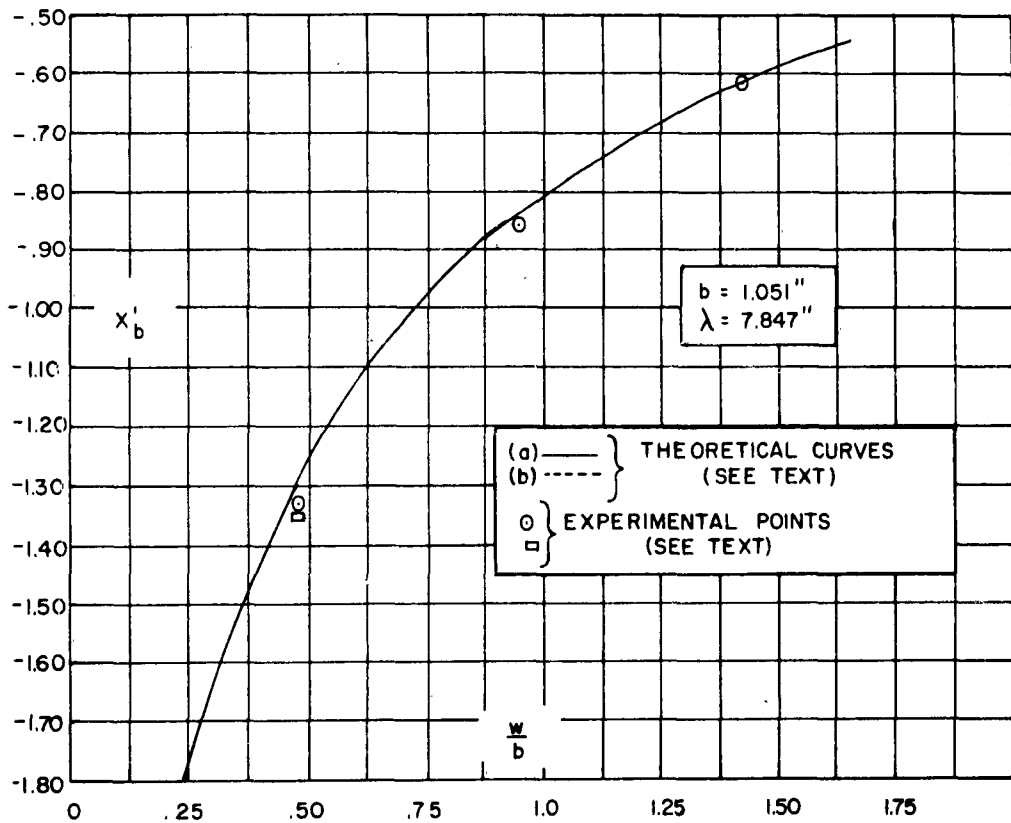


Fig. 8-49b. REACTANCE TEE NETWORK PARAMETERS FOR RIGHT ANGLE BENDS

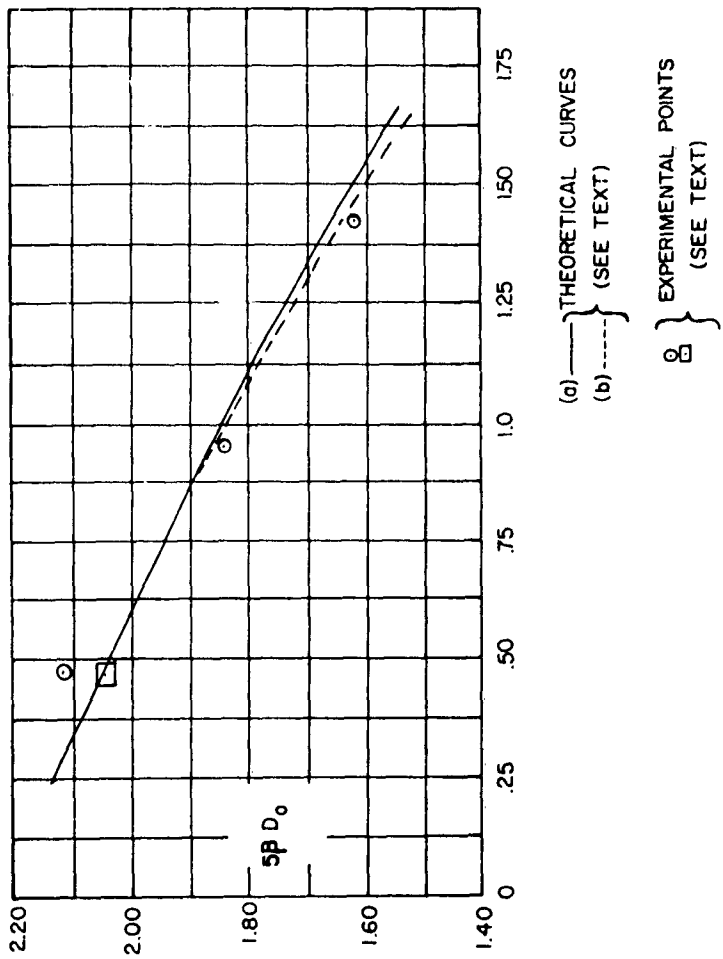


Fig. 8-50a TANGENT NETWORK PARAMETERS FOR RIGHT ANGLE BENDS

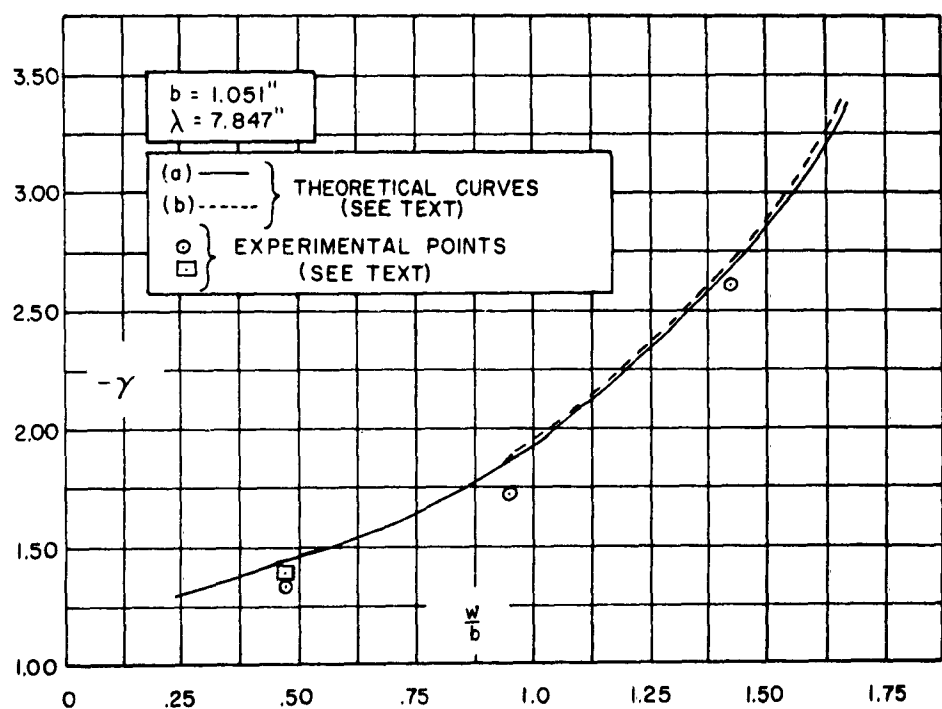


Fig. 8-50b TANGENT NETWORK PARAMETERS FOR RIGHT ANGLE BENDS.

Angle Bend. Fig. 8-51a illustrates the resultant discontinuity.

The distance between bends, d , as well as the nominal angles were hard to maintain so that average values were taken. Fig. 8-51b

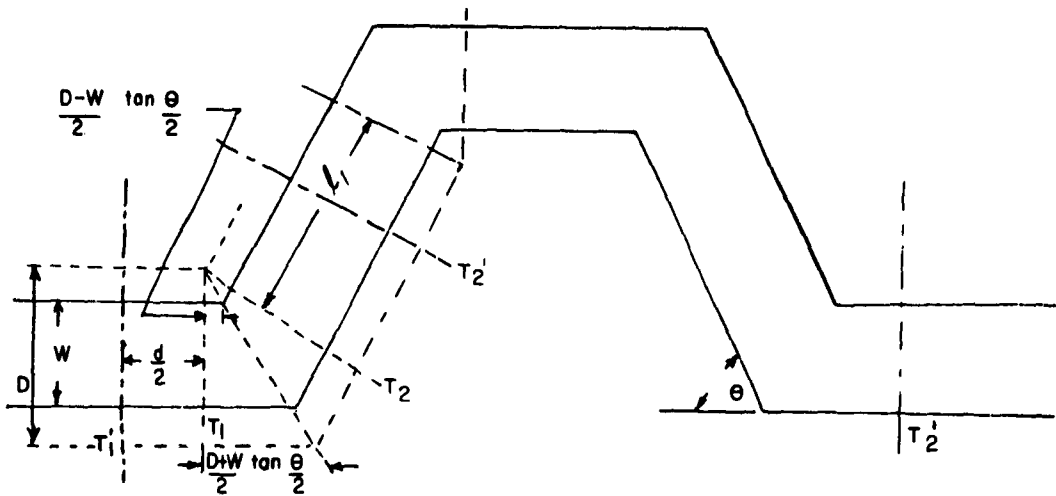


Fig. 8-51a: Four-Cornered Sharp Angle Bend in the Center Conductor.

illustrates the quantities referred to in eq. 8-144, which is an average value for d .

$$d = 1/6 [E_1 + E_2 + E_3 + E_4 + F + H] - D \tan \theta/2 \quad (8-144)$$

Fig. 8-51c defines D_R for the Four-Cornered Bend. In order to obtain the parameters of interest, it is only necessary to replace equation 8-66 with eq. 8-144 and equation 8-142 with equation 8-145 in the development for the Right Angle Bend.

(Sec. E-9a)

$$D_O' = D_O - [D_R - 2.02" - h] - d/2 + \frac{D - W}{2} \tan \theta/2 \quad (8-145)$$

The second method is concerned with the measurement of acute angle bends ($\theta < 90^\circ$). A three-angle bend is constructed, cascading a known bend of angle θ_k between two unknown bends of angles $\theta_k/2$. Fig. 8-52a illustrates the discontinuity in

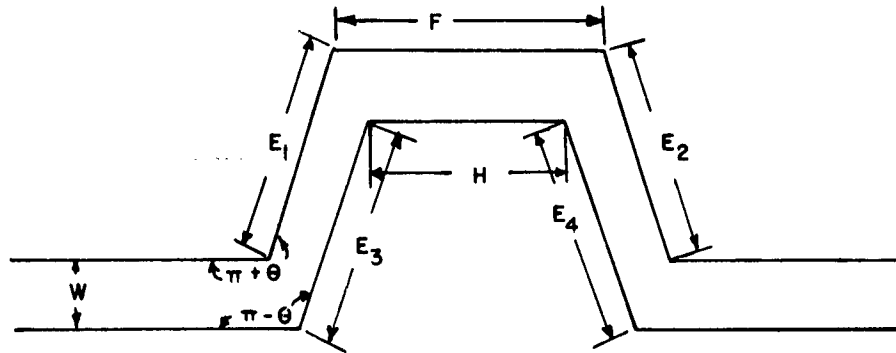


Fig. 51 b. DISTANCES TO BE MEASURED FOR FOUR CORNERED BEND MEASUREMENT ($\theta \pm 90^\circ$)

E_1, E_2, E_3, E_4, F, H ; Various values of d for average value of d .
 $\pi \pm \theta$; Various values of $(\pi \pm \theta)$ for average value of θ .

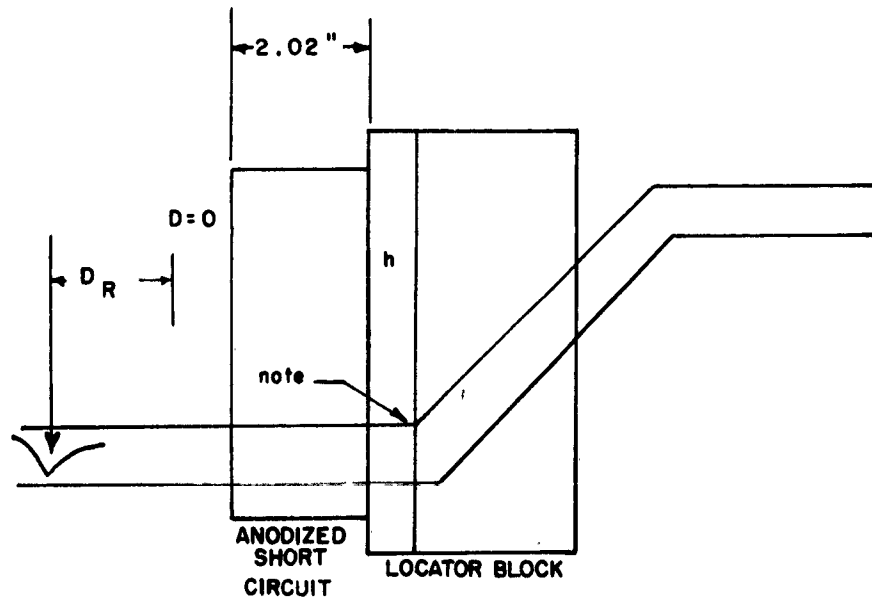


Fig. 51c. DEFINITION OF D_R FOR FOUR CORNERED BEND MEASUREMENT ($\theta \pm 90^\circ$)

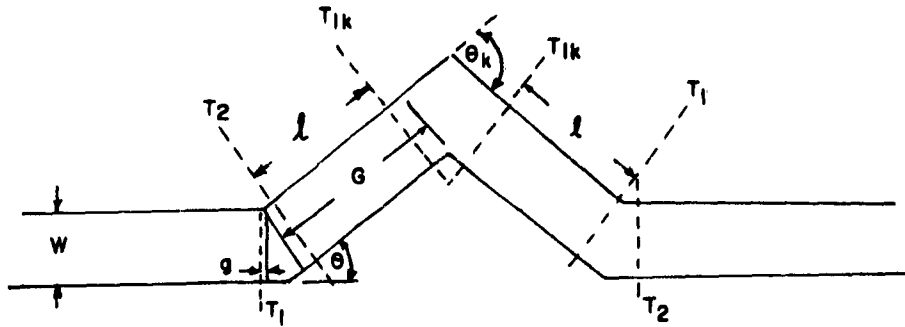
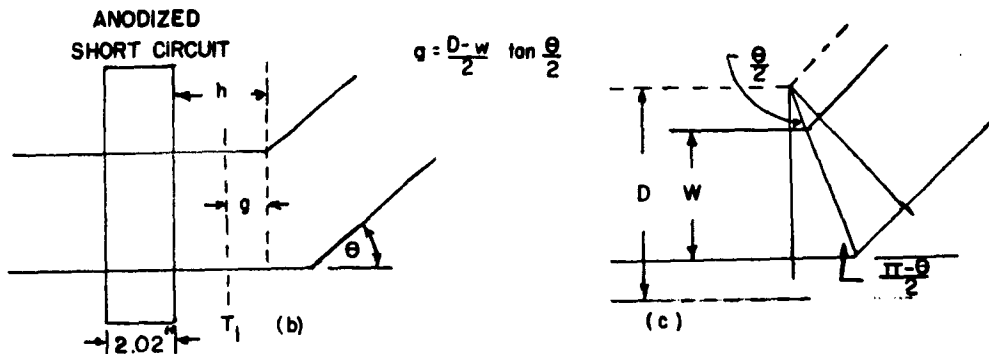


Fig. 8-52a: Three Cornered Bend in the Center Conductor ($\theta < 90^\circ$).

question. Figs. 8-52b and c define several of the parameters



Figs. 8-52b and c: Definitions of D_R ; g for Three Cornered Bend Measurements ($\theta < 90^\circ$).

appearing in the development of the Reactance Tee from the Tangent measurements.

Measurement:

D_R at T_1

$$D_R = D_R' - (2.02" + h) + g$$

$$g = \frac{D_1 - w}{2} \tan \theta/2$$

Given:

D_o , γ , D_R , λ_g , Z_o , θ , θ_k , w , G (corner to corner) a_k , b_k (the a b c d element of bend θ_k at T_{1k} , T_{2k}).

Find:

$$x_a', x_b'$$

$$\varphi = 2 \pi (D_o - D_R) / \lambda_C \quad (8-146)$$

From equation 8-55

$$E = \mp \left(\frac{1}{2} \frac{\gamma}{\sqrt{-\gamma}} \right) \sin 2 \varphi \quad (8-55)$$

$$F = \mp Z_o (\sqrt{-\gamma} \cos^2 \varphi \mp \frac{1}{\sqrt{-\gamma}} \sin^2 \varphi)$$

From Fig. 8-52a

$$l = G - \frac{D - w}{2} [\tan \theta/2 + \tan \theta_k/2] \quad (8-147)$$

Stillman⁶⁴ states that if the elements a_k and b_k are from a previous Three-Cornered Measurement, eq. 8-147 is to be used.

If a_k and b_k are from a previous Four-Cornered Measurement, use

$$l = G - \left(\frac{d_k}{2} - w \right) - \left[\frac{D - w}{2} \tan \theta/2 \right] \text{ (for } \theta_k = 90^\circ \text{)} \quad (8-148)$$

and

$$l = G - \frac{D - w}{2} (\tan \theta/2 + \tan \theta_k/2) - \frac{d_k}{2} \text{ (for } \theta_k \neq 90^\circ \text{)} \quad (8-149)$$

In equation 8-148, G and the second bracketed term are from the Three-Cornered Structure, while the first bracketed term is from the Four-Cornered Structure. On the other hand, in eq. (8-149), G , $\frac{D - w}{2}$ and $\tan \theta/2$ are from the Three-Cornered Structure while $\tan \theta_k/2$ is from the Four Cornered Structure.

Knowing "l", we then rearrange equation 8-65 slightly to obtain equation (8-150) and (8-151) which represent matrix elements at the shifted reference planes.

$$a' = a_k (\cos^2 \beta_1 - \sin^2 \beta_1) - \sin \beta_1 \cos \beta_1$$

$$x \left[\frac{b_k}{Z_o} + \frac{Z_o (1 - a_k^2)}{b_k} \right] \quad (8-150)$$

$$b' = b_k \cos^2 \beta_1 - \left(\frac{1 - a_k^2}{b_k} \right) Z_o^2 \sin^2 \beta_1$$

$$+ 2 a_k Z_o \sin \beta_1 \cos \beta_1 \quad (8-151)$$

Now that the elements a' and b' at the shifted reference planes are known, we may proceed to solve for the unknown bends represented by a symmetrical matrix with elements "a" and "b". In Appendix XII, it is shown that

$$a = \frac{(A + a')}{\sqrt{\frac{(a' B + b' A)^2}{Bb} - \frac{(B - b')^2}{Bb}}} \quad (8-152)$$

and

$$b = \frac{(B - b')}{\sqrt{\frac{(a' B + b' A)^2}{Bb} - \frac{(B - b')^2}{Bb}}} \quad (8-153)$$

The parameters of the final equivalent network are then realized by solving the elements of the matrix 8-56 for X_a' and X_b' .

$$X_a' = \frac{b}{Z_o (1 + a)} \quad (8-154)$$

$$X_b' = \frac{X_a}{a - 1} \quad (8-155)$$

The third method is concerned with obtuse angle bends ($\theta > 90^\circ$). The overall discontinuity structure now consists

of an unknown bend of angle θ cascaded between the known bends of angle $\theta - 2\alpha_k$. The measurement reference plane is taken half way between adjacent bends as shown in Fig. 8-51.

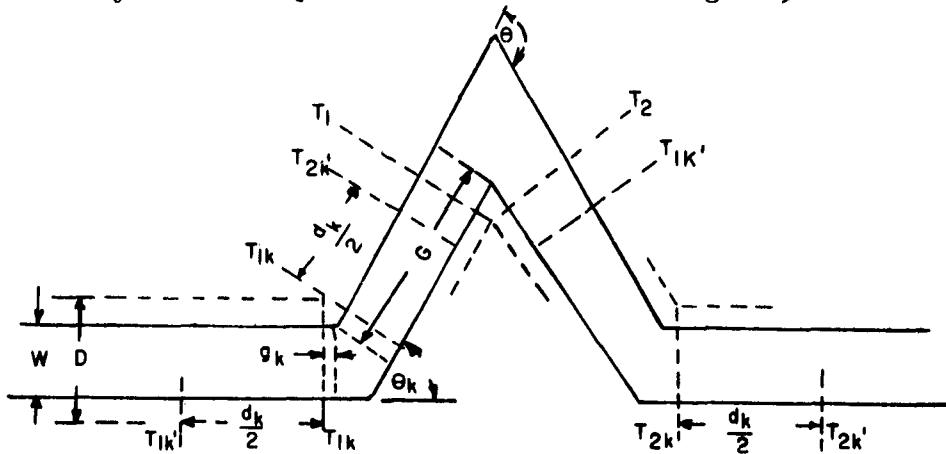


Fig. 8-53: Sharp Angle Bend in Center Conductor (Obtuse Angle, $\theta > 90^\circ$) Series Reactance Network at Specified Reference Planes from D_o , S_o , γ .

Measurement:

$$D_R \text{ at } T_{1k}' ; D_R = D_R' - (2.02 + h) + g_k + \frac{d_k}{2} ;$$

d_k is the d from the previous Four-Cornered Bend measurement.

Given:

D_o , γ , D_R' , G , Z_o , θ , θ_k , D , W , a_k , b_k
(a , b , c , d elements), d_k at reference
planes T_{1k}' and T_{2k}' obtained from a and
 b of previous Four-Cornered Bend Measurement.

Find:

$$x_a', x_b'$$

I

$$\varphi = \frac{2\pi(D_o - D_R')}{\lambda g} \quad (8-146)$$

From eq. 8-55

$$E = \mp \left(\frac{1 - \gamma}{2\sqrt{-\gamma}} \right) \sin 2\varphi \quad (8-55)$$

$$F = \mp z_o (\sqrt{-\gamma} \cos^2 \varphi \mp \frac{1}{\sqrt{-\gamma}} \sin^2 \varphi)$$

E and F are the normalized elements at T_{1k}' , T_{2k}' of the overall structure. For the case of the obtuse angle, we have an unknown bend sandwiched between two known bends. It is shown in Appendix XIII that if we solve for the matrix elements of the unknown bend in terms of those for the known bends, we get

$$a = a_k (a_k A + b_k C) + c_k (a_k B - b_k A) \quad (8-156)$$

$$b = -b_k (a_k A + b_k C) + a_k (a_k B - b_k A) \quad (8-157)$$

Figure 8-52 illustrates several of the parameters of the obtuse

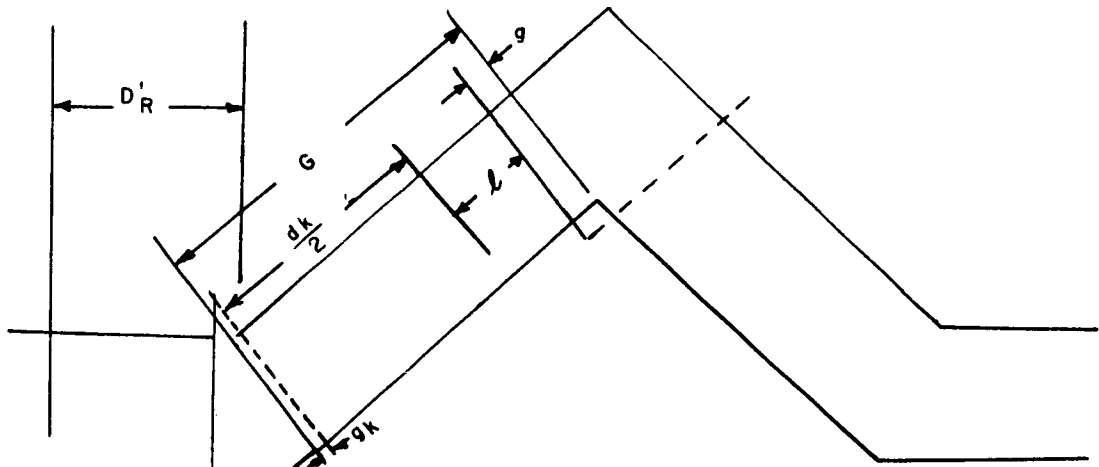


Fig. 8-54: Definition of D'_R , d_k , g_k for Three Cornered Bend Measurement.

Three Cornered Bend. From this Figure we see that

$$l = G - g - g_k - \frac{d_k}{2} \quad (8-158)$$

Also from the previous development

$$g = \frac{D - w}{2} \tan \theta/2 \quad (8-159)$$

We now have enough information to find the elements of the unknown matrix, a and b .

$$a = a_k (\cos^2 \beta l - \sin^2 \beta l) - \sin \beta l \cos \beta l$$

$$x \left[\frac{b_k}{Z_o} + \frac{Z_o (1 - a_k^2)}{b_k} \right] \quad (8-150)$$

$$b = b_k \cos^2 \beta l - \left(\frac{1 - a_k^2}{b_k} \right) Z_o^2 \sin^2 \beta l \\ + 2 a_k Z_o \sin \beta l \cos \beta l \quad (8-151)$$

Knowing a and b , we find the parameters of the equivalent circuit through use of eqs. 8-154 and 8-155.

$$X_a' = \frac{b}{Z_o (1 + a)} \quad (8-154)$$

$$X_b' = \frac{X_a}{a - 1} \quad (8-155)$$

The above four equations were discussed under the subject of the acute angle bend.

Experimental results on the sharp angle bend are compiled in Table 8-4. The parameters recorded include the angle of the bend θ , the insertion V.S.W.R., the final Reactance Tee parameters, the Reactance Tee parameters at 180° shifted reference planes, the reflection coefficient and the input line length. The data in Table 8-4 is plotted in Figures 8-53 and 8-54. The solid curves represent the theoretical results which were based on the theoretical expressions for the parameters of E-plane

TABLE 8-4

SHARP BEND OF ANY ANGLE IN CENTER CONDUCTOR

$$W = 1.000" \quad b = 1.051" \quad \lambda_g = 7.874"$$

θ°	$ \Gamma $		X_a'		X_b'		\bar{X}_a'		\bar{X}_b'	
Theo.	Exp.	Theo.	Exp.	Theo.	Exp.	Theo.	Exp.	Theo.	Exp.	
120	0.6137	0.6932	0.4003	0.6018	-0.4926	-0.4349	-0.5349	-0.2680	0.4926	0.4349
100	0.3969	0.2250	0.3530	0.4712	-0.7159	-0.8703	-1.0788	-1.2694	0.7159	0.8703
90	0.3050	0.2652	0.3275	0.3936	-0.8532	-0.8636	-1.3789	-1.3336	0.8532	0.8536
60	0.1155	0.1039	0.2408	0.2618	-1.4778	-1.4586	-2.7148	-2.6554	1.4778	1.4535
45	0.0503	0.0651	0.1905	0.1733	-2.0593	-2.1198	-3.9290	4.0613	2.0598	2.1198
30	0.0255	0.0264	0.1346	0.1448	-3.1542	-2.9912	-6.2338	-6.8376	3.1842	2.9912
22.5	0.0122	---	0.1041	---	4.2393	---	-3.4745	---	4.2393	---
15	0.000	0.0148	0.0717	0.005	-6.4807	-50.3384	-12.8897	-100.6818	6.4807	50.3384

TABLE 8-4 (Continued)

θ°	γ		βD_0		MEASURED AS
	Theo.	Exp.	Theo.	Exp.	
120	4.1768	5.5190	1.6450	1.4309	3-Cornered Bend
100	2.3163	1.5805	1.8128	1.8024	4-Cornered Bend
90	1.8818	1.7218	1.8843	1.8469	4-Cornered Bend
60	1.2637	1.2318	2.0619	2.0479	4-Cornered Bend
45	1.1295	1.1393	2.1373	2.1482	3-Cornered Bend from 90° Bend
30	1.0523	1.0543	2.2131	2.2077	3-Cornered Bend from 60° Bend
22.5	1.0243	----	2.200	----	
15	1.000	1.0301	1.5708	----	3-Cornered Bend from 30° Bend

(a) — THEORETICAL CURVES
 (b) - - - (SEE TEXT)
 ◎ EXPERIMENTAL POINTS

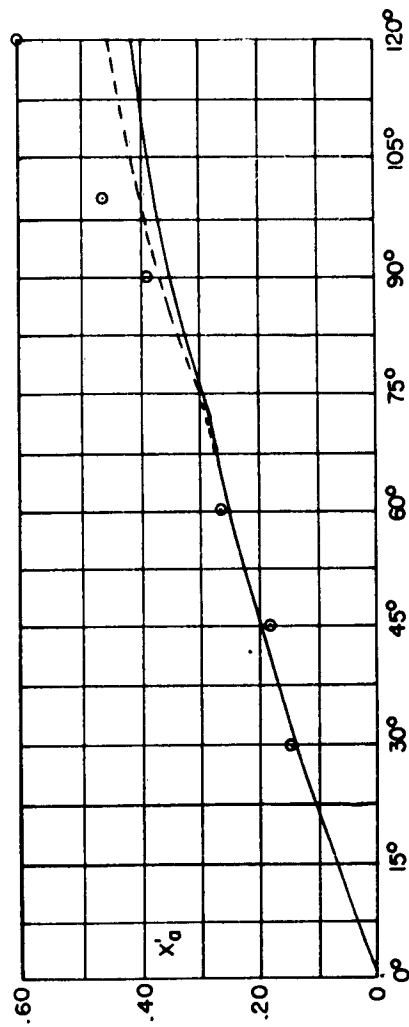


Fig. 8-53a REACTANCE TEE NETWORK PARAMETERS FOR SHARP ANGLE BENDS

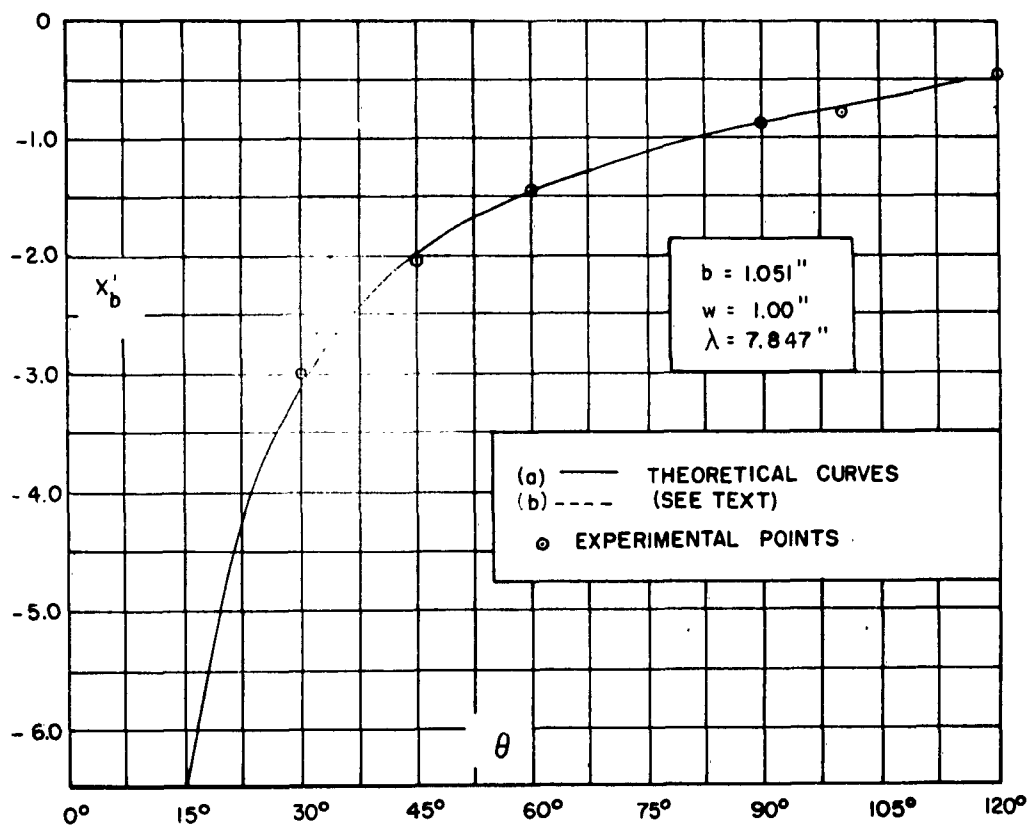


Fig. 8-53b. REACTANCE TEE NETWORK PARAMETERS FOR SHARP ANGLE BENDS

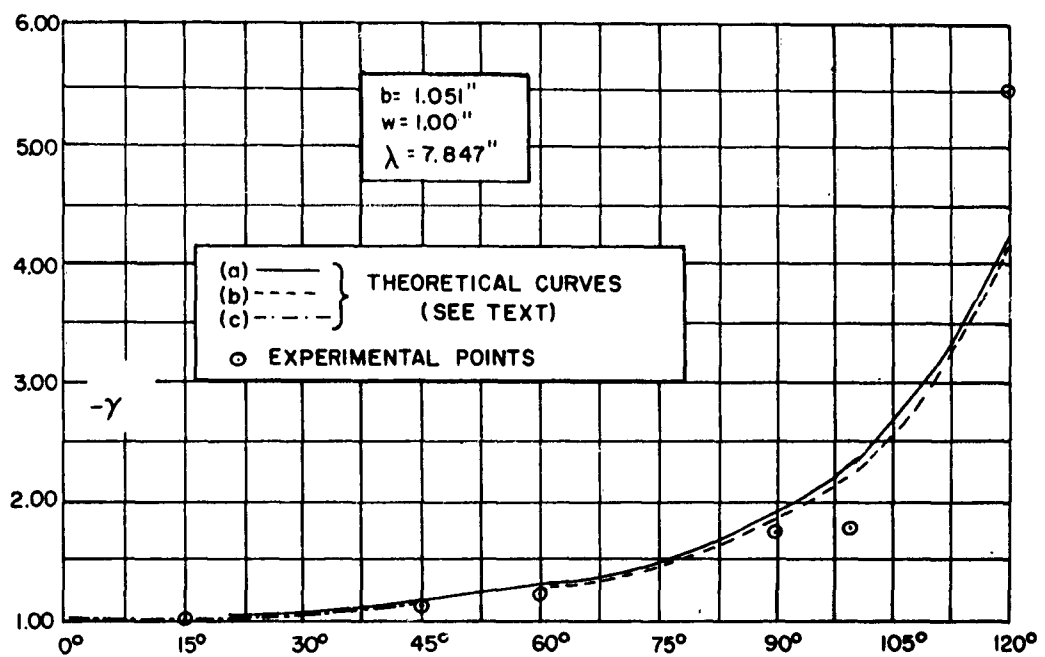


Fig. 8-54 a. TANGENT NETWORK PARAMETERS FOR SHARP ANGLE BENDS

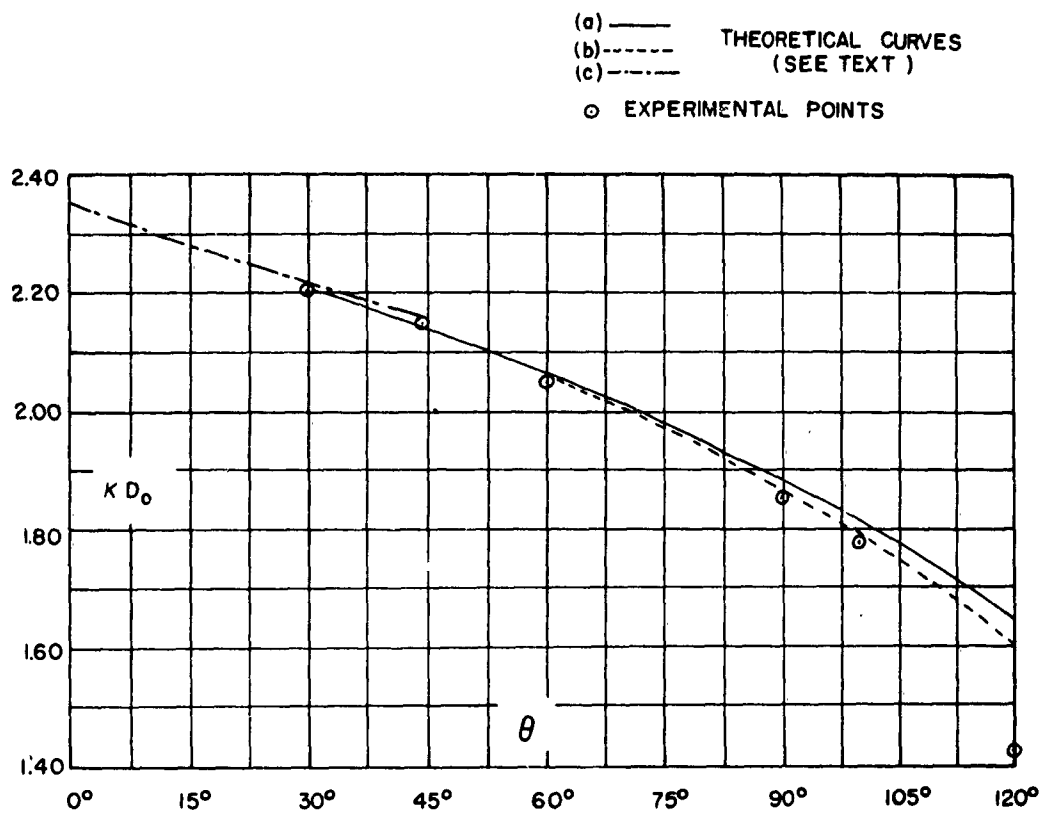


Fig. 8-54b.TANGENT NETWORK PARAMETERS FOR SHARP ANGLE BENDS

bends in rectangular waveguide. The dashed curve for X_a (for $\theta > 60^\circ$), is on the other hand, based upon experimentally obtained values for the parameter of E-plane bends in rectangular waveguide. Part of the discrepancy between theory and measurement is consequently due to errors already existing in the theoretical result (X_a only) for the rectangular waveguide bend. The discrepancy between Stripline measurements and the dashed curve is somewhat larger. This discrepancy is believed to be due to an imperfection in the Babinet equivalent model for the bend. In contrast to the Babinet model which has impenetrable walls, the actual Stripline possesses a fringing field which permits an additional small interaction to occur between the center conductor on one side of the bend and that on the other. This effect, not taken into account in the Babinet model, becomes more marked as the band angle θ becomes larger.

Altshuler and Oliner⁶² have shown that, once X_a' and X_b' are known, the expressions required for the abstraction of the parameters of the tangent network (γ , D_o , S_o) can be derived.

$$-\gamma = C + \sqrt{C^2 - 1} \quad (8-156)$$

where

$$C = \frac{1 + 2(X_a' + X_b')^2 + X_a'^2(X_a' + 2X_b')^2}{2X_b'^2}$$

$$k D_o = \tan^{-1} \alpha \quad (8-157)$$

where

$$a = \frac{\gamma - X_a' (X_a' + 2X_b')}{(X_a' + X_b') (1 + \gamma)}$$

$$k S_o = k D_o \pm \pi/2 \quad (8-158)$$

For θ small ($C \approx 1$)

$$-\gamma \approx 1 - (2X_a' + 1/X_b') \quad (8-159)$$

$$\alpha \approx 1/X_b' - 1 \quad (8-160)$$

For small angle bends ($\theta < 30^\circ$), the expressions for abstracting γ and D_o from X_a' and X_b' become very sensitive leading to large computational errors. The small angle approximations are, however, quite good and are in fact more substantially reliable than the "exact" expressions in this range. The theoretical values of γ and D_o obtained through their use are shown in the form of dot-dash waves. The $-\gamma$ vs. θ curve points up the fact that it is better to employ two or three smaller bends in place of one large bend. As an example, consider the experimental points at $\theta = 30^\circ$, 45° and 90° . The 90° bend has an insertion V.S.W.R. of 1.75. On the other hand, two 45° bends in tandem (and "far" from each other so as not to interact) can have a maximum V.S.W.R. of 1.25 and three 30° bends can have a maximum V.S.W.R. of 1.15.

F. Conclusions:

Equivalent circuits have been developed for a great number of stripline discontinuities. In many cases experimental evidence was also obtained and a comparison made between theory

and measurement. In general correlation is good, but the reader should check the correlation and its range of validity before attempting to use the design formulas. Discontinuities may arise in two different ways: (1) Unavoidably--In any configuration there will be bends, tees, etc. which need to be described and, (2) Transfer or Driving Point Function Synthesis--If a desired transfer or driving function can be mathematically described and meets the realizability criteria for two ports (or n ports for that matter) it can first be synthesized in a standard fashion using Passive Synthesis, then reduced to holes, slots, gaps, etc. in stripline. Since at high frequencies the lumped constant network would probably not be realizable anyway, due to the small values involved plus fringing problems, design utilizing stripline discontinuities should prove to be a useful tool.

C

BIBLIOGRAPHY

59. A. A. Oliner, "Equivalent Circuits for Discontinuities in Balanced Strip Transmission Lines," IRE Transactions on Microwave Theory and Techniques, Vol. MTT-3, No. 2, March 1955, pp. 134 - 143.
60. M. Suzuki, "Circuit Parameters of a Tuning Post in a Rectangular Waveguide and Its Applications," Microwave Research Institute, Polytechnic Institute of Brooklyn, N. Y., Report No. R-591-57, PIB-519, July 1957.
61. E. Jahnke and F. Emde, "Tables of Functions," Dover Publications, Inc., New York, N. Y., p. 16; 1945.
62. H. M. Atlschuler and A. A. Oliner, "Discontinuities in The Center Conductor of Symmetric Strip Transmission Line," IRE Transactions on Microwave Theory and Techniques, Vol. MTT-8, No. 3, May 1960, pp. 328 - 339.
63. S. B. Cohn, et al. "Research on Design Criteria for Microwave Filters," Stanford Research Institute, Menlo Park, California, pp. 115 - 116, June 1957.
64. M. S. Stillman, "Measurement of Discontinuities in Symmetric Strip Transmission Line," M.E.E. Thesis, Polytechnic Institute of Brooklyn, N. Y., June 1958.
65. Airborne Instrument Laboratories, Report 2830-2, 1 Dec 1955, Contract No. AFM (604) 780.
66. Franco and Oliver "Symmetric Strip Transmission Line Tee Junction." IRE Transactions on Microwave Theory and Techniques, Vol. MTT-10, No. 2, March 1962.

APPENDIX XI

Relationship Between Series Reactance Network and Tangent Network:

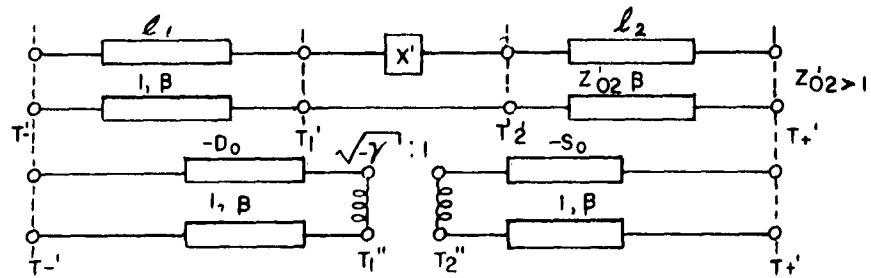


Fig. AII-1: Tangent and Series Reactance Networks.

Given

$$D_o, S_o, -\gamma$$

$$X', l_1, l_2$$

The Tangent Network parameters $D_o, S_o, -\gamma$ are obtained at T_{+}' and T_{-}' , while the Series Reactance parameters are obtained at reference planes T_1' and T_2' . In the Tangent Network the fact that the two Characteristic Impedances are different is already implicitly contained in $-\gamma$. In the Reactance Network all impedances are normalized to the Characteristic Impedance of the input transmission line; i.e., $X = X/Z_{01}$ and $Z_{02}' = Z_{02}/Z_{01}$.

According to King,⁵⁰ page 76, the reflection coefficient Γ of a transmission line may be expressed by

$$\Gamma = \frac{Z_o - Z_c}{Z_o + Z_c} = \frac{Z_o/Z_c - 1}{Z_o/Z_c + 1} \quad (\text{AII-1})$$

where Z_o = output impedance

Z_c = characteristic impedance

If T_+ ' is terminated in a match (Z_{02}' for the Reactance Network and one for the Tangent Network) then at T_1' for the Reactance Network $Z_{in}' = Z_{02}' + j X'$; for the Tangent Network V.S.W.R. = - γ . Under these conditions, the reflection coefficient for the Reactance Network (eq. All-1) becomes

$$\Gamma = \frac{Z_{in}' - 1}{Z_{in}' + 1} \quad (\text{All-2})$$

$$= \frac{Z_{02}' + j X_1' - 1}{Z_{02}' + j X_2' + 1}$$

Since primary interest is in $|\Gamma|$, we can take the absolute value of eq. (All-2) to obtain

$$|\Gamma| = \sqrt{\frac{(Z_{02}' - 1)^2 + X_1'^2}{(Z_{02}' + 1)^2 + X_1'^2}} \quad (\text{All-3})$$

Since the input V.S.W.R. of the Tangent and Reactance Networks must be the same, we can equate the reflection coefficient of the Reactance network with that of the Tangent network in the formula

$$\rho = -\gamma = \left| \frac{\Gamma}{\Gamma} + \frac{1}{-1} \right| \quad (\text{All-4})$$

or solving for $|\Gamma|$

$$|\Gamma| = \frac{\rho - \frac{1}{\rho}}{\rho + \frac{1}{\rho}} \quad (\text{All-5})$$

Squaring both sides

$$|\Gamma|^2 = \frac{\rho^2 - 2\rho + 1}{\rho^2 + 2\rho + 1} \quad (\text{All-6})$$

Substituting the value of $|\Gamma|$ from eq. (All-3)

$$\frac{[(z_{02}')^2 + x'^2 + 1) - 2z_{02}']}{[(z_{02}')^2 + x'^2 + 1) + 2z_{02}']} = \frac{\rho^2 - 2\rho + 1}{\rho^2 + 2\rho + 1} \quad (\text{All-7})$$

Solving eq. (All-7) for x' and letting $\rho = -\gamma$ we obtain

$$x' = \pm \left[\frac{z_{02}'}{\sqrt{-\gamma}} (\gamma^2 + 1) - (z_{02}')^2 + 1 \right]^{1/2} \quad (\text{All-8})$$

At the reference planes T_1' and T_2'' , the network can be redrawn as Fig. All-2.

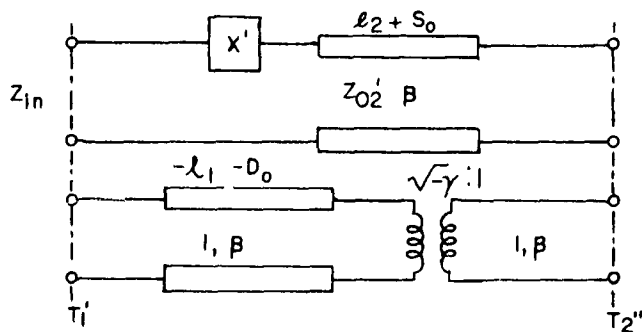


Fig. All-2: Equivalent Tangent and Reactance Network Representation.

For lossless open circuited transmission lines

$$Z_{in} = -j Z_o \cot \beta s \quad (\text{All-9})$$

where Z_o = Characteristic Impedance

s = distance from open

Since both networks are to be equivalent, one may equate their input impedances with the output open circuited. For

the reactance network

$$Z_{in} = j X' - j Z_{02}' \cot \beta (l_2 + s_o) \quad (All-10)$$

For the tangent network

$$Z_{in_2} = - j \cot \beta (-l_1 - D_o) \quad (All-11)$$

Equating eqs. (All-10) and (All-11), we get

$$X' - Z_{02}' \cot \beta (l_2 + s_o) = - \cot \beta (-l_1 - D_o) \quad (All-12)$$

But

$$\cot (-x) = - \cot x \quad (All-13)$$

So

$$X' - Z_{02}' \cot \beta (l_2 + s_o) = \cot \beta (l_1 + D_o) \quad (All-14)$$

For a lossless short circuited line

$$Z_{in} = j Z_o \tan \beta s \quad (All-15)$$

where

Z_o = Characteristic Impedance

s = distance from open

For the reactance network, with the output short circuited

$$Z_{in_1} = j X' + j Z_{02}' \tan \beta (l_2 + s_o) \quad (All-16)$$

and for the tangent network (shorted output)

$$Z_{in_2} = j \tan \beta (-l_1 - D_o) \quad (All-17)$$

but

$$\tan (-x) = - \tan x \quad (All-18)$$

so

$$Z_{in_2} = - j \tan (l_2 + D_o) \quad (All-19)$$

Equating eqs. (All-16) and (All-19), there results

$$x' + z_{02}' \tan \beta (l_2 + s_o) = - \tan \beta (l_1 + d_o) \quad (\text{All-20})$$

From eq. (All-14)

$$\begin{aligned} - \tan \beta (l_1 + d_o) &= \frac{-1}{\cot \beta (l_1 + d_o)} \\ &= -x' + z_{02}' \frac{1}{\cot \beta (l_2 + s_o)} \end{aligned} \quad (\text{All-21})$$

Equating eq. (All-20) and (All-21)

$$[-x' + z_{02}' \cot \beta (l_2 + s_o)] [x' + z_{02}' \tan \beta (l_2 + s_o)] = 1 \quad (\text{All-22})$$

Regrouping eq. (All-22) and using a trigonometric identity, we find that

$$\frac{\cot^2 \beta (l_2 + s_o) - 1}{\cot \beta (l_2 + s_o)} = \frac{1 + x'^2 - z_{02}'}{x' z_{02}'} \quad (\text{All-23})$$

$$\text{Let } \cot \beta (l_2 + s_o) = \eta \quad (\text{All-24})$$

Making this substitution, eq. All-23 simplifies to

$$\frac{\eta^2 - 1}{\eta} = \frac{1 + x'^2 - z_{02}'}{x' z_{02}'} \quad (\text{All-25})$$

or

$$\eta^2 - \left(\frac{1 + x'^2 - z_{02}'}{x' z_{02}'} \right) \eta - 1 = 0 \quad (\text{All-26})$$

$$\text{Let } \varphi = \left(\frac{1 + x'^2 - z_{02}'}{x' z_{02}'} \right) \quad (\text{All-27})$$

Equation All-26 then becomes

$$\eta^2 - \varphi \eta - 1 = 0 \quad (\text{All-28})$$

Using the quadratic formula

$$\begin{aligned}\eta &= \varphi/2 \pm \sqrt{\frac{\varphi^2 + 4}{4}} \\ &= \varphi/2 \pm \sqrt{(\varphi/2)^2 + 1} \quad (\text{All-29})\end{aligned}$$

or substituting eq. All-24 and All-27

$$\begin{aligned}\cot \beta (l_2 + s_o) &= \frac{1 + x'^2 - 2 z_{02}'}{2 x' z_{02}'} \\ &\pm \sqrt{\left(\frac{1 + x'^2 - z_{02}'}{2 x' z_{02}'} \right)^2 + 1} \quad (\text{All-30})\end{aligned}$$

Define

$$\xi = \varphi/2 = \left(\frac{1 + x'^2 - z_{02}'}{2 x' z_{02}'} \right) \quad (\text{All-31})$$

Then

$$\cot \beta (l_2 + s_o) = \xi \pm \sqrt{\xi^2 + 1} \quad (\text{All-32})$$

We may now solve eq. (All-32) for l_2 in a straightforward manner. The result is

$$l_2 = 1/\beta \left[\cot^{-1} \left(\xi \pm \sqrt{\xi^2 + 1} \right) \right] - s_o \quad (\text{All-33})$$

In a similar manner eq. All-14 may be solved for l_1 resulting in

$$l_1 = 1/\beta \cot^{-1} [x' + z_{02}' \cot \beta (l_2 + s_o)] - d_o \quad (\text{All-34})$$

APPENDIX XII

Derivation of the Transfer Matrix Elements for an Unknown Sharp Angle Bend (Acute Angle, $\theta < 90^\circ$)--Three-Cornered Bend:

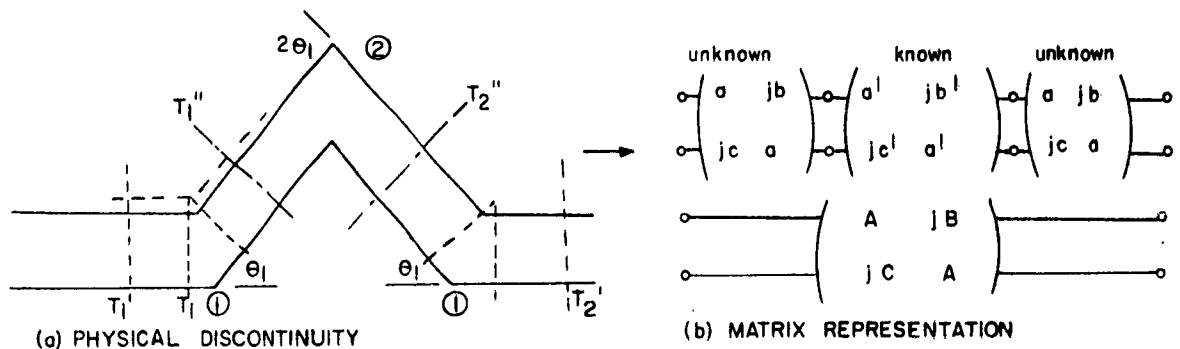


Fig. A12 - 1: Discontinuity Structure for Study of Acute Angle Bends.

The Three-Cornered Bend used in the evaluation of acute angle bends is shown as part a of Figure A12-1. It is represented in matrix form by part b of the same figure. The matrix representation is that of three cascaded bends, one of which is known while the other two are identical. To find the elements of the resultant matrix, we proceed by straightforward matrix multiplication.

$$\begin{pmatrix} A & jB \\ jC & A \end{pmatrix} = \begin{pmatrix} a & j b \\ j c & a \end{pmatrix} \begin{pmatrix} a' & j b' \\ j c' & a' \end{pmatrix} \begin{pmatrix} a & j b \\ j c & a \end{pmatrix} \quad (\text{Al2-1})$$

where

$$A = (2a^2 - 1) a' - a b c' - a c b'$$

$$B = (2 a b) a' - b^2 c' + a^2 b'$$

The final expression for A uses the restriction for

r. l. s. networks (eq. 8-6 with $a = d$)

$$a^2 + b c = 1 \quad (8-6)$$

Now, it may be shown that

$$a (B - b') = b (A + a') \quad (A12-2)$$

or

$$A = K b \quad (A12-3)$$

where

$$K = \frac{A + a'}{B - b} = a/b \quad (A12-4)$$

If $K = a/b$ is inserted in the equation B and the result is solved for b , we obtain

$$b = \pm \sqrt{\frac{B}{2 K a' - c' + K^2 b'}} \quad (A12-5)$$

Now using the fact that

$$K = \frac{A + a'}{B - b} \quad (A12-6)$$

and

$$c' = \frac{1 - a'^2}{b} \quad (A12-7)$$

(from eq. 8-6), we find that

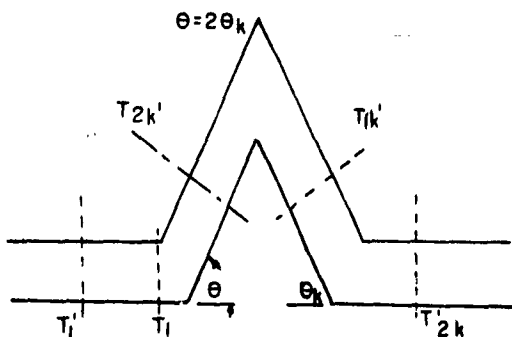
$$b = \pm \sqrt{\frac{(B - b')}{\frac{(A b' + a' B)^2}{B b'} - (B - b')^2}} \quad (A12-8)$$

and using eq. A12-3, that

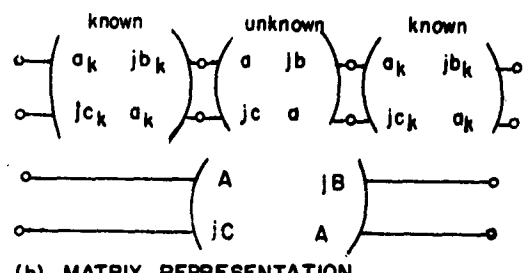
$$a = \pm \sqrt{\frac{(A + a')}{\frac{(A b' + a' B)^2}{B b'} - (B - b')^2}} \quad (A12-9)$$

APPENDIX XIII

OVERALL MATRIX: A, B, a_k, b_k , are known for measurement.
 a, b are unknown



(a) PHYSICAL DISCONTINUITY



(b) MATRIX REPRESENTATION

Fig. A13-1: Discontinuity Structure for the Study of Obtuse Angle Bends.

In this appendix we wish to solve for the elements a and b of the unknown matrix in terms of the known parameters a_k, b_k, c_k and A, B and C . We begin by defining several symbols.

Set:

$$t = \begin{pmatrix} a & jb \\ jc & a \end{pmatrix} \quad (\text{A13-1})$$

$$t_k = \begin{pmatrix} a_k & jb_k \\ jc_k & a_k \end{pmatrix} \quad (\text{A13-2})$$

and

$$T = \begin{pmatrix} A & JB \\ JC & A \end{pmatrix} \quad (\text{A13-3})$$

Therefore, by definition

$$T = (t_k) (t) (t_k) \quad (\text{A13-4})$$

Premultiply both sides of eq. (A13-4) by the inverse of t_k ,
namely t_k^{-1}

$$(t_k)^{-1} T = (t_k)^{-1} (t_k) (t) (t_k) \quad (\text{A13-5})$$

Now

$$(t_k) (t_k)^{-1} = 1 \quad (\text{A13-6})$$

so

$$(t_k)^{-1} T = (t) (t_k) \quad (\text{A13-7})$$

Post Multiply both sides of eq. A13-7 by $(t_k)^{-1}$

$$\begin{aligned} (t_k)^{-1} T (t_k)^{-1} &= (t) (t_k) (t_k)^{-1} \\ &= t \quad (\text{by eq. A13-6}) \end{aligned} \quad (\text{A13-8})$$

We must proceed by finding the matrix elements of $(t_k)^{-1}$.

From eq. A13-2

$$t_k = \begin{pmatrix} a_k & j b_k \\ j c_k & a_k \end{pmatrix} \quad (\text{A13-2})$$

The inverse elements are given by

$$a_{ij} = \frac{a_{ij}}{|a|} \quad (\text{A13-9})$$

where: i, j are integers

$|a|$ is the determinant of the original matrix. For
the matrix under discussion (eq. A13-2)

$$|t_k| = a_k^2 + b_k c_k = 1 \quad (\text{A13-10})$$

Therefore

$$(t_k)^{-1} = \begin{pmatrix} a_k & -j b_k \\ -j c_k & a_k \end{pmatrix}$$

Inserting the definitions of $(t_k)^{-1}$ and T into eq. A13-8, we get

$$\begin{aligned} t &= \begin{pmatrix} a_k & -j b_k \\ -j c_k & a_k \end{pmatrix} \begin{pmatrix} A & j B \\ j C & A \end{pmatrix} \begin{pmatrix} a_k & -j b_k \\ -j c_k & a_k \end{pmatrix} \\ &= \begin{pmatrix} a & j b \\ j c & a \end{pmatrix} \end{aligned}$$

Performing the indicated multiplication and equating to the elements of the (t) matrix, we obtain the final result, which is

$$a = a_k (a_k A + b_k C) + c_k (a_k B - b_k A) \quad (\text{A13-12})$$

$$b = -b_k (a_k A + b_k C) + a_k (a_k B - b_k A) \quad (\text{A13-13})$$

ABSTRACT

The entire analysis of stripline is based on the assumption that operation is in the TEM mode. Since mode jumping is possible, it is necessary to know what limitations must be placed on stripline dimensions in order to assure propagation in the TEM mode. To determine these limitations, a transverse resonance procedure is used. When tied into an existing relation for the E-plane bifurcation in waveguide and upon application of stripline boundary conditions, the desired result is obtained. Cutoff wavelength for the first higher mode is given and a condition for propagation of discrete higher order modes is established. Finally, experimental verification is given through measurements made by the Airborne Instruments Laboratory on "trough waveguide."

TABLE OF CONTENTS

Chapter	Page
IX Higher Mode Propagation in stripline	
A. Introduction	1
B. Cutoff Wavelength of the First Higher Mode	2
C. Discussion of the Higher Mode Spectrum	8
D. Experimental Verification.	12
Bibliography.	15

LIST OF FIGURES

Figure	Page
9-1 First Higher Mode in Stripline.	2
9-2 Side View of an E-Plane Bifurcation in Waveguide	3
9-3 Cross Section of Stripline Taking Fringing Capacity into Account.	4
9-4 Graph for the Cutoff Wavelength of the First Higher Mode	6
9-5 Fractional Error in the Use of the Approximate Formula	7
9-6 Approximate Rule for Determining λ_c in Stripline	8
9-7 Electric Field Lines for (a) a class of discrete modes, (b) a contribution to the continuous spectrum	8
9-8 Stripline Geometry.	9
9-9 The Trough Waveguide (A.I.L.)	12
9-10 Transmission Characteristics of Trough Waveguide	14

Chapter IX

HIGHER MODE PROPAGATION IN STRIPLINE

A. Introduction:

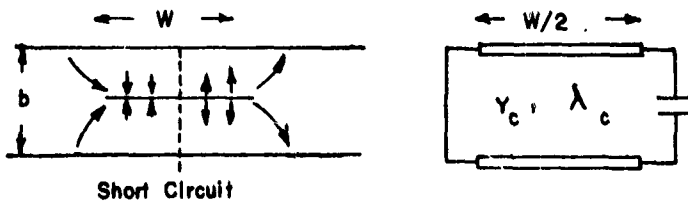
All the previous chapters on the properties of stripline have assumed that operation was taking place in the Transverse Electromagnetic (TEM) mode. Because of this assumption, it is possible to use standard transmission line techniques for evaluation of Characteristic Impedance, Attenuation, Transient Response, etc. The TEM mode is particularly easy to evaluate since it satisfies Laplace's Equation ($\nabla^2 V = 0$). As such, a static solution can be assumed (although the field is certainly not static). Assumption of a static field greatly simplifies calculations.

In order to justify the assumption that a TEM mode is being supported, it is necessary to know what limitations must be placed on stripline dimensions. Should these limitations not be met, stripline can easily jump into an infinite number of Transverse Electric or Transverse Magnetic modes depending on the boundary conditions satisfied.

Basic work on this problem has been done by Jasik¹ and Oliner.² The author obtained the original derivation done by Dr. Jasik through a private communication with that author. Dr. Oliner derived a similar relation independently which was similar in form to that of Dr. Jasik but was somewhat easier to evaluate. In this chapter the best features of both derivations will be presented.

B. Cutoff Wavelength of the First Higher Mode:

The cutoff wavelength of the first higher order mode in stripline will be computed through the use of a transverse resonance procedure. The approximate field distribution of this mode is shown in part (a) of Fig. 9-1.



a. Electric Field Distribution

b. Network for Transverse Resonance

Fig. 9-1: First Higher Mode in Stripline

In contrast to the dominant mode, which possesses a magnetic wall or open circuit at its mid-plane, the first higher mode has an electric wall or short circuit there. It is in fact the lowest mode with this symmetry property. Since the first higher order mode is symmetric about this short circuit, it is sufficient to consider one half of the configuration of Fig. 9-1a. The fringing capacity may be considered as a lumped element. These simplifications lead to the equivalent circuit of Fig. 9-1b.

The value of the lumped capacitive element is given by the E-plane bifurcation in the Waveguide Handbook⁵⁹ on page 353.

Formula 2a on that page is

$$\frac{2\pi d}{\lambda} = \frac{2b}{\lambda} \left(\frac{b_1}{b} \ln \frac{b}{b_1} + \frac{b_2}{b} \ln \frac{b}{b_2} \right) + S_1 \left(\frac{2b_1}{\lambda}, 0, 0 \right) - S_1 \left(\frac{2b_2}{\lambda}, 0, 0 \right) \quad (9-1)$$

where

$$S_1(x, 0, 0) = \sum_{n=1}^{\infty} \left(\sin^{-1} \frac{x}{n} - \frac{x}{n} \right)$$

Fig. 9-2 illustrates the various parameters of eq. 9-1.

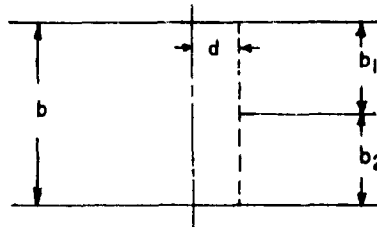


Fig. 9-2: Side View of an E-Plane
Bifurcation in Waveguide.

Equation 9-1 can be somewhat simplified for the case of stripline where $b_1 = b_2 = 1/2 b$. Applying this simplification to equation 9-1, there results:

$$\frac{2\pi d}{\lambda} = \frac{2b}{\lambda} \ln 2 + S_1 \left(\frac{2b}{\lambda}, 0, 0 \right) - 2 S_1 \left(\frac{b}{\lambda}, 0, 0 \right) \quad (9-2)$$

The parameter d must be determined by considering the transverse resonance condition. As an alternate to figure 9-1b, the fringing capacity from center strip to ground can be considered to be compensated for by an additional width of the center strip of d on each side as shown in Fig. 9-3.

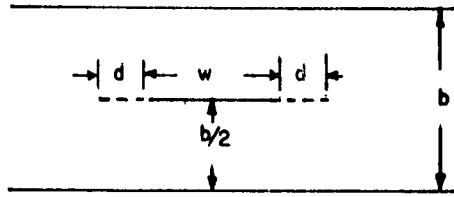


Fig. 9-3: Cross Section of Stripline Taking Fringing Capacity into Account.

Field distribution is symmetrical about the center strip so it is sufficient to consider one half of the configuration of Fig. 9-3, say the lower half. The condition of resonance is readily obtained from the boundary condition and is

$$w + 2d = \frac{n\lambda}{2} \quad (9-3)$$

Since our interest is in the lowest order mode, $n = 1$. If eq. 9-3 solved for d and the result inserted in eq. 9-2, the desired expression results. It can be seen to be;

$$\begin{aligned} \frac{\lambda_c}{2b} &= \frac{w}{b} + \frac{2}{\pi} \ln 2 + \frac{\lambda_c}{\pi b} s_1 \left(\frac{2b}{\lambda_c}, 0, 0 \right) \\ &\quad - \frac{2\lambda_c}{\pi b} s_1 \left(\frac{b}{\lambda_c}, 0, 0 \right) \end{aligned} \quad (9-4)$$

where

$$s_1(x, 0, 0) = \sum_{n=1}^{\infty} (\sin^{-1} x/n - x/n)$$

b = ground plane spacing

w = center strip width

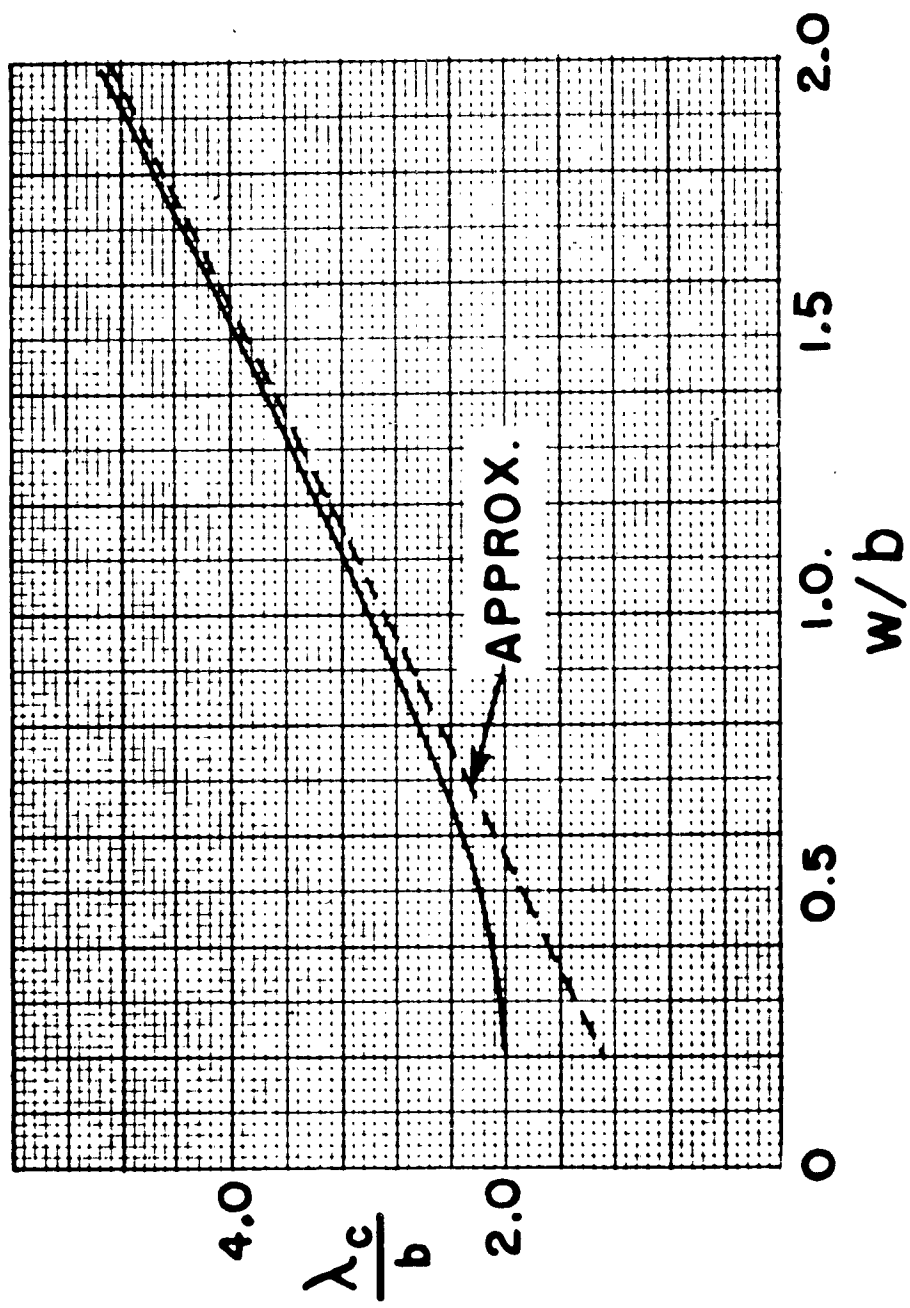
λ_c = cutoff wavelength of the first higher mode.

Equation (9-4) is arranged as shown because the arcsine sum contributions are not major, although significant. In employing eq. (9-4) for calculations, one should solve w/b for values of b/λ_c . The variation of λ_c/b with w/b is presented as the solid line of Fig. 9-4.

When the arcsine sums are neglected, the dashed line of Fig. 9-4 is obtained. The latter is useful as an approximate formula, particularly for w/b large, i.e., for the low impedance range. The error in the use of the approximate formula is shown as Fig. 9-5 as the fractional error encountered as a function of w/b. It is seen that for w/b > 1, the error is less than 3%. The neglect of the arcsine sums, whose value is a function of the cutoff wavelength is equivalent to employing for the fringing capacity in the network of Fig. 9-16 the static value used for the approximate determination of the Characteristic Impedance of the dominant (TEM) mode.

The solid curve of Fig. 9-4, corresponding to the accurate solution, can be extended as far as desired in the w/b direction, but does not exist below w/b = 0.2075, i.e., $\lambda_c/b = 20$ (the reason for the latter statement will be discussed in the next section). However because of inaccuracies introduced by higher mode interaction (due to the edges of the strip being too close together) the curve cannot be trusted quantitatively below about w/b = 0.5.

Fig.9-4. Graph for the cut-off wavelength of the first higher mode



SYMMETRIC STRIP LINE

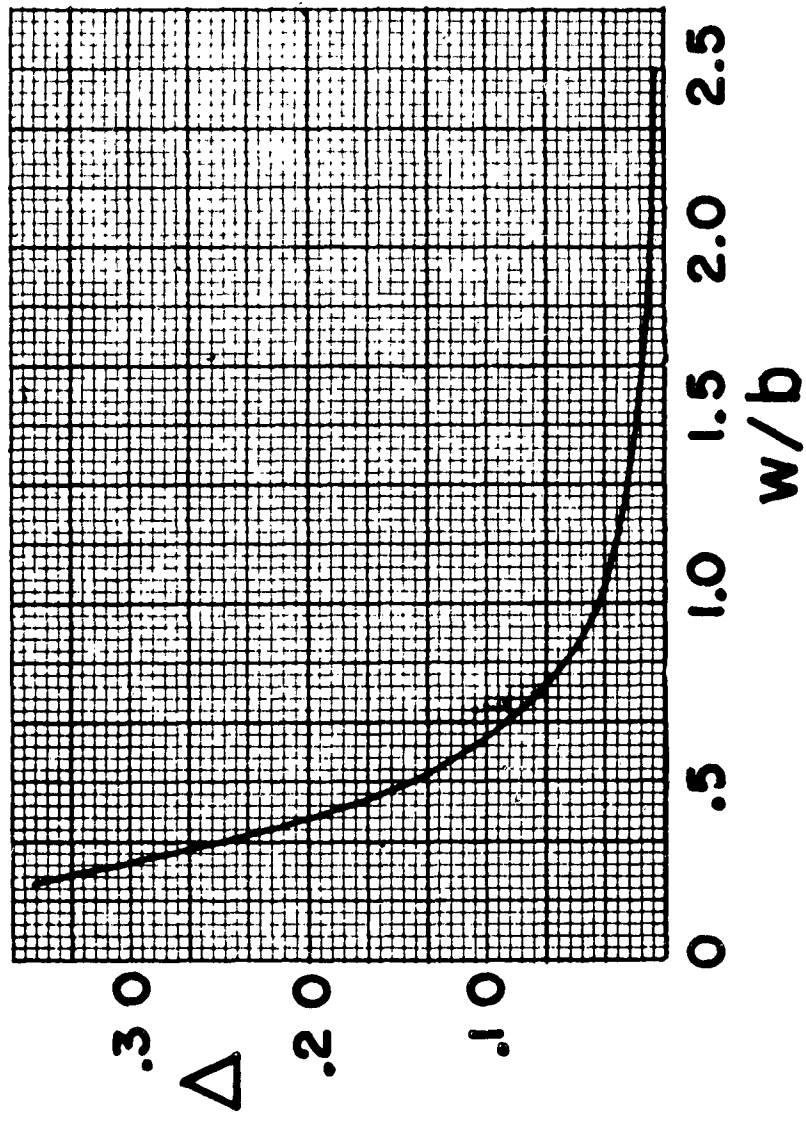


Fig.9-5. Fractional error in the use of the approximate formula

Oliner² points out that an approximate rule can be developed for the cutoff wavelength. When $b/2$ is small compared to the wavelength in Stripline, the cutoff wavelength is equal to the circumference measured around the Stripline center conductor as shown in Fig. 9-6. As $b/2$ increases, the distance from the conductor at which the circumference is to

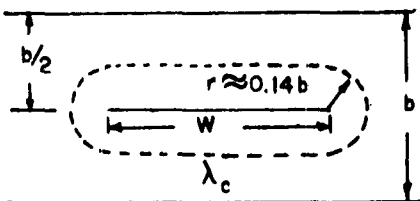


Fig. 9-6: Approximate Rule for Determining λ_c in Stripline.
be measured will increase such that at $b = 0.4 \lambda_c$, $r \approx 0.17 b$,
and at $b = 0.5 \lambda_c$, $r \approx 0.25 b$.

C. Discussion of the Higher Mode Spectrum:

It was remarked above that the solid curve of Fig. 9-4 does not exist below the value $\lambda_c/b = 2.0$. Oliner² has shown that below this value the mode is no longer a discrete, proper mode but becomes a portion of the continuous spectrum. The following discussion is essentially that of Oliner's.

The electric field lines in the case of one class of discrete modes is shown in Fig. 9-7a.

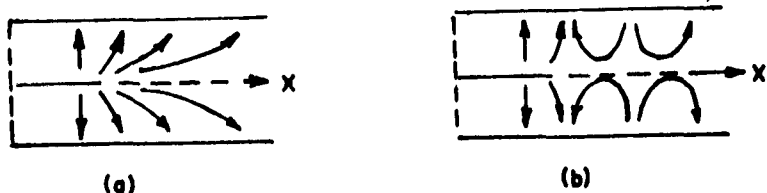


Fig. 9-7: Electric Field Lines for (a) a class of discrete modes, (b) a contribution to the continuous spectrum.

In the region external to the strip in the x direction, the field acts like a mode below cutoff. The wavenumber k_{xe} is satisfied by $k_{xe}^2 < 0$. The field configuration of Fig. 9-7b is characteristic of a propagating mode in the x direction, imposing the condition that $k_{xe}^2 > 0$. Such a mode cannot be associated with a discrete mode in the z direction, but rather with the continuous spectrum.

Consider the stripline cross section shown as Fig. 9-8. Let this cross section be divided into two regions: region one in the central portion and region two in the exterior portions including the fringing regions in the neighborhood of the strip edges. In region one, away from the strip edges,

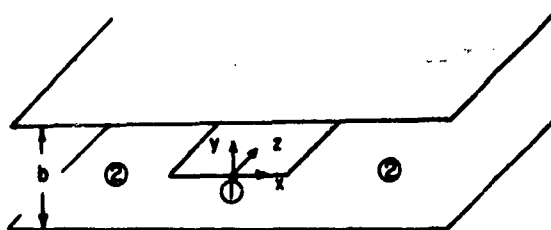


Fig. 9-8: Stripline Geometry.

the wavenumbers in the respective directions are related by

$$k_z^2 = k^2 - k_c^2$$

where

$$k = 2\pi/\lambda$$

$$k_z = 2\pi/\lambda_g$$

$$k_c = 2\pi/\lambda_c$$

and where λ , λ_g and λ_c are respectively, the free space wavelength, the higher mode stripline wavelength and the higher mode cutoff wavelength. For the first higher mode, λ_c is given by eq. 9-4. In regions two of Fig. 9-8, the wavenumbers are related by

$$k_z^2 = k^2 - k_{xe}^2 - k_{ye}^2 \quad (9-6)$$

k_{ye} and k_{xe} are numbers characteristic of the field variation in the x and y directions in the exterior region. For the first higher mode, boundary conditions impose the condition that $k_{ye} = n/\lambda$.

Since for any given mode the values of k_z in regions one and two must be the same, one finds on equating eq. (9-5) and (9-6)

$$\begin{aligned} k_{xe}^2 &= k_c^2 - k_{ye}^2 \\ &= \left(\frac{n\pi}{\lambda_c}\right)^2 - \left(\frac{n\pi}{b}\right)^2 \end{aligned} \quad (9-7)$$

Now for a discrete mode, $k_{xe}^2 < 0$. Inspection of eq. 9-7 shows that $k_{xe}^2 < 0$ when

$$b < \frac{n\lambda_c}{2} \quad (n \text{ an integer}) \quad (9-8)$$

Any practical stripline configuration imposes the condition

$$b < \frac{\lambda_c}{2} \quad (9-9)$$

Even though the dominant (TEM) mode (for which $\lambda_c = \infty$) will propagate as a discrete mode for any value of b , any discontinuity in the line will set up radial line modes similar

to TE_1 (or TM_1) modes in parallel plate line, which will propagate if eq. (9-9) is not satisfied.

We may summarize the above discussion by considering the class of modes characterized by the field plots of Fig. 9-7. Let it be assumed that a higher mode is propagating, so that $\lambda < \lambda_c$ for this mode. Since $n = 1$ for this mode, it can be seen that if eq. 9-9 is satisfied eq. 9-8 will be also. If the mode is propagating, therefore, and $b < \lambda/2$ the mode will always be a discrete mode. If $b > \lambda/2$, the mode may still be a discrete mode, or it may radiate real power away from the center strip, according to whether or not eq. 9-8 is satisfied.

Should the higher mode be below cutoff, additional restrictions arise. Since now $\lambda > \lambda_c$ satisfaction of eq. 9-9 does not influence eq. 9-8. If eq. 9-8 is satisfied, a discrete mode exists; if it is not satisfied, the mode is improper and a member of the continuous spectrum. The question of whether or not the continuous spectrum radiates real power or not must be considered. If real power is radiated, every discontinuity structure of stripline must contain resistive elements in its equivalent circuit. Since the mode is improper and part of the continuous spectrum which exists only as a complex, it is conceivable that certain components of this spectrum contain components which would interfere destructively thus preventing radiation of real power. In this case higher mode power would be completely stored and the equivalent circuits of discontinuity structures would be purely reactive.

Considerations quite independent of the above line of reasoning (e.g., the spectrum of a line source between parallel plates supporting an exponentially decaying current distribution, the possibility of the existence of leaky waves of the type encountered in traveling wave antennas, etc.) indicate that the mode complex is bound and that discontinuities are lossless. Thus, the continuous spectrum, for $b > \lambda/2$, occurs only when the higher modes are below cutoff, and is non-radiating.

D. Experimental Verification:

Airborne Instruments Laboratory³ has made an experimental verification of eq. 9-4. The structure used for the evaluation is termed "trough line" and was originated by AIL. Fig. 9-9 illustrates the geometry of "trough waveguide." Note that its cross section corresponds to one half of the geometry of Fig. 9-1a with an electric short circuit or magnetic wall at its midpoint. Trough waveguide does not support the TEM mode, but, as may be seen from its symmetry properties does support

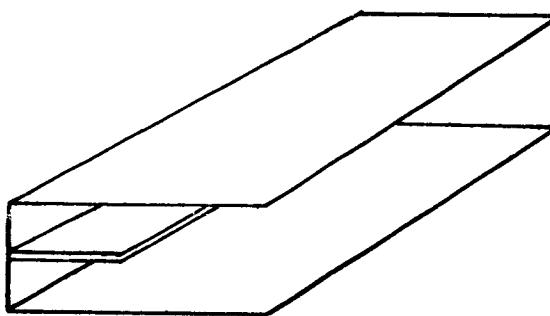


Fig. 9-9: The Trough Waveguide (A.I.L.)

the first higher order mode of Stripline as its dominant mode. Measurement of the transmission characteristics of trough

waveguide as a function of frequency are shown in Fig. 9-10.⁴
The value of cutoff frequency, computed from eq. 9-4 and shown
on Fig. 9-10 as a dashed line, can be seen to correspond to
the measured value of cutoff quite well.

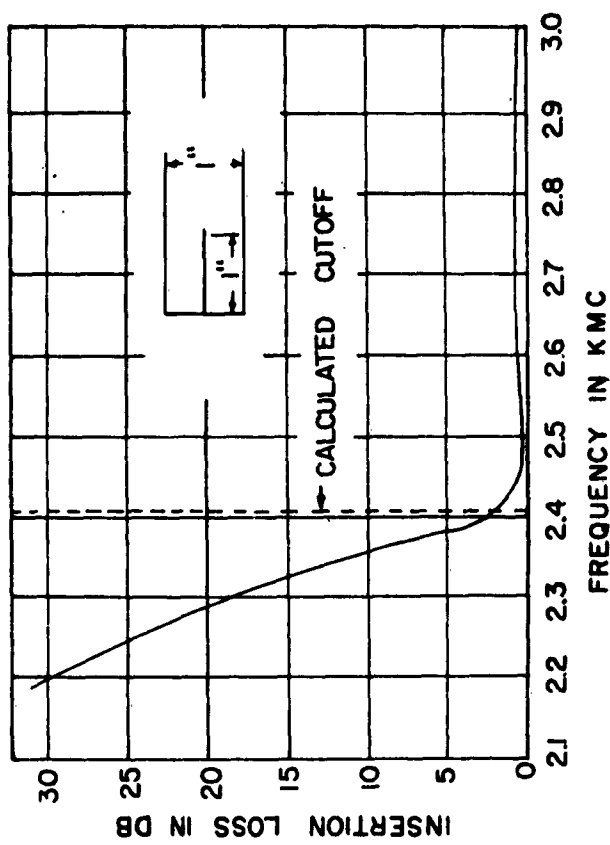


Fig-9-10. TRANSMISSION CHARACTERISTICS OF TROUGH WAVEGUIDE

BIBLIOGRAPHY

1. H. Jasik, memorandum to E. G. Fubini, 30 July 1953. Also contained in Progress Report No. 2830-L-3 on Contract No. AF 19(604)-780, Airborne Instruments Laboratory, 2 Nov 53.
2. A. A. Oliner, "Theoretical Developments in Symmetrical Strip Transmission Lines," Proceedings of the Symposium on Modern Advances in Microwave Techniques, pp. 387 - 392, Ann Arbor, Michigan, Edwards Brothers Inc., 1955.
3. Progress Reports No. 2830-L-1, -2, -9, -14, -16, on Contract NO. AF 19(604)-780, Airborne Instruments Laboratory, 1 September 1953, 1 October 1953, 3 May 1953, 1 October 1954, and 1 December 1954.
4. Figure 4 of Progress Report No. 2830-L-2, 1 October 1953.
See reference 3.